DIS-SIMILAR FRICTION STIR WELDED JOINT QUALITY IMPROVEMENT THROUGH REINFORCEMENT AND PROCESS PARAMETER OPTIMIZATION

A Thesis submitted to the Delhi Technological University, Delhi in fulfillment of the requirements for the award of the degree of

DOCTOR OF PHILOSOPHY

IN

MECHANICAL ENGINEERING

By

PREETY RANI

(2K16/PhD/ME/28)

UNDER THE SUPERVISION OF

Prof. R. S. MISHRA

Department of Mechanical Engineering,

Delhi Technological University

DEPARTMENT OF MECHANICAL ENGINEERING

DELHI TECHNOLOGICAL UNIVERSITY

NEW DELHI-110042, INDIA

DECLARATION

I hereby declare that the research work presented in this thesis, entitled **"Dis-similar friction stir welded joint quality improvement through reinforcement and process parameter optimization"** is an original work carried out by me under the supervision of Prof. R.S. Mishra, Professor, Department of Mechanical Engineering, Delhi Technological University, Delhi. This thesis has been prepared in conformity with the rules and regulations of the Delhi Technological University, Delhi. The research work reported and results presented in the thesis have not been submitted either in part or full to any other university or institute for the award of any other degree or diploma.

PREETY RANI
(2K16/Ph.D/ME/28)
Research Scholar
Department of Mechanical Engineering
Delhi Technological University, Delhi

CERTIFICATE

This is to certify that the work embodied in this thesis entitled **"Dis-similar friction stir welded joint quality improvement through reinforcement and process parameter optimization"** submitted by **Preety Rani, (Roll No. 2K16/Ph.D/ME/28)** in partial fulfillment of requirements for the award of degree of **DOCTOR OF PHILOSOPHY** in **Mechanical Engineering** is a bonafide record of original research work carried by him under my supervision in accordance with the rules and regulations of the institute.

This is also certified that this work has not been submitted to any other institute or university for the award of any other diploma or degree.

Prof. (Dr.) R.S. Mishra
Professor
Department of Mechanical
Engineering,
Delhi Technological University, Delhi

ACKNOWLEDGEMENTS

The work presented here would not have been possible without the help of many talented and learned people. First and foremost, I would like to thank my supervisor Prof. R.S. Mishra, Delhi Technological University, Delhi, for extending his full support and encouragement. I am greatly benefitted from his experience and skills which he shared with me with utmost generosity. I am thankful to the supervisor to help me to get access to all the necessary facilities in DTU including welding laboratory.

I would like to express, a sincere gratitude to Prof. S. K. Garg, Chairman, DRC, and Head of the Department, Mechanical Engineering, Delhi Technological University, for their valuable help, motivation and extending all the necessary processing and experimental facilities during my research work.

My sincere thanks to all the faculty and staff members of Department of Mechanical Engineering (DTU), who supported me during my entire course work and research work. I am grateful to Mr. Girish Anand for their technical and experimental support.

I am short of words to express my sincere gratitude to my parents. Whatever I have achieved in my life; it is because of them. I can't express in words their efforts to nurture me. I am grateful to my husband Mr. Narender Malik for his support and encouragement during my overall research work.

PREETY RANI

ABSTRACT

This research work focuses on a comparative study on weld quality of reinforced friction stir welded joints of dissimilar aluminum alloys AA5083 and AA6061 incorporated with two different types of reinforcement particles. To fabricate dissimilar reinforced FSWed joints, AA5083 and AA6061 plates of thickness 6 mm were used as base materials and micro-sized Al_2O_3 and SiC particles were used as reinforcing candidates. Response surface methodology (RSM) based full factorial face-centered central composite design using three process parameters along with their three levels was employed to develop the design of experiments. Different tool rotational speed (750-1150 rpm), traverse speed (25-45 mm/min) and number of FSW passes (1-2) were considered as process parameters to multi-optimize the output response parameters (tensile strength, %elongation and microhardness) using desirability function in Response surface methodology. Multi-response mathematical model was developed to predict the response output parameters. To analyze the tensile strength, %elongation and microhardness of reinforced FSWed joints of AA6061 and AA5083, empirical relationships were developed at 95% confidence level. Microstructural characterization is carried out using optical microscopy and Field emission scanning Electron Microscope (FESEM) equipped with energy-dispersive X-ray spectroscopy (EDS). The results showed that increasing rotational speed, decreasing the traverse speed and increasing numbers of FSW passes leads to improve the dispersion pattern of reinforcing particles of (Al_2O_3 and SiC) in the SZ of reinforced FSWed joints.

The highest tensile strength (254.42 MPa), %elongation (30.9%) and micro-hardness (124.2 HV) for Al_2O_3 microparticles reinforced FSWed joints were observed at rotational speed of 950 rpm, traverse speed of 35 mm/min after three passes of FSW. The optimum value of tensile strength, %elongation and micro-hardness at the SZ are 258.09 MPa, 31.3% and 124.69 HV respectively, whereas the optimum value of rotational speed, traverse speed and number of FSW passes are 995.38 rpm, 29.79 mm/min and 3 passes, respectively was found for Al_2O_3 microparticles reinforced FSWed joints.

The highest tensile strength (266.97 MPa), %elongation (32.7 %) and microhardness (128.4 HV) for SiC microparticles reinforced FSWed joint were observed at rotational speed of 950 rpm, traverse speed of 35 mm/min after three passes of FSW. The

optimum value of tensile strength, %elongation and micro-hardness at the SZ are 269.62 MPa, 32.75 % and 128.47 HV, respectively, whereas the optimum value of rotational speed, traverse speed and number of FSW passes are 994.57 rpm, 29.40 mm/min, and 3 passes, respectively was found for SiC microparticles reinforced FSWed joints.

TABLE OF CONTENTS

LIST OF FIGURES

LIST OF TABLES

CHAPTER-1
INTRODUCTION

1.1 FRICTION STIR WELDING

This is a solid-state joining process used to join two work pieces by using a non-consumable tool. Heat generates between rotating tool and work piece surface due to friction. A soft region develops in work piece near the tool. Tool transverses along the joint line which intermixes the metals of both the pieces mechanically and generates the mechanical pressure to forge the hot softened material. It is like the joining of clay or dough. FSW is used to join wrought or extruded aluminum. It is also used in trains and aerospace applications because of high strength in welded joints [1].

1.1.1 WORKING PRINCIPLE

In FSW, the cylindrical tool is mounted on the friction stir welding machine's rotating spindle. Furthermore, the work piece plates must be firmly secured on a fixture in such a way that the base plate faces are not driven apart. The revolving tool is then lowered gradually between the separating lines of the two plates to be welded [2]. Frictional heat is generated owing to friction between the work piece and rotating tool, softening the material without melting it.

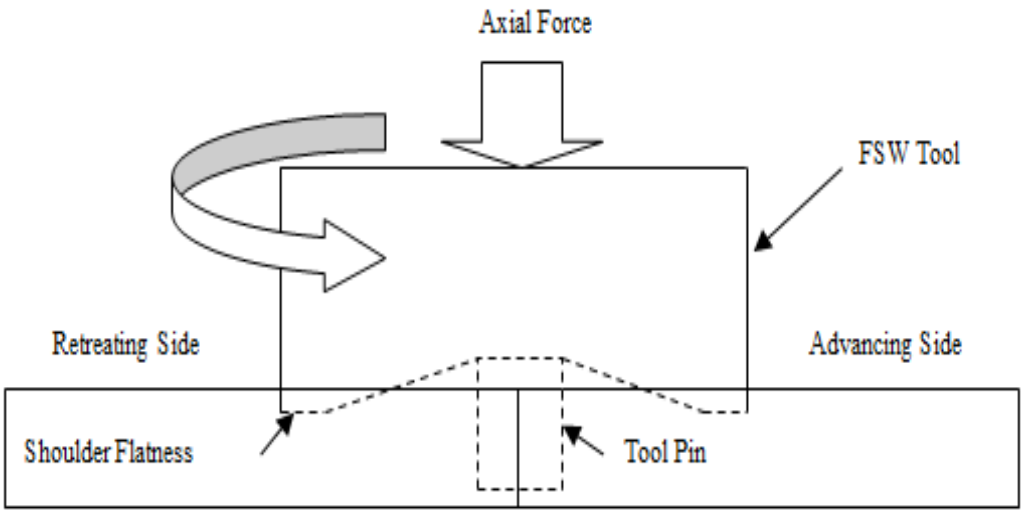

Figure 1.1: Schematic diagram of FSW

During welding, the friction heat also assists the tool in moving along the parting line of the base plates. The high temperature achieved is on the order of 0.8 times the melting point of material. The plasticized material is transported to the tool pin's trailing edge

and forged by the tool shoulder's close contact with the pin profile. Because a hole to admit the pin is created and may be filled during the welding operation, the procedure is referred to as a solid-phase keyhole welding approach [2]. The friction stir welding principle is demonstrated in Fig. 1.1.

1.1.2 MERITS & DEMERITS OF FSW:

There are several advantages of FSW over fusion welding methods. FSW is a solid state welding technique that creates joints with a low defect concentration without using any material melting. In this, there is no involvement of any liquid phase. Problems like porosity, solidification cracking and liquation cracking are not faced. Low concentration of defects is there.

Although there may be some unique defects also causes like insufficient temperature due to high translation speed or low rotation speed which may results in tunnel defects along the weld on the surface. Forging action may be limited due to low temperatures which reduces the bond continuity between materials.

Some advantages over conventional welding methods are as follows:

- Good mechanical properties at welded area
- Safe process due to absence of harmful spatter and fumes of molten metal.
- No filler material required
- Does not consume material, a short pin can weld up to 1 km length of joint.
- Less setup cost. A designed fixture easily can convert a conventional vertical milling machine in an FSW setup.
- No weld pool hence can be processed in vertical and horizontal position as well.
- Good surface appearance and requires less processing after weld.
- Minimum surface preparation.
- Environment friendly
- Economic and energy efficient.
- It gives better performance over fusion welding at lower cost.

Along with advantages, some disadvantages are also there in FSW which are as follows:

- Hole is left at the exit of the pin.
- To keep the plates together, strong clamping is needed.

- Requires rigidity to balance the large down forces.
- Less flexible for the variations in plate thickness. Different tools are required for different plate thickness.
- Lesser transverse rate than some other welding processes. This may compensate if others require multi passes.

1.1.3 APPLICATIONS

1.1.1.1 *Aerospace industry*

At the meantime, the aerospace sector uses FSW to join space vehicle elements. Friction stir welded and successfully tested circumferential lap welds and longitudinal butt welds of Aluminum alloys fuel tanks for space vehicles. As a result, FSW procedure can be utilized for:

- Fuselages.
- Scientific and Military rockets.
- Cryogenic fuel tanks.
- External throwaway tanks.
- Fuel tanks.

1.1.1.2 *Marine industries*

The marine industries were among the first to use the technology for commercial purposes. The following applications are suited for the process:

- Panels for bulkheads.
- extrusions.
- Superstructures and Hulls.
- Transport and Marine structures.
- Sailing boats.

1.1.1.3 *Rail-way industry*

The first commercial manufacture of high-speed trains consisting of aluminum extrusions that can be linked via FSW has been declared. The following are some examples of applications:

- High-speed trains.

- Railway tankers and rolling stock.
- Underground carriages.
- Container bodies.

1.1.1.4 *Construction industry*

It is feasible to employ portable FSW equipment for the following purposes:

- Window frames
- Aluminum bridges
- Facade panels
- Fabrication of Pipes
- Pipelines of aluminum
- Air conditioners and heat exchangers
- power plants reactors

1.1.1.5 *Land transportation*

Several automobile businesses and suppliers to this industry are now experimenting with the FSW technology for commercial use. The following are examples of possible applications:

- Truck bodies
- Chassis cradles
- Wheel rims
- Mobile cranes
- Airfield transportation vehicles and Buses
- Fuel tankers
- Bicycle and Motorcycle frames
- Tail lifts for lorries

1.1.1.6 *Electrical industry*

FSW is becoming increasingly utilized in the electrical sector for:

- Electrical connectors
- Electric motor housings
- Encapsulation of electronics
- Bus bars

1.1.1.7 *Other industries*

FSW is a viable substitute for:

- Gas cylinders.
- Joining of copper or aluminum coils.
- Refrigeration panels.
- Cooking equipment.

1.2 DECSRIPTION OF THE ROTATING TOOL

The tool has two essential elements, the shoulder and pin as depicted in Fig. 1.2. The pin has generally a cylindrical form that projects from the shoulder surface and a longitudinal axis that is parallel to the shoulder longitudinal axis. During welding, the pin creates heat and stirs the material. At working temperatures, the pin must be big enough to keep above the plastic stress level.

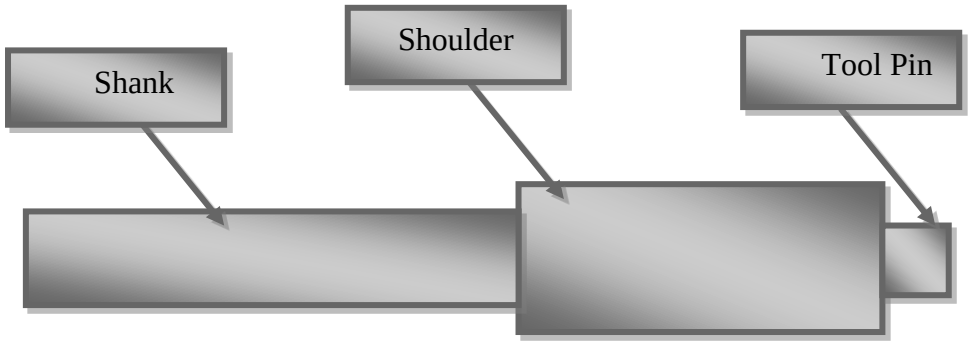

Figure 1.2: Tool outline for FSW

The weld quality is also affected by the profiles of tool pin. Cylindrical, cylindrical threaded, trapezoidal, square, and other pin profiles are available. The tool shoulder has two purposes: to produce more heat at the work-piece/ tool frictional contact and to cap the "stirred" plasticized material. The plasticized material during FSW tends to extrude from the tool's leading to the trailing side, but is restrained by tool shoulder, resulting in a smooth surface finish.

1.3 TOOL MATERIAL

Friction stir welding, is carried out by thermomechanical deformation in which the tool temperature approaching base metal's solidus temperature. Welding/processing takes place at temperatures between 70 and 90 % of the base material's melting point, thus the material of tool should be enough strong enough to sustain twisting and breaking at

this temperature. Fractures become undesirable as a result of a tool losing its dimensional stability and other desired properties [3].

The following factors must be considered while selecting a tool material:

- Strength at ambient and elevated temperature
- Tool reactivity
- Machinability
- Fractural toughness
- Wear resistance
- thermal expansion coefficient
- Elevated temperature stability.

An FSW/FSP tool used may be made of various materials including H-13 tool steel, tungsten-based, Ni-alloys, polycrystalline-cubic boron nitride (PCBN), and other materials. A tool composed of H13 tool steel that has been heat treated and oil quenched was employed in this study.

1.4 TOOL STEEL

Tool steel like H13 is very common tool material which is used in FSW/FSP for magnesium alloy, aluminum alloy, and copper alloy. The advantages of tool steel include easy machinability and availability, low cost and have excellent mechanical properties. The tool steel H13 can be used for similar or dissimilar aluminum alloy. H13 tool steel have a resistance to damage from deformation and abrasion in the FSW of aluminum alloys.

1.4.1 NICKEL COBALT BASE ALLOY

The Nickel cobalt-based alloys are fabricated to reveal high strength and excellent corrosion protection. The operating temperature should be less than the precipitation temperature ranges from 600-800°C to prevent the dissolution and precipitate over-aging. Nickel cobalt base alloy tool is mainly designed for aircraft engine components.

1.4.2 REFRACTORY METALS

The refractory metals such as molybdenum, tantalum and tungsten are utilized for high temperatures and high densities parent materials for friction stir welding. These metals are the strongest alloy having melting point from 1000-1500^{0}C. The refractory metals

tools are mainly design for welding of aluminum alloy, copper, steels and tungsten base alloy, but the main drawback of refractory metals is high cost, long lead time and difficult to machining.

1.4.3 CARBIDES AND METAL MATRIX COMPOSITE

Because of superior mechanical and physical properties (i.e. fracture toughness, wear resistance and ambient temperature) of carbide they are mainly used as machining tools. Friction stir welding tool such as tungsten carbide is reported to have fine and uniform welded surface with or without pin thread. Tungsten carbide is brittle in nature and have very high strength due to bonding between tungsten and carbide atoms. Tis bonding also leads to have high melting point about 2800^0C. This tool is mainly used for copper, steel and aluminum alloy welding.

1.5 MICROSTRUCTURE OF FSWED JOINT

The material of work pieces gets soften by heat generated by rubbing action of the tool shoulder and the work piece surface. The tool pin stirs the soften material to produce a sound joint of the two work pieces. The material of the joint also exhibits the axial force exerted by the tool and a heat cycle due to elevation of the temperature [4]. The microstructure in the FSWed joint is presented in Fig. 1.3, which can be divided in following regions:

(a) Nugget zone (NZ)

(b) Thermo-mechanical affected zone (TMAZ)

(c) Heat-affected zone (HAZ)

(d) Base material (BM)

Figure 1.3: Representation of various zones in FSW [4]

(a) Nugget zone (NZ)

Weld nugget refers to the recrystallized region in the TMAZ. Since the grain structure is frequently distinct in this location—clearly a component of the TMAZ—the area

immediately below the tool shoulder needs to be given its own category. The intent is to regard this region as a distinct sub-zone of the TMAZ. So, this zone exhibits highest strength and hardness among all other regions of the joint.

(b) Thermo-mechanical affected zone (TMAZ):

The material has been plastically deformed by the tool in this area, and the heat generated by the operation will have an impact on both the material's characteristics and microstructure. Consequently, grains are stretched, distorted, and bent as a result of the tool pin's shearing action in this zone. The plastic strains make the region of least strength and hardness. This zone exhibits the thermal cycle and mechanical stresses as well; therefore, it is called as TMAZ.

(c) Heat affected zone (HAZ)

It is obvious that this area is closer to the weld center. In this region, the material underwent a heat cycle that changed the mechanical and/or microstructure characteristics. However, in this area, there is no plastic deformation.

(d) Base material (BM):

The BM or unaffected area of the welding joint is remote from the welding region. This material may exhibit some thermal heat cycle but not affected in terms of microstructure and mechanical properties.

1.6 MATERIAL SUITABILITY

FSW is not affected by gravity. As a result, it may be employed to weld in any orientation, including annular vertical, and horizontal. As a consequence, FSW has been utilized to produce circumferential welds of fuel tanks in spacecraft. Regular corner and fillet welds as well as double V-butt joints, and other applications are also possible with FSW within given parametric tolerances, the following aluminum alloys might be successfully welded to produce consistent high integrity welds:

2XXX aluminum series	(Al-Cu)
3XXX aluminum series	(Al-Mn)
4XXX aluminum series	(Al-Si)
5XXX aluminum series	(Al-Mg)
6XXX aluminum series	(Al-Mg-Si)

7XXX	aluminum series	(Al-Zn)
8XXX	aluminum series	(Al-Li)

1.6.1 OTHER MATERIALS

FSW method has also been employed to other materials, on which research is now being conducted. The following are a few of them:

- Magnesium and its alloys
- Lead
- Titanium and its alloy
- Mild steel
- Copper and its alloys
- Zinc

1.7 ALUMINUM ALLOY

The various aluminum alloys are utilized in automobile and aerospace engineering industries. The major alloying elements which are used in different Al-alloys are Copper, manganese, Magnesium, Silicon, Magnesium, Zinc, and tin. The most important aluminum alloy is silicon base alloy (Al-Si), where high percentage 3.5 to 12% silicon is used. Silicon base aluminum alloy have excellent casting characteristics. These alloys are widely utilized in automobile sector, aerospace engineering such as metal skinned aircraft etc. The second widely used alloy is magnesium base aluminum alloy. These alloys are lighter than the all-aluminum alloys. Aluminum alloy have an attractive appearance in its natural finish, which may be shiny, lustrous and soft. Aluminum alloy can re recycle from the scrap value and providing environmental benefits and economics. It has easily fabrication and joining ability. The physical, chemical and mechanical characteristics of Al-alloys depend on composition of alloying elements (i.e. Cu, Si, Mg, Mn, Zn, Sn, and Fe), grain size and microstructure. The total amount of alloying elements should be less than or equal to 10% and the impurity elements should be less than 0.15% [5]. Compared to steel, aluminum alloy has a wide variety of mechanical and physical qualities which are as given below.

- The density of aluminum alloy is only 1/3rd that of steel.
- Aluminum alloys may have high ductility, high toughness and have high strength to weight ratio.

- Aluminum alloy have a high resistance to corrosion under critical service conditions and it's also used for cryogenic application.
- Aluminum alloys are highly reflective material and it is a good electricity and heat conductor.
- Aluminum alloys are nontoxic and non-ferromagnetic material and it can have used for food and beverages containers.

1.7.1 CLASSIFICATION OF ALUMINUM ALLOYS

Cast aluminum alloys and wrought aluminum alloys are the two main divisions of aluminum alloys [6]. For wrought aluminum alloys, the American Society for Testing and Materials (ASTM) established a four-digit identification system, while for cast aluminum alloys, it adopted a three-digit and decimal designation system. These two divisions are further divided into number series from 1xxx-9xxx for wrought alloys and 1xx.x–9xx.x of cast alloys, as presented in Figure 1.1. The major alloying elements decide the series of the aluminum alloy. These classified number series are also subdivided under non-heat treatable and heat treatable alloys in both wrought and cast categories. In the wrought aluminum alloys 1xxx, 3xxx, 4xxx, 5xxx series and 1xx, 2xx series in cast alloy are classified or grouped in non-heat treatable sub category. 2xxx, 6xxx, 7xxx and 3xx, 4xx of wrought and cast aluminum alloys are grouped under heat treatable alloys [7]. The desired properties of heat treatable alloys can be enhanced due to thermal or mechanical treatments of these alloys.

1.7.2 DESIGNATION SYSTEM OF ALUMINUM ALLOYS

In four-digit designation system of wrought alloys, the first digit (Xxxx) describes the main constituent, which has been mixed to aluminum as presented in Figure 1.4. The second digit (xXxx) other than 0 describes the condition of modification of specific alloy, whereas, second digit in 1000 series describes the amount of aluminum (above 99%) in the alloy. For each alloy in the series, the third and fourth numbers (xxXX) are randomly selected.

The first digit (Xxx.x) of three-digit plus decimal designation system of the cast alloys, describes the primary alloying element of aluminum alloy. Second and third digits (xXX.x) give the identity to a particular alloy in the series. The digit following the decimal point specifies whether alloy is a casting (xxx.0) or an ingot (xxx.1 or .2). The

prefixed capital letter represents a modification to the alloy.

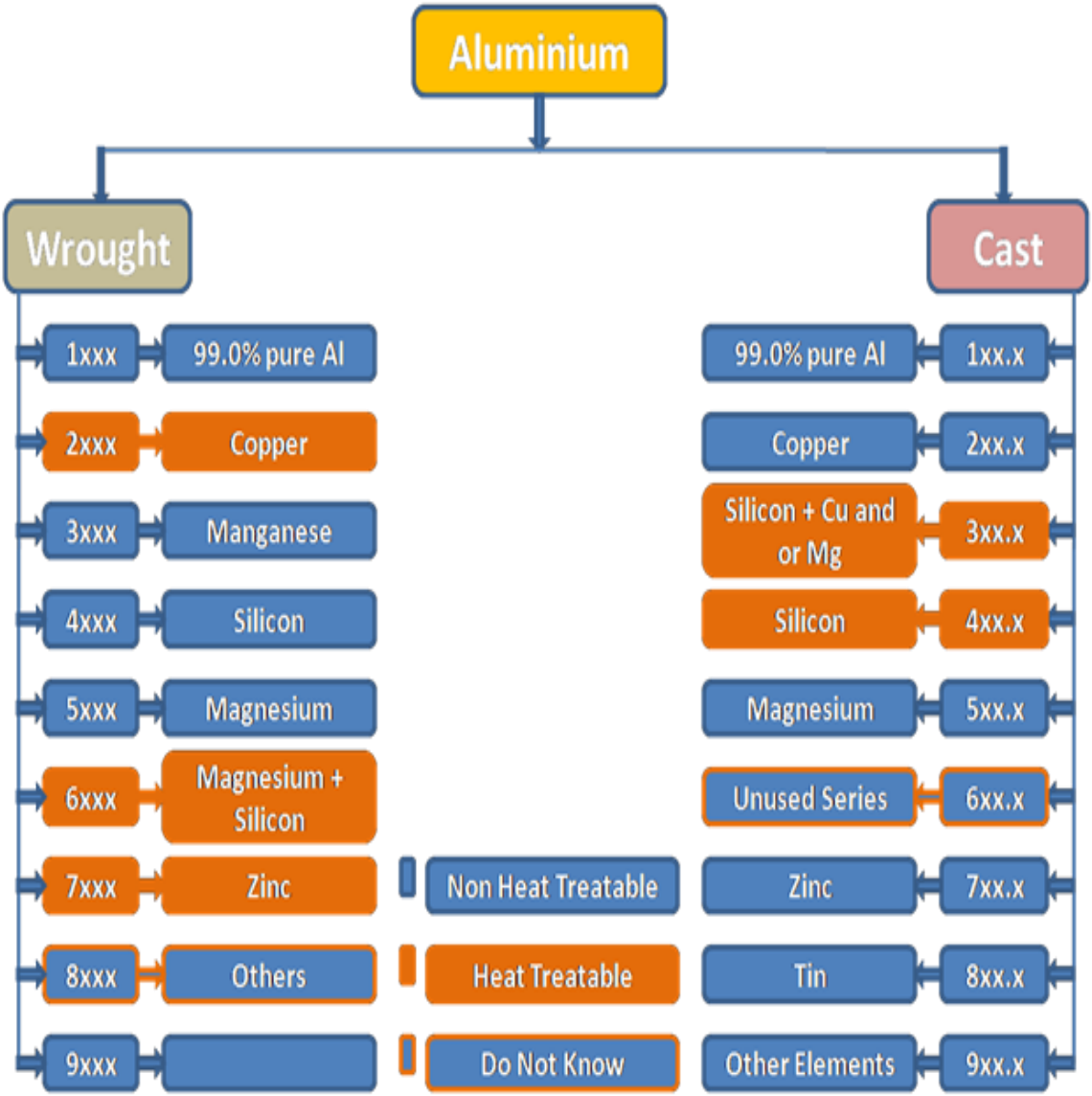

Figure 1.4: Classification of aluminum alloys [8]

Solution heat treatments and age hardening are the most common thermal treatments used to provide optimum mechanical properties to the heat treatable alloys. The optimum mechanical characteristics are acquired by non-heat treatable alloys through strain hardening. Application of cold working processes to enhance mechanical properties is known as strain hardening. The designation system adapted to these temper conditions of aluminum alloys is called temper. The temper designation system follows the alloy designation numbers in form of letters and numbers which is connected by a hyphen. Example: AA6063-T6, AA6061-T4, AA5083-H112. Table 1.1 provides the temper designation scheme.

Table 1.1: Temper designation system [9]

S. No.	Letter	Description
1	F	As Fabricated
2	O	Annealed
3	H	Strain Hardened
4	W	Solution Heat Treated
5	T	Thermally Treated

H temper (Strain Hardening) and degree of hardness illustrated in Table 1.2 and Table 1.3, respectively and T temper (Thermal Treated) is further subdivided as presented in Table 1.4.

Table 1.2: Subdivisions of H temper [9]

The first digit following H (Basic operation)		
S. No.	**Letter**	**Description**
1	H1	Strain hardened only
2	H2	Strain Hardened & Partially Annealed
3	H3	Strain Hardened & Stabilized
4	H4	Strain hardened & Lacquered

Table 1.3: Designation of extent of strain hardening [9]

S. No.	Letter	Description
1	HX2	Quarterly Hard
2	HX4	Half hard
3	HX6	Three Quarters Hard
4	HX8	Fully Hard
5	HX9	Extra Hard

Table 1.4: Subdivisions of T temper [9]

The first digit after T		
S. No.	**Letter**	**Description**
1	**T1**	Naturally aged

2	**T2**	Cold worked after cooling
3	**T3**	Solution heat treated
4	**T4**	Solution heat treated and naturally aged
5	**T5**	Artificially aged after cooling
6	**T6**	Solution heat treated with artificially aged
7	**T7**	Solution heat treated with over aged
8	**T8**	Solution heat treated, cold worked with artificially aged
9	**T9**	Solution heat treated, artificially aged with cold worked
10	**T10**	Cold worked following cooling

1.7.3 TYPES OF ALUMINUM ALLOYS

On the basis of alloying elements, the aluminum alloy may be classified into different categories which are as given below.

1XXX series

In wrought aluminum having 1XXX series have present various elements as inherent impurities in the smelter grade. AA 1100 and 1135 are the 1XXX series alloys. These alloys have specified minimum and maximum copper contents. Corrosion resistance, thermal conductivity and electrical conductivity of 1XXX series alloys is very high and may also obtained high tensile strength via strain hardening. The silicon, copper and iron are the alloying elements present in the highest percentage in 1XXX series.

2XXX series

In this series, magnesium is the secondary alloying element, with copper (Cu) being the primary alloying element. For obtaining optimum mechanical and physical properties, these alloys required heat treatment. The mechanical properties of 2XXX series are very similar or sometimes exceed the low carbon steel, after heat treatment. The corrosion protection properties of these alloys are not good as compare to other aluminum alloys or sometimes it shows intergranular corrosion. These alloys are commonly used to make suspension parts, structural part and aircraft wheel etc., and it also have high strength to weight ratio.

3XXX series

The main alloying element in the 3XXX series is manganese (Mn), the strength of 3XXX series alloys have 20% more than 1XXX series alloys. They are not heat-treated alloys, but having good corrosion properties. The alloying element Mn is limited (up to 1.5%) present in the aluminum solid solution and form precipitates Al_{12} (Mn, Fe)$_3$Si or Al_6(Mn, Fe) phase. These alloys are frequently utilized in cooking equipment, architectural product, chemical equipment's and resistance to corrosion.

4XXX series

In this aluminum alloys series, the silicon is the major alloying element and it may be added upto 11% to the lowering the melting point without increasing of brittleness. The Al-Si alloys are mostly used as a welding filler wire with different grade for joining similar or dissimilar aluminum alloys. Mostly these alloys are not heat treatable. ER4043 is widely used as a filler wire. Due to containing of silicon they are demanded in architectural application, production of forged engine piston etc.

5XXX series

In this series, magnesium (Mg) is the main alloying element. When it is used with manganese (Mn), high strength alloy would get. Mg is more effective than Mn as harder. 0.8% magnesium is equal to 1.25 manganese for hardened the alloys. The 5XXX series shows good corrosion resistance in marine atmosphere and also has excellent welding characteristics. Magnesium base aluminum alloy like ER5356 used as a filler wire to join the different aluminum alloys with TIG or MIG welding processes.

6XXX series

The principal alloying elements in 6XXX series are Mg and Si, typically less than 1% each, and minor amount of chromium, copper, zinc and manganese. The magnesium silicate Mg_2Si was found in 6XXX series which is the hardening constituent. This alloy series are heat treatable, excellent corrosion resistance, versatile, highly formable, high strength, and excellent weldability, the weld metal cracking may be prevented by the use of different filler metal such as ER4043, and ER5356. These alloys shouldn't be welded by an arc without filler since they are inherently susceptible to solidification cracks. Depending on the service and application requirements, 4xxx and 5xxx series

filler material may be used for welding. These alloys are commonly used for automotive components and architectural extrusions.

7XXX series

In this alloy series, zinc (Zn) is the principal alloying element, and it may be varied from 2 to 10%. Due to its excellent mechanical characteristics, these alloys are used in high performance application i.e. competitive sporting equipment, aerospace and aircraft engineering, automobile industries etc.

The inclusion of magnesium further complicates the issue by forming additional ternary eutectics and complicated intermetallic, which provide dispersion hardening and $MgZn_2$ precipitates. The copper zinc system produces $CuAl_2$ and an intermetallic, which together add to the precipitation's hardness. When welding, the zinc instantly turned into an oxide, lowering the weld pool's surface tension and increasing the chance of fusion defects, which is a problem specific to the 7XXX series. This necessitates the employment of welding processes that use a welding current that is 10–15 percent greater than that of a 5XXX alloy. It's also been discovered that using a shorter arc than usual improves material transfer to virtually globular levels.

8XXX series

This series is frequently utilized to designate alloys, such as 8001 (Aluminum-Ni-Fe) and 8020 (Aluminum-Ni-Fe) (Aluminum-Sn), that don’t easily fit into any of the prior groups. The Al-Li alloys, however, are a relatively recent class of high-strength alloys that offer a higher Young's modulus and significant weight reductions of about 15% compared to some other alloys of high-strength. Each 1% increase in lithium resulted in a weight loss of about 3%. These benefits indicate that lighter, weldable Al-Li alloys can replace high strength alloys, as of 2XXX family, in the design of aircraft structures, leading to considerable weight savings.in the design of aircraft structures, resulting in significant weight reductions.

After being given a name, the family of alloys known as "scandium-containing alloys" may also fit under this category. These are brand-new alloys that are still in the early stages of development. Scandium has been discovered to be quite successful in enhancing strength through grain refinement and age hardening, the latter of which is especially advantageous in welding of materials. Scandium maybe combined with

additional alloying materials like zinc, magnesium, zirconium or lithium to produce tensile strengths of above 600 N/mm^2 in laboratory tests.

1.8 WELDING OF ALUMINUM ALLOYS

Fusion welding was generally used to weld the aluminum and its alloys in early stages of use of aluminum in industries. The melting of material from the edges to be weld due to heat input by the heat source and then solid recasting of the same material produce the weld joint. But High thermal conductivity, shrinkage during solidification, high thermal expansion and high hydrogen solubility in the molten state make the welding of aluminum alloys challenge for designer and researcher. The above-said properties of aluminum leads to the less fusion due to a layer of oxides, the inclusion of slag, partial penetration, thermal cracks, hot tears, undercut and porosity in the welds. gas metal inert welding (MIG) and Gas tungsten inert welding (TIG) and are in trending for welding of aluminum since early of 20th century. But the defects, low joint strength and extreme grain evolution in heat affected zone (HAZ) were still a challenge for designers. There are three major types of defects which may occur in the weld of aluminum alloys when welded by fusion or TIG or MIG welding techniques.

- Stress corrosion cracking
- Porosity
- Hot cracking

The solubility of hydrogen in molten superheated aluminum is very high but it reduced drastically with the decrease in temperature during solidification. The contaminated hydrogen converts in to bubbles at a lower temperature due to lower solubility in aluminum at a lower temperature and faster solidification due to the higher thermal conductivity of aluminum. These bubbles cannot escape due to solidification of metal which causes porosity as presented in Figure 1.5.

Figure 1.5: Porosity defect in aluminum weld joint [10]

The hydrogen present within the parent and filler metal, hydrogen oxide layer of the same metals, contamination (oil and greases) and presence of moisture in shielding gases are the main source of the hydrogen for porosity in the aluminum during welding [10].

Hot cracking is occurring when a molten metal solidifies at the surface but the inner material is in liquid form. The inner molten metal shrinks during solidification which produces residual stresses on the outer slid surface. These stresses cause cracks in the outer surface which are known as hot cracks as presented in Fig. 1.6. These cracks are occurring due to solidification so also called solidification cracks or thermal cracks. Hot cracks are generally found occur in weld region but it may occur in HAZ also if grains of the same region partially melted.

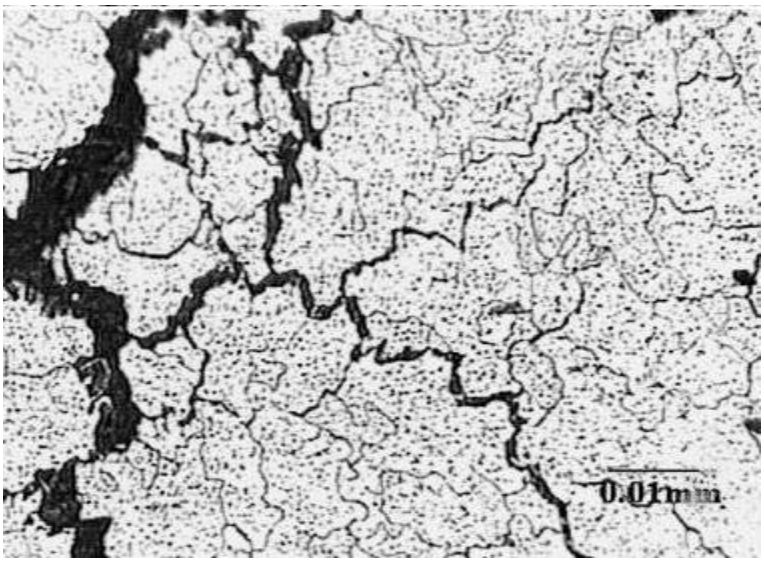

Figure 1.6: Hot cracking in the weld zone [11]

High thermal conductivity causes the rapid cooling of the outer surface of the material (molten) in the weld zone, which induces residual stresses. The combination of the tensile stresses (residual stresses) and the corrosive environment cause stress corrosion cracking. The welds joint which have heterogeneous microstructure are more sensitive for stress corrosion cracking. These types of cracks are initiated from the corrosion pit and propagate along with the grain boundaries due to the chemical and tensile condition. A colony of this type of cracks is shown in Fig. 1.7.

Figure 1.7: Colony of stress corrosion cracks

The problem associated with the welding of aluminum alloys is due to the melting and recasting of the material in weld zone. High temperature also causes unwanted grain growth in HAZ. Solution to these problems is to produce the weld at lower temperature than the melting point of the aluminum. Researchers and designers have developed some welding methods such as resistance welding, Thermit welding, pressure welding, friction welding etc. However, FSW which is proved to be the most significant process for welding aluminum alloys.

1.9 MECHANISM OF COMPOSITE FABRICATION IN FSW/FSP

FSP is considered a variant of the FSW method. FSW is used to weld materials in solid-state, particularly those with low melting points, such as aluminum alloys. The research by Mishra et al. [12] in 1999 was the first to utilize the phrase "friction stir processing" as a keyword. It was suggested in 2003 that FSP may be used to successfully manufacture light metal alloy surface composites (SCs) [13]. After this accomplishment, FSP became known as a surface modification and grain refinement approach, and it became a key milestone in solid-state material processing techniques.

The working concept of FSP is similar to that of FSW, excluding that FSP is used for the processing of the base materials to improve desirable features such as grain refinement, mechanical and surface properties enhancement, and so on

Composite fabrication is accomplished by adding reinforcing particles to the base material matrix from the outside and then executing FSP. There are two steps to composite manufacturing using FSP. The incorporation of reinforcing particles (RPs) into the base material-matrix is the first stage, and the FSP of the RPs incorporated base matrix is the second stage. RPs (also known as reinforcement approaches) can be pre-placed in a variety of ways. Groove techniques, Direct pasting of RPs, spray techniques, and other approaches are among them [14-19]. Each technique of reinforcement preplacement has its own set of stages and advantages and disadvantages. The approach of direct pasting RPs onto the base matrix was used to begin the production of SCs. It is a rapid procedure that does not require any preparation stages such as drilling holes or grooves, but it has a substantial problem of RP waste during FSP [20]. During the process, a small percentage of RPs sputters out, resulting in RP waste. To avoid sputtering during FSP, various reinforcement schemes have been developed. The groove method, spray technique, hole technique, and hollow tool technique are examples of these. The groove method is the most popular. The groove method entails machining a groove on the surface of plate with predetermined dimensions [21, 22]. The RPs are then poured into the groove and squeezed. The groove entrance is sealed with a pinless tool after the RPs are packed. FSP is then conducted using a specifically developed instrument with a pin. Fig. 1.8 depicts the typical stages involved in the groove approach. However, the groove can be covered with a thin sheet or piece of tape to avoid having to seal the groove.

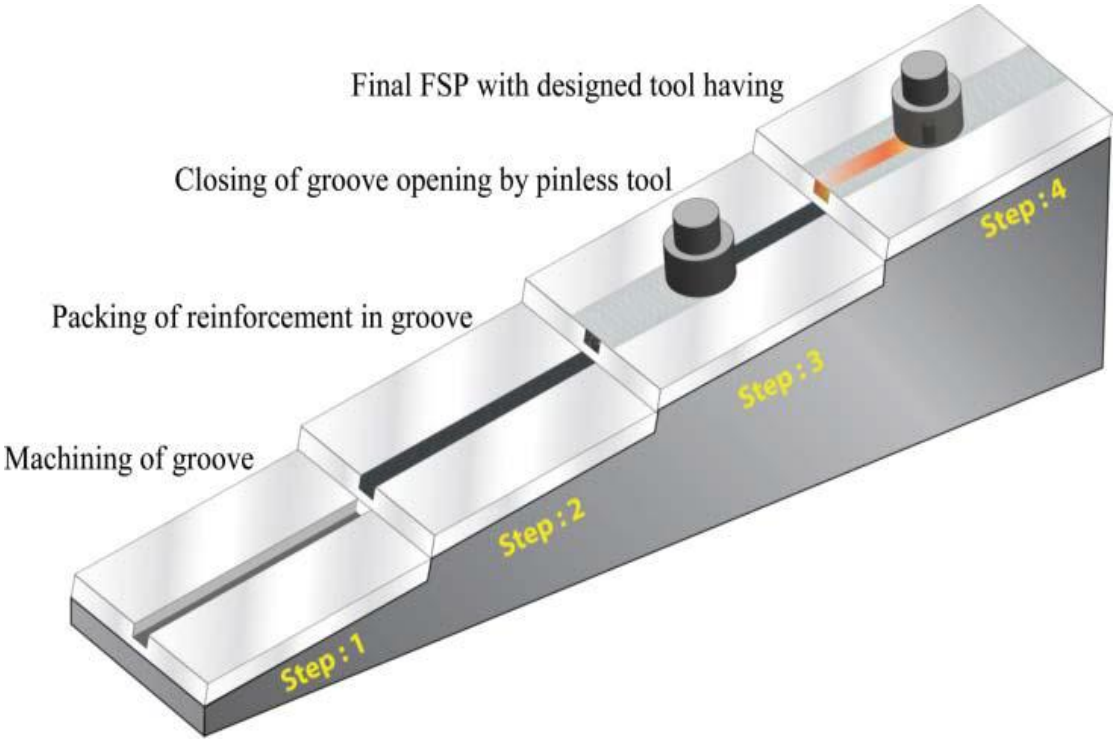

Figure 1.8: Steps in composite fabrication via groove method [23]

The hole technique entails drilling holes of appropriate diameters in the base material [24]. Half of the tool shoulder was proposed to covers the next hole ahead of the hole's. The spray technique is another approach for eliminating the closing phase. The base plate does not even need to be machined. A slurry of reinforcing particles is sprayed on surface of base plate using plasma spray, and other methods, followed by FSP. Reinforcing particles are formerly immersed in the hollow tool, which is then flowed out to penetrate the area limited between the shoulder of the tool and deformed zone in the hollow tool process. As the rotating tool moves longitudinally, these RPs compress into the workpiece. However, a deeper SCs layer requires more work in this manner. As a consequence, it can be determined that a variety of reinforcing techniques are in use, each of which leads in a different RP dispersion and developed different composite characteristics.

In a comparative analysis, Rathee et al. [25] found that direct pasting of reinforcing particles is a simpler approach but produces less homogeneous surface composites than the hole and groove method. Furthermore, as compared with the blind hole approach, the groove with tool-offset approach produces more uniform composites.

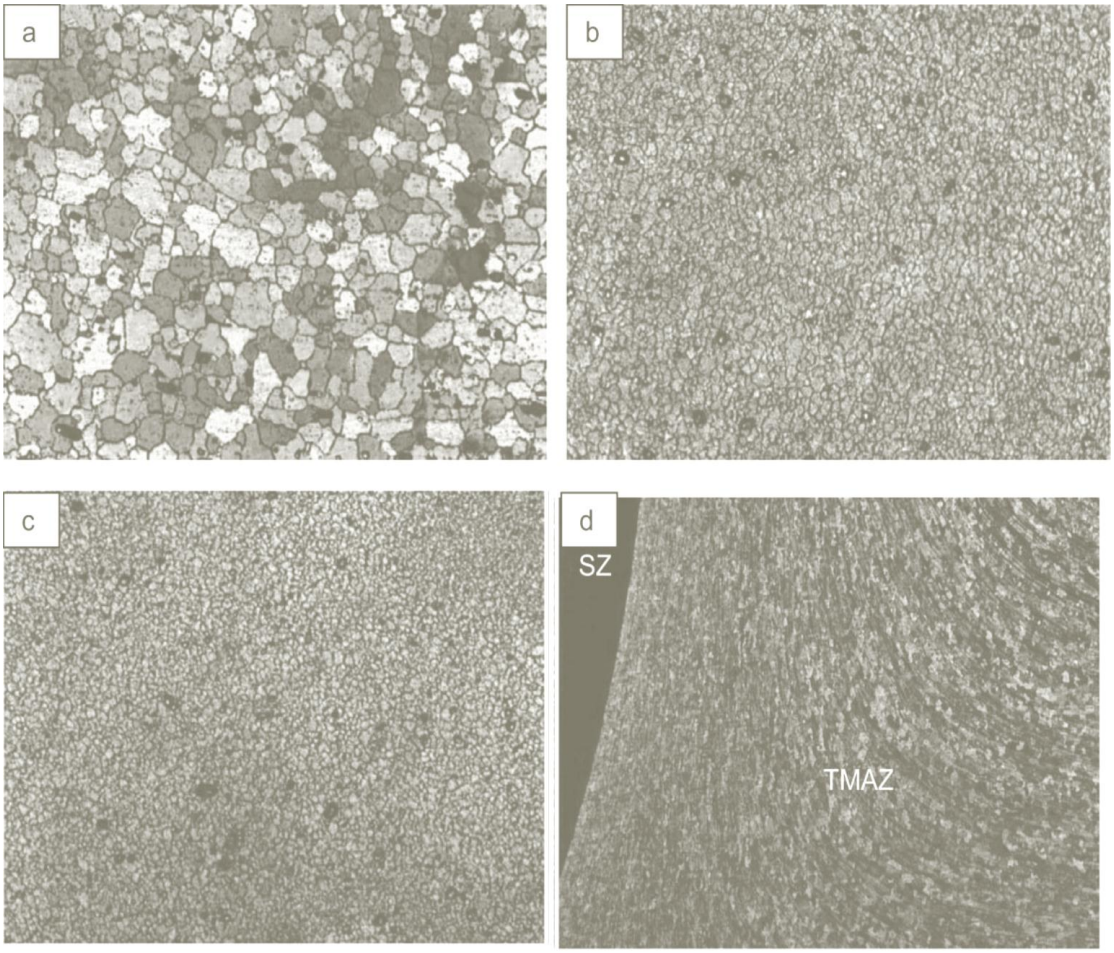

Figure 1.9: Microscopic graphs of: (a) Parent material, (b) FSPed without RPs, (c) FSPed with RPs of CNT, (d) Upward flow pattern of composite interface [25]

To generate defect-free, sound, and uniform ex-situ surface composites, an appropriate reinforcing procedure should be used. The following is a summary of the composite manufacturing mechanism utilizing FSP. The development of friction heat across the region joining the revolving tool and the work material resulting in softening and plasticization of the workpiece material during FSP [26, 27]. The microstructure of as received AA5083 with 21 µm grain size as depicted in Fig. 1.9 a. the grain size was decreased to 6.31 µm after employing FSP without RPs as depicted in Fig. 1.9 b. On addition of RPs of CNT, the size of grains was further decreased to 3.98 µm as revealed in Fig. 1.9 c [28]. So, the study revealed that the degree of grain size reduction mainly depends on base material, type and size of RPs, number of passes and selection of optimum process parameters.

1.10 FACTORS AFFECTING WELD QUALITY

Improvements in composite microstructure and mechanical characteristics are entirely dependent on how reinforcing particles are dispersed in the base matrix, which changes depending on the reinforcing technique used and the variable combinations used in composite production.

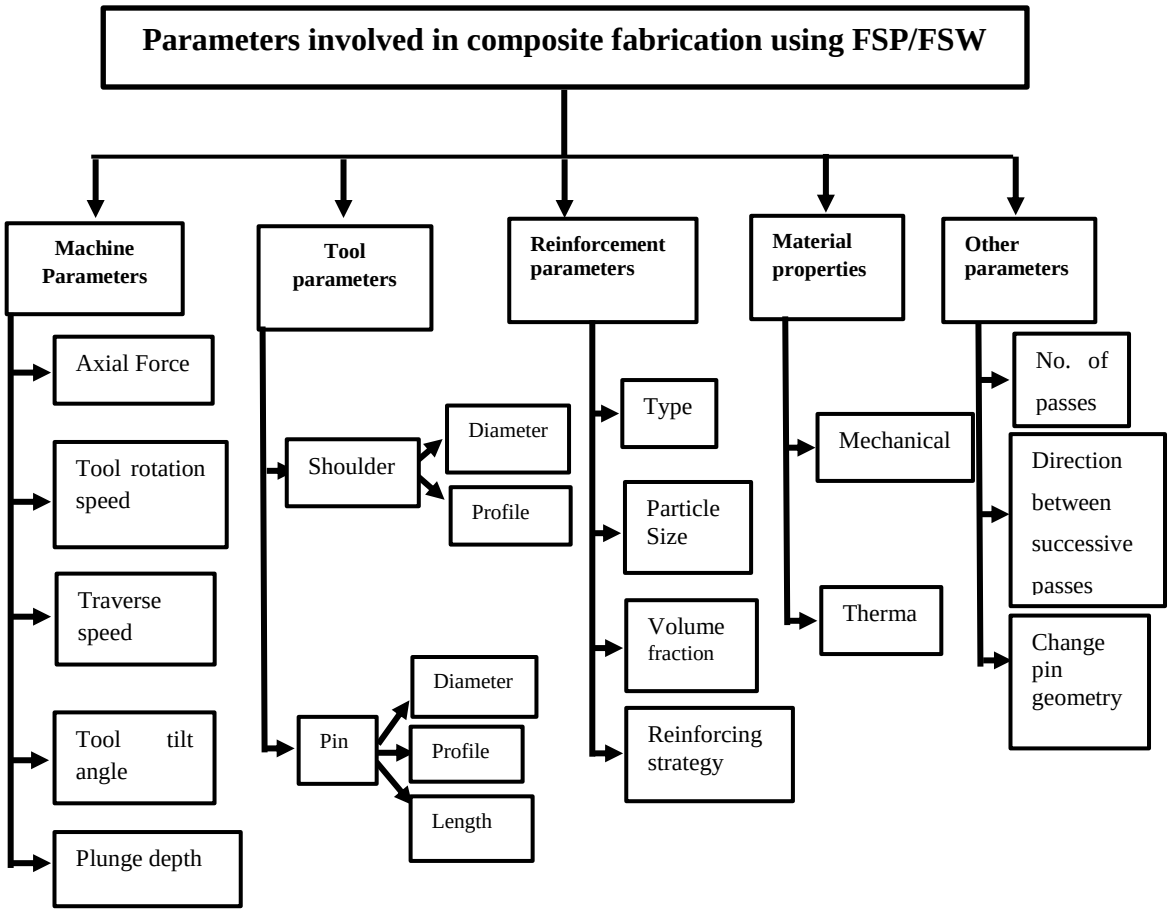

Figure 1.10: Illustration of the many elements involved in composite production.

Fig. 1.10 is an illustration of the many elements involved in composite production. These parameters may be categorized into five categories according on their impact on SC properties: machine particular, tool particular, reinforcement particular, material property precise, and other strategies. When compared to other factors, some contribute more to property enhancement.

1.10.1 TOOL ROTATION SPEED (RS)

The rate at which the tool revolves around its axis is known as the tool rotation speed. It is an essential factor in FSP/FSW. The heat input in the workpiece during welding is also affected by tool rotation speed. It is expressed in rpm.

1.10.2 TRAVERSE SPEED

The traverse speed influences the joint properties as well. This refers to the rate at which the revolving tool moves forward on the workpiece. During welding, the deviation of the heat input in the workpiece depending on the traverse speed.

1.10.3 AXIAL FORCE

The download force utilized between the tool and the work piece is another essential element in FSW. The tool is kept in touch with the parent material's surface by the downward force.

1.10.4 TOOL TILT ANGLE

The tool angle in relation to the work-piece during FSW also affects the quality of the weld.

The angle is usually 900, however it can vary up to 30 in special circumstances.

1.10.5 PLUNGE DEPTH

The link between plunging depth and tool inclination is substantial. Tilt inclinations and plunging depths may be modified concurrently to produce desired tool-work piece contact areas. Increased tilt inclinations while keeping constant plunge depths result in reduced heat production because there is less contact surface between the workpiece surface and the shoulder of tool. Higher tool penetration depths are required to compensate for the loss in surface contact and consequently the quantity of heat produced.

1.10.6 SHOULDER DIAMETER

When processing or welding, the tool's shoulder diameter is used to produce additional heat and to cover the plasticized material when it is "stirred. The weld quality is also impacted by the tool shoulder diameter. The weld zone will be larger as the tool shoulder diameter increases.

1.10.7 TOOL PIN LENGTH

This is a crucial consideration for determining joint properties. The pin length should be a bit smaller than the thickness of the work-piece. The tool pin length may thus be regarded as a crucial factor in FSW.

1.10.8 TOOL PIN DIAMETER

The diameter of the tool pin is utilized to generate friction heat and agitate the material during welding. In FSW, the tool pin diameter is a critical parameter. Friction heat in the treated zone will increase as the tool pin diameter increases.

1.10.9 TOOL PIN PROFILE

The weld properties and flow pattern of the plasticized material are influenced by the tool pin profile or probe geometry. While shoulder of the tool encourages mass flow of material, pin of the tool supports a layer by layer material flow. Generally used tool pin profiles are cylindrical, conical, square, triangle, pentagonal and cylindrical threaded etc.

1.10.10 REINFORCEMENT PARTICLES TYPE, SIZE, AND VOLUME PERCENT

The size and type of RPs can affect the properties of produced composites. Various types of reinforcement particles like silicon carbide (SiC), carbon nanotubes, graphite, boron carbide (B_4C), aluminum oxide (Al_2O_3), and others have been used to fabricate SCs utilizing FSP. Several researchers created hybrid composites employing two or more RPs at varying ratios of hybrid, in addition to mono composites.

1.10.11 OTHER PARAMETERS

The dispersion of reinforcing particles improves with the enhancement in the number of passes during composite manufacture through friction stir processing, as does the change in direction and pin shape.

The following factors are being combined in order to better regulate the process, which is currently being researched.

1.11 TYPES OF REINFORCEMENT PARTICLES

Despite their wide range of technical uses and exceptional features, Al alloys have limited yield strength, stiffness, and wear resistance in some applications. Their strengthening is required to make them appropriate for certain technical applications. The young' modulus, yield strength and wear resistance of ceramic particles incorporated in Aluminum matrix rises. AMMCs are gaining prominence in the aerospace, defense, car, and marine industries as a result of their enhanced

characteristics. To take advantage of their hard character, a variety of reinforcement particles have been introduced to aluminum-matrix utilizing FSP. Ceramic particle forms of reinforcements are described in this section. Silicon carbide (SiC), graphite, titanium carbide (TiC), titanium diboride (TiB_2), boron carbide (B_4C), aluminum oxide (Al_2O_3), carbon nanotubes, and other reinforcing particles are often employed. In addition to process factors, MMC characteristics are influenced by the type, size, volume percentage, and spatial orientation of RPs [29]. Here, the characteristics of various RPs, as well as their fabrication challenges and applications, are examined.

1.11.1 CARBON NANO TUBES (CNTS)

CNTs are another essential reinforcing candidate that has been demonstrated to be useful in the production of MMCs. These are graphitic carbon materials that are tube-shaped and have a high modulus of elasticity (up to 1 TPa) and stiffness (up to 63GPa). These have excellent thermal and electrical properties in addition to excellent mechanical characteristics. These can be metallic or semiconductor depending on their shape and size [30].

AMMCs reinforced with carbon nanotubes are becoming more popular in a range of structural applications. However, CNTs' ability to tolerate severe plastic deformation at higher temperatures is a serious drawback. High shear stresses cause CNTs to fail, and they turn into fine spheres, as in the ball milling [31]. When CNT walls are broken, new structures such as carbon onions may form. CNTs, on the other hand, have been shown to withstand a variety of SPD processes, including equal channel angular processing, accumulative roll bonding, and so on.

1.11.2 BORON CARBIDE (B_4C)

Boron carbide is another prominent reinforcing material. It has a low density (nearly 2.52 g/cm^3) and hardness of about 2800 kg/mm^2 . It has a melting temperature of 2,763 ^oC. Composites of Al/B_4C are useful for nuclear power reactors as neutron absorbers. The particles of boron carbide are also utilized to improve the aluminum alloys' ballistic performance. These composites are commonly utilized in the construction of bicycle frames, ballistic jackets, armour vehicles and tanks, car parts, and other items due to higher hardness, remarkable bonding capability, and strong thermal and chemical stability [32].

1.11.3 TITANIUM DIBORIDE

Titanium diboride (TiB_2) is a high-density material with a density of 4.52 g/cm^3, a hardness of about 2,500 kg/mm^2, and a melting temperature of 3,225 ºC . It is thermally stable and has a high Young's modulus (about 565 GPa). Because of its considerable hardness, and excellent thermal stability, it is being used in MMCs. In standard liquid state composite manufacturing approaches, however, mixing the particles of TiB_2 necessitates additional effort due to TiB_2 particles settling down due to its higher density and low wettability differential than aluminum alloys [33]. FSP/FSW overcomes these issues because it is a solid-state approach.

1.11.4 TITANIUM CARBIDE (TiC)

Titanium carbide (TiC) has such a high melting temperature of 3067 ºC and a density of 4. 91g/cm^3. TiC has a high elastic modulus and the grain refining capability when compared to aluminum alloys. Al/TiC composites are challenging to produce due to TiC's high density, poor wettability, and substantial CTE discrepancy between Al and TiC.

1.11.5 CERIUM OXIDE (CeO_2)

Cerium oxide (CeO_2) seems to be another significant reinforcement that is gaining popularity in aluminum-based MMCs for sectors such as the shipping sector, where corrosion resistance is critical. In general, the addition of RPs (especially SiC) lowers the corrosion resistance of aluminum-based MMCs. CeO_2 is commonly used as a corrosion protection promoter because it serves as a cathodic blocker, slowing down cathode activities. [34].

1.11.6 ALUMINUM OXIDE (Al_2O_3)

Aluminum oxide is another essential reinforcing candidate used in the production of MMCs. It has a low melting point of roughly 2,050 ° C. and a high density (4.08 g/cm3). Because of their superior wettability, low melting point, and inexpensive cost, they are becoming increasingly popular.

In the FSP manufacturing of surface composites, some researchers used micro and nano-sized Al2O3 particles. Zarghani et al. [35] created Al6082/Al_2O_3 surface composites. The introduction of nano-sized Al_2O_3 particles increased microhardness by 168 % and increased wear resistance by two to thrice. Particles dispersion consistency,

wear resistance and microhardness all improved as FSP passes increased. Raaft et al. [36] discussed the synthesis of monocomposites of A356 with graphite and Al_2O_3 particles. In terms of wear and mechanical properties, the scientists discovered that A356/Al_2O_3 based composites beat A356/ graphite-based composites. A maximum improvement in microhardness of 82 percent was also observed in Al_2O_3-based composites.

1.11.7 SILICON CARBIDE (SiC)

One of the most common reinforcements used in AMMC is silicon carbide (SiC). It has a low density (3.20 g/cm^3) and melting temperature (2700 ºC). High variations in thermal expansion coefficients between two constituent components (SiC and Al) generate problems during solidification, which is a common concern when synthesizing Al–SiC composites using standard composite production processes. FSP overcomes these issues because of its solid-state nature [37].

Therefore, in the present study, micro sized particles of SiC and Al_2O_3 are used as reinforcing candidates.

CHAPTER-2

LITERATURE REVIEW

2.1 REVIEW of LITERATURE

The main aim of this chapter is to report the previous research work related to FSW done by various researchers based on influence of input parameters on the integrity of FSWed joint. FSW was invented and patented in December 1991 by TWI [38]. The initial set up was developed for the welding of aluminum with a cylindrical tool pin and flat shoulder surface. The first commercial application was reported to manufacture the hollow aluminum panel for deep freezing of fishes in fish boats in 1996 [39]. But in current scenario FSW is used in aerospace, shipbuilding, transport, railway, defense, structure fabrication and recently in computer and mobile industry due to continuous efforts of researchers and designers. FSW can be applied for welding of soft materials such as aluminum, magnesium as well as hard materials such as titanium and steel with the change in time span. FSW can also be applied for welding of thick plates (60 mm, used for thin plate at initial stage of development). These developments in process of FSW are because of the continuous efforts of researchers.

The literature survey is carried out for material selection, parameters selection, selection of working range for parameters, selection of appropriate optimization technique etc. The reviewed literature is segregated in different groups such as materials (similar/dissimilar), use of reinforcements, processing parameters mainly tool rotational speed, traverse speed, shoulder diameter and tool tilt angle etc. and considered responses. The following sections of this chapter are dedicated for the selection of above said parameters for the experimental study. The detailed report of literature survey is presented in following sections:

2.2 COMPARISON OF FSW WITH OTHER WELDING TECHNIQUES

Many researchers have compared the performance of FSWed aluminum alloy joint with the joints fabricated by other welding processes like TIG and MIG etc.

Haagensen et al. [40] investigated the fatigue strength of FSWed joints of AA6082 in T4 condition and compared the same with joints fabricated by TIG welding process.

The study found that the grains of HAZ of FSWed joints are finer and the fatigue strength of the same was more than 50% higher than the joints fabricated by TIG.

Ericsson and Sandstrom [41] investigated the fatigue performance of AA 6082 in T4 and T6 temper condition joined by FSW, MIG and TIG welding processes. The experiments were performed on various welding speeds. The study found the joints fabricated by FSW are sound in fatigue strength and also showed less effect of welding speed on the same in comparison of MIG and TIG processes.

Mahmoud Abbasi et al. [42] compared the TIG welding, FSW and friction stir vibration processing (FSVP) in terms of microstructure and mechanical characteristics of AA6061 joints. The specimen is vibrated when FSP is performed in FSVP. FSW has been adjusted to create FSVW, in which the connecting specimens vibrate parallel to the welding line. According to the findings, the smaller grains in the weld zone for FSVW and FSW were observed. The grains in FSVW were finer than the FSW ones. The findings also indicated that the FSVW joints had better strength, toughness and hardness values than the joints made by FSW and TIG. The growth of finer grains was facilitated by the vibration that occurred during FSW. FSVW had a weld efficiency of around 81%, whereas FSW and TIG had weld efficiencies of about 74% and 67%, respectively.

Squillance et al. **[43]** compared the micro-hardness and corrosion resistance behavior of 2 mm and 3 mm thick sheets of AA 2024-T3 joined by FSW and TIG welding processes. TIG welding requires more heat to fabricate joints, so the high temperature during welding results in the decay of micro-hardness of the welding joints. Whereas, the joint fabricated by the FSW showed a different pattern of micro-hardness owing to the combined effects of dynamic plastic deformations and low heat input. HAZ and weld bead of TIG welding process were found more sensitive for passive corrosion than the joint fabricated by FSW. The overheat input caused loss of micro-hardness due to over aging and phase transformation in HAZ of joints welded by TIG.

Yeni et al. [44] utilized three deferent welding techniques, i.e. solid-state joining process FSW, fusion welding TIG and MIG. The welded joints have been analyzed as far as their microstructures, mechanical characteristics and hardness. Microstructural evolution uncovers that finer grain sizes are acquired in FSW, through grain development has been seen in TIG and MIG welds. The outcomes demonstrate that among the three welding techniques utilized. The hardness profiles of weld cross section of TIG, MIG and FSW of AA7075 is presented in Fig. 2.1.

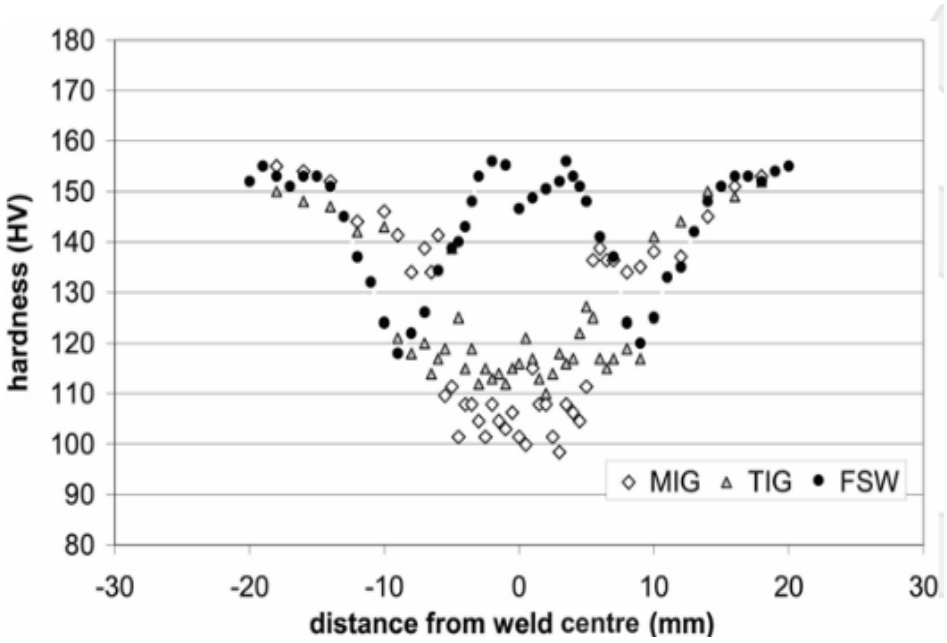

Figure 2.1: Hardness profiles of weld cross section of TIG, MIG and FSW of AA7075 [44]

Sik et al. [45] compared the joints of 4 mm thick plates of AA2014-O welded by TIG and FSW processes. The joints were tested for hardness, tensile and fatigue strength. Due to lower heat input the joint of FSW were found distortion free weld bead. Weld bead's surface finish of FSW was also better than that of TIG weld bead. The study found that the FSW is the better alternate for the welding of AA2024-O.

Kumar et al. **[46]** compared the heat input (kJ/mm) and joint efficiency of joints fabricated by TIG, MIG and FSW. The study used 6 mm plates of AA6061 for experimentation which were welded by above mentioned welding processes. Study found that the heat input in process is 38% and 51.2% lesser than the TIG and MIG processes, respectively. Joint efficiency was also found highest for FSWed joints than other two processes. The joint efficiency was 64.5%, 51.6% and 80% for TIG, MIG and FSW, respectively.

Elanchezhian et al. [47] compared the weld strength of AA7075 by tensile test and impact test for TIG, MIG and FSW welding processes. The study found that the impact strength and tensile strength of FSWed joints was higher than other joints fabricated by two processes.

Bodukuri et al. [48] compared the tensile strength, microhardness, microstructure and cracks and porosity of the AA5083 welded by TIG and FSW. The FSWed joints three to four times better tensile strength than the joints fabricated by TIG. Micro-hardness

of joints fabricated by TIG was 81.3 HV whereas the joints fabricated by FSW achieved 86.1 HV. The samples of FSWed joints found with porosity and cracks in HAZ in microstructural analysis buy TIG welded joints were free of these.

Lailesh Kumar et al. [49] studied the impact of different welding techniques on welded joints' tensile strength of mild steel. The study revealed that the tensile properties of FSWed joints were higher i.e. 356 MPa and 22%, respectively than fusion arc welding technique.

Navneet Khanna et al. [50] analyzed the defect formation and tensile strength of the TIG welded and FSWed for comparison. AA6063-T6 was utilized for experimentation and the specimens were tested by X ray radiography and UTM. The results of the study reveal the higher tensile strength and less defect formation in FSWed joints than TIG welded joints. Therefore, study verified that the FSW is a better option than TIG welding process to weld AA6063.

2.3 SELECTION OF PROCESS PARAMETERS

As discussed earlier parameters of any process decides the efficiency and the effectiveness of process. This section of the chapter is dedicated to the literature survey of research for impact of processing parameters on mechanical behavior of FSWed joints.

The efficiency and quality of FSWed joint is decided by the two inputs i.e. heat input to the process (per unit length) or heat generated and the flow of material to be welded in soft condition during process. These two inputs are affected by the parameters of process and design of tool used for welding. FSW parameters may be categorize in four categories viz machine process parameters, tool design parameters, material parameters and other parameters. Some parameters of these categories are also having considerable influence on the microstructural and mechanical characteristics of FSWed joint as discussed follows:

2.3.1 TOOL ROTATIONAL SPEED (RS) AND TRAVERSE SPEED (TS)

Tool rotation speed (RS) and traverse speed (TS) are considered as the most significant process parameters which decides the quality of FSWed joints. Rotational and traverse speeds affect the frictional heat generation between two surfaces i.e. tool shoulder and work material. Higher the RS and lower the TS higher will be the heat generation and

affect the material flow. The literature related to rotational speed and traverse speed is reported as below:

Moataz M. Attallah et al. [51] investigated the abnormal grain growth (AGG) in the nugget zone of FSW of AA2095 in the post-welding heat treatment. The AGG is mostly determined by the welded joint's process parameters. The grain refining in the weld zone was done with a lower heat input, i.e. a lower rotating speed and a high feed rate. Following post-weld heat treatment, aberrant grain development becomes excessive, causing the welded joint's strength to decrease.

G. Buffa et al. [52] suggested a 3D-thermo mechanical-coupled numerical method for FSW that employs a visco-plastic material description for the seam of weld. This model can forecast the influence of input factors on the process thermodynamics, like material flow, strain rate, temperature strain, and forces. With a drop in advancing speed, an extension of the HAZ was discovered, as well as an increase in the nugget's maximum temperature and maximum strain. The asymmetrically distributed flow in the weld zone (WZ) is found because the flow of material is largely influenced by rotating and advancing speeds.

S. R. Ren et al. [53] observed the impact of input parameters on tensile properties of FSWed joints of Mg, Si base aluminum alloy of Al-Mg-Si, and it was found that the higher tensile strength revealed at RS 1200 rpm, TS 400 mm/min of with 45° shear fracture, while lower tensile strength was observed at RS 600 rpm, TS 100 mm/min. The higher hardness profile was noticed at RS 1200 rpm with a TS 400 mm/min.

Z. Zhang et al. [54] established the thermo-mechanical model to estimate the distribution of temperature and material deformation. According to this model, the maximum temperature in the FSW is increased as RS increases. The TS can lead to enhance the efficient power input for friction stir welding system. The increasing RS and decreasing TS may lead to enhanced stirring of the rotating tool and modify the weld properties. When the traverse speed increases than the increment in the rotational speed is necessary to avoid welding defect. When the TS and RS is increased, residual stress also increased.

Omar S. Salih et al. [55] investigated the mechanical behavior of aluminum matrix-composite (AMC) fabricated by FSW which was dependent on both FSW processing parameters and composition of AMC, hence the mechanical behavior of FSW welded joint evaluated consequently. Formation of new grains structure with the enhancement of reinforcement grains in the weldment by controlling the processing parameters with

different amount of heat was observed in the microstructure of AMC. The FSW process parameters i.e. tilt angle, TS, and RS have a substantial impact on heat input and strength of welded joints.

L. Commin et al. [56] found that the temperature distribution is consistent over the weld length but asymmetric between the AS and RS because of the heat input created by the plastic deformation. Grain growth was detected with a rise in the processing parameters that endorse heat generation, and stress levels were greater on the RS. The grain size evolution follows the models proposed, which take into consideration the strain rate and processing temperature.

Ravi Kumar et al. [57] investigated the impact of processing parameters (RS 800-1000 rpm, and TS 90-110 mm/min) on mechanical behavior of FSWed joint of AA7075 and AA6061 by FSW. The lowest tensile stress i.e. 205.23 MPa was noticed at a RS of 900 rpm with the TS 100 mm/min. The benign mixing of both metals was observed at high rotational speed with a lower feed rate.

Jerry Wong et al. [58] welded the AA6061 plates of 1 mm thickness and studied the impact of a rotating tool; the revolving and advancing speeds were adjusted. To assess joint strength, the specimens were sectioned. Vickers microhardness indentations and metallographic investigations were performed. As a result of crystallization, higher value of feed rates and intermediate value of rotational tool speed provide a better weld joint in the stir zone. The tensile test also shows that higher value of feed rates and intermediate values of rotational speed produce a better weld joint. Due to the heat input, lower advance and feed rates result in the dissolving of hardening precipitates, Mg_2Si in this case, and increased precipitation.

Jianqing Su et al. [59] employed the FSP on a 2mm thick plate of Ti-6Al-4V by different feed rate (1-4 IPM) and RS (800 rpm- 1000 rpm). The nugget zone of the FSP specimens shows a fully β transformed micro-structure characterized by basket weave lamellar structure (α/β). The higher TS and lower RS resulted in α colony and fine β grains size which gives the higher strength. The higher tensile and yield strength was observed 1156 MPa and 1067 MPa respectively without losses of ductility at RS 900 rpm and a TS of 4 IPM.

J.F. Guo et al. [60] examined the effect of constant RS of 1200 rpm and TS range 2-5 mm/sec on FSWed dissimilar materials between AA7075 and AA6061 and analyzed that the grain size of welded joints reduces on increasing TS. The micro hardness was less than that base materials. The minimum value of hardness was found in HAZ

towards AA6061 and all the joints were fractured in HAZ of AA6061 where the minimum hardness was situated.

Nilesh Kumar & R.S Mishsra [61] produced defect free, uniform, ultrafine and equiaxed grain structure by adjusting the FSP process parameters using severe-plastic deformation mechanism. The aluminum alloy Al-Mg-Sc was processed with three different tools rotational speed (325, 400, and 800 rpm). Depending on the process parameters, the grain size of the welded joint varied from 0.39 to 0.89 μm. When the Zener-Hollman parameter is increased, the reduction of grain size was observed. It was discovered that dynamic recrystallization during FSP might not be achievable under the existing deformation and microstructural conditions.

Lee et al. [62] performed experiments on AA6061 by FSW with two different rotational speeds and compared the specimen for microstructure and mechanical properties. Researchers used 1250 and 3600 rpm with two different TS i.e. 87 and 267 mm/min. The results revealed that all specimens were free of defects rather than joint fabricated by 3600 rpm and 267 mm/min parameters. The maximum UTS was achieved in the same joint i.e. 200 MPa UTS, 80 MPa YTS and 10% elongation in comparison of 250 MPa, 150 MPa and 15% UTS, YTS and EL, respectively of base material.

Elangovan and Balasubramanian [63] performed tests to investigate the ductile attributes and microstructural description of AA2219 compound joints as function of RS. The joints were manufactured at a RS of 1500 rpm, 1600 rpm and 1700 rpm keeping other parameters fixed. The outcomes demonstrated that the joint manufactured with 1600 rpm RS show predominant joint quality than the partners.

Hou et al. [64] studied the effects of tool RS on mechanical behavior of FSWed joints of AA6061. The investigation utilized variation of rotational speed and shoulder diameter as 400, 500, 600, 700 and 800 rpm and 12, 14, 16, 18 mm, respectively. The traverse speed was kept constant as 150 mm/min. The results of the study revealed that defect free joints were produced at 400 and 600 RPM rotational speeds. The joint were produced by 800 rpm rotational speed was found with maximum hardness in NZ.

Wang et al. [65] discussed the adjustment strategy for Underwater FSW (UFSW) parameters such as RS and TS for spray formed AA7055. The experiments were performed in three groups with the changing of RS and TS. The test specimens were tested for the, micro-hardness, tensile properties and microstructure. Findings revealed that in water environment the RS has a wider range of adjustment. Precipitates of $MgZn_2$ were maintained due to balanced heat input and dissipation at high RS.

Kundu and Singh [66] analyzed the effect of variation of rotational speed for FSWed joints of AA5083. For the welding process RS was varied from 355 to 2000 rpm along with TS, tilt angle and pin profiles. The results of the study uncover that the maximum strength was achieved in the specimen joined by 1000 rpm as presented in Fig. 2.2.

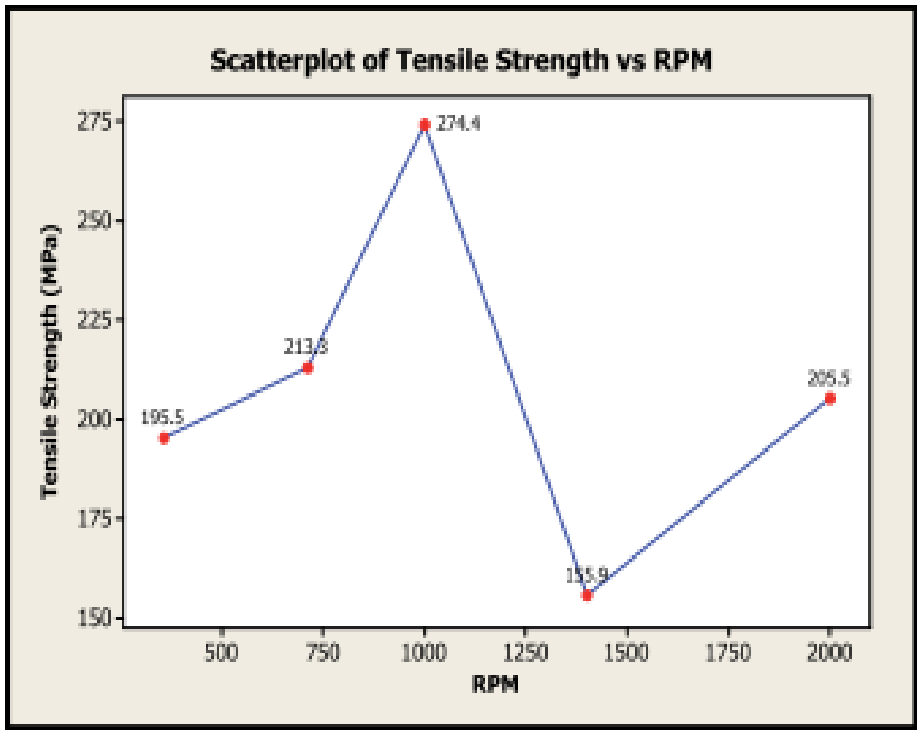

Figure 2.2: Scatter plot of tensile strength vs. tool rotational speed [66]

Zhou et al. [67] investigated the impact of RS of tool variation on mechanical characteristics of self-reacting FSWed joints of Al-Mg-Si alloy. 300, 400, 500, and 600 RPM tool rotational speed was utilized for the welding. The results of the study revealed that the lower rotational speed produced defective joints. Whereas higher rotational speeds were produced defect free joints of FSW. There was a little change in grain size found with the increase in RS.

Shashi Kumar et al. [68] depicted the effect of RS along with TS, downward force and tool tilt angle on FSWed joints of AISI 316L stainless steel. The experimentation were planned by the Box Benkhen approach of RSM. Statistical analysis such as ANOVA and F-test were performed to develop a regression model for UTS as a function of considered parameters. The results exposed that the maximum UTS was 604 MPa found in the joints fabricated with 597 rpm.

Zhang et al. [69] investigated the impact of RS on the weld quality of the FSWed AA2024 and AA7075 . The experiments were carried out with different RS i.e. 600,

950, 1300, and 1650 RPM. The fabricated joints were tested for mechanical and microstructural properties. The results revealed that increasing RS caused the thicker TMAZ at advancing side. Higher RS caused the coarsening of the grains in NZ which caused the fall in hardness of the joints in NZ. The maximum hardness was found of the joint which was fabricated with 600 rpm. The maximum UTS was found in the joints were fabricated with 1650 rpm, 950 rpm and 950 rpm for similar AA 7075, similar AA 2014 and dissimilar joints, respectively.

Deepak Kumar and Jatinder Singh [70] experimentally analyzed the mechanical properties of FSWed joints of AA6101-T6. For process parameters optimization three parameters i.e. RS, TS and TA were varied at three levels. Experiments were designed by Taguchi approach of DOE. The results showed that 1000 rpm RS caused the maximum micro-hardness and higher tensile strength i.e. 154 MPa with 25 mm/min TS and 1000 rpm RS.

The frictional heat generation by the contact of surfaces of the tool and work piece and the same is affected by the rotational speed, shoulder diameter axial force, etc. traverse speed of the process is the transverse distance traveled by the tool in per unit of time in the direction of abutting line. The heat input during process is decided by the traverse speed. After RS, traverse speed is the second essential process parameter. The effects of TS on properties of FSWed joints analyzed by researchers reported as follows:

R Prasanth and K Hans Raj [71] conducted experiments for dissimilar FSW of AA6351-T6 and AA6061-T6 to optimize the process parameters. All three considered parameters utilized at three different levels and experiments were designed by RSM. The fabricated joints were tested for tensile test. The results of the study depicted that the increment in considered input parameters caused an increase in UTS, YTS and EL. The higher values of responses are obtained at 60 mm/min TS with 900 rpm RS and 6 KN axial force.

K T Thilagham and S Muthukumaran [72] fabricated dissimilar FSWed joints of AA6082-T6 and AA2014-T87 to analyze the microstructural and tensile properties. The Taguchi approach was utilized for DOE of three factors i.e. RS, TS and TA at three different levels. The results of ANOVA revealed that 70 mm/min is the optimized value of TS with 800 rpm of RS and 2^{o} of TA. The optimized set of parameters can fabricate the FSWed joint with 72% strength of base material.

Salih et al. [73] developed the interactional relationship to recognize the microstructural development through FSW of Al-Mg-Si alloy. Two most important

process parameters i.e. RS and TS were varied for experimentation and the specimens were tested for EBSD and TEM for microstructural description. The results of the study depicted that the quality and microstructure of FSWed joints were significantly influenced by the ratio of TS and RS. The results also revealed that the increased TS caused high strength, fine grains and re- precipitation of strengthening precipitates.

Deepak Kumar and Jatinder Singh [70] experimentally analyzed the mechanical and properties of FSWed joints of AA6101-T6. For process parameters optimization three parameters i.e. RS, TS and TA were varied at three levels. Experiments were designed by Taguchi approach of DOE. The results showed that the 25 mm/min TS caused the maximum micro-hardness and higher tensile strength i.e. 154 MPa with 1000 rpm and 2^{o} TA.

2.3.2 TILT ANGLE (TA)

Tilt of the tool is the angle at which tool is inclined to the surface of work material, where 0^{o} denotes the perpendicular position of tool in respect of base material as presented in Fig. 2.3. Tool tilt angle affects axial force exerted on material, material flow behind the tool pin during transverse movement of tool.

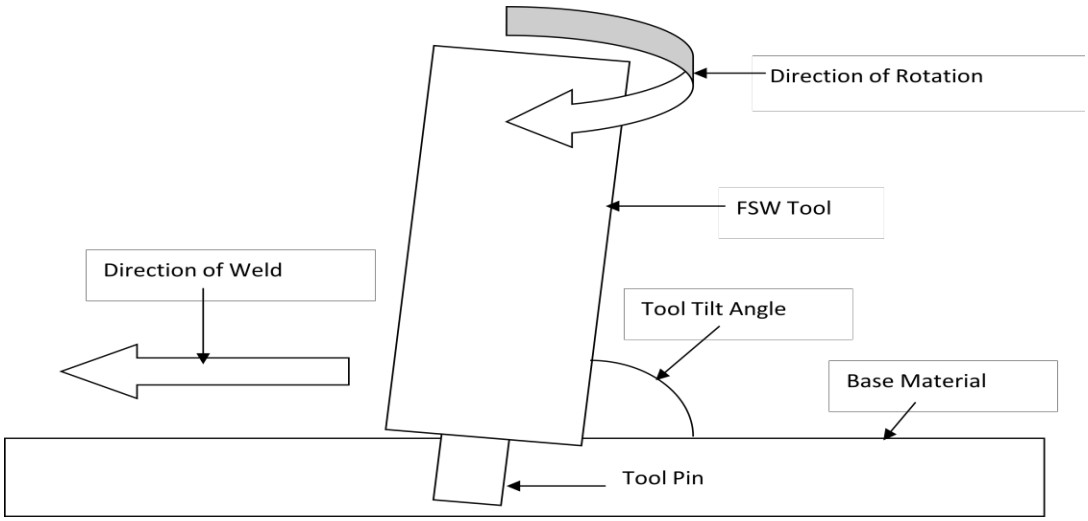

Figure 2.3: Presentation of tool tilt angle

Chen et al. **[74]** examined the influence of tilt angle of tool on defect formation of FSWed joints of AA5456. For experimentation the tilt angle of the tool was changed from 1.5 to 4.5^{o}. The results revealed that tilt angle below 2^{o} produced defective welding joints. Tensile strength of the welded specimens was observed to increased when tilt angle was changed to 1.5^{o} to 3.5^{o}, then start to decreased on further increment in tilt angle.

Barlas and Ozsarac [75] determined the impact of FSW parameters on macrostructure, microstructural and mechanical characteristics of FSWed joints of $AlMg_3$ AA5754. The results of the testing were showed that the tilt angle considerably affected the results of microstructure and mechanical characteristics. The finer grains and maximum tensile strength of joints were found when tilt angle was 2^o.

Kadaganchi et al. [76] created a mathematical model for the variation of responses to predict the influences of variation of RS, TS, tilt angle and pin profile for FSW of AA 2014-T6. The adequacy of the developed model was checked by confirmatory test. The experimentation was designed using CCD approach via RSM, which suggested 30 numbers of experiments in total. The results of the study indicated that the maximum UTS and YTS were observed for the joints which were produced with 3.5^o tilt angle. But EL was maximum when tilt angle was 3^o.

Kundu and Singh [70] conducted the experiments to fabricate dissimilar FSWed joints of AA5083 and AA5086 to examine the impact of variation of process parameters on considered responses. RS, TS, TA and PP were varied to predict the effect on tensile strength and EL of FSWed joints. Considered input parameters were varied for five levels. The results revealed that the TA has a significant effect on considered responses and also decide the surface characteristic of the joint as presented in Fig. 2.4.

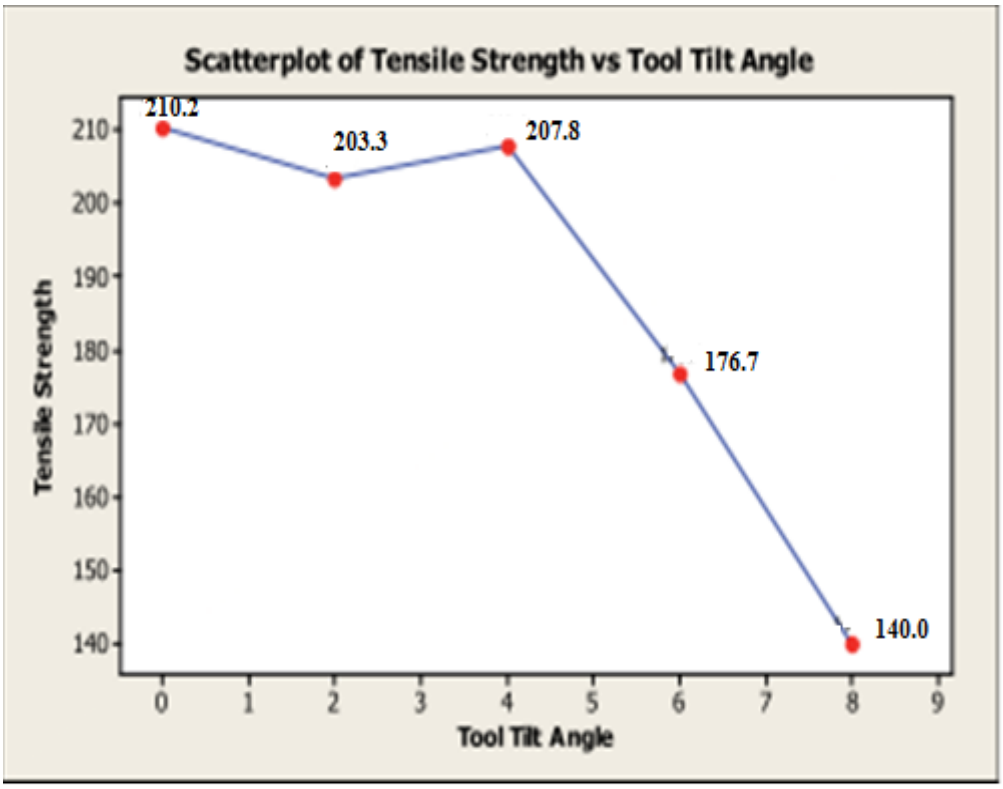

Figure 2.4: Scatter plot of tensile strength vs. tool tilt angle [76]

Long et al. [77] established a thermo mechanical model coupled with finite element model to recognize the impact of tilt angle on temperature, flow path and stress during FSW process. It was showed by the simulated results that the warm holes type of defects appeared with zero degree tilt angle while these defects were not observed at tilt angle of 2º. This 2º angle also caused peak temperature and compressive force on the material.

Banik et al. [78] analyzed weld attributes of FSWed joints of AA6061-T6 for mechanical properties by variation of tool tilt angle. To assess the effects of tilt angle for taper and taper threaded tool pin, torque and other forces acting at the tool work-piece interface are speculatively approximated. Results showed that when tilt angle enhanced, torque and forces linked to FSW also increased. When compared to taper pins, taper threaded pins have higher torque and Z forces, but the X forces are lower. Welding forces found to be fluctuated with increased tilt angle for taper tool pin but this was opposite for the taper threaded pin.

Verma et al. [79] studied the impact of tool tilt angle, RS and TS on mechanical characteristics of FSWed armor-marine grade AA7039. The CCD technique of RSM was used to design the tests. The results of the study revealed that optimized valued of above said parameters 1325 rpm, 35 mm/min and 1.65 degree for RS, TS and tilt angle, respectively.

Goyal and Garg [80] fabricated FSWed butt joints of 5 mm thick rolled plate of AA5086-H32. Experiments were performed by varying six process parameters at five levels. A mathematical model was designed using RSM to establish a relationship between the parameters and the considered responses. The specimens were tested for the tensile properties. The results revealed that the maximum UTS and YTS were found at 1.5º of tilt angle.

Kumar et al. [49] investigated the effect of RS along with TS, downward force and tool tilt angle on FSWed joints of AISI 316L stainless steel. The experimentation was designed using Box Benkhen approach. Statistical analysis such as ANOVA and F-test were performed to develop a regression model for UTS as a function of considered parameters. The results exposed that the maximum UTS was 604 MPa found in the joints fabricated with 1.5º tilt angle.

Deepak Kumar and Jatinder Singh [70] experimentally analyzed the mechanical and properties of AA6101-T6 weld joints. For process parameters optimization three parameters i.e. RS, TS and TA were varied at three levels. Experiments were designed

by Taguchi approach of DOE. The results showed that the 2o TA caused the maximum micro-hardness and higher tensile strength i.e. 154 Mpa with 1000 rpm and 25 mm/min TS.

2.3.3 TOOL PIN PROFILE

Initially a simple cylindrical tool pin was used to fabricate the FSWed joints of various aluminum alloys. But researchers have developed and analyzed the effects of the same parameter on the integrity of the joints. Works of some researchers are reported here as follows:

Boz and Kurt [81] analyzed the impact of tool pin profile on bonding of FSWed material of AA1080. For this purpose five pin profiles were utilized i.e. one square and four cylindrical with differ screw pitches such as 0.85, 1.10, 1.40 and 2.1 mm. The results showed that pin profile and screw pitch pin affected the bonding of the joints significantly.

Elangovan and Balasubramanian [63] used five deferent pin profiles and three rotational speeds to evaluate their effects on metallurgical and mechanical characteristics of FSWed joints of AA2219. The study utilized straight cylindrical, threaded cylindrical, triangular, taper cylindrical and square pin profile for comparison as presented in Fig. 2.5. The welded joints were tested for FSP zone and mechanical properties for joint also correlated with this zone. The results revealed that the FSWed joints produced with square pin attained highest tensile strength and found free of defects.

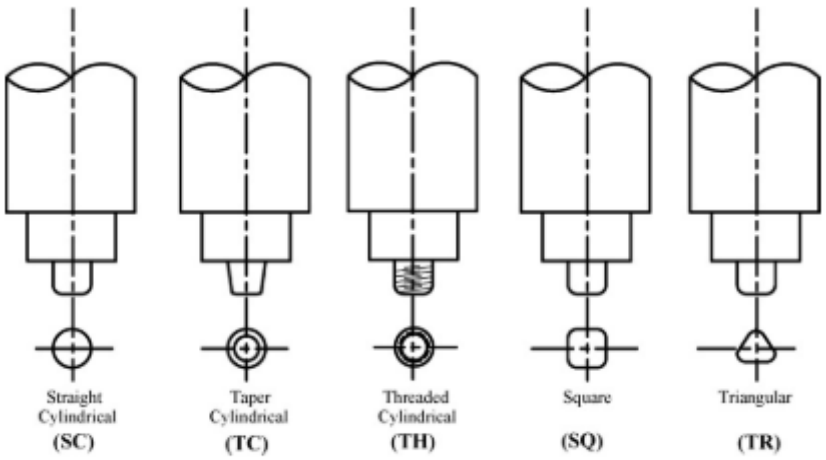

Figure 2.5: FSW tool pin profiles [63]

Elangovan and Balasubramanian [82] fabricated FSWed joint of AA6061 with different RS, TS, axial force and pin profiles. The study utilized straight cylindrical,

taper cylindrical, threaded cylindrical, triangular and square profiles of tool pin. The results of the study uncovered that the square pin profile fabricated the joints of higher tensile strength and joint efficiency.

Mohnty et al. [83] revealed the effects of pin profiles on mechanical behavior of FSWed joints of Al-Cu-Si alloy. The study utilized trapezoidal, tapered cylindrical and cylindrical tool pin profiles for experimentation. The findings demonstrated that the pin geometry has significant effect on considered responses and the straight cylindrical was found more effective than others two profiles.

Palanivel et al. [84] generated a regression model to anticipate the impact of tool pin profile, RS and TS on the mechanical characteristics of FSWed joints of AA6351 and AA5083. Study utilized different pin profiles including tapered octagonal, straight hexagonal, tapered square, straight octagonal and square. The welded specimens were tested for UTS. The trials were created using the RSM's central composite rotatable design, and a total of 31 trails were performed as recommended. The results of study showed that the maximum UTS were found in joints which were fabricated by straight square pin.

Yuqing et al. **[85]** employed five tool pin profiles to fabricate the FSWed joints of 20 mm thick plates of AA7075-T6. Threaded taper, triangular, square, three grooves and conical profiles of pin were utilized to predict their effects on tensile strength and ductility. The results of the study revealed that the joints fabricated by triangular, square and three grooves were found free of defects. The joint fabricated by three grooves pin profile were exhibited the maximum tensile strength and ductility among all used profiles..

Krishna et al. [86] finds the impact of different pin profiles on tensile and hardness behavior of AA6061 and AA7075 FSWed joints. The different pin profiles employed for experimentation were: straight cylindrical, straight square and tapered hexagonal. Specimens were tested for the YTS and micro-hardness. The results of the study uncovered that the YTS was found better in joints fabricated by straight cylindrical and the micro-hardness was maximum in joints fabricated by straight square pin profile.

LIU et al. [87] developed the weld joints of AA 5A05 plates of thickness 10 mm. The study's findings demonstrated that pin with and without flat surfaces had an impact on material flow. The tensile characteristics of the welded specimens were also examined, and it was discovered that the joint efficiency achieved by the plane profile, which was used to build it, was 95%.

Raturi et al. [88] fabricated AA7075/ AA6061 FSWed joints, in order to assess the impact of RS, TS, tool pin profiles and axial force on the mechanical characteristics. Various pin profiles were employed, including cylindrical, cylindrical grooved with flutes, trapezoidal, cylindrical grooved, and cylindrical tapered. The findings showed that joints made with pins with three faces had greater tensile characteristics.

Olivier Lorrain et al. [89] An investigation has been done on FSW of Al alloy with two different tool pin profiles. The first pin was unthreaded with a flat surface, whereas the second pin was unthreaded without a flat surface. In order to investigate the materials, the longitudinal-section and cross-section of the weldment with or without the use of material marking were observed. The material flow via the classic thread tool has the same characteristics as the flow of material via the classical thread tool. The macro weld cross-section shows that when product of the thrust force and the RS is increased, the area affected by the rotation of the shoulder in the thickness direction is thicker than the tapered pin with three flats.

Dawood H.I et al. [90] examined the impact of profile of tool pin on the weld quality of the FSWed joint of Al-6061. It was found that the triangular pin revealed the sound mechanical characteristics in comparison to other pin profile, whereas the minimum hardness and strength were observed with the square pin profile. The fractured surface shows that the square and threaded tapered cylindrical specimens break with brittle fractured due to excess heat generation during FSW, while ductile fractured was observed in the triangular pin profile.

2.3.4 SHOULDER DIAMETER (SD)

Shoulder diameter decides the contact area of tool surface with the surface of the work material. This area affects the rate of heat generation, which is the most important factor to affect the integrity of the FSWed joints. Many researchers have done work for SD; some of those are reported here as follows:

Elongovan and Balasubramanian [63] investigated the effects of shoulder diameter along with RS, TS, axial force and pin profile on formation of processed zone and mechanical behavior of AA6061 weld joint. The results of study revealed that the joints produced by 18 mm and 21 mm shoulder diameters were found defects free but 15 mm shoulder diameter produced joints with tunnel defects. The study also found that the maximum mechanical strength was achieved by joint which was developed using 18 mm diameter of shoulder.

Commin et al. [91] investigated the relationship between variation of process parameters, heat generation and plastic deformations. AZ31 Mg was utilized as raw material for the study. The trails were carried out with the variation of RS, TS and shoulder diameters. The results revealed that the increase in RS and shoulder diameter and decrease in TS caused in increase in heat which results in grain growth.

Arora et al. [92] investigated the mechanical behavior of AA6061 FSWed joints. The study's objective was to maximize shoulder diameter for traction-required torque. According to the study, as shoulder diameter grew, so did the needed torque and heat production. Maximum UTS and YTS values were reported for specimens with a shoulder diameter of 18 mm.

Hou et al. [64] examined the effects on tensile characteristics of weld joints of AA6061 of shoulder diameter and RS, by using self-reacting tool shoulder. The experiments were performed by using different shoulder diameters on upper and lower sides. The results uncovered that the smaller diameter of tool shoulder caused the tunnel defect. Increase in shoulder diameter and RS results in the increase in heat generation. The maximum tensile strength was noticed in the joints produced using 16 mm and 18 mm lower and upper diameters, respectively.

Saravanan et al. **[93]** studied the impact of variation of shoulder to pin diameter ratio on the microstructural, microstructural and tensile properties of FSWed joints of AA2014/AA7075 . The above said ratio was used varied at 2, 2.5, 3, 3.5 and 4 for experimentation. The results showed that the 2 and 2.5 ratios of diameters produced joints with pin holes and banded structure due to improper mixing of material. The maximum 356 MPa tensile strength was found in specimens fabricated with 3 ratios of diameters.

A. Gill [94] investigated the effects of process parameters on impact toughness of FSWed joints of aluminum alloy. The RS, TS and shoulder diameter were varied at two levels. The experiments were carried out as per L8 orthogonal array of Taguchi's approach of DOE. The significance of parameters and adequacy of the model were tested by F and t tests. The study's findings showed that as shoulder diameter increased, the impact strength decreased. The maximum impact toughness was achieved by specimen fabricated by 18 mm shoulder diameter.

Joshi and Badheka [95] investigated the dissimilar FSWed joints of copper and stainless steel to optimize the shoulder diameter. The experiments were performed by various shoulder diameters including 16, 18, 20 and 22 mm. the fabricated joints

were tasted for tensile strength and microstructure. The results of research revealed that only 18 mm diameter was able to fabricate defect free joints rather than others. The maximum 76% joint efficiency and maximum UTS were attained specimens joined by same shoulder diameter.

2.3.5 SHOULDER PROFILE

Surface of the shoulder which comes in the contact with the surface of working material caused frictional heat generation for the joining of the material. Initially a flat featureless shoulder was used to join the aluminum alloys. But then it came in the focus of researchers that the generation of heat and flow of material also can be controlled by the end surface features of shoulder. The shoulder profile of the feature at the end of the same also affects the flow of material. Some studies are report here for the shoulder profiles.

M De Giorgi et al. [96] explored the effect of shoulder end features on the tensile strength and fatigue life of FSWed joints of 1.5 mm thick sheets of AA6082-T6. Three shoulder geometries i.e. scroll; shallow cavity and flat surface were utilized for experimentation. The results exposed that the grains size in NZ was finer in joint fabricated by shoulder with cavity than others.

Luis Trueba et al. [97] fabricated FSWed joints of AA6061 with six different shoulder profiles i.e. recessed A, recessed B, raised C, Raised D, recessed E and ramp F as presented in Fig. 2.6.

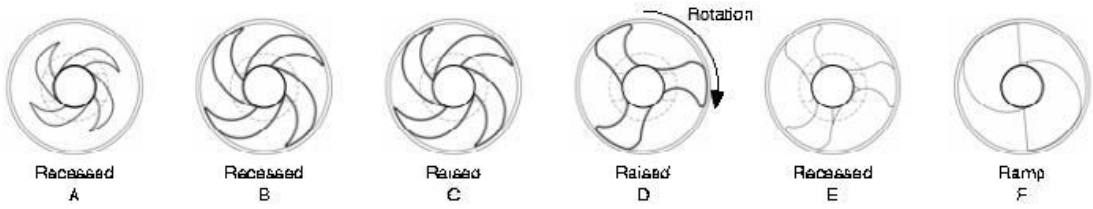

Figure 2.6: Shoulder profiles used for FSW [97]

The results of the study revealed that raised spiral (tool C) can fabricate the joints of better quality than other profiles.

Giuseppe Casalono et al. **[98]** investigated the surface roughness and grain size of FSWed joints of AA5754 with different shoulder geometries. For testing, four distinct shoulder end geometries were used. The results of the study depicted that geometry of

shoulder significantly affects the considered responses and finer weld surface was found in case of conical surface shoulder.

Periyasamy et al. [99] explored the impact of shoulder concavity angle and pin profiles on the mechanical behavior of dissimilar FSWed joints of AA7075 and AA6061. Three concavity angles i.e. 1.5º, 3º and 4.5º were used to fabricate the joints. The results of the work found that 3o angle of concavity with square pin profile can fabricate the joints with higher strength.

Many researchers have used a cavity at the end shoulder surface, that serves as a reservoir for the material displaced by tool pin during plunge in to the depth. This material is utilizing when the tool travels forward. The area at the end of the shoulder surface other than this cavity is remain flat and comes in contact with material surface for friction. The shoulder flatness is scarcely used by researchers as parameter for variation.

2.3.6 TOOL PIN DIAMETER

The size of the tool pin determines how much material will be stirred in order to create a joint while welding soft materials. This volume also affects the heat generated due to plastic deformations of material. The previous research work carried out for this parameter is reported as follows:

Y Javadi et al. [100] explored the influence of processing parameters on residual stresses in FSWed joints of AA5086. Taguchi approach was utilized for DOE and pin diameter, feed rate, rotational speed and shoulder diameter varied. The findings showed that that pin diameter and shoulder diameter have no dominating effects toward the change in residual stresses FSWed joints.

B Ravi Sankar and P Umamaheswarrao [101] attempted to optimize the input parameters for hardness and tensile strength of FSWed joints of AA6061. Rotational speed of tool, pin diameter and traverse speed were varied. The findings showed that 5 mm pin diameter can fabricate the joint of higher tensile strength.

Mostafa Akbari et al. [102] investigated the effects of variation of pin length, shoulder and pin diameter and on tensile properties of FSWed joint. Three pin diameters i.e. 4.5, 6 and 7.5 mm were utilized for experimentation. The results revealed that axial force increased with increment in pin diameter. The tensile strength was found higher when D/d ratio was 3 i.e. 6 mm pin diameter.

H.W. Zhang et al. [103] analyzed the material flow under various FSW processing parameters using FEM. The modification of the axial load can impact the equivalent plastic strain dispersion in NZ, however HAZ and TMAZ were not affected. The corresponding plastic strain in the NZ can be raised as the axial load increases. The plastic-strain distribution was not symmetric but the plastic strain on advancing side is maximum.

2.3.7 NUMBER OF PASSES

Indrajeet Charitet al. [104] created the multi-sheet structure by FSW and studied using diffusion bonding. Superplastic 7475 Al-alloy was employed in this experiment. For a 2.5 mm thick lap junction, they employed a single pass and six passes joint welding process. Six passes produced a finer grain size than a single pass. The base material's grain size was 10 μm whereas, the grain size of after one and six-pass welded joints was 3.2 and 2.2 μm, respectively. The microstructure of the six-pass welded joint remained stable, and the superplastic characteristics were maintained. The tensile strength of base material, welded joints after single-pass and six-passes was observed as 511, 402 and 451 MPa, respectively.

Z.Y Ma et al. [105] investigated multi-pass FSP on silicon- aluminum base A356, and found that as the distance from the fifth pass of FSP, improves the strength of the TMAZ and NZ diminishes. The strength and ductility after the fifth-pass are essentially identical to those of after the single-pass. Furthermore, in the current 5-pass FSP A356, the yield and tensile strength of various micro-structure regions produced by mining tensile specimens is higher than that of big specimens. The particles distribution, aspect ratio, and grain size of the welded plate were not affected by multi-pass FSP. During the multiple-pass procedure, the silicon particles were evenly dispersed.

Su et al. [106] studied the microstructure commercial AA7075 after friction stir processing. The FSW area's microstructure did not have a homogeneous dispersion of grain size. The mean grain size falls somewhat from top to bottom. Diffraction rings were also found, which confirms the massive misorientations between the individual grains, according to them. Even with equal grain sizes, the dislocation density was not homogeneous inside the stir zone; this result showed that unusual plastic deformation was imparted in the grains. Any chosen plate size may be treated to an ultra-fined-grain microstructure by executing many overlapping passes. The research have shown that

several simultaneous passes are an effective way to create big bulk ultrafine grain material with evenly dispersed microstructure.

Z.Y. Ma [107] explored the impact of double passes on the mechanical behavior of FSPed AA 7075. Almost similar grain sizes range from 5.3 to 5.8 μm were found in both single and double FSP pass. The higher temperature was observed in a double pass on comparison with single pass. Double FSP pass found an enhancement in superplastic elongation as compared to single-pass Al-7075. The double FSP pass on Al-7075 had the highest superplastic elongation of 1220 percent at 480°C. The main superplastic distortion approach for both double and single-pass FSP is grain boundary sliding, according to superplastic analysis.

2.3.8 FSW OF DISSIMILAR MATERIALS

FSW has many advantages over other conventional welding techniques. One of those is that FSW is able to join dissimilar materials with high efficiency without any difficulty.

Navneet Khanna et al. [108] emphasizes on the FSW of dissimilar weld joint of AA6061 and AA8011. The effect of base plate location and tool offset on different characteristics is investigated while maintaining other welding settings (RS-1070 rpm, TS- 50 mm/min, and tilt angle- 2°). When the 1 mm tool offset towards the advancing side (softer alloy), the tensile testing results reveal higher strength and elongation of 77.88 MPa and 21.96 percent elongation, respectively. The various parameters have no effect on the hardness readings. To determine the quality of the weld surface, a visual inspection is performed. In order to have a broader insight of subsurface defects and material mixing, a radiography test is also performed. Time–temperature graphs are shown to evaluate the heat distribution throughout the welded zone, and the asymmetric shape of the graph reveals higher temperature on the advancing side. Microstructure examination reveals consistently dispersed grains, implying improved tensile characteristics, as well as a material flow pattern. The characterization data led to the conclusion that the softer material should be placed on the advancing side for better weld quality.

A. Barcellona et al. [109] studied the metallurgical characteristics of different aluminum alloys AA7075 and AA2024 and discovered that the proportion of insoluble particles reduces owing to tool pin action. Both the base metal (AA7075 and AA2024) and the welded area were studied for grain size and dimensions. Due to precipitate

density drops, the weldment's lowest hardness value was discovered at the thermo-mechanically impacted zone.

M. Ilangovan et al. [110] employed FSW was utilized to join AA6061 and AA5086 the welding of similar or dissimilar aluminum alloys to remove the problem, faced during fusion welding,. The microstructure of different zone was observed by optical and SEM machine, the fine grain structure was noticed in the NZ. The joint efficiency was improved by 56%, this was occurring owing to the development of grain size strengthening. The stir zone had a hardness of 115 HV, which was more than the base metal and other adjoining zones.

Harish Suthar et al. [111] examined the failure behaviour of AA6061 and AA7075 FSWed joints and found that the dissimilar FSW of AA7075/AA6061 softened at HAZ in the advancing side, which had a softer material (AA6061-T6) and a lower hardness value recorded in the area. The fracto-graphy revealed a decreased density of tiny dimples, indicating a lower strain during rupture with facet caused by insufficient material fusing at the Stir zone (SZ) and TMAZ interface.

Avinash et al. [112] studied the feasibility of dissimilar welding of AA7075-T6 and AA2024-T3. Above mentioned both materials were non weldable by fusion welding. These materials were welded successfully and the welded joints were tested for the microstructure and tensile characteristics. The findings found that considered process parameters i.e. RS, TS, and pin profile have significant effect on responses.

P Jayaseelan et al. [113] developed the dissimilar FSWed joints of AA6061-T6 and AISI304 by different tool pin diameters in water medium. The pin diameter was varied as 4, 5 and 6 mm. The axial force during process and tensile strength were analyzed. The findings revealed that the axial force increased with the increment in pin diameter and tensile strength was also affected by this parameter.

Zhang et al. [114] fabricated the joint of AA7075 T651 and AA2024 T351 by FSW process to determine the effect of RS on the quality of the joints. 600, 950, 1300, 1650 rpm RS were used to perform the experiments in similar and dissimilar FSW. The samples underwent tests for hardness, tensile strength, and grain size.

Raturi et al. [88] examined the impact of pin profile, RS and TS on the integrity of FSWed joints of AA6061/AA7075 T651. The fabricated samples were tested for flexural load and tensile strength. The findings showed that maximum flexural load and tensile strength were attained for the joint fabricated with 900 RPM and 132 mm/min RS and TS, respectively.

P Jayaseelan et al. [113] developed the dissimilar weld joints of AA6061-T6 and AISI304 by different tool pin diameters in water medium. The pin diameter was varied as 4, 5 and 6 mm. The findings of the study demonstrated that the axial force increased with the increment in pin diameter and tensile strength was also affected by this parameter.

2.3.9 REINFORCING PARTICLES

Sameer Mohammed and Anil Kumar Birru [115] investigated friction stir welded AA6082-T6 plates with a thickness of 2 mm, employing Al_2O_3 nanoparticles as reinforcement materials between adjacent plates. The joining was accomplished using a tungsten carbide hexagonal pin profile tool at RS of 710 and 900 rpm. The welds were passed two and three times each, with a constant TS of 40 mm/min. An optical microscope and SEM were employed to examine the microstructure. The microstructural data reveal that the welded at 710 rpm RS, 40 mm/min TS, and 3 passes has an excellent distribution of Al_2O_3 particles. The average grain size of the reinforced welded sample in three passes was 16.02, and it also had the greatest tensile strength and strain of 227.61 MPa, and 10.5 %, respectively. The weld nugget zone of the reinforced welded sample had the maximum hardness value of 74 HV.

Naresh Parumandla and Kumar Adepu [116] produced Al/SiC and Al/Al_2O_3 surface nanocomposites. As reinforcement, and SiC and Al_2O_3 nanoparticles were employed, while the matrix material was 6061-T6 aluminum alloy. Experiments were carried out at 1150 rpm and 15 mm/min with different volume percentages of nano reinforcements (2, 4, and 6). The method compared the impacts of nano reinforcement on surface nanocomposites' mechanical, microhardness, microstructural, and wear characteristics. Microstructure analysis indicated that SiC and Al_2O_3 nano particles were mostly arranged in clusters in the processed region. Additionally, the defect generation rate increases as the volume % of nano reinforcement increases. The mechanical characteristics of the surface nanocomposites were investigated using Vickers microhardness and tensile tests. Along the stir zone, superior microhardness qualities were attained. Microhardness increases with adding of ceramic particles in the material matrix; however yielding strength drops while wear resistance increases. Al/SiC composites had a lower average coefficient of friction than Al/Al_2O_3 composites. With enhancing the volume percentage of nano particles, the effect of reinforcing particles on wear resistance was enhanced.

Saeed Ahmadifard et al. [117] investigated the impact of Ti_3AlC_2 MAX phase into AA7075 by FSP in addition of nano-sized Al_2O_3 particles. After three FSP passes with 1000 rpm and 28 mm/min, these composites were effectively manufactured. The produced surface hybrid nanocomposites were characterized tensile, microhardness, and wear testing along with using optical microcopy and SEM. Due to enhanced grain refinement and excellent dispersion of nanoparticles, the Al-100 percent Al_2O_3 composite acquired the highest hardness and tensile strength. The Ti_3AlC_2 MAX phase improved tribological characterization due to its laminar structure, whilst Al_2O_3 nanoparticles improved mechanical characteristics. For AA7075, the wear mechanism is adhesive; for nanocomposite specimens, it is adhesive-abrasive, according to scanning electron microscope examinations.

A. Abdollahzadeh1 et al. [118] placed silicon carbide (SiC) nano-powders into the adjacent side of AZ31 magnesium plates. FSP using a pin-less tool was used to ensure a proper dispersion of these nanoparticles. Second, utilizing a frustum pin tool, the best conditions for FSW of AA6061 and AZ31 alloy to were obtained by combining TSs and RSs . When compared to the FSPed joint without nanoparticles, the FSPed joint manufactured at 35 mm/min and 650 rpm showed a 28 % higher tensile strength and increased in elongation of threefold. SiC nanoparticles improved the microstructure of the stir zone and helped refine the grains. The reinforced samples exhibit higher hardness in comparison to that of the nonreinforced samples owing to reduced grain size and the SiC articles with a high hardness. The non-reinforced sample fractured totally brittle, but the reinforced samples fractured in a ductile manner.

Mohsen Bahrami et al. [119] studied the impact of SiC nano-particles on the mechanical behavior of FSWed AA7075. FSW at 1250rpm and 40mm/min was used to achieve this. Experiments were conducted with and without the nano-sized SiC particles. Optical microscopy and SEM were employed to examine the cross-sectional microstructures of the joints (SEM). Furthermore, the volume proportion of the reinforcing particles was revealed to be 20%. SEM images revealed a good dispersion of SiC reinforcements, along with excellent bonding. The results of atomic force microscopy (AFM) were likewise quite similar to those of a recent SEM microstructure. Tensile strength, % elongation, fatigue life, and joint toughness all increased dramatically as a result of the presence of SiC nanoparticles. The morphologies of the fractures were in good accord with the ductility values.

Yahya Bozkurt et al. [120] demonstrated the viability of friction stir welding to weld identical AA2124 plates with SiC/25p. The weld zone features and performance were evaluated using microstructure parameters, microhardness, and tensile testing. XRD was employed to analyze the phase structure of a comparable composite weld. The weld zone temperature was measured by employing thermo-couples to show that the composite joint may be shown without melting. The finding showed that FSW may be utilized to weld AA2124/SiC that are comparable. The SiO_2 phase was observed according to XRD measurements. Peak temperatures that were measured 15 mm out from the weld region varied from 201 to 270 ºC. It was also observed that the tensile strength of the composite joints made by the AA2124/SiC was around 20% less than that of the basic composite. The novelty of this research stems from one of FSW's preliminary experiments on the mechanical features of the composite joint.

F. Cioffi et al. [121] studied the mechanical characteristics of composite joint (AA2124/ SiCp -25%vol) developed by FSW at different RSs with a higher volume fraction of SiCp, The initial particle-free zones vanish during the stirring, resulting in a uniform distribution of particles. Sometimes large particles are shattered. At low RS, tunnel flaws appear, while at high RS, they disappear. The TMAZ, expands in size as RS increases**.** In compression testing, the welds acquire a ductility of 10–15 percent, however in tension tests, the welds exhibit a brittle behavior. Between compression and tensile tests, a strength differential, SD, effect is achieved. This explains why the FSW method has such a minor negative impact on the matrix–reinforcement interaction. The existence of a microscopic residual stress is thought to be the cause of the SD effect.

D. A. Dragatogiannis et al. **[122]** developed dissimilar FSW of thick plates of aluminum alloys incorporated with nano-sized TiC particles. In compared to an unreinforced weld, defect-free welds have better material mixing between the materials, as well as better particles dispersion and grain refinement. The generated metal matrix composites' local mechanical behaviour was investigated and compared to that of their bulk equivalents and source materials. Microstructure and the fillers are linked with observed mechanical parameters at the micro- and nanoscale (particularly hardness and elastic modulus). The inclusion of TiC nanoparticles increases the ultimate tensile strength, hardness, yield values, elastic modulus and %elongation.

S. Gopalakrishnan and N. Murugan [123] fabricated titanium carbide (TiC) based aluminum matrix composite (Al/TiCp) by indigenously designed stir-casting method. Weld joints are made using the FSW. For the analysis, welding factors such as TS, RS,

% TiC, axial force, and tool pin profile were taken into account. The tensile strength of FSWed joints is predicted by employing a mathematical modeling. A different set of characteristics investigated in FSWed specimens without any post-weld heating revealed a good joint efficiency in comparison to the tensile strength of AA6061. The welding speed and pin shape shows a greater impact on the tensile strength, according to the model's analysis.

K. Kalaiselvan et al. **[124]** developed the AMC of AA6061/B_4C via stir-casting route with using K_2TiF_6 as flux. FSW was used to successfully butt weld them (FSW). A RS of 1000 rpm, and a TS of 80 mm/min, were used in the FSW. A square pin profile tool was employed for FSW. Optical microscopy and SEM were employed to examine the microstructure of the welded junction. Four zones were visible in the welded junction, which are typical of FSW aluminum alloys. Fine granules and homogeneously distributed B_4C particles were visible in the weld zone. Under the experimental conditions, a joint efficiency of 93.4 percent was achieved. FSW, on the other hand, lowered the composite's ductility.

Atul Kumara et al. [125] studied the processes of simultaneous enhancement of tensile characteristics, corrosion resistance and wear behavior, of stir cast Al7075 with micro and nano SiC/2%wt composites using FSP. After the FSP, the nanoparticles reinforced composite outperformed the microparticles reinforced composite in terms of mechanical characteristics. With the simultaneous improvement in ductility, wear resistance (10 times) and tensile strength (>3 times) were shown to rise considerably. Reduced grain size, uniformly distributed SiC nano-sized particles inside the matrix, increased the matrix-particle interface properties, and removal the flaws of casting like porosity following the FSP are all credited with the improvement. Following the FSP, the as-cast composites' corrosion potentials altered in a noble direction. Following the FSP, corrosion resistance is said to have improved due to the reduction in surface irregularity and uniformly distributed particles. Because of the increased matrix/particle interface properties and dispersion strengthening, the nano-composite was shown to be superior to all of these positive impacts.

Seung-Joon Lee et al. [126] developed composites with the aid of multi-walled-carbon nanotubes (MWCNT) in aluminum metal matrix by employing FSW and studied the mechanical properties and microstructural behaviour by controlling volume of MWCNT by 1 and 3%, and the plunging load of 400 and 600 kg. After the FSW, MWCNT exhibited some grain coarsening, uneven shear texturing, and accumulating

dislocations; however, the differences produced by varying MWCNT and plunging load were insignificant. The FSWed composite produced with 600 kg plunging load and 3% MWCNT shows a two-fold better balance between ductility and strength than those of the base metal.

Ashok kumar and M.R. Thansekhar et al. [127] employed cumulative impact of FSW and FSP on dissimilar AA1350 and AA6101-T6. Alumina particles are utilized to strengthen the interface region. For different diameters of grooves, FSW and FSP are done at the same time. Mechanical and wear tests are used to evaluate the welding quality and surface changes. The smallest groove, with a depth of 1 mm and width of 0.5mm and has the highest bending and tensile strengths, while the largest groove of width and depth 2mm and 3mm, respectively shows the highest wear resistance as and hardness. The Taguchi approach reveals that width of groove is the most important factor.

2.4 RESEARCH GAP

After going through the literature, the following gaps have been identified:

- A few experimental studies have been reported on the influence of process parameters of friction stir welding on weld quality of dissimilar aluminum alloy AA6061 and AA5083 with reinforcement particles.
- A limited studies are available on the incorporation of reinforcing particles in case of joining dissimilar materials by FSW.
- A little Research work has been done the comparison of the different types and sizes of the reinforcement particles on the weld region.
- A few researchers have investigated the effects of hybrid metal matrix composite using friction stir welding.
- Very few researchers have been carried out on the optimization of processing parameters of FSW

2.5 RESEARCH OBJECTIVES

From the literature survey the research gaps were identified. Accordingly, the following objectives are formulated:

- To fabricate reinforced joints of dissimilar aluminum alloys (AA5083/AA6061) using micro-sized Al_2O_3 and SiC particles.

- To study the influence of various process parameters (i.e. rotational speed, traverse speed and number of FSW passes) on weld quality dissimilar reinforced FSWed joints.
- To obtain the Multi-response optimization of parameters for Friction stir welded dissimilar aluminum alloy joints using Response Surface Methodology (RSM).
- To characterize the reinforced joints by microstructural analysis such as Field emission Scanning Electron Microscope (FESEM) and Optical Microscope (OM).
- To study of mechanical characteristics of reinforced joints such as tensile strength, %elongation and micro-hardness.

CHAPTER-3

RESPONSE SURFACE METHODOLOGY

3.1 INTRODUCTION

The Response Surface Methodology (RSM) technique, which is an important subject in statistical experiment design, is a set of statistical and mathematical approach that can be employed for the analysis and modeling of the problems in which a desired response is impacted by multiple variables and the goal is to optimize the response. [128].

3.2 RESPONSE SURFACE METHODOLOGY

The RSM approach is a set of mathematical and statistical strategies for the analysis and modelling of the problems in which a respondent is impacted by multiple variables and the purpose is optimizing that response [129]. It is a significant topic in statistical experiment design. Independent components can be represented quantitatively in various experimental circumstances (equation 3.1).

$$y = f(x_1, x_2) + e \qquad (3.1)$$

This describes the relationship between $x_1, x_2 \ldots, x_k$ of k quantitative factors and response y. The response function or response surface is denoted by function f. The experimental errors are measured by the residual 'e'. A characteristic surface is generated for a given collection of independent variables. A polynomial can be used to accurately predict f's mathematical form when it is unknown within the experimental domain. The relationship increases with increasing polynomial degree, while experimental costs increase.

Multiple regression equations were developed using RSM to represent the quality attributes of FSWed joints produced by the FSW in this study. The dependent parameter is regarded as a surface on which a mathematical model is fitted when using the response surface approach. The second order response surface has been considered for the formulation of regression equations:

$$y = \beta_0 + \sum_{j=1}^{q} \beta_j x_j + \sum_{i=1}^{q} \beta_{jj} x_j^2 \sum\sum_{i<j} \beta_{ij} x_i x_j + \varepsilon \qquad (3.2)$$

Where $x_i = (x_1, x_{2i}, \ldots\ldots, x_{iq})$, $\beta = (\beta_1, \beta_2, \ldots\ldots, \beta_q)$

This assumes that variable xj's linear, cross and squared product terms are present on surface y. The regression coefficient can be estimated using a variety of methods.

3.2.1 CENTRAL COMPOSITE DESIGN

The findings of any experiment may be used to estimate the standard error (SE) "e," of Y on the fitted surface at any point. The SE is a function of the point's xj's coordinates. The SE is the similar for all points that are equidistant from the region's center because of the rotatability criterion and meet the equation:

$$x_1^2 + x_2^2 + \ldots\ldots x_k^2 = \delta^2 = constant \qquad (3.3)$$

However, in RSM a polynomial response surface has many benefits and certain drawbacks. One drawback is that when extended outside of the experimental zone, the polynomials are unreliable. Another significant drawback of utilizing second order polynomials is that with more than three X variables or levels, the size of trials increases too large and analysis becomes too difficult. A well-designed experimental strategy, on the other hand, can significantly minimize the overall number of trials. One of these methods is central composite designs (CCD). Continuing on, it has been shown that the second-order central composite designs are the most effective technique for establishing the mathematical relationship of the response surface with minimum feasible tests without sacrificing accuracy.

CCD is the most popular class of designs used for fitting second-order models. Generally, the CCD consists of a 2k factorial (or fractional factorial of resolution V) with n_F factorial runs, 2k axial or star runs, and n_c center runs,

i.e., total runs in CCD = n_F factorial runs + 2k axial or star runs + n_C center runs

Fig. 3.1 shows the CCD for k = 2 and k = 3 factors. Total runs for k = 2 can be calculated as:

Total Runs = 4 factorial runs (i.e., corner points) + 4 axial runs + 5 times-repeated center runs = 13.

The practical deployment of a CCD often arises through sequential experimentation. That is, a 2k has been used to fit a first-order model, this model has exhibited lack of fit, and the axial runs are then added to allow the quadratic terms to be incorporated into the model. The CCD is a very efficient design for fitting the second-order model.

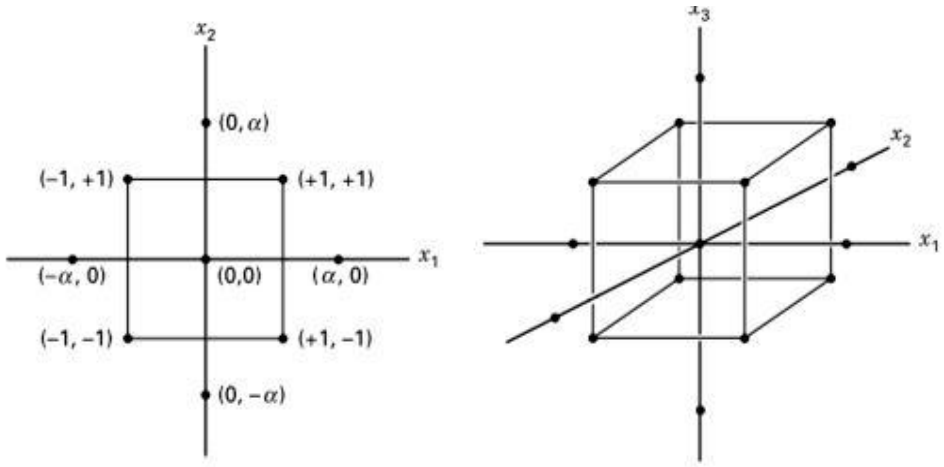

Figure 3. 1: CCD for k = 2 and k = 3 variables

There are two important parameters in the design that must be specified: (i) the distance **α** of the axial runs from the design center and (ii) the number of center points nC. We now discuss the choice of these two parameters:

Rotatability (it relates the distance α of the axial runs from the design center): It is important for the second-order model to provide good predictions throughout the region of interest. One way to define "good" is to require that the model should have a reasonably consistent and stable variance of the predicted response at points of interest z. Box and Hunter (1957) suggested that a second-order response surface design should be rotatable. This means that the variance is the same at all points z that are at the same distance from the design center. That is, the variance of predicted response is constant on ***spheres***. A central composite design is made rotatable by the choice of **α**. The value of **α** for rotatability depends on the number of points in the factorial portion of the design; in fact, $\boldsymbol{\alpha} = (n_F)^{1/4}$ yields a rotatable CCD where n_F is the number of points used in the factorial portion of the design. For example, k = 2 factors, there is $4(2^2)$ factorial runs means default $\boldsymbol{\alpha = (4)^{1/4} = 1.414.}$ k = 5 factors, there is $32(2^5)$ factorial runs means default $\boldsymbol{\alpha = (32)^{1/4} = 2.378.}$ The designs are shown in Figure 7 posses these **α** values then CCD said to be rotatable.

Spherical CCD: Rotatability is a spherical property; that is, it makes the most sense as a design criterion when the region of interest is a sphere. However, it is not important to have exact rotatability to have a good design. For a spherical region of interest, the best choice of α from a prediction variance viewpoint for the CCD is to set $\alpha = k^{1/2}$. This design, called a spherical CCD, puts all the factorial and axial design points on the surface of a sphere of radius k1/2. For example, k = 2 factors means α (for spherical CCD) = $(2)^{1/2} = 1.414$. k = 5 factors means α (for spherical CCD) = $5^{1/2} = 2.236$.

Face-Centered CCD: In many situations, the region of interest is cuboidal rather than spherical. In these cases, a useful variation of the CCD is the face-centered CCD (or the face-centered cube), in which α = 1. This design locates the star or axial points on the centers of the faces of the cube, as shown in Figure 8 for k = 3. This variation of the CCD is also sometimes used because it requires only three levels of each factor, and in practice it is frequently difficult to change factor levels. However, note that face-centered CCDs are not rotatable. In the present study, full factorial face centered CCD design was employed.

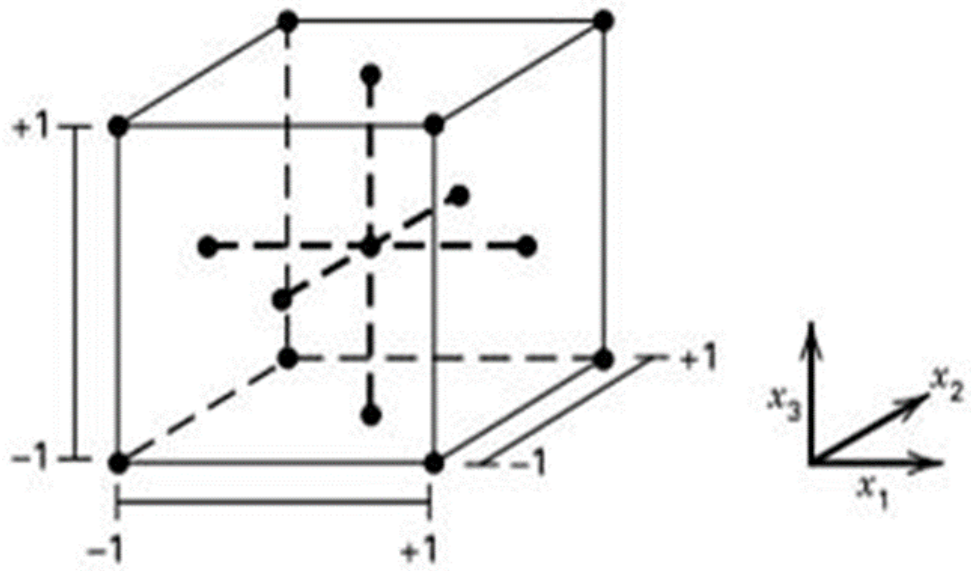

Figure 3. 2: A face-centered CCD for k = 3

Center Runs in the CCD (n_C): The choice of **α** in the CCD is dictated primarily by the region of interest. When this region is a sphere, the design must include center runs to provide reasonably stable variance of the predicted response. Generally, three to five center runs are recommended.

CCD is sectioned into three parts as following [130]:

- 2k design points, where 2 indicates number of levels used to maintain the parameters during testing. and k denotes the number of parameters.

- Extra points known as star points, which are positioned on the co-ordinate axes to construct a core composite design with a size star arm.

- A few additional points were added to the center to offer the response Y with a radius of one substantially identical accuracy.

The factor α denotes sphere or circle's radius on which the star points are located. Table 3.1 demonstrates the components of a second order central composite rotatable design for various numbers of parameters.

Table 3.1: Components of second order Central Composite Design [131]

Variables (k)	Factorial Points(2^k)	Star Points (2k)	Centre Points (n)	Total (N)	Value of α
3**	8	6	6	20	1.0000
4	8	8	5	21	1.00000
5	16	10	6	32	2.00000
6	32	12	10	54	2.37841
****This is used in Present Work,**					

3.2.2 ESTIMATION OF THE COEFFICIENTS

As previously indicated, the regression equation for the response surface of second order was expected to be (Eq. 3.4):

$$Y = \beta_0 + \sum_{j=1}^{q} \beta_j x_j + \sum_{i=1}^{q} \beta_{jj} x_j^2 + \sum\sum_{i<j} \beta_{ij} x_i x_j + \varepsilon \quad (3.4)$$

Where, the estimated response is Y, the coefficients are β's, and the independent variables are xj's. To calculate the regression coefficients, the least squares approach can be employed.

3.2.3 SIGNIFICANCE TEST OF THE COEFFICIENTS

To evaluate the significance of specific coefficients, a null hypothesis must be established, and the estimated coefficients must be tested for difference from their mean by utilizing student's t-test [132]. When the design is totally randomized, the analysis of variance can be used to compare two treatments instead of the t-test. This is because a one-tailed F-test with 1 and n DOF (degrees of freedom) equals a two-tailed t-test

with n DOF (t2 = F for 1 DOF). As a result, the F test with 1 and n0 DOF was employed to examine the significance of individual coefficients, where n0 is the total observations of the centre-point response surface.

3.2.4 ANALYSIS OF VARIANCE

The goal of product or process development is to enhance the product's or process' performance qualities in relation to consumer wants and expectations. The goal of experimentation should be to limit and regulate variances in a product or process, and then judgments on which parameters impact a product's or process' performance must be made. ANOVA is a statistical tool for interpreting and making judgments based on experimental data. Sir Ronald Fisher created the approach in the 1930s as a tool to analyses the findings of agricultural research. ANOVA is connected with a lot of mathematical elegance. It is a decision-making technique based on statistics for identifying any differences in the average performance among the groups of items under consideration.

3.2.5 RSM AND ROBUST DESIGN

RSM is a crucial component of experimental design. RSM is an important tool for creating new processes and improving their performance. RSM may frequently be used directly to achieve quality improvement goals such as reduced variability and improved process and product performance. Variation in key performance criteria is widely established to lead to poor process and product quality. During the 1980s, process quality received a lot of attention, and a methodology for applying experimental design was established, especially for the following:

- To develop or design products and procedures that are resistant to component variation.
- To minimize variability in a product's or process's output response around a target value.
- For the purpose of creating goods and processes that are resistant to environmental conditions.

By robust, we mean that the product or process meets its objectives consistently and is generally unaffected by difficult-to-control circumstances. RSM implies that these noise components are uncontrolled in the field, but that they can be controlled during the creation of a process for the sake of a controlled experiment.

Table 3.2: ANOVA for Second Order Central-Composite Design

S. No.	Sources	Sum of Squares	DOF
1	First order terms	$\sum_{q=1}^{k} b_i \left(\sum_{q=1}^{N} x_{iq} Y_q \right)$	K
2	Second order terms	$b_o \left(\sum_{q=1}^{N} y_q \right) + \sum_{i=1}^{k} b_{ii} \left(\sum_{q=1}^{N} x_{iq}^2 Yq \right) + \sum_{i<j}^{k} b_{ij} \left(\sum_{q=1}^{N} x_{iq} x_{jq} y_q \right) - \frac{\left(\sum_{q=1}^{N} y_q \right)^2}{N}$	$\frac{k\,(k\,-1)}{2}$
3	Experimental error	$\sum_{s=1}^{n_o} (y_s - \bar{y}_o)^2$	n_o -1
4	Lack of fit	Found by subtraction	$N - n_o - \frac{k(k+3)}{2}$
5	Total	$\left(\sum_{q=1}^{N} y_q \right)^2 - \left[\frac{\left(\sum_{q=1}^{N} y_q \right)^2}{N} \right]$	N - 1

The F-ratio is specified as:

$$F(1, n_0) = \frac{b_i^2 / c_{ii}}{S_e^2} \tag{3.5}$$

Where c_{ii} = Element of error matrix (X' X) $^{-1}$

b_i =Regression Coefficient

S_e = Standard deviation of experimental error measured from the replicating observation at zero level:

$$S_e^2 = \frac{1}{n_o - 1} \sum_{s=1}^{n_o} (y_s - \bar{y}_o)^2 \tag{3.6}$$

Where, $y_0 = \frac{1}{n_0}\sum_{s=1}^{n_0} y_s$

Y_s = s^{th} response value at center

This estimated F value may be compared to the theoretical F value at 95% confidence level. If the calculated F value for a coefficient is more than theoretical value, the impact of that term is substantial. The irrelevant second-order elements in the equations can be removed, and the remaining coefficients recalculated [132].

3.2.6 MODEL ADEQUACY

The predicted regression equation is checked for adequacy of fit:

Evaluate the residual sum of square using:

$$S_1 = \sum_{q=1}^{K}\left(Y_q - \overline{Y_q}\right)^2 \quad (3.7)$$

Where the observations at experimental locations are denoted by Yq, and the mean of all observations is denoted by $\overline{Y_q}$. Where, k denotes the total variables, and N denotes the total observations. The DOF for residual sum of sum of squares will be computed as follows:

$$f_1 = N - \frac{(k+2)(k+3)}{2}$$

- The error sum of squares may be calculated using repeated observations at the centre point as follows:

$$S_2 = \sum_{S=1}^{n_0}(Y_s - Y_0)^2 \quad (3.8)$$

Where, y_s denotes the s^{th} response value at centre.

- Determine the total of squares fit inadequacy.

$$S_3 = S_1 - S_2 \quad (3.9)$$

For which the DOF is

$$f_3 = f_1 - f_2 = N - \frac{(k+1)(k+2)}{2} - n_0 - 1 \quad (3.10)$$

- Apply F- test to test the adequacy of fit as:

$$F = \frac{S_3/f_3}{S_2/f_2} \tag{3.11}$$

If FF0.05 (f3, f2) at confidence level of 95% or F F0.99 (f3, f2) at confidence level of 99%, the generated regression equation fits the data sufficiently.

CHAPTER-4

RESEARCH METHODOLOGY

4.1 INTRODUCTION

Gaps in the literature are identified with the help of the literature survey, these gaps helped to formulate the main objectives of the present research work. The aim of the present study is to fabricate weld joints of dissimilar AA5083 and AA6061 with the incorporation of micro-sized SiC and Al_2O_3 particles using friction stir welding. The following sequence of experimental activity was intended to achieve the key objectives:

1. Cutting of AA 5083 and AA 6061 plates in the dimensions of 150*40*6 mm for the proper clamping in the fixture of FSW machine. And evaluation of their chemical composition and mechanical characteristics.
2. Evaluation of chemical composition of SiC and Al_2O_3 microparticles.
3. Fabrication of slots on the adjoining surfaces of AA5083 and AA6061 for incorporating reinforcement particles.
4. Design of experimentation (DOE) was obtained using full-factorial central composite design (CCD) by Response surface methodology to observed optimized input and output responses.
5. Fabrication of reinforced FSWed joints of AA5083 and AA6061 using DOE of different process parameters such as tool rotational speed and traverse speed and number of FSW passes using different reinforcement particles.
6. Evaluation of tensile characteristics of the reinforced FSWed joints and fracture surface was examined via scanning electron microscope.
7. Microhardness of various zones was performed using Vickers hardness tester.
8. Determination of significance of process parameters: F-test of ANOVA is performed to determine the significance of considered process parameters. Individual as well as instructional influence of the above said parameters are studied and explored in detail.
9. Development of the regression model was carried out with the help of RSM, mathematical models are developed for all output responses.
10. Multi-optimization of the response parameters was carried out using desirability approach in RSM.

11. Confirmatory tests were performed with the suggested set of optimized process parameters to verify the validity of developed mathematical models.
12. Characterization of FSWed joints using optical microscope (OM), field emission scanning-electron microscopy (FESEM), and Energy-dispersive X-rays spectroscopy (EDS) to reveal the material flow behavior, grain size, grain orientation and joint quality.
13. Perform the comparative analysis between the FSWed joints incorporated with Al_2O_3 and SiC micro particles.

The flow chart is a condensed version of the detailed work. Fig. 4.1 depicts the flow chart for the present work, which shows the step-by-step approach or methodology used during the work.

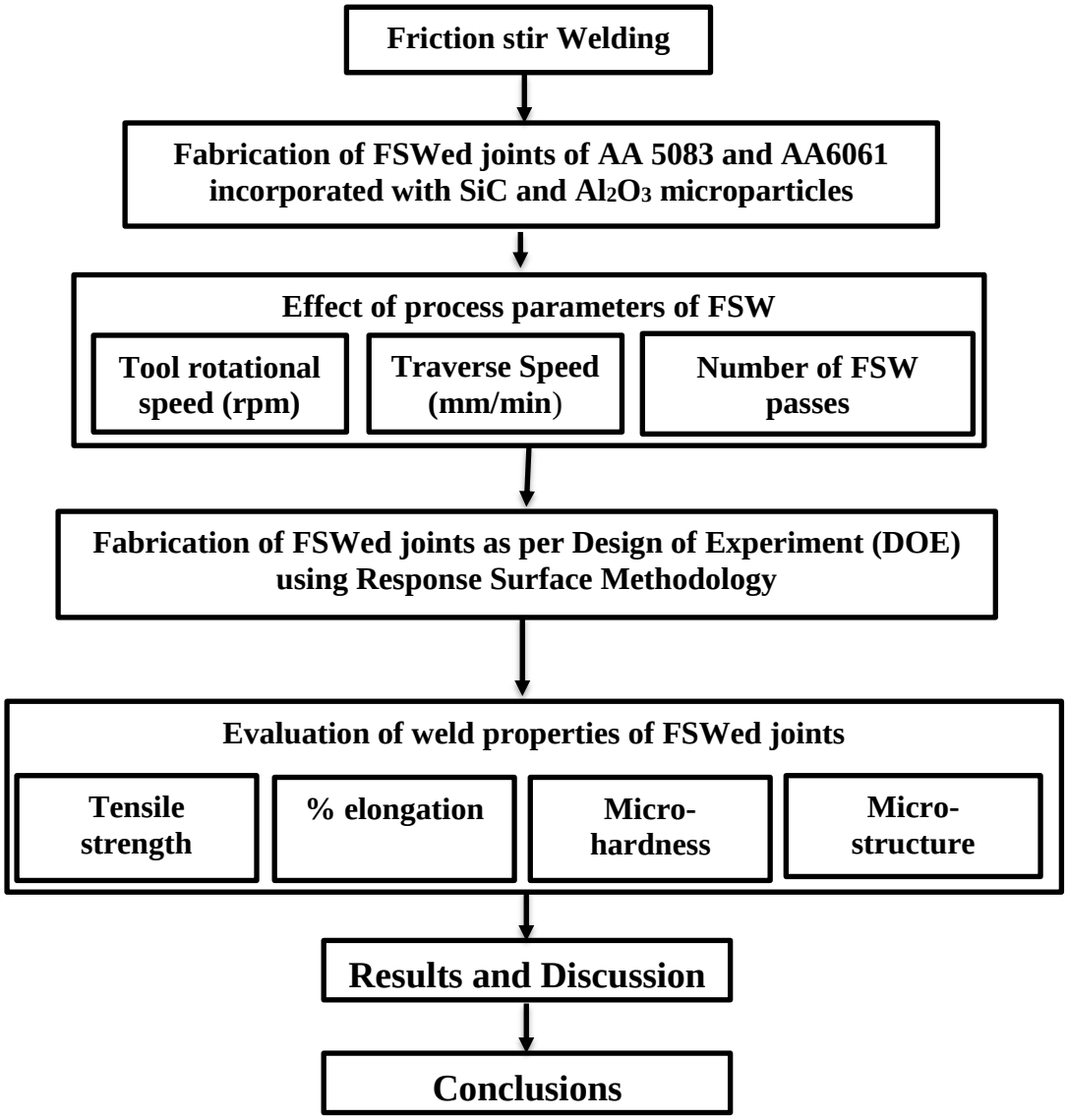

Figure 4.1: Work Plan

4.2 BASE MATERIALS

FSW of AA6xxx and AA5xxx has recently attracted a lot of interest from researchers because to its extensive use in the automotive and aviation sectors [133]. AA5083 is a strain hardenable alloy with exceptional corrosion resistance. Additionally, it has high weldability [134]. As a result, AA5083 is frequently used in the construction of ships and armored vehicles, in addition to the automotive and aerospace sectors [135]. AA 6061 is the most popular alloy in the 6xxx aluminum group, with uses in the automobile industry including wheel rims, truck bodywork, vehicle chassis, and fuel tanks [136]. It's utilized to make aircraft wings, fuselages, and fuel tanks in the aerospace industry [137]. Container bodies, cargo wagons, carriages, and trams are all made with it in the railway industry [138]. It may also be used in shipbuilding and helicopter platform construction [139]. Due to extensive applications and excellent weldability, dissimilar welding of these alloys (AA6061 and AA5083) has attracted the great attention of almost all industries [140]. The improvement of these alloys' joint strength will be extremely useful in a variety of technical fields, which encourages us to conduct this research work. Therefore, in the present study, the composite metal matrix was fabricated on dissimilar aluminum alloys AA5083/AA6061. The influence of induced reinforcing particles along with multi-pass FSW on the microstructural and mechanical characteristics of FSWed dissimilar aluminum alloys AA5083/AA6061 was investigated. The main alloying components in AA6061 are silicon (Si) and magnesium (Mg) whereas AA5083 containing magnesium (Mg) have major alloying elements. The raw plates of base materials (AA6061 and AA5083) is depicted in Fig. 4.2.

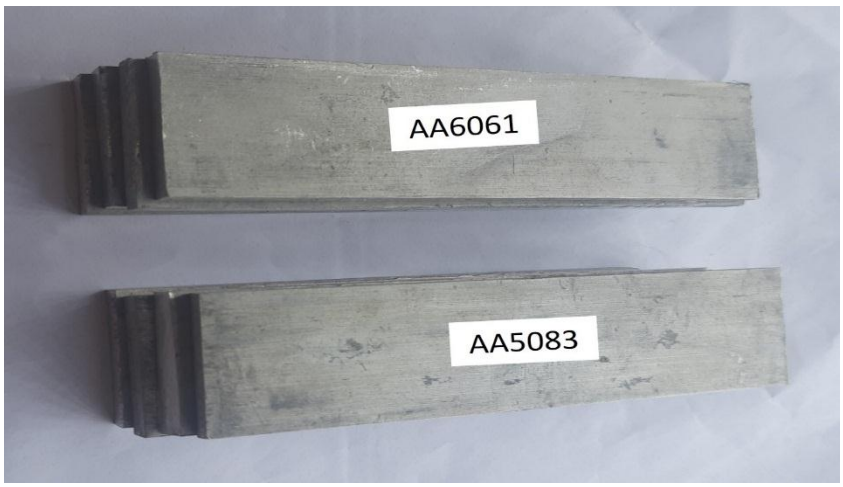

Figure 4.2: Base plates of AA6061 and AA5083

Table 4.1 displays the chemical compositions of base materials obtained by chemical spectroscopy. The optical and FESEM micrographs, and chemical compositions as obtained by electric dispersive X-ray spectroscopy (EDS) of AA 5083 and AA6061 are delineated in Fig 4.3 (a-c) and (d-f), respectively. Mechanical and wear characteristics of base materials are tested as per ASTM standard and tabulated in Table 4.2.

Table 4.1: Chemical composition of parent materials

Parent Materials	Si	Fe	Cu	Mg	Zn	Mn	Ti	Cr	Al
AA6061	0.87	0.62	0.74	0.73	0.17	0.09	0.02	0.04	Bal.
AA5083	0.50	0.13	0.03	4.94	0.04	0.43	0.02	0.05	Bal.

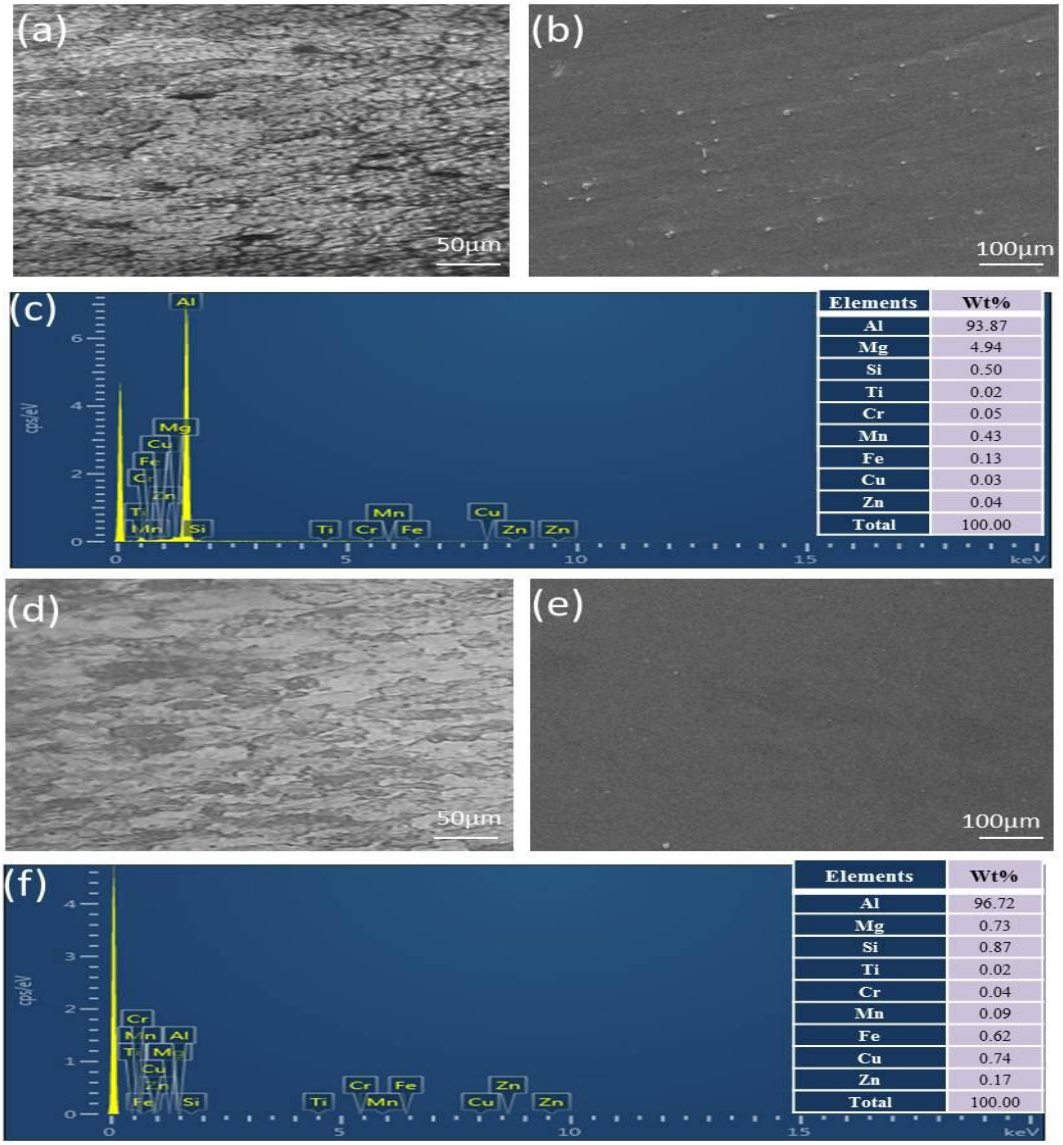

Figure 4.3: Optical and FESEM micrographs and EDS peaks of base materials (a-c) AA5083, (d-f) AA6061

Table 4.2: Mechanical characteristics of AA5083 and AA6061

Base materials	Tensile strength (MPa)	%Elongation (%)	Microhardness (HV)
AA5083	290.20	21.9	85.4
AA6061	310.04	20	98.1

4.3 REINFORCING PARTICLES

The SiC particles were adopted as reinforcing particles, due to its lower melting point and density than other reinforcing particles such as TiC etc. FSW may be used to fabricate Al-SiC composites due to its solid state nature without encountering the common issue of significant discrepancies in the thermal expansion coefficients of SiC and aluminum during solidification [141]. By fabricating Al-SiC composites using FSW/FSP, several researchers improved the material's mechanical and wear characteristics. By using different volume fraction of 5, 8 and 13% of SiC nanoparticles sound weld joints of AA7075/AA2024 were established. With 5% SiC particle inclusion, which resulted in uniform SiC particle dispersion, the best weld quality was achieved [142]. The FSWed joint of AA1350 and AA6101 embedded with Al_2O_3 nanoparticles showed better mechanical characteristics and wear resistance than SiC particles. [143].

Al_2O_3 is an important reinforcing material in the development of MMCs. It exhibits high density (about 4.08 g/cm^3) and low melting temperature (around 2,050 ºC). Its popularity is growing because of good wettability, low melting temperature, and inexpensive cost. Several researchers used Al_2O_3 particles in surface matrix composites through FSP/FSW. Zarghani et al. [144] developed surface composites using Al6082/Al_2O_3. The employment of nano Al_2O_3 particles resulted in two to threefold increase in wear resistance and a 168% increase in microhardness. With increasing FSP pass counts, consistency in particles dispersion, wear resistance and microhardness improved. Raaft et al. [145] developed the mono base metal matrix composites of A356 using graphite and Al_2O_3 particles. It was found that that A356/Al_2O_3 composites (MMC) outperform A356/graphite composites in terms of wear and mechanical characteristics. In Al_2O_3-based composites, a maximum increase in microhardness of 82 % was also observed. Therefore, in the present research, micro sized particles of SiC and Al_2O_3 ware utilized as reinforcing candidates. The FESEM micrograph and EDS

analysis of micro-sized SiC and Al_2O_3 particles are also delineated in Fig. 4.4 and 4.5, respectively.

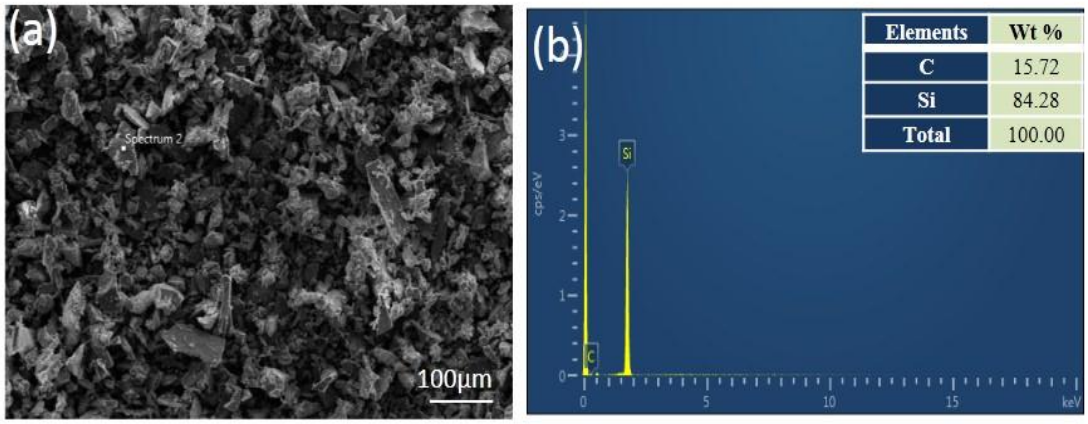

Figure 4.4: SiC micro particles (a) SEM micrograph (b) EDS analysis

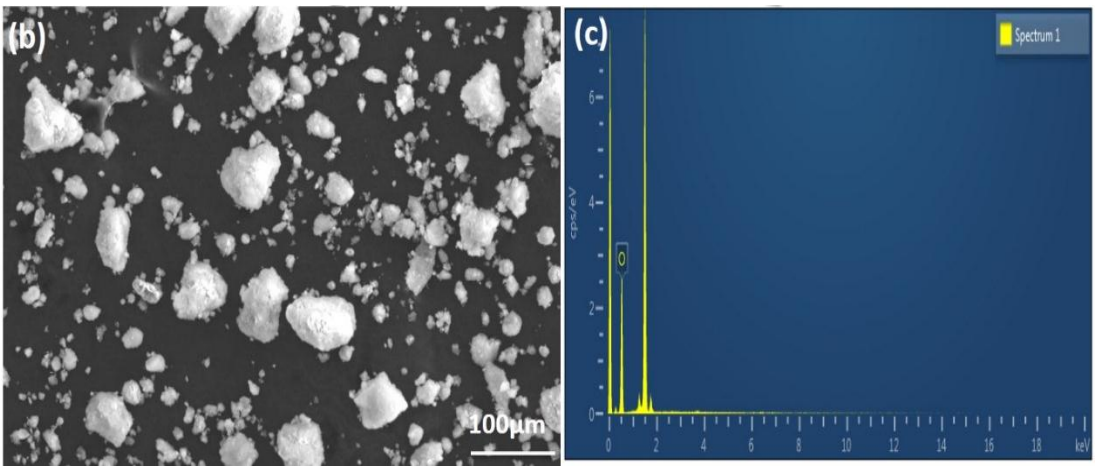

Figure 4.5: Al_2O_3 microparticles (a) SEM micrograph (c) EDS analysis

4.4 EXPERIMENTAL PROCEDURE

Experimentation work was carried by using friction stir welding machine (R.V. machine tools, FSW4T-HYD) (15 hp; 3000 rpm; 25 kN) as depicted in Fig. 4.6. The tool is held by a vertical spindle, and the work piece is held by a fixture with four hydraulically driven clamps and a backing plate with groove of size 200×80 mm. The backing plate groove is designed to securely support the work component. The spindle's maximum operating speed is 3000 rpm. On this machine, traverse speed and rotational speed can be varied easily. The reinforced joints of AA6061 and AA5083 plates of thickness 6 mm was fabricated using reinforcing particles. The friction stir processing is done on incorporated reinforced plates of AA6061 and AA5083 with different processing parameters. The following steps are as given below.

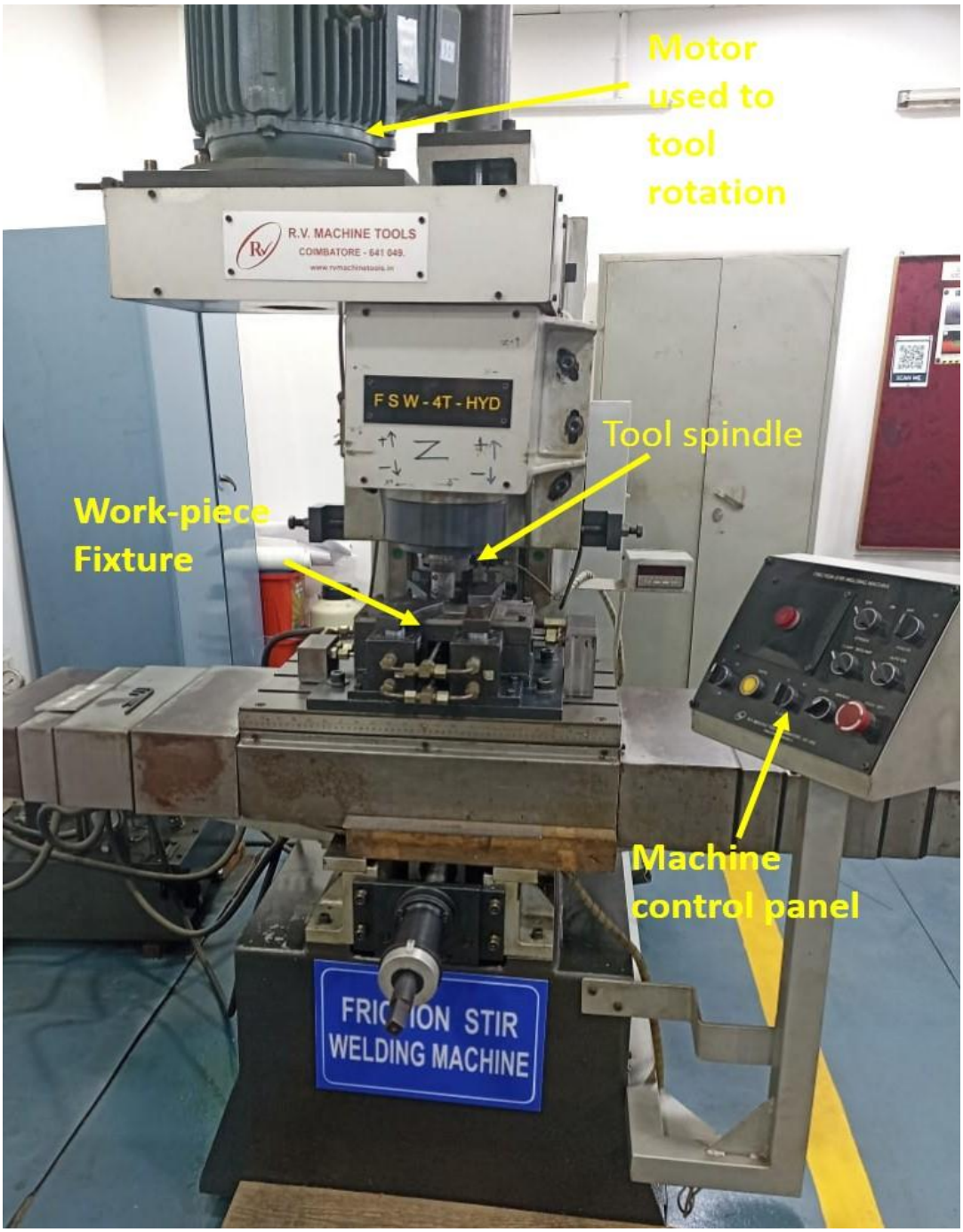

Figure 4.6: Friction stir welding machine

4.4.1 TEST SAMPLES PREPARATION

Plates of AA6061 and AA5083 of thickness 6 mm were utilized as base materials for the present work. Aluminum plates a dimension of 150 x 40 mm were cut with the help of milling cutter and grinding done at the edge to smooth the surface to be joined as depicted in Fig. 4.7.

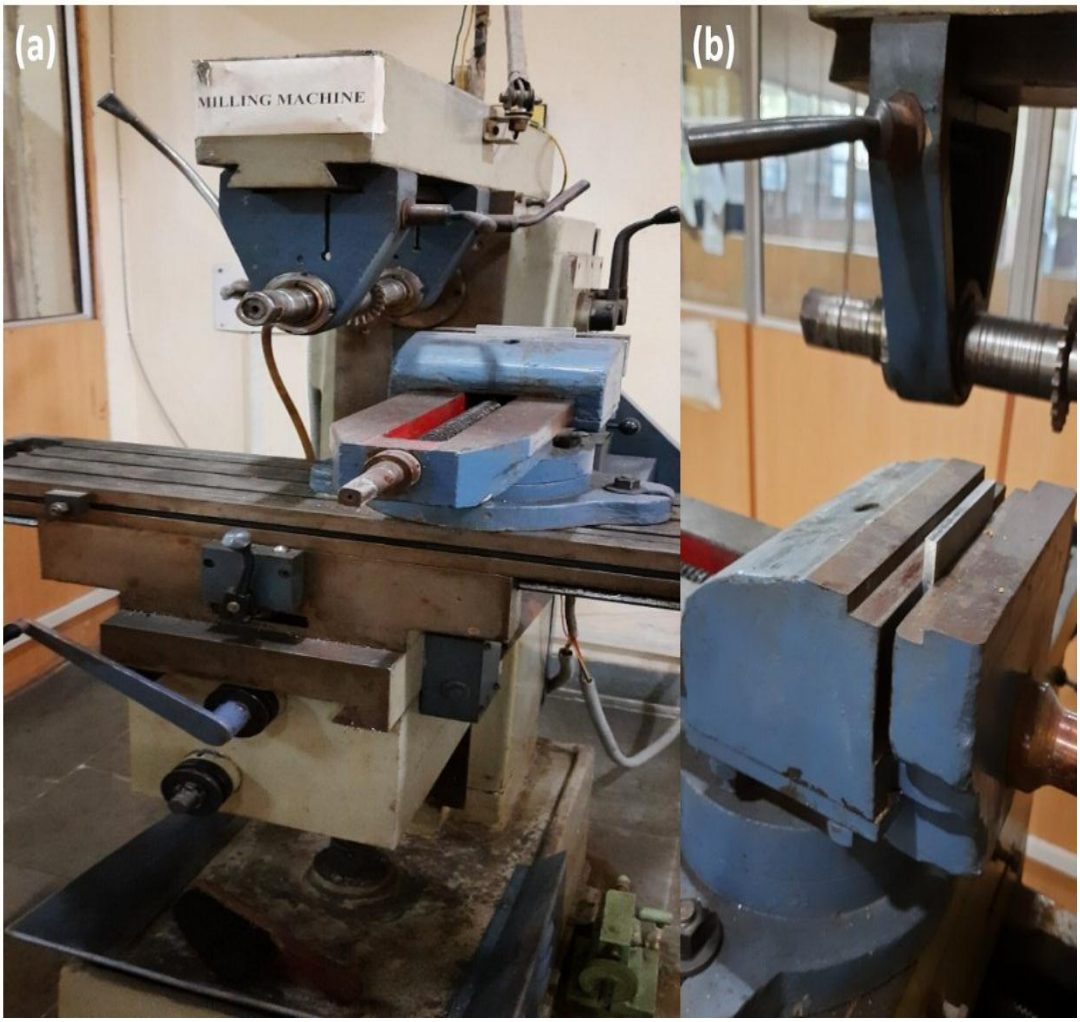

Figure 4.7: Sample preparation for FSW using milling machine

4.4.2 GROOVE PREPARATION

To incorporate the reinforcing particles in the weld region, grooves of 3 mm depth were plowed by using milling machine along the adjoining faces of base plates from the top surface as depicted in Fig. 4.8. The surface grinder was employed for better surface finish and dimensional accuracy. The groove of width 0.18 mm on each plate of AA 5083 and AA 6061 was plowed to incorporate the reinforcing particles in the processed zone.

4.4.3 INCORPORATION OF REINFORCING PARTICLES

For the appropriate filling of reinforcement particles into the stir zone, a thick slurry of reinforcing particles was prepared using 99% pure ethanol. To prevent contamination, the grooves were thoroughly cleaned using acetone before filling. Thereafter, the grooves were filled with the slurry of reinforcement particles and allowed to dry at room temperature for about an hour as depicted in Fig. 4.8.

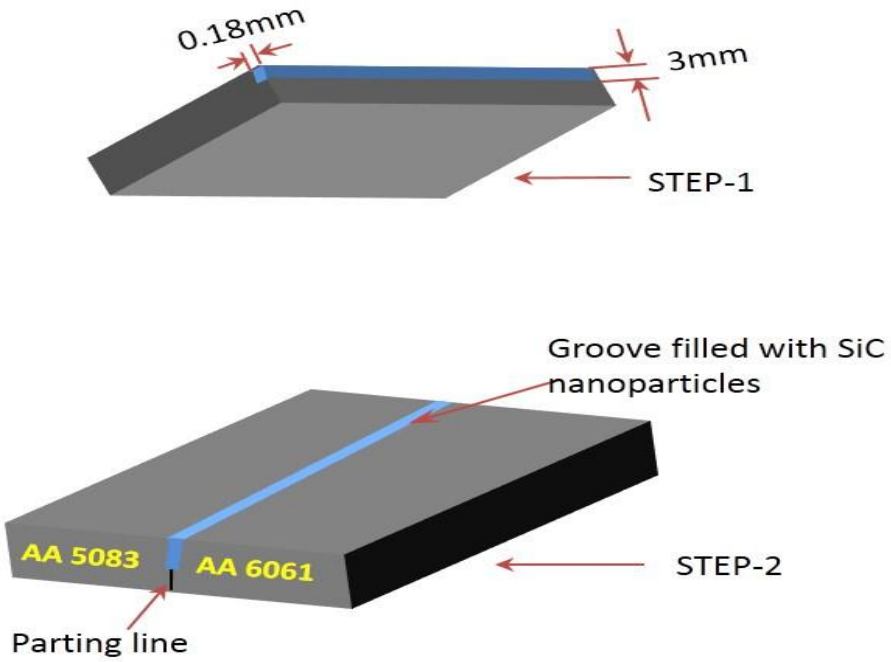

Figure 4.8: Groove for filling reinforcing particles

4.5 FABRICATION OF FSWED REINFORCED JOINT

4.5.1 MANUFACTURING OF FSW TOOL

In this work, the threaded cylindrical pin profiled tool was utilized to fabricate the reinforced FSWed joint because of the threaded pin profile yield defect-free joints and it is preferred over the other pin profile [146] and the material was used for the manufacturing the tool is H13 tool steel due to its high wear and shock resistance among different tool steel grades. The process of manufacturing of tool pin profile as depicted in Fig. 4.9-4.11.

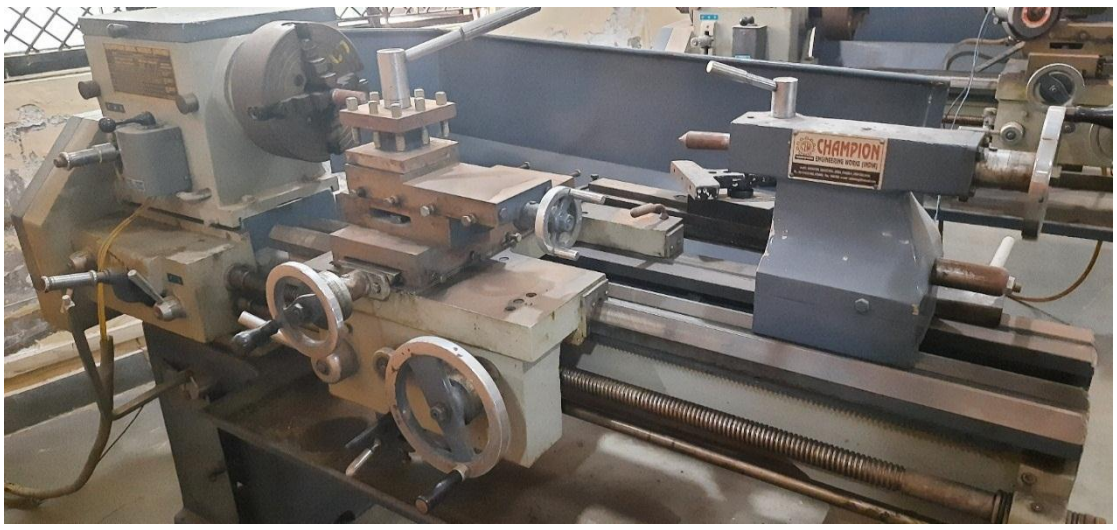

Figure 4.9: Lathe machine used for making FSW tool

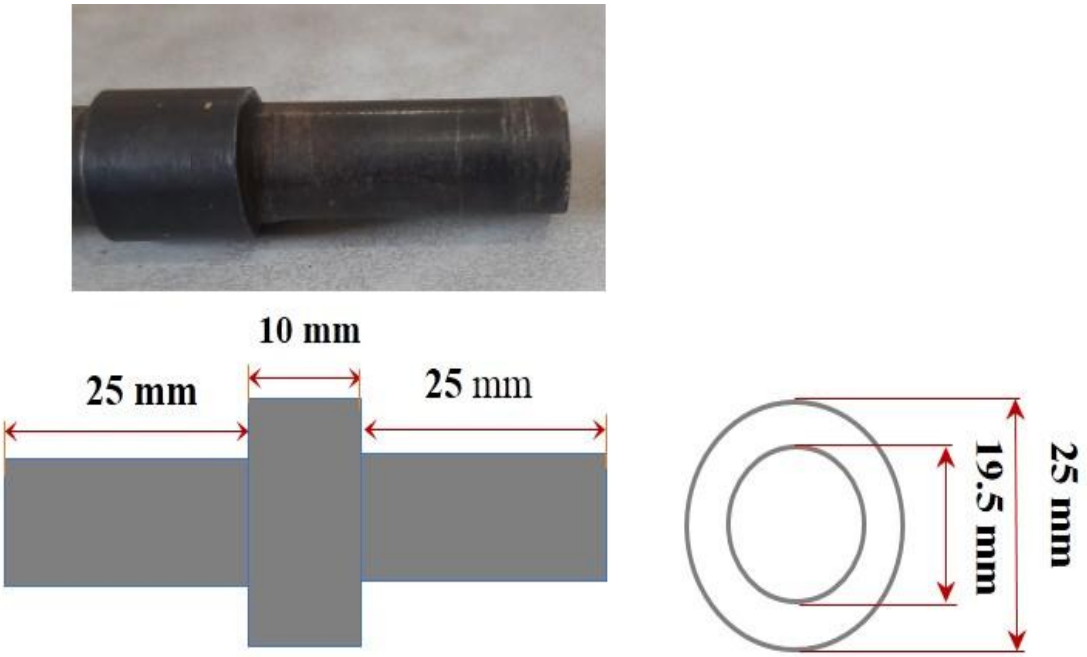

Figure 4.10: Dimensional features of FSW pin-less tool

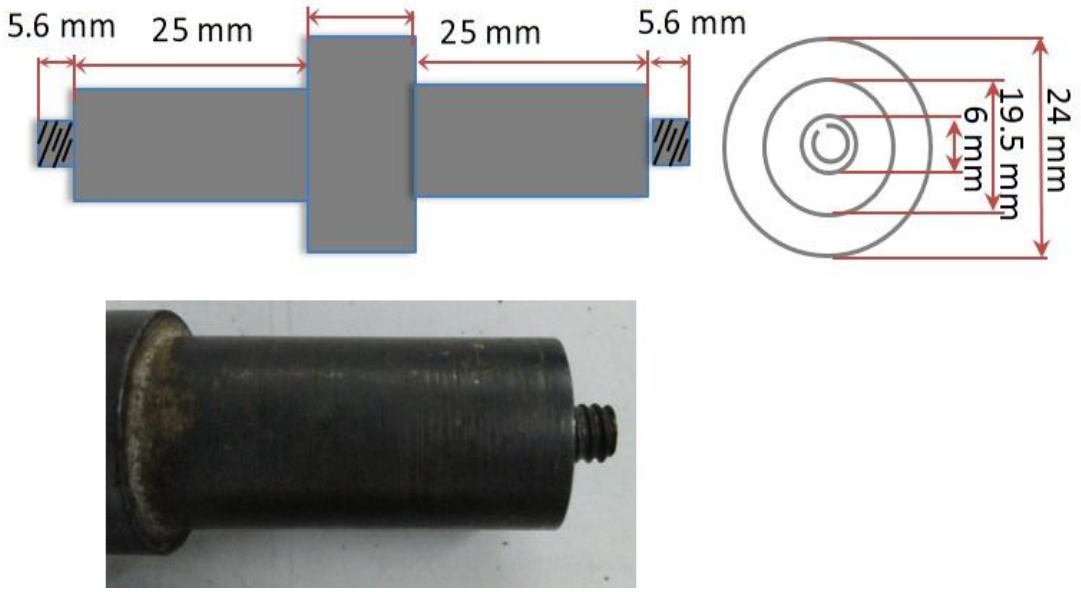

Figure 4.11: Dimension features of FSW tool

4.6 FRICTION STIR WELDING

In the present study, an indigenously developed NC-FSW machine was employed to produce the dissimilar joints of AA5083 and AA6061. The slurry made of reinforcing particles and ethanol was filled into the grooves made at the adjoining faces of the base plates as depicted in Fig. 4.12 (a-d). Thereafter, AA5083 and AA6061 plates were securely secured to prevent the plates from abutting during processing. A pin-less tool made of H-13 tool steel was employed to close the groove prior welding. Thereafter, a

non-consumable tool manufactured of tool steel H13 was employed for experimentations. The dimensional features of pin-less tool and FSW tool are depicted in Fig. 4.10.

For FSW, the rotating tool was plunged slowly into the parting line of base plates of AA 5083 and AA6061 until the tool pin is completely inserted into the base plates. The tool was maintained at this position for a dwell period of around 60 sec in order to preheat the material. Thereafter, the tool was allowed to move along the parting line of the base plates at a particular traverse speed.

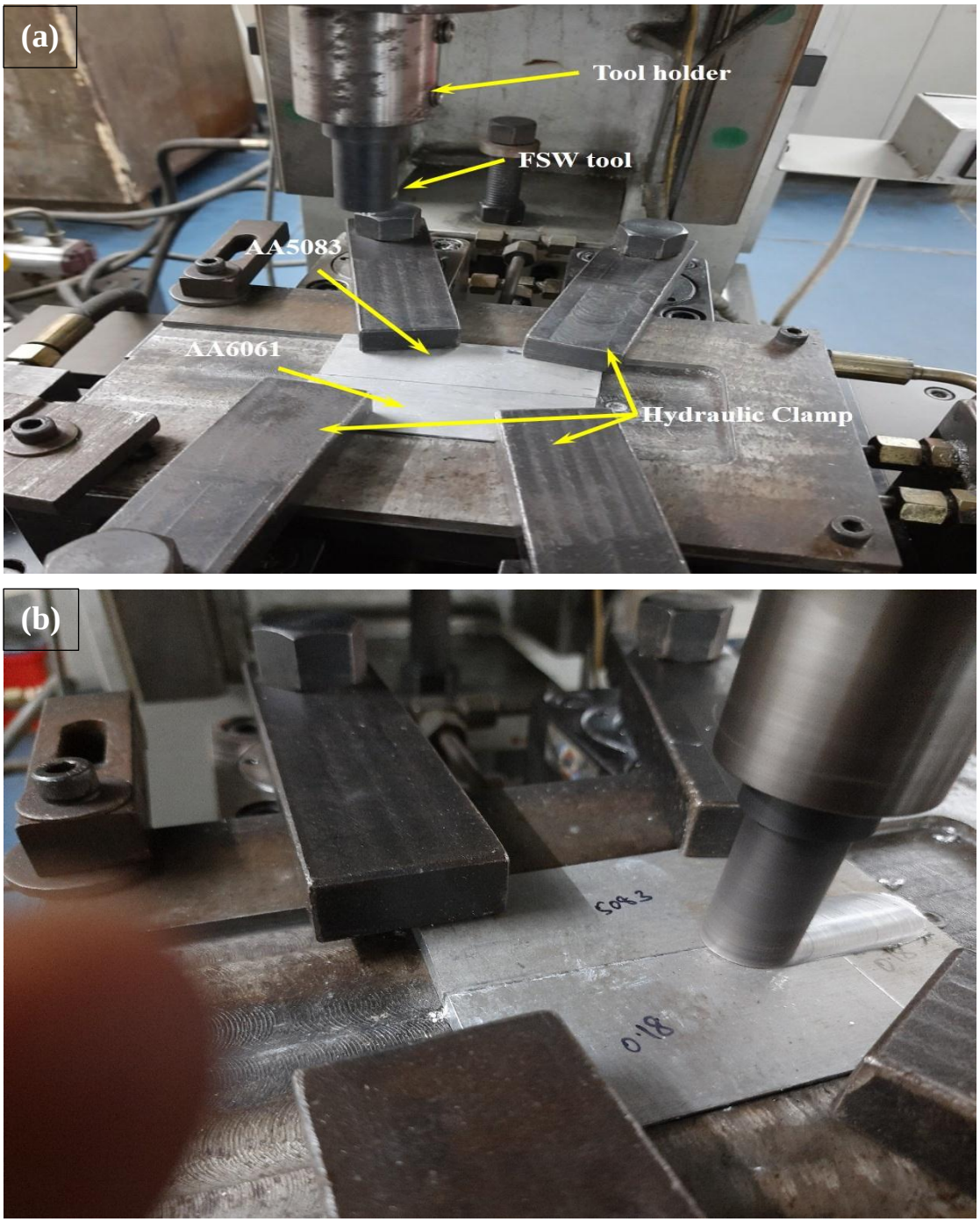

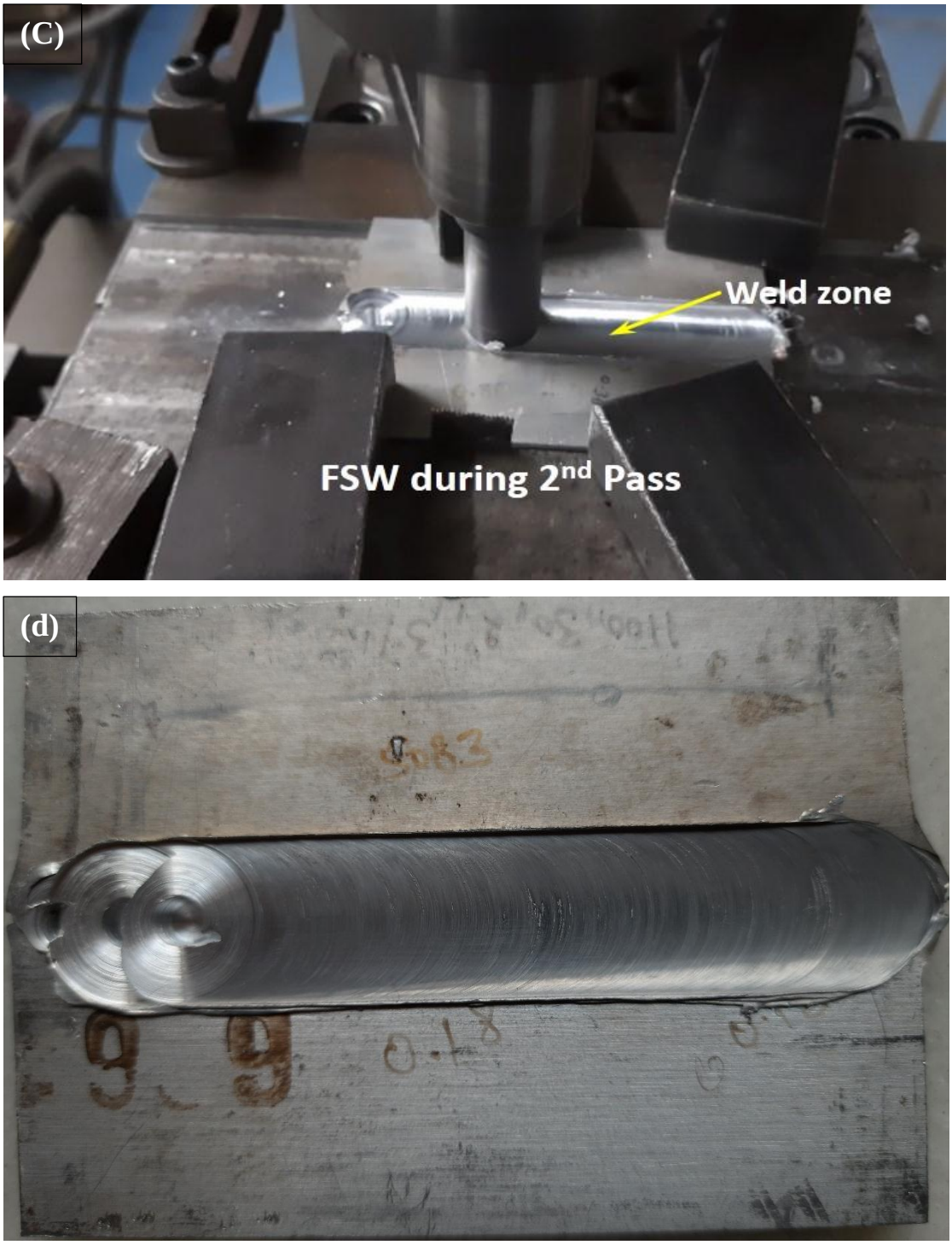

Figure 4.12: Steps of FSW process

The particle's dispersion pattern, temperature distribution and subsequent microstructural evolution of the processed zone are all mainly influenced by the tool rotational speed, traverse speed and number of FSW passes. The process parameters such as tool rotation speed of 750-1150 rpm, tool traverse speeds of 25-45 mm/min and number of FSW passes 1-3 were utilized to fabricate the FSWed joints shown in Fig. 4.12. The process parameters along with their levels used in this study are illustrated in

Tables 6 and 7. A threaded pin profile tool was utilized for fabrication of the FSWed joints embedded with micro- sized SiC and Al_2O_3 particles. The dimensional features of threaded pin tool and the images of the tool during manufactured are depicted in Fig. 4.11. There are total twenty number of experiments were performed obtained as per design matrix of full factorial face centered central composite design using response surface methodology (RSM) and illustrated in Table.7. The reinforced FSWed joints after experimentation are depicted in Fig. 4.13.

Table 4.3: Processing parameter and its level used for FSW

Process Parameters	Units	Notation	Range	Levels		
				-1	0	1
Tool rotational Speed	rpm	A	750-1150	750	950	1150
Traverse Speed	mm/min	B	25-45	25	35	45
Number of passes	--	C	1-3	1	2	3

Figure 4.13: Various reinforced friction stir welded joint

Table 4.4: Design of Experiments

Std	Run	A: Tools Rotations Speeds (rpm)	B: Traverses Speeds (mm/min)	C: Number of FSW passes (%)
7	1	750	45	3
5	2	750	25	3
20	3	950	35	2
12	4	950	45	2
2	5	1150	25	1
15	6	950	35	2
10	7	1150	35	2
18	8	950	35	2
14	9	950	35	3
8	10	1150	45	3
9	11	750	35	2
6	12	1150	25	3
11	13	950	25	2
16	14	950	35	2
17	15	950	35	2
13	16	950	35	1
1	17	750	25	1
4	18	1150	45	1
3	19	750	45	1
19	20	950	35	2

4.7 TEST SAMPLES PREPARATION

The samples required for tensile testing, micro-hardness test, and microstructural characterization were extracted from the friction stir welded reinforced joints by employing CNC wire cut EDM (Electrical Discharge Machining) for higher dimensional accuracy, as shown in Fig. 4.14.

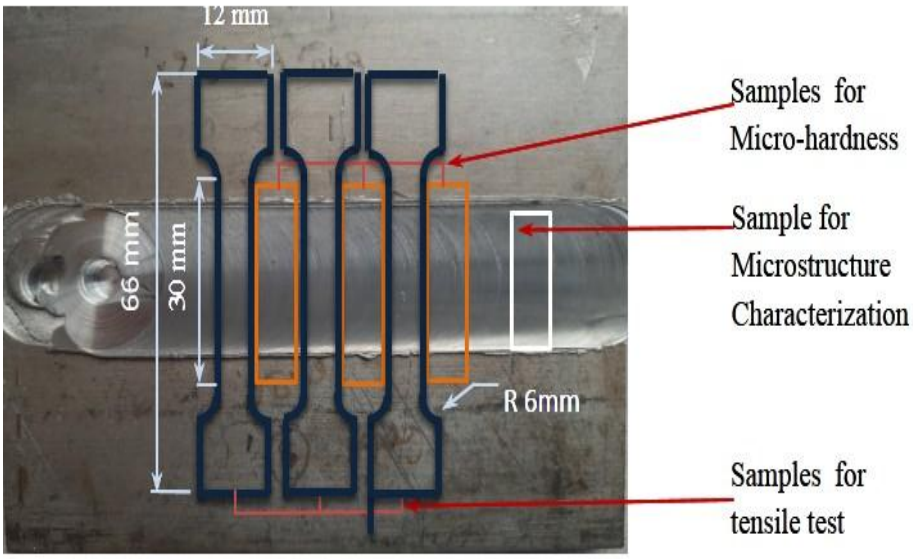

Figure 4.14: Dimensional characteristics of different test samples

4.7.1 TENSILE TEST

The strength of the material undergoing a basic lengthening operation is determined by tensile testing. The main functions of the testing apparatus are to produce the curve of load vs displacement and the curve of stress vs strain. Tensile test results can be applied for engineering applications in the selection of materials. Tensile properties are commonly involved in material specifications to assure quality. The samples for tensile tests were extracted as per the ASTM-E8 standard as presented in Fig. 4.14. In this work, a single sheet size is 150 x 40 mm which is to be butt joint with the same size of the sheet. After the processing, the total fabricated sample is 150 x 80 mm in size with 80 mm for cross-sectional side. Due to this, a sub-size tensile samples (66 mm length of tensile sample) is preferred as depicted in Fig. 4.15.

Figure 4.15: Tensile sample as per ASTM-E8 standard

Tensile testing of reinforced FSWed joint samples was carried out by Universal Testing Machine (Model: Biss UT-02-0100) as shown in Fig. 4.16. Three samples were extracted for each FSWed specimen and the tensile tests were performed at room temperature and the average of three results were reported. Make sure samples free from crack or notches or other defects that would disparagingly affect the test results.

Figure 4.16: Universal testing machine (UTM)

4.7.2 MICROHARDNESS TEST

The microhardness variation of the reinforced FSWed joints of AA5083 and AA6061 processed under different combinations of processing parameters were evaluated using Vickers hardness tester. The ASTM (E 384-99) standards were followed for sample

preparation and testing methods for micro-hardness measurements. The samples for microhardness were properly polished using emery papers (400-1200 grade) before indentation. The double disc polishing machine utilized for polishing is depicted in Fig. 4.17.

Figure 4.17: Double disc polishing machine

The indentations were made on the lateral surface at 3 mm below the top. By taking a 1 mm gap between the indentations and using a 100 gm load for a 15 s dwell duration, the Vickers microhardness tester (Fig. 4.18) was used to assess the hardness profile.

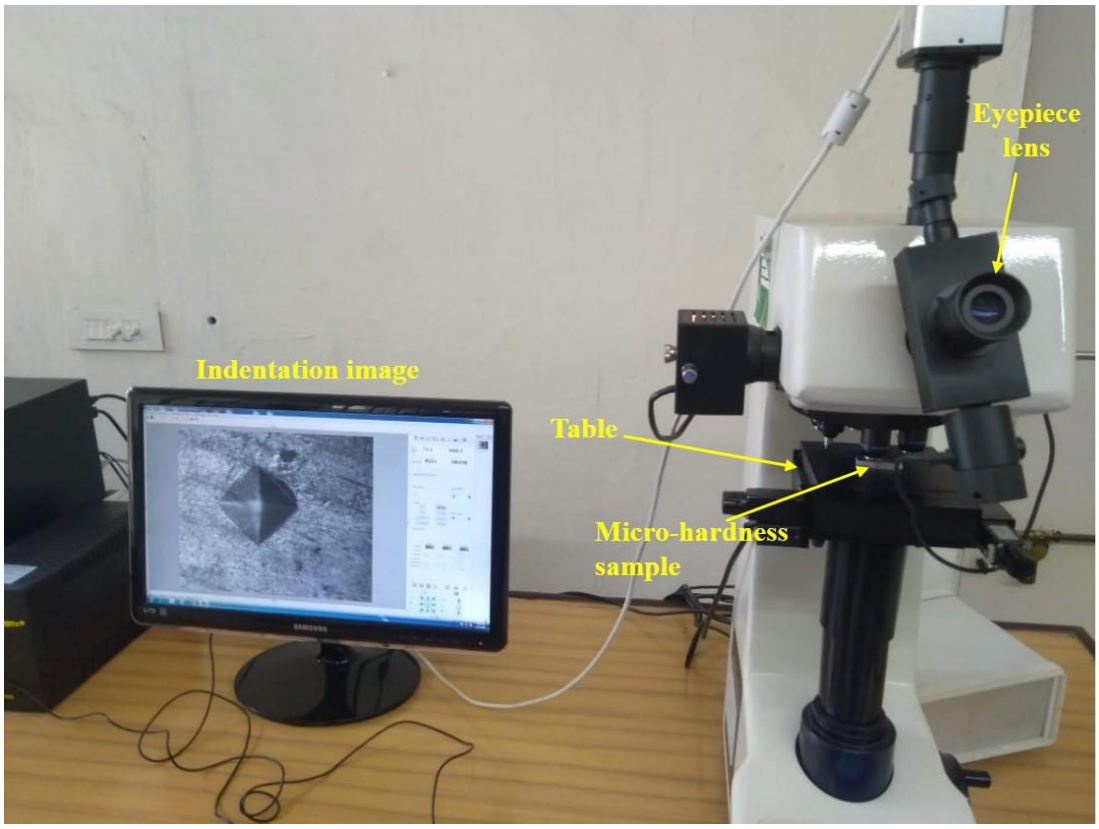

Figure 4.18: Vickers micro hardness testing process

4.7.3 MICROSTRUCTURAL EVALUATION

The microstructural study of the reinforced FSWed joints was examined by a number of characterization approaches.

- The specimens having the dimensions (10 mm x 5mm x 6mm) were extracted from the reinforced FSWed joints.
- The samples were polished with emery papers from grit size from 100 to 2000 grade to get fine polish. The polishing machine used is depicted in Fig. 4.17.
- Final polishing was done using alumina powder with emery cloth using double disc polishing machine. After that, the samples were etched with Keller reagent (HNO_3, HF, and HCL) as per ASTM E407 standard.
- The chemical etchants were mopped and washed in running water after that the samples were placed in the optical microscope machine (as depicted in Fig. 4.19) to analyze the microstructure of the FSWed joints.
- Thereafter, the samples were analyzed using FESEM machine (JEOL: JSM 7610 F plus) to evaluate the particles dispersion pattern in the stir zone. FESEM machine used for microstructure evaluation is depicted in Fig. 4.20 (a, b).

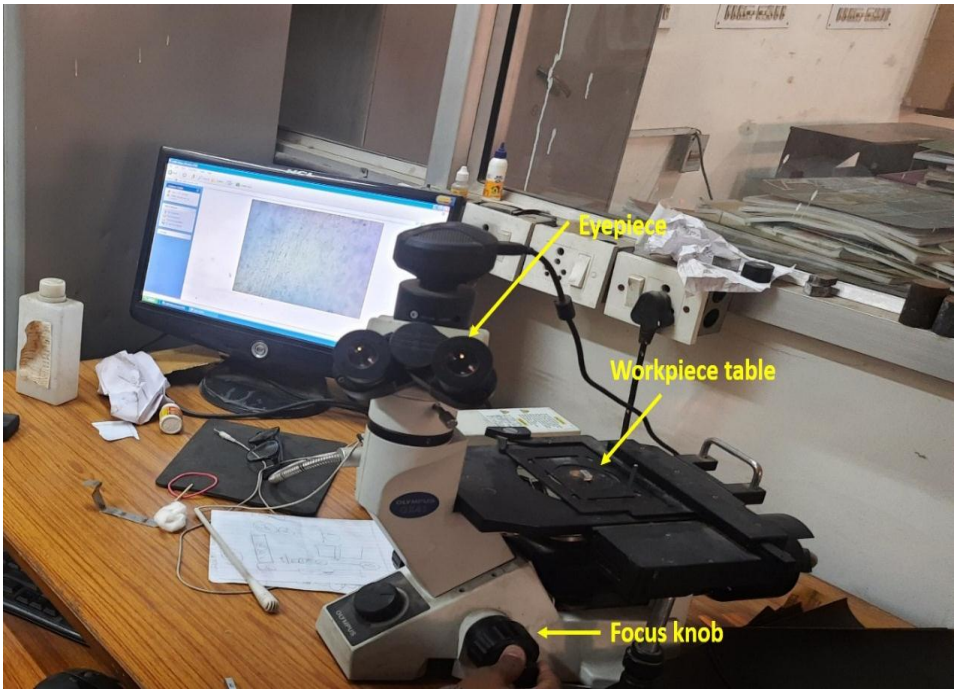

Figure 4.19: Optical microscope used to grain structure evolution

Figure 4. 20: FESEM and EDX machine during testing

- To analyze the fracture surface of the samples extracted from the tensile test, the fractured surfaces were analyzed using FESEM. The fractured surface was examined to better understand the failure mechanism of the reinforced FSWed joints.
- The chemical composition of the base material and reinforced FSWed joints were analyzed using EDX/EDS analysis.

CHAPTER-5

RESULT AND DISCUSSION

5.1 PARAMETRIC OPTIMIZATION OF Al_2O_3 MICROPARTICLES REINFORCED FSWED JOINTS

The friction stir welding was performed to successfully fabricate the dissimilar reinforced joints of AA5083 and AA6061 embedded with of 6 % volume fraction of Al_2O_3 micro-particles (Al_2O_3-mp), in order to investigate the effects of FSW parameters, Al_2O_3 particles and multi-pass FSW on the microstructural and mechanical characteristics of the reinforced FSWed joints as depicted in Fig. 5.1.

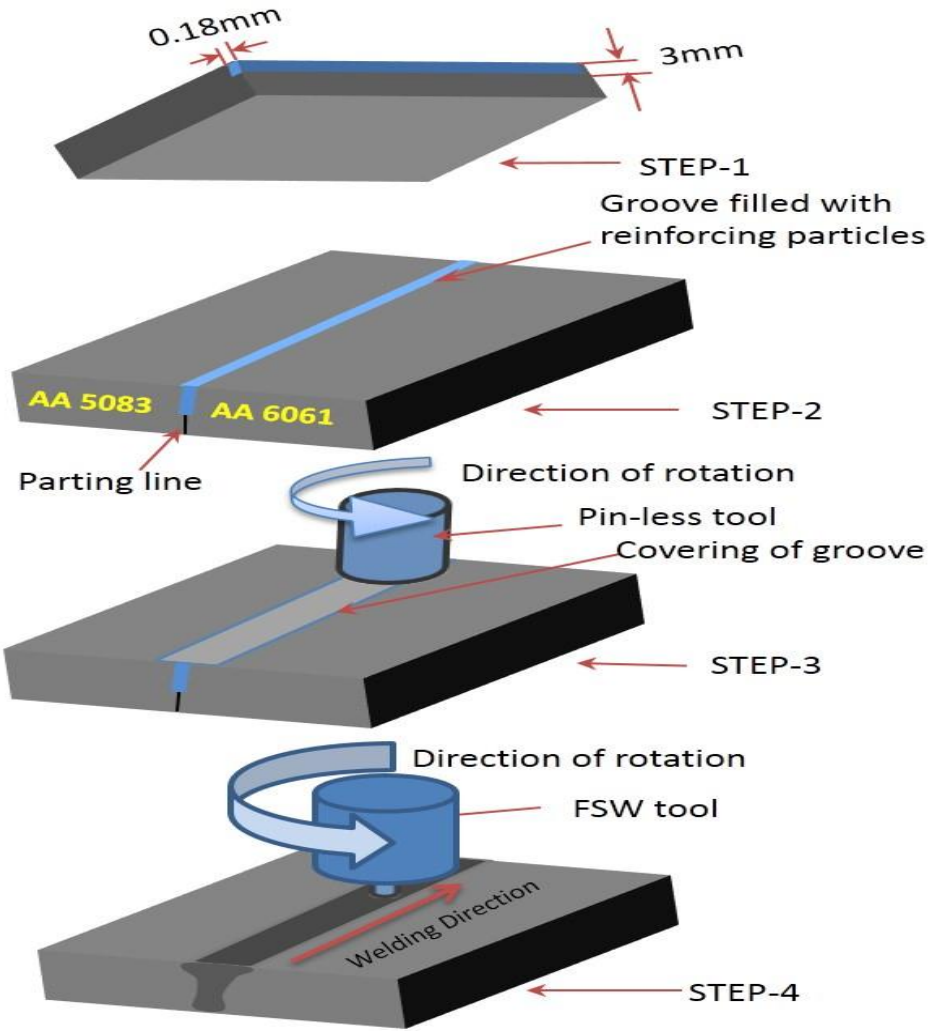

Figure 5.1: Systematic diagram of FSW approach

A non-consumable with threaded profiled pin manufactured of tool steel (H-13) was utilized for experimentation. The input processing parameters for FSW technique have

been taken as rotational speed (750–1150 rpm), traverse speed (25-45 mm/min) and number of FSW passes (1-3).The samples for various testing were extracted from the reinforced FSWed joint using wire-cut CNC EDM. The samples' dimensions for the tensile test were taken in accordance with ASTM E8-standard, as mentioned in the Fig. 5.2. A computer-controlled UTM machine was employed to conduct the tensile tests. Three tensile samples were tested from each reinforced FSWed joint and average result was reported. As per design expert software recommendation, there are twenty FSWed joints embedded with 6% Al_2O_3 micro-particles were fabricated under different processing conditions as depicted in the Fig. 4.13.

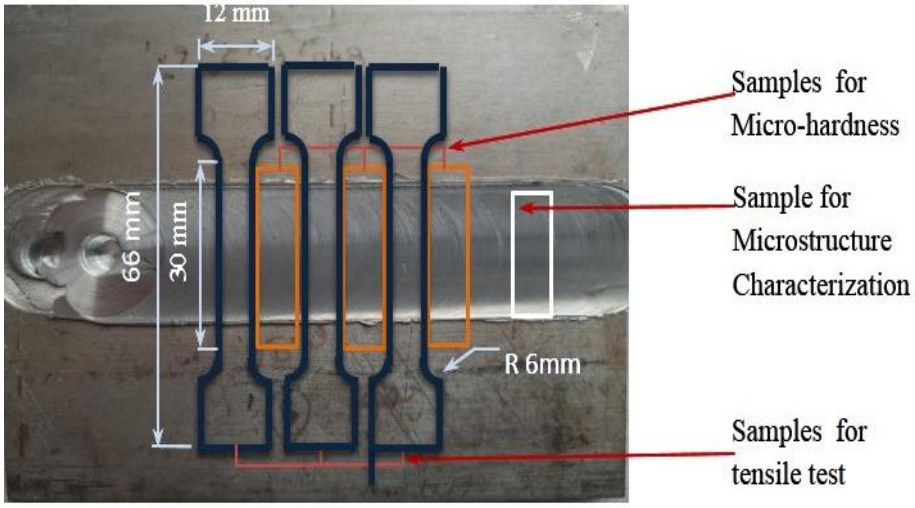

Figure 5.2: Dimension features of various test samples

Various researchers have utilized a variety of experimental design strategies for the development of regression equations but central-reinforced design (CCD) is one of the best and most accurate design approaches [147, 148]. To obtained the design of experiments (DOE) based on face centered full-factorial CCD, the process parameters and their levels were assigned, where the samples upper and lower values were coded as +1 and -1 respectively.

Table 5.1: Processing parameter of FSW-Al_2O_3-mp with their levels

Parameters	Symbols	Units	Range	Levels		
				-1	0	1
Rotational Speed (RS)	A	rpm	750-1150	750	950	1150
Traverse speed (TS)	B	mm/min	40-60	25	35	45
Number of passes (NOPs)	C	-----	1-3	1	2	3

The face centered central reinforced design contains twenty experimental combinations with three independent input parameters namely tool rotational speed (RS), traverse speed (TS) and number of FSW passes (NOPs) with their three levels. The Processing parameter of FSW and their levels are tabulated in Table 5.1.

5.2.1 TENSILE STRENGTH

In order to investigate the influence of rotational speed, traverse speed and number of FSW passes on the tensile properties of dissimilar reinforced FSWed joint of AA5083 and AA6061, embedded with 6% volume fraction of Al_2O_3 micro-particles, the tensile samples were extruded transversely to weld joint using Wire-cut CNC EDM for better dimensional accuracy. The tensile tests were performed on the tensile samples at room temperature and observed the tensile strength of different reinforced joints. The average tensile strength and %elongation of various Al_2O_3-mp reinforced FSWed joints under various parametric conditions were illustrated in Table 5.2.

The tensile strength for as received AA5083 and AA6061 were observed to be 290.20 and 310.04 MPa, respectively, whereas %elongation was observed to be 20 and 21.9 %, respectively. From Table 5.2, it can be observed that the tensile strength of the various reinforced multi-pass FSWed joint is less than the parent metal [149]. The stress- strain plots of the various reinforced joints are depicted Fig. 5.3. The reinforced joints' tensile strengths ranged from 178.95 MPa to 254.42 MPa, as depicted in Fig. 5.4. Grain size was the main factor in determining the mechanical properties of the FSWed joint when no reinforcing particles were used. But with the addition of Al_2O_3-mp particles, additional factors like RPs size, the strength of the bonding between the matrix and the precipitates, RPs dispersion pattern, and the location created by the matrix's uneven thermal expansion coefficient all contribute to the mechanical properties of the reinforced FSWed joint [150]. The bonding between the RPs and the parent metal, dislocation density, and grain size all affect the reinforced FSWed joint's tensile strength [151]. The reinforced FSWed joints produced at lower RS of 750 rpm, higher TS of 45mm/min after one FSW pass (specimen no. 19) exhibited lower tensile strength due to clustering of Al_2O_3-mp caused by inadequate material mixing due to insufficient plastic strain as low rotational speed. The smaller clusters of Al_2O_3-mp were observed after two and three FSW passes at lower RS of 750 rpm due to repeated plastic strain resulting in breaking of clusters of Al_2O_3-mp.

Table 5.2: Mechanical properties of various reinforced FSWed joints

Specimen no.	Process parameters			Response parameters			
	RS (rpm)	TS (mm/min)	NOPs	UTS (MPa)	Joint efficiency (%)	%elongation (%)	Micro-hardness (HV)
1	750	45	3	203.34	70.07	20.6	103.0
2	750	25	3	210.65	72.59	20.0	108.1
3	950	35	2	236.62	81.54	26.9	116.1
4	950	45	2	231.56	79.79	24.6	110.3
5	1150	25	1	216.43	74.58	23.8	109.2
6	950	35	2	239.66	82.58	27.1	116.9
7	1150	35	2	226.54	78.06	25.1	112.1
8	950	35	2	238.98	82.35	27.3	116.6
9	950	35	3	254.42	87.67	29.8	124.2
10	1150	45	3	246.64	84.99	27.5	107.2
11	750	35	2	193.43	66.65	19.3	102.2
12	1150	25	3	240.84	82.99	28.2	119.5
13	950	25	2	239.56	82.55	27.2	118.2
14	950	35	2	241.64	83.27	27.1	117.4
15	950	35	2	239.67	82.59	28.1	114.9
16	950	35	1	230.28	79.35	25.6	113.2
17	750	25	1	186.56	64.29	18.2	95.1
18	1150	45	1	210.32	72.47	21.3	104.3
19	750	45	1	178.95	61.66	17.1	96.5
20	950	35	2	239.7	82.60	27.4	115.2

Due to considerable strain being induced by the increased RS of 950 rpm, significant material mixing and uniform dispersion of Al_2O_3-mp were observed. The effective material mixing with uniform dispersion of Al_2O_3-mp was observed in the SZ of reinforced joint produced at RS of 950 rpm, TS of 35 mm/min after three-passes of FSW (specimen no. 9). The increase in the number of FSW passes enhanced the dispersion of RPs in the SZ. More homogenous dispersion of particles provides higher obstacles to prevent grain growth, which further reduces grain size [152].

Because of the pinning effect of uniformly dispersed Al_2O_3-mp and dynamic recrystallization (DRX), which leads to higher grain refinement, specimen no. 9 produced at 950 rpm, 35 mm/min, and three passes of FSW exhibits the finer grains. The grain size in reinforced FSWed joint was very small as compare to base materials because of the presence of Al_2O_3-mp presented in the stir zone which reduced the grain size as per Zener pinning effect [153].Whereas, the grain structure become coarsen at higher RS of 1150 rpm due to the dominating effect of higher heat input in comparison with DRX and pinning effect of Al_2O_3-mp. According to the Hall-patch relation $\sigma_1 = \sigma_i + kd^{(-1/2)}$, tensile strength is inversely related to grain size [154]. Consequently, specimen no. 9 produced at 950 rpm, 35 mm/min after three passes of FSW exhibited the maximum tensile strength of 254.42 MPa with joint efficiency of 87.60%. On the basis of the base material AA5083's tensile strength, the joint efficiency of the reinforced FSWed joints was calculated. The minimum value of tensile strength (178.95 MPa) was observed in the reinforced joint (specimen no. 19) produced at RS of 750 rpm, TS of 45 mm/min after one FSW pass, which is about 61.66 % of the tensile strength of as received AA5083 as tabulated in Table 5.2. The %elongation of reinforced FSWed joints was observed higher than that of as received AA5083 and AA6061, the higher percentage improvement of %elongation of 30.9% was found at RS of 950 rpm, TS of 35 mm/min, after three-passes of FSW (specimen no. 9) which was about 36.07% higher than that of as received AA 5083.

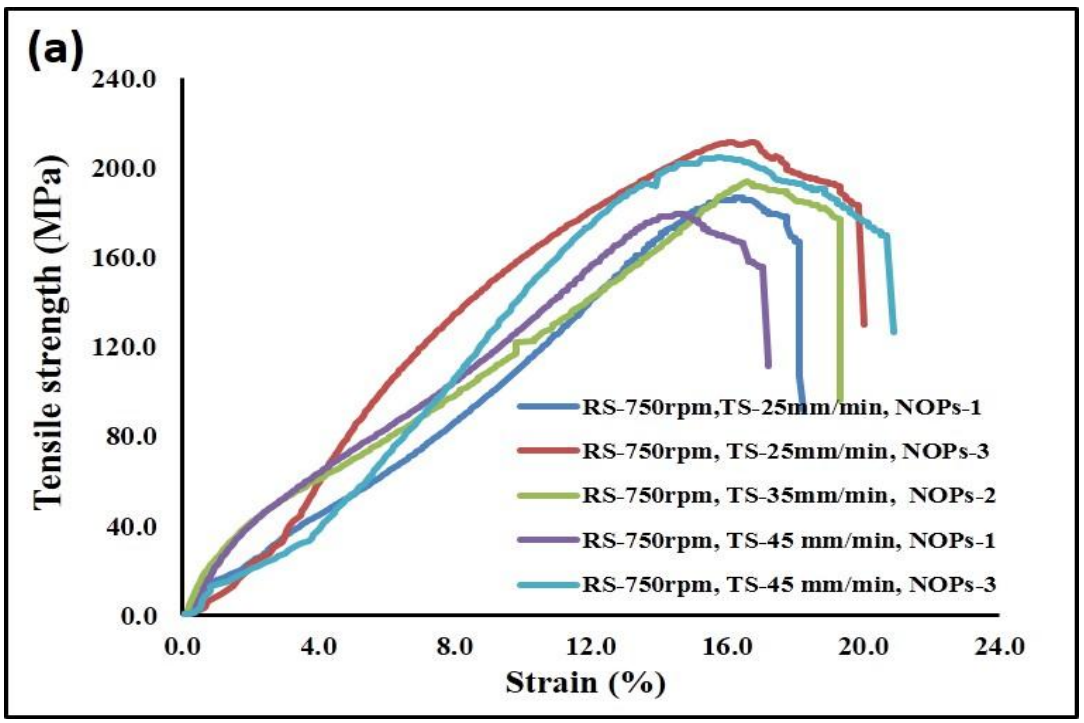

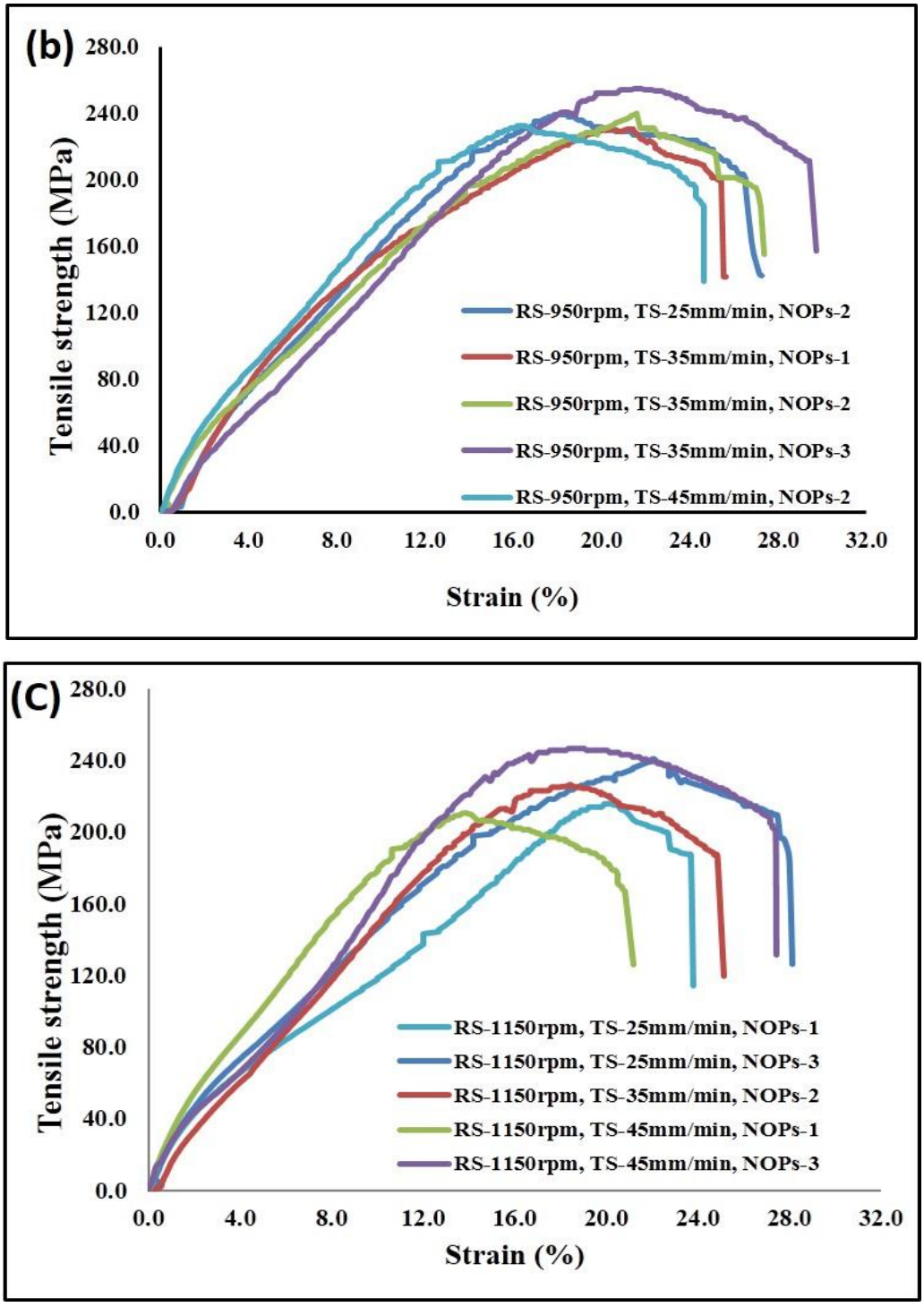

Figure 5.3: Stress-strain plots of reinforced joints produced at, (a) 750 rpm, (b) 950 rpm, (c) 1150 rpm.

The intermetallic particles are considerably refined and evenly distributed throughout the matrix by the FSW passes. The amount of stress imparted on individual particles is significantly reduced by decreasing the aspect ratio and increasing the number of particles per unit area, which enhances the particles' resistance to breaking and/or detaching from the matrix and results in higher ductility [155-157].

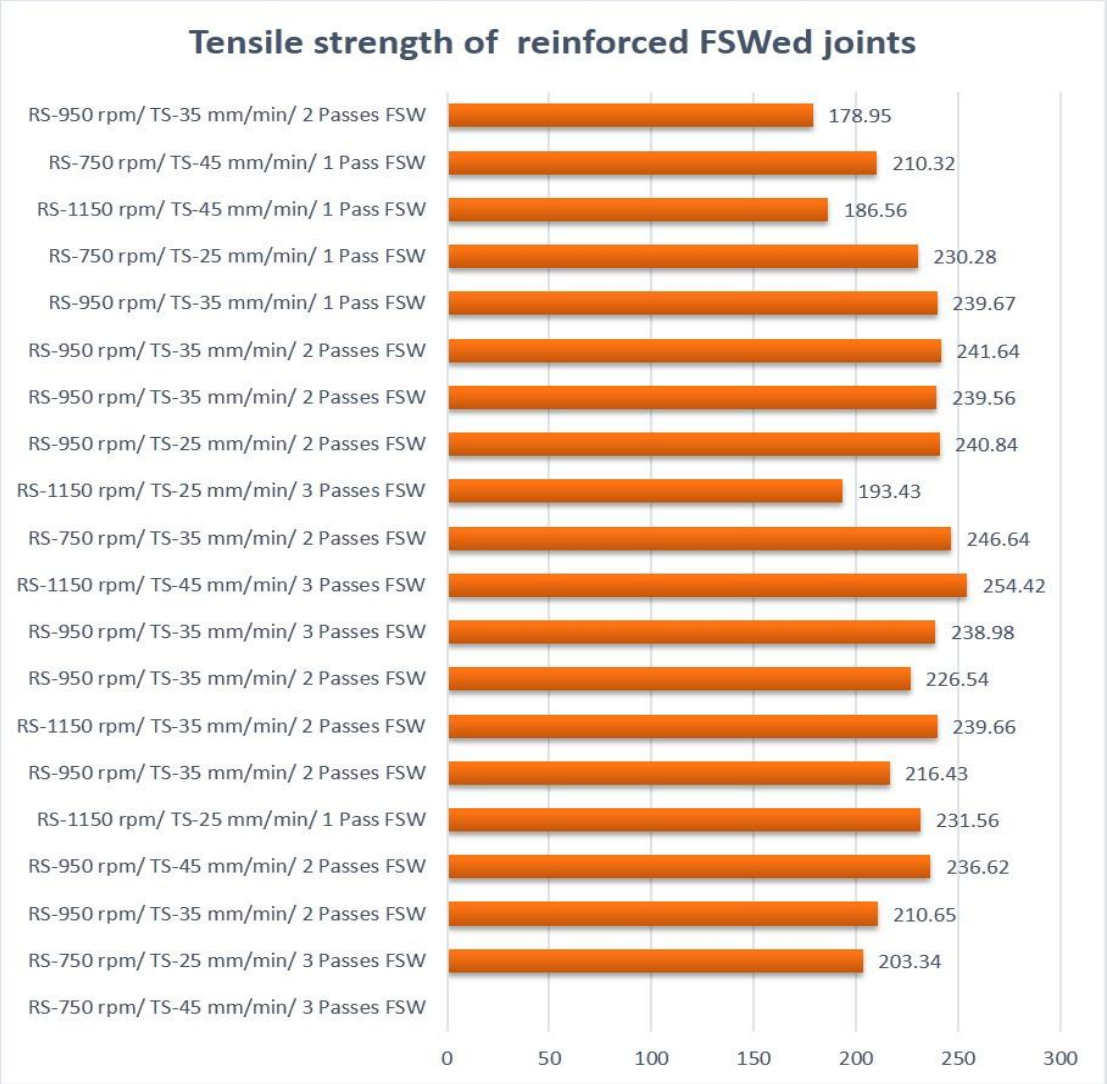

Figure 5.4:UTS of various reinforced FSWed joints

5.2.2 MICROHARDNESS

The variation in microhardness in the processed zone of FSWed reinforced joints of AA6061 and AA5083 processed under various processing conditions was analyzed using Vickers hardness tester, as depicted in Fig. 5.5. The hardness profile was assessed, using a Vickers micro-hardness tester with a gap of 1 mm between the indentations, at a load of 100 gm and dwell time of 15 s. The mean microhardness value at the weld center of all the reinforced FSWed joints is illustrated in Table 5.2. The asymmetric distributions of microhardness in the weld zone as a result of the irregular plastic flow in the processing region's retreating and advancing sides [158]. The microhardness variation from the center of the weld zone towards both sides of all the reinforced joint embedded with 6 % volume fraction of Al_2O_3-mp is delineated in Fig. 5.6 (a-c).

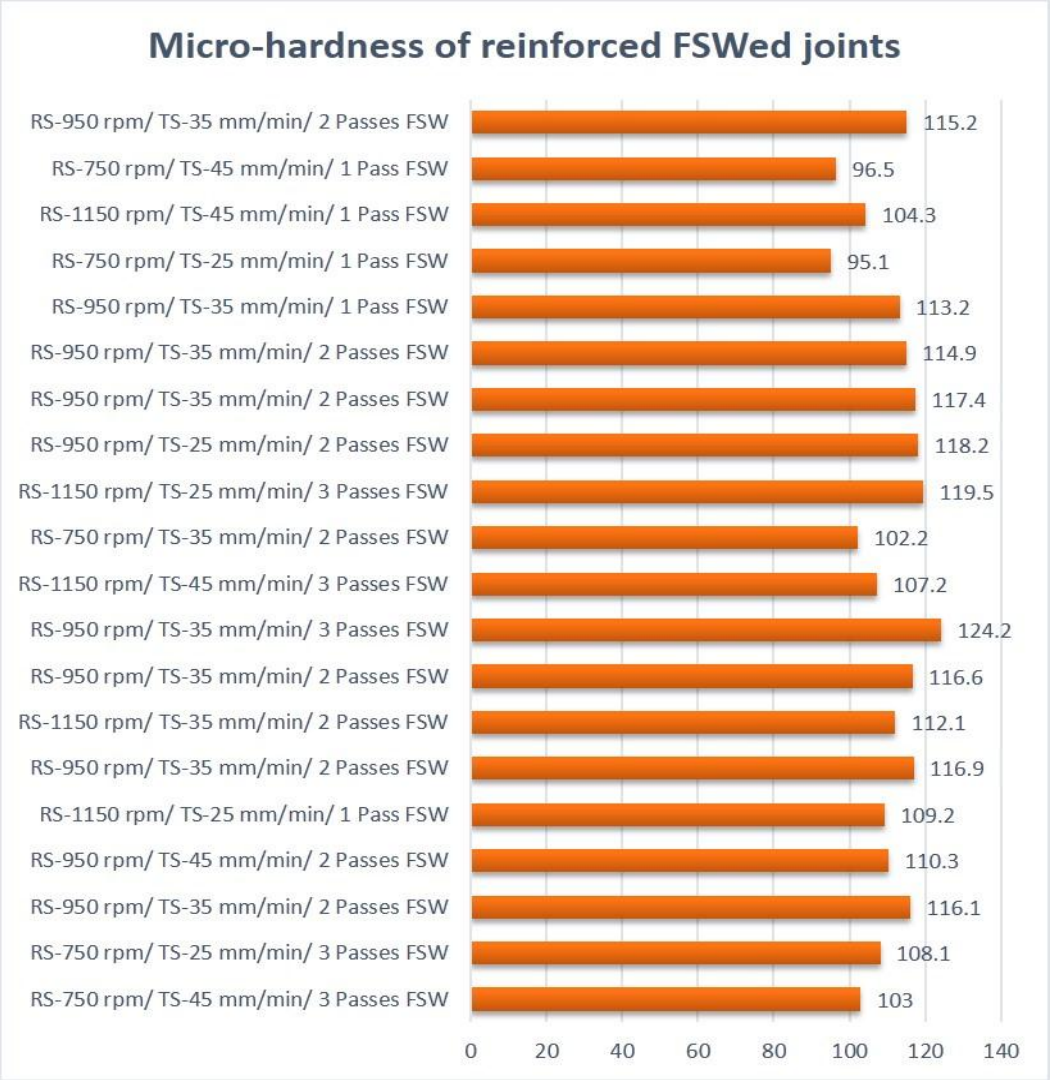

Figure 5.5: Micro-hardness variation to the processing parameters

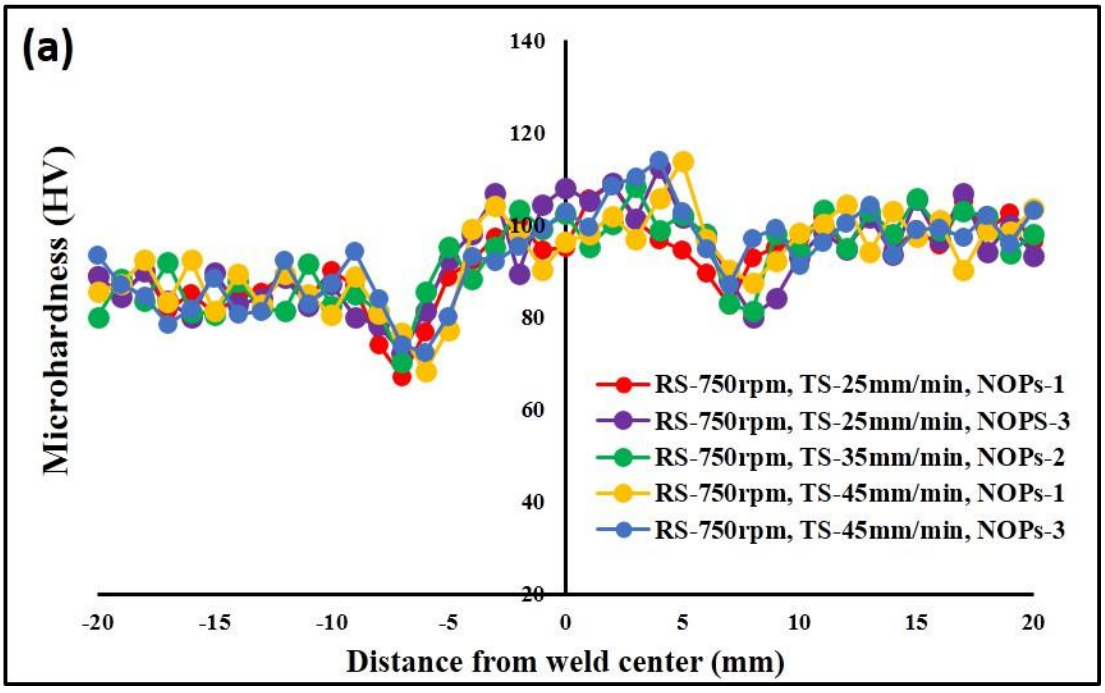

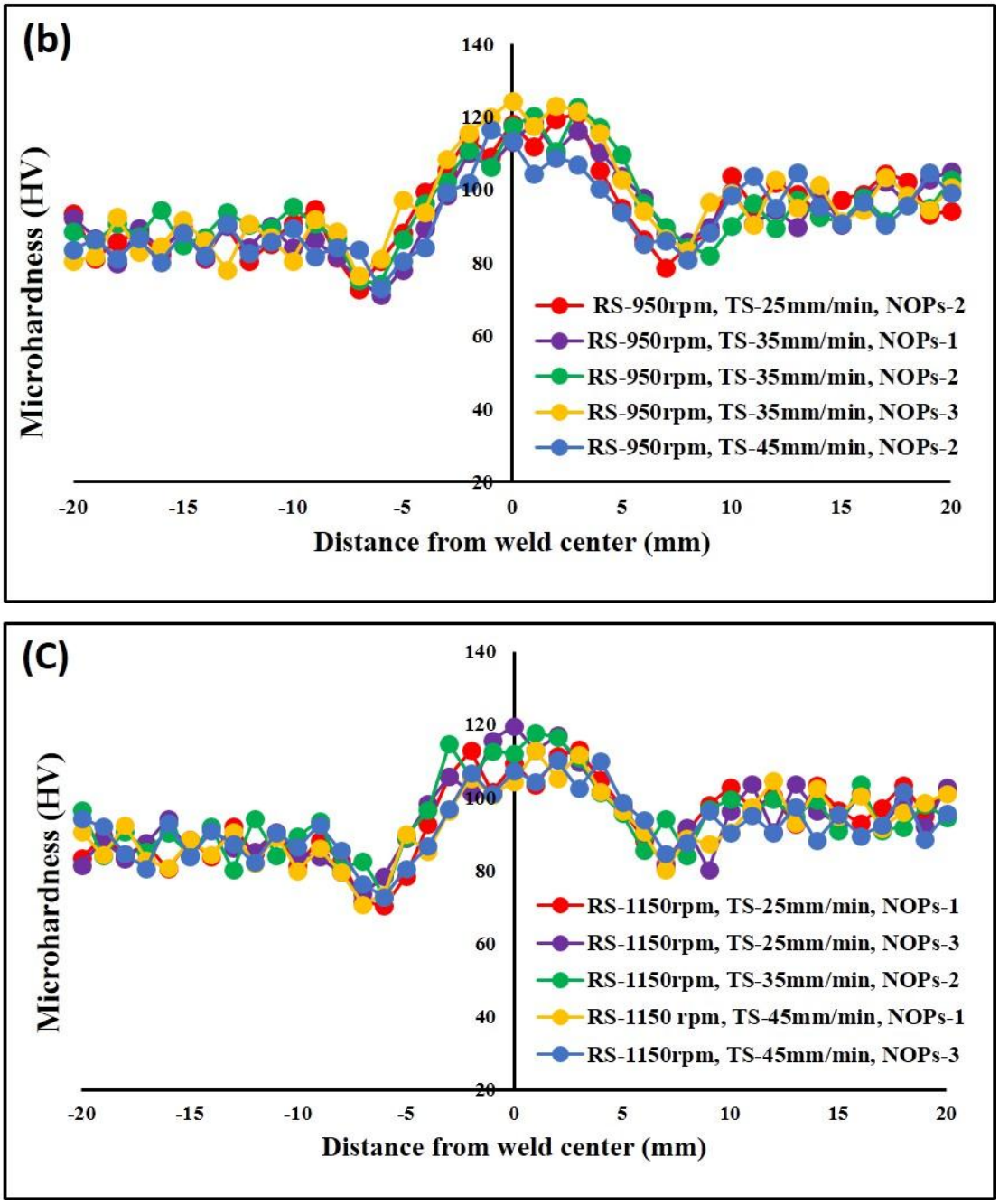

Figure 5.6: Micro-hardness distribution of various reinforced joints, (a) at 750 rpm, (b) at 950 rpm, (d) at 1150 rpm

Base materials, AA5083 and AA6061 exhibited mean micro-hardness values of 85.4 and 98.1 HV, respectively. The microhardness of reinforced joints can be ascribed to heat input, grain refinement and presence of Al_2O_3-mp dislocation density [150]. The minimum hardness of 95.1 HV was found at lower RS of 750 rpm and TS of 25 mm/min after one pass of FSW (specimen no. 17) owing to low heat input and clustering of Al_2O_3-mp. Whereas, the micro-hardness at RS of 950 rpm, TS of 35 mm/min after one and two passes of FSW (specimen no. 16 and 17) was found to be 113 and 117.4 HV,

respectively. Among all the reinforced joint specimens, the FSWed joint (specimen no. 9) produced at TS of 35 mm/min and RS of 950 rpm after three-passes of FSW reveals the maximum microhardness of 124.2 HV due to the dynamic recrystallization, higher grain refinement via pinning effect and enhanced material mixing rule homogenous dispersion of Al_2O_3-mp in the SZ as compared to other FSWed joints. The micro-hardness of the reinforced FSWed joints was also enhanced due to the addition of hard Al_2O_3-mp. The highest micro-hardness was observed in the SZ in comparison with the other adjacent zones due to fine and equiaxed grain structure due to pinning effect of Al_2O_3-mp and dynamic recrystallization, whereas TMAZ and HAZ exhibit low micro-hardness due to coarsening of grain, elevated temperatures, over aging during the FSW [159]. According to the Hall-Patch relation, smaller grains reveal higher hardness [160]. The reinforced FSWed joints produced at higher RS of 1150 rpm, also shows more uniform distribution Al_2O_3 particles. Whereas the microhardness of the SZ reduces due to domination of annealing effect of higher heat input at higher RS of 1150 rpm resulting in coarse grain structure. Therefore, the reinforced FSWed joint produced at TS of 25 mm/min and RS of 1150 rpm after three passes of FSW (specimen no. 12) exhibits lower microhardness of 119.5 HV in the SZ.

5.2.3 DEVELOPING THE MATHEMATICAL MODEL

ANOVA techniques was employed the empirical correlation for the response variable was developed by which are presented in equations. 5.1-5.6. The actual experimental condition of processing parameters and their level as tabulated in Table 5.1. Fisher's F test was used to evaluate the developed models with a confidence level of 95%. The ratio of variance within a factor to variance between factors is known as the F-value. P-value of less than 0.05 is required, P stands for probability. The percentage of the independent factors' impact on the responses is known as contribution and implies the factor’s sensitivity. The output of the response will be significantly changed by changing the value of the factor with the largest percentage contribution. The standard F-value must exceed the estimated F-value in order for the model to be considered adequate. The models are significant when the lack of fit is not significant. Tables 5.3–5.5 provide the results of the ANOVAs for the responses such as, tensile strength, microhardness and %elongation at the stir zone for reinforced FSWed joints.

The final mathematical model equations developed in terms of coded variables are given below.

Tensile strength = $+ 239.00 + 16.78 \times A - 2.32 \times B + 13.33 \times C + 1.83 \times A \times B + 1.53 \times A \times C + 1.53 \times B \times C - 28.46 \times A^2 - 2.88 \times B^2 + 3.91 \times C^2$ (5.1)

%elongation = $+ 27.18 + 3.07 \times A - 0.63 \times B + 2.01 \times C - 0.34 \times A \times B + 0.66 \times A \times C + 0.44 \times B \times C - 4.78 \times A^2 - 1.08 \times B^2 + 0.72 \times C^2$ (5.2)

Micro-hardness = $+116.53 + 4.74 \times A - 2.88 \times B + 4.37 \times C - 1.69 \times A \times B - 0.79 \times A \times C - 1.74 \times B \times C - 9.90 \times A^2 - 2.80 \times B^2 + 1.65 \times C^2$ (5.3)

The final mathematical model equations in terms of actual variables are represented in equations 5.4-5.6.

Tensile strength = $+239.00 + 16.78 \times \text{Rotational speed} - 2.32 \times \text{Traverse speed} + 13.33 \times \text{Number of FSW Passes} + 1.83 \times \text{Rotational speed} \times \text{Traverse speed} + 1.53 \times \text{Rotational speed} \times \text{Number of FSW Passes} + 1.53 \times \text{Traverse speed} \times \text{Number of FSW Passes} - 28.46 \times \text{Rotational speed}^2 - 2.88 \times \text{Traverse speed}^2 + 3.91 \times \text{Number of FSW Passes}^2$ 5.4

%elongation = $+ 27.18 + 3.07 \times \text{Rotational speed} - 0.63 \times \text{Traverse speed} + 2.01 \times \text{Number of FSW Passes} - 0.34 \times \text{Rotational speed} \times \text{Traverse speed} + 0.66 \times \text{Rotational speed} \times \text{Number of FSW Passes} + 0.44 \times \text{Traverse speed} \times \text{Number of FSW Passes} - 4.78 \times \text{Rotational speed}^2 - 1.08 \times \text{Traverse speed}^2 + 0.72 \times \text{Number of FSW Passes}^2$ 5.5

Micro-hardness = $+116.53 + 4.74 \times \text{Rotational speed} - 2.88 \times \text{Traverse speed} + 4.37 \times \text{Number of FSW Passes} - 1.69 \times \text{Rotational speed} \times \text{Traverse speed} - 0.79 \times \text{Rotational speed} \times \text{Number of FSW Passes} - 1.74 \times \text{Traverse speed} \times \text{Number of FSW Passes} - 9.90 \times \text{Rotational speed}^2 - 2.80 \times \text{Traverse speed}^2 + 1.65 \times \text{Number of FSW Passes}^2$ 5.6

Table 5.3: ANOVA table of full quadratic model for tensile strength

Tensile Strength						
Sources	SS	DOF	MS	F value	P value	
Model	8636.77	9	959.64	217.80	< 0.0001	significant
A-RS	2817.03	1	2817.03	639.34	< 0.0001	
B-TS	53.96	1	53.96	12.25	0.0057	
C-NOPs	1778.22	1	1778.22	403.58	< 0.0001	
AB	26.68	1	26.68	6.06	0.0336	
AC	18.76	1	18.76	4.26	0.0660	
BC	18.64	1	18.64	4.23	0.0668	
A^2	2226.78	1	2226.78	505.38	< 0.0001	
B^2	22.82	1	22.82	5.18	0.0461	
C^2	42.02	1	42.02	9.54	0.0115	
Residual	44.06	10	4.41			
Lack of Fit	30.91	5	6.18	2.35	0.1849	not significant
Pure Error	13.15	5	2.63			
Cor. Total	8680.83	19				
SD	2.10	R^2		0.9949		
Mean	225.29	Adjusted R^2		0.9904		
C. V. %	0.93	Predicted R^2		0.9413		
		Adeq. Precision		53.181		

Table 5.4: ANOVA table of full quadratic model for %elongation

%elongation						
Sources	SS	DOF	MS	F value	P value	
Model	273.10	9	30.34	122.64	< 0.0001	significant
A-RS	94.25	1	94.25	380.91	< 0.0001	
B-TS	3.97	1	3.97	16.04	0.0025	
C-NOPs	40.40	1	40.40	163.28	< 0.0001	
AB	0.91	1	0.91	3.68	0.0839	
AC	3.51	1	3.51	14.19	0.0037	
BC	1.53	1	1.53	6.19	0.0321	

A^2	62.88	1	62.88	254.13	< 0.0001	
B^2	3.22	1	3.22	13.01	0.0048	
C^2	1.42	1	1.42	5.73	0.0377	
Residual	2.47	10	0.25			
Lack of Fit	1.59	5	0.32	1.79	0.2701	not significant
Pure-Error	0.89	5	0.18			
Cor. Total	275.58	19				
SD	0.50	R^2		0.9910		
Mean	24.61	Adjusted R^2		0.9829		
C. V. %	2.02	Predicted R^2		0.9559		
		Adeq Precision		37.020		

Table 5.5: ANOVA table of full quadratic model for microhardness

Micro-hardness						
Sources	SS	DOF	MS	F value	P value	
Model	1132.83	9	125.87	93.19	< 0.0001	significant
A-RS	224.68	1	224.68	166.34	< 0.0001	
B-TS	82.94	1	82.94	61.41	< 0.0001	
C-NOPs	190.97	1	190.97	141.38	< 0.0001	
AB	22.78	1	22.78	16.87	0.0021	
AC	4.96	1	4.96	3.67	0.0843	
BC	24.15	1	24.15	17.88	0.0017	
A^2	269.28	1	269.28	199.36	< 0.0001	
B^2	21.49	1	21.49	15.91	0.0026	
C^2	7.53	1	7.53	5.57	0.0399	
Residual	13.51	10	1.35			
Lack of Fit	8.72	5	1.74	1.82	0.2633	not significant
Pure-Error	4.79	5	0.96			
Cor Total	1146.34	19				
SD	1.16	R^2		0.9882		
Mean	111.01	Adjusted R^2		0.9776		
C. V. %	1.05	Predicted R^2		0.9419		
		Adeq Precision		33.467		

The coefficient of tool rotational speed (A) is positive, it implies that higher value of RS, improves the mechanical characteristics of reinforced FSWed joints such as tensile strength, %elongation and microhardness because at lower value of rotational speed produced insufficient plastic strain resulting in agglomeration of Al_2O_3-m pin the stir zone. Whereas increasing value of traverse speed produces the adverse effect on the mechanical characteristics of reinforced joints. The number of FSW passes is also significantly affecting the mechanical characteristics of reinforced joints. The reinforced joints processed under higher number of FSW passes exhibits higher tensile strength, %elongation and micro-hardness. Uniform plastic flow and symmetric microstructure were noticed at higher RS of 950 rpm and after three FSW passes. The heat input and rotational speed are directly related. High heat input at higher rotational speed produces the sufficient strain resulting in proper material flow [161]. Whereas, the increase in traverse speed gives the adverse consequence on mechanical properties of reinforced joints.

Table 5.3-5.5 demonstrated that the F value for tensile strength, microhardness and %elongation are 217.80, 93.19 and 122.64, respectively and indicated that model terms are significant. The P value in mathematical model for RS (A), TS (B) and NOPs (C) for reinforced FSWed joints is less than 0.05 indicating that they are significant. Lack of fit is found not significant in the ANOVA tables 5.3-5.5, as the P-value is higher than 0.1. The R^2 value demonstrates how well the models are fit. Predicted R^2 values for all response parameters are relatively close to adjusted R^2 values. The maximum number of points that can fall within the regression line depends on how closely projected R^2 and modified R^2 values coincide. The main distinction between predicted and adjusted R^2 is that predicted R^2 makes the assumption that each individual variable can account for all of the variation in dependent variable. Only the independent variables that have an actual impact on the dependent variable are revealed by the adjusted R^2. The R^2 value for the tensile strength is 0.9949 reveals 99.49% of the complete variability which is evaluated by the model after taking into account the essential factors. The difference between value of R^2 (99.49%) and adjusted R^2 (99.04%) is 0.45%, indicating that the model does not explain 0.45% of the total variation and the model is not over fitted.

5.2.4 EFFECT ON THE RESPONSE PARAMETERS

Fig. 5.7 depicts the predicted values vs actual experimental values for response parameters including tensile strength, microhardness and %elongation of reinforced FSWed joint incorporated with 6% volume fraction of Al_2O_3-mp.

(a)

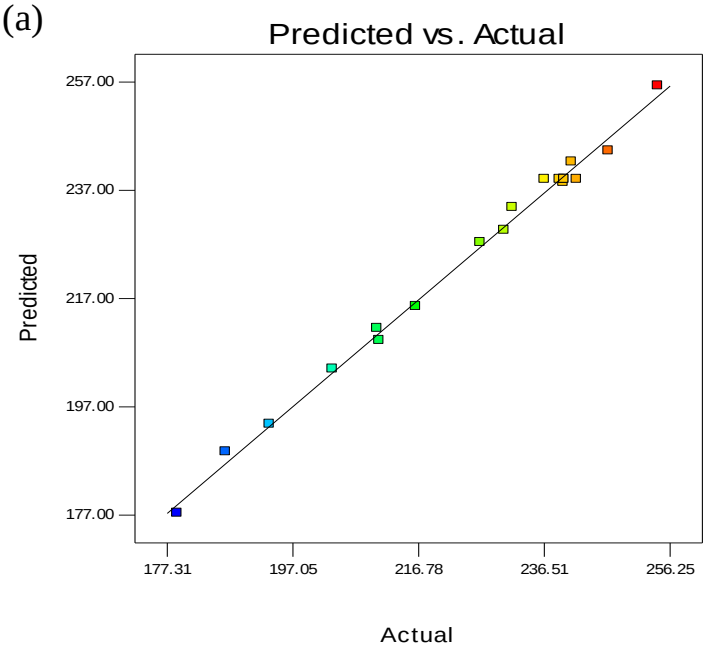

(b)

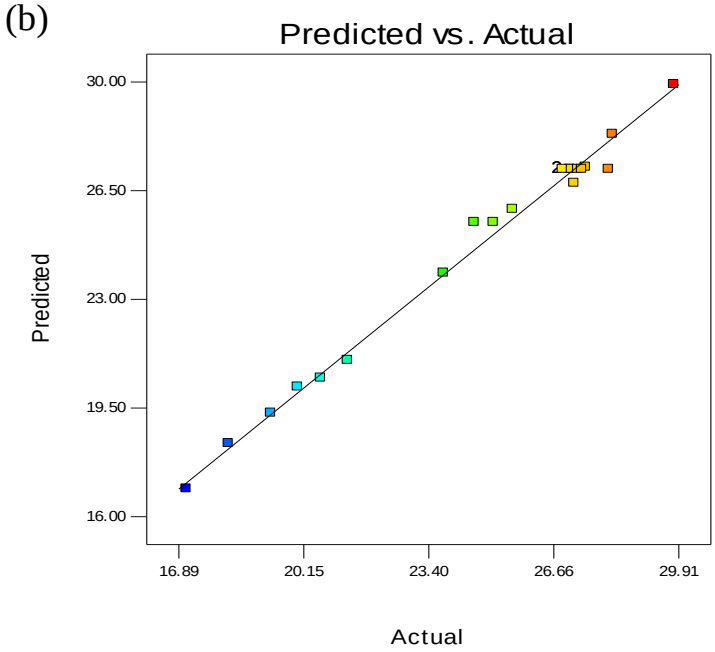

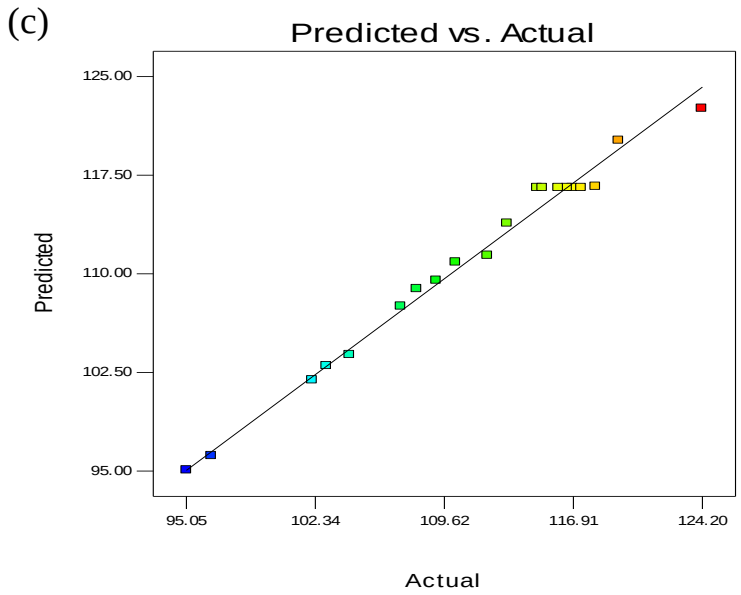

Figure 5.7: Plots between Predicted vs actual values, (a) Tensile strength, (b) %elongation, (c) Microhardness.

The scattered plots show that the response variables are lying very close to the straight lines indicating the uniform scattering of error throughout the model. The plot of the response values' experimental and anticipated values demonstrates remarkable correlation. The aforementioned correlation reveals that the regression models are adequate.

The 3D responses surfaces and contour plots of the regression model for tensile strength, microhardness and %elongation at stir zone are shown in Figs. 5.8-5.10. The apex of the response surfaces represents the optimum output responses. By analyzing the 3D responses surfaces and contour plots, it is easy to examine the impact of different factors on the responses. The significance of grain refinement can be revealed by dynamic recrystallisation and pinning effect caused by Al_2O_3-mp. It was observed that as the RS increases from 750 rpm to 950 rpm, tensile strength, microhardness and %elongation increases due to more uniform dispersion of speed Al_2O_3-mp resulting in enhanced pinning effect and reduced the grain size. Additionally, it was shown that reinforced FSWed joints' tensile strength increased with a decreasing value of TS. Tensile strength (178.95 MPa) and %elongation (17.2%) were both observed to be minimum at lower RS of 750 rpm and higher TS of 45 mm/min and after one FSW pass, whereas as minimum value of microhardness (95.1 HV) was found at lower RS and TS of 750 rpm and 25 mm/min respectively, after one FSW pass due to insufficient mixing of material which caused clustering of Al_2O_3-mp in the SZ.

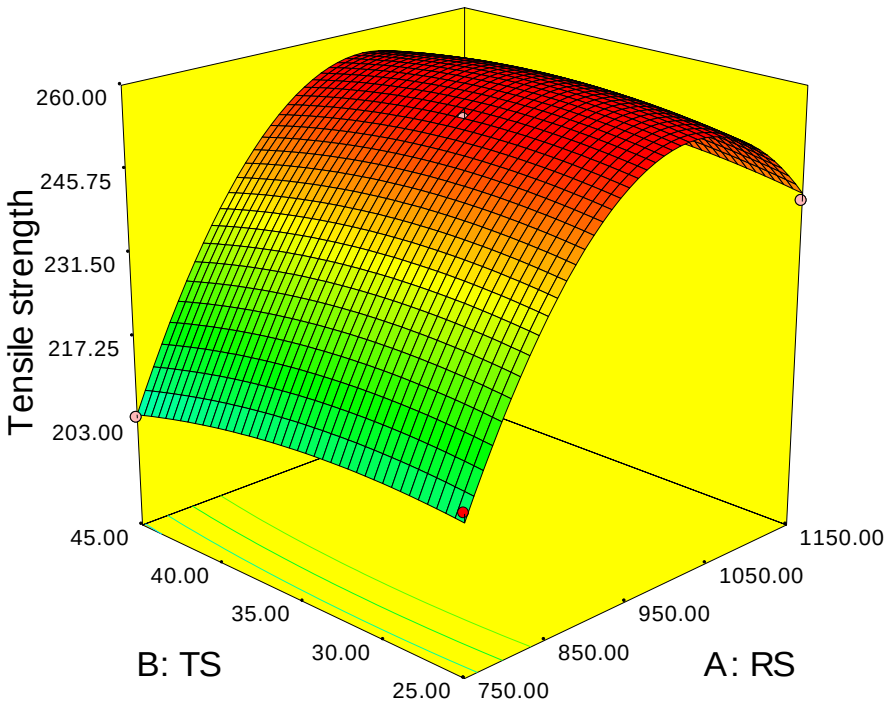
Tensile strength
260.00
245.75
231.50
217.25
203.00
45.00
40.00
35.00
30.00
25.00
B: TS
750.00
850.00
950.00
1050.00
1150.00
A: RS

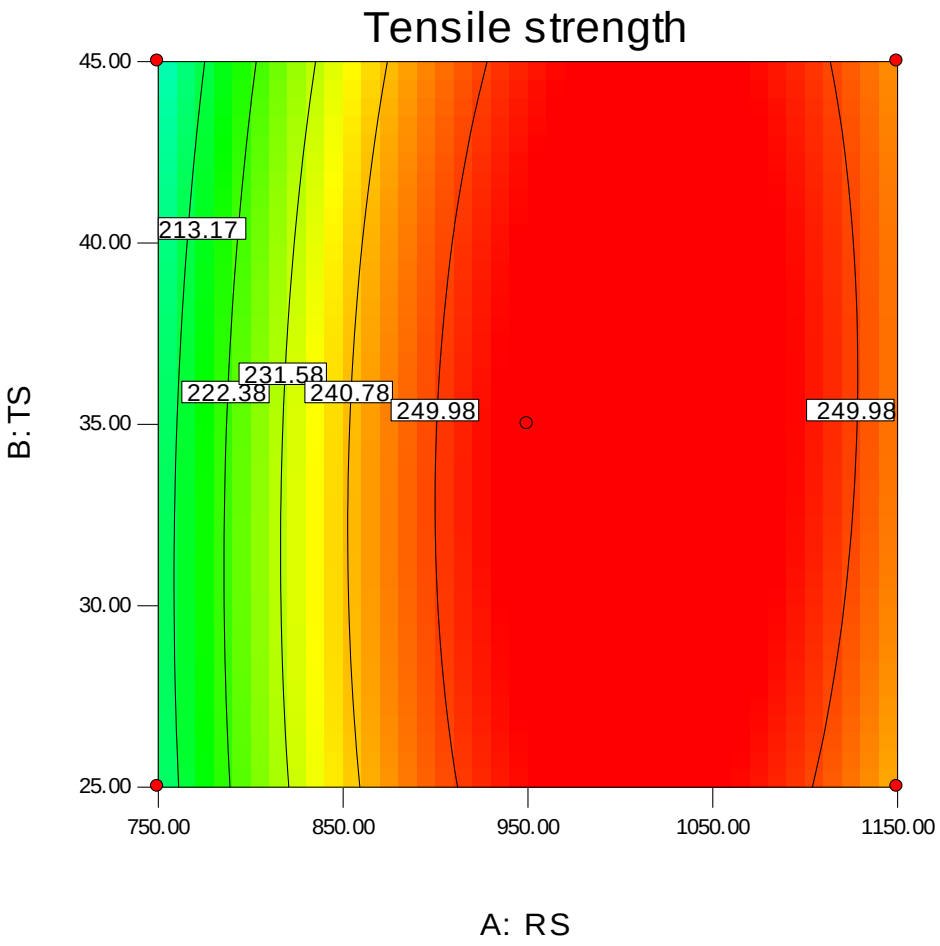
Tensile strength
45.00
40.00
35.00
30.00
25.00
B: TS
213.17
222.38
231.58
240.78
249.98
249.98
750.00
850.00
950.00
1050.00
1150.00
A: RS

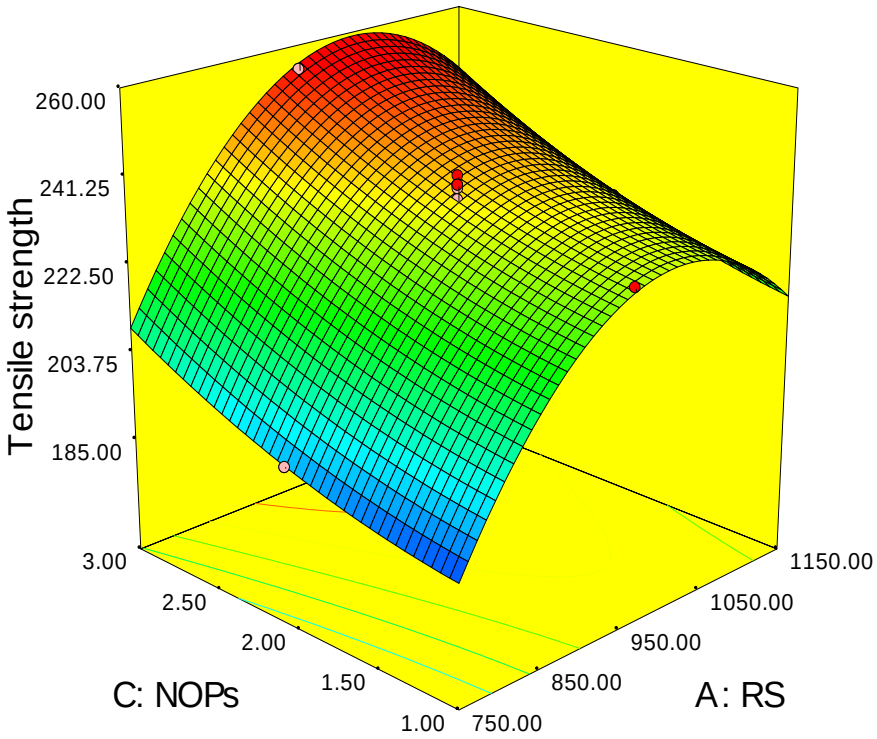
Tensile strength
260.00
241.25
222.50
203.75
185.00
3.00
2.50
2.00
1.50
1.00
C: NOPs
750.00
850.00
950.00
1050.00
1150.00
A: RS

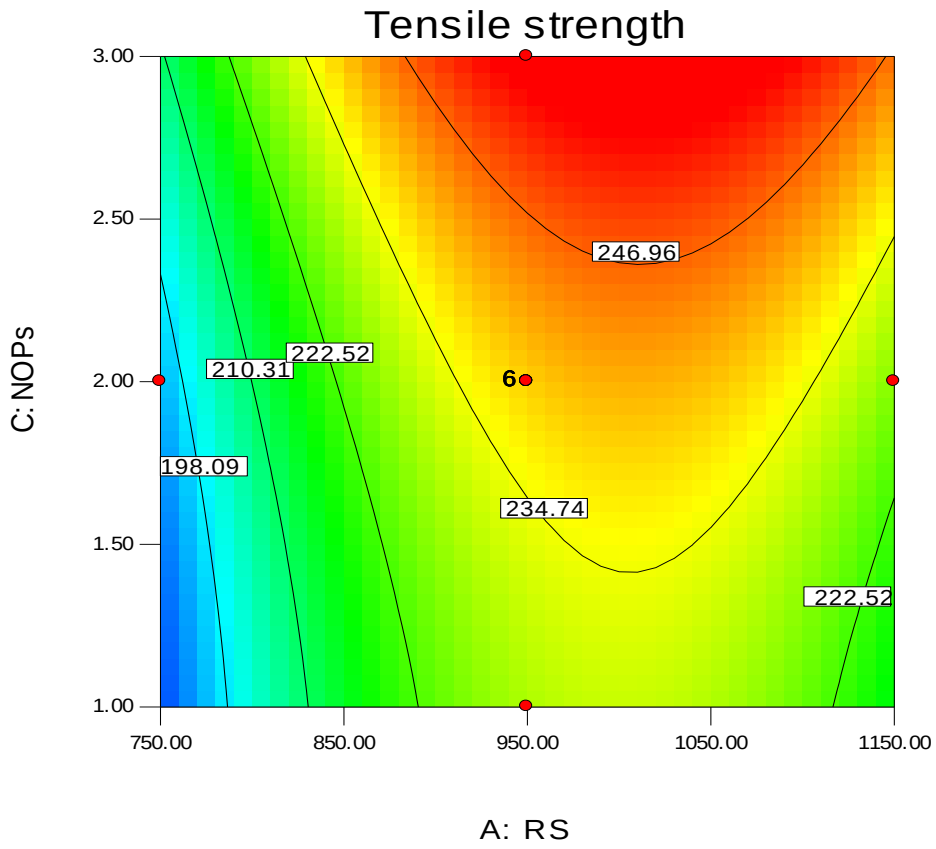
Tensile strength
3.00
2.50
2.00
1.50
1.00
C: NOPs
246.96
222.52
210.31
198.09
234.74
222.52
6
750.00
850.00
950.00
1050.00
1150.00
A: RS

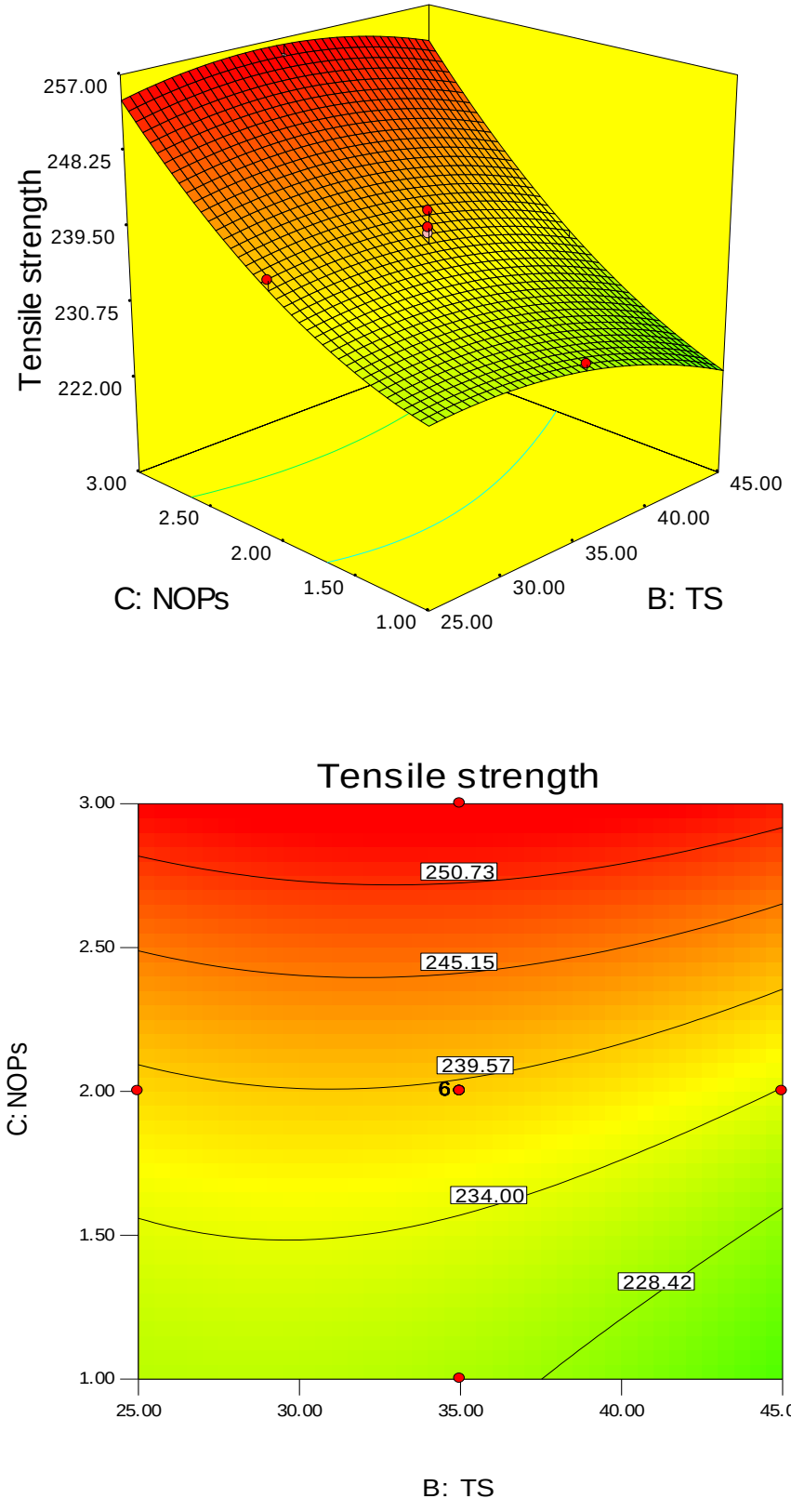

Figure 5.8: 3D response contour and surface plot of tensile strength of reinforced FSWed joint embedded with Al_2O_3-mp

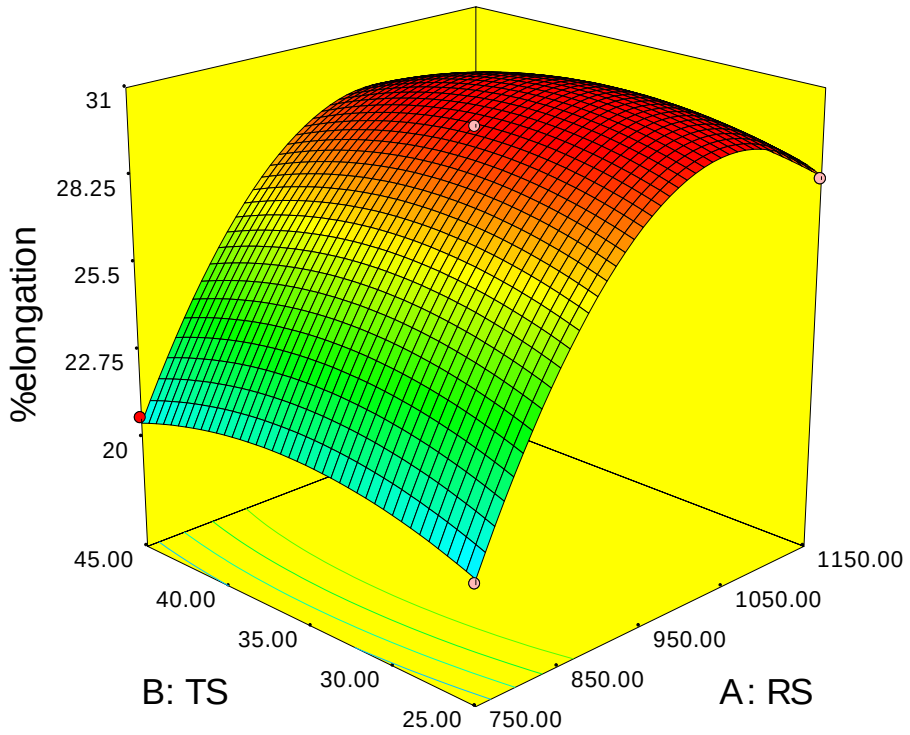
%elongation
31
28.25
25.5
22.75
20
45.00
40.00
35.00
30.00
25.00
B: TS
750.00
850.00
950.00
1050.00
1150.00
A: RS

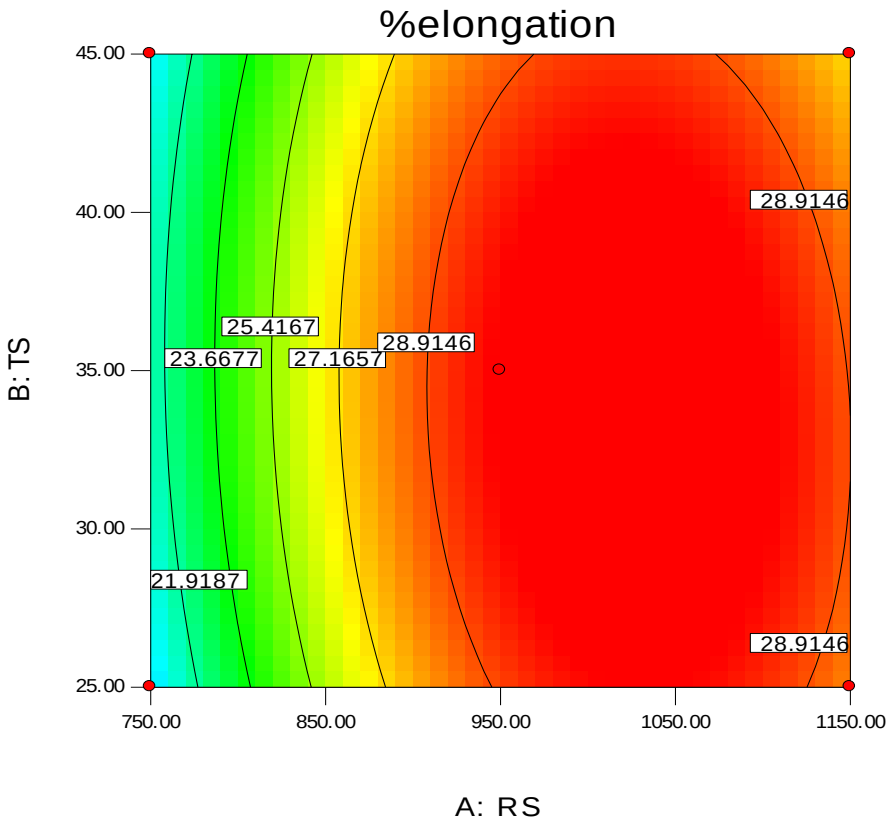
%elongation
45.00
40.00
35.00
30.00
25.00
B: TS
28.9146
25.4167
23.6677
27.1657
28.9146
21.9187
28.9146
750.00
850.00
950.00
1050.00
1150.00
A: RS

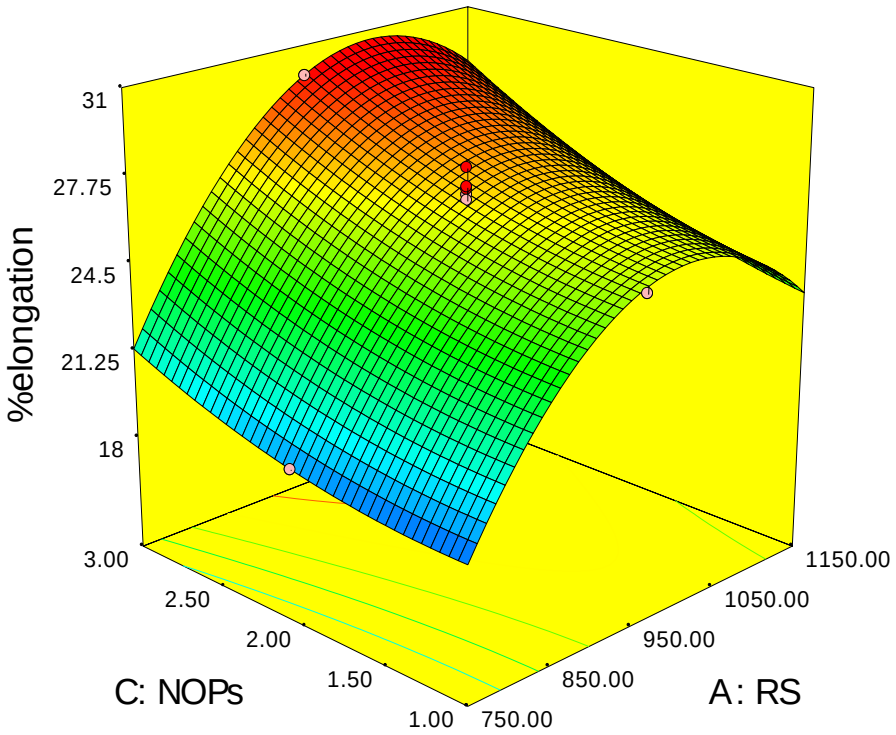
%elongation
31
27.75
24.5
21.25
18
3.00
2.50
2.00
1.50
1.00
C: NOPs
750.00
850.00
950.00
1050.00
1150.00
A: RS

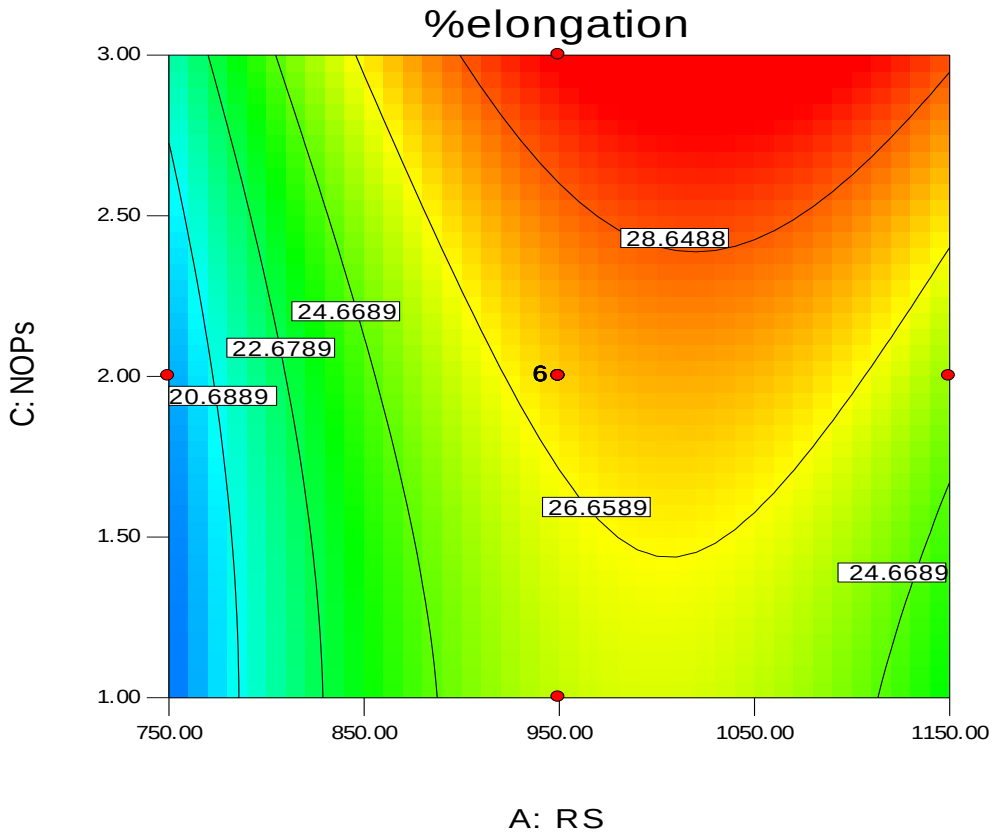
%elongation
3.00
2.50
2.00
1.50
1.00
C: NOPs
28.6488
24.6689
22.6789
20.6889
6
26.6589
24.6689
750.00
850.00
950.00
1050.00
1150.00
A: RS

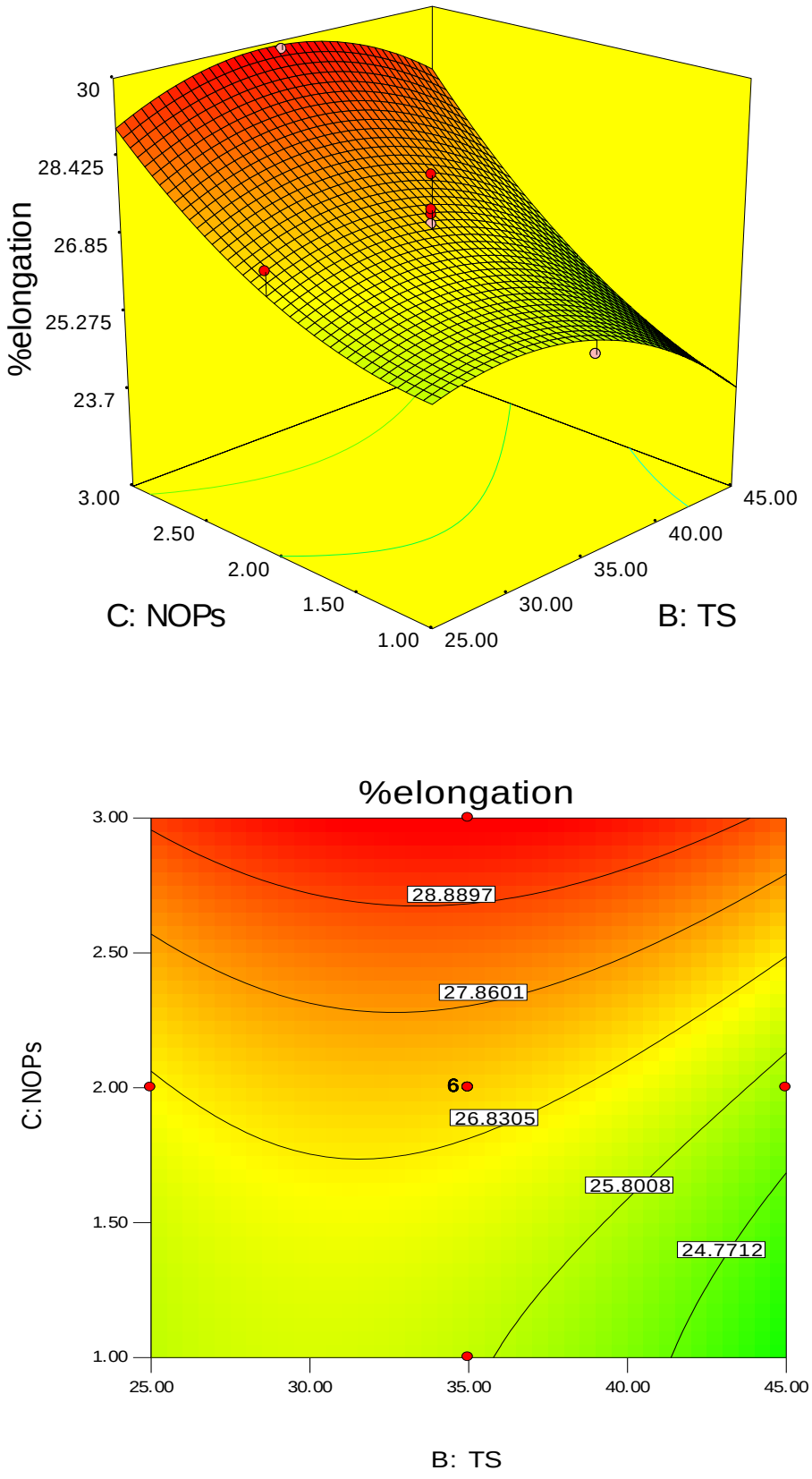

Figure 5.9: 3D response contour and surface plot of %elongation of reinforced FSWed joints embedded with Al_2O_3-mp

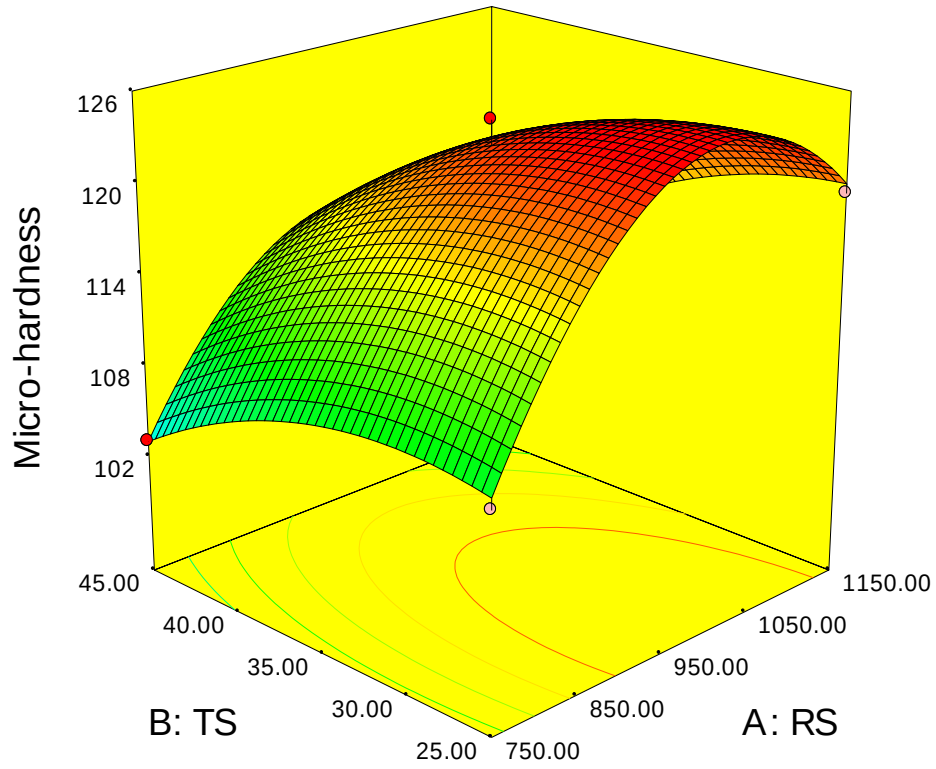
Micro-hardness
126
120
114
108
102
45.00
40.00
35.00
30.00
25.00
B: TS
750.00
850.00
950.00
1050.00
1150.00
A: RS

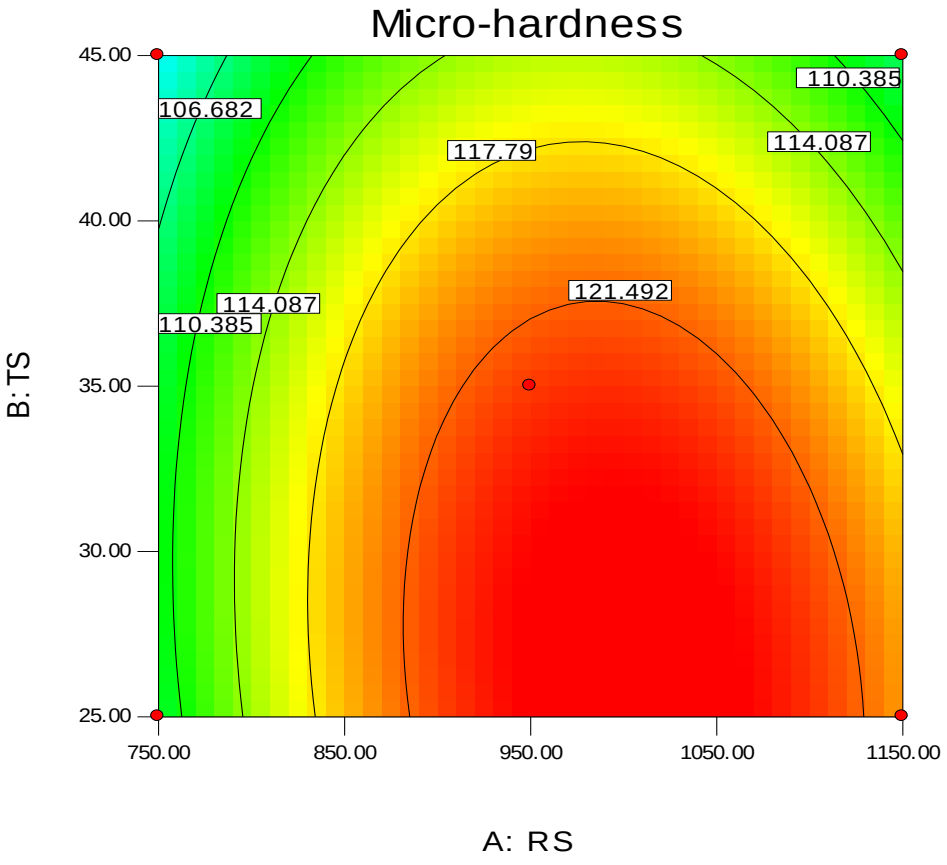
Micro-hardness
45.00
40.00
35.00
30.00
25.00
B: TS
106.682
110.385
114.087
117.79
121.492
114.087
110.385
750.00
850.00
950.00
1050.00
1150.00
A: RS

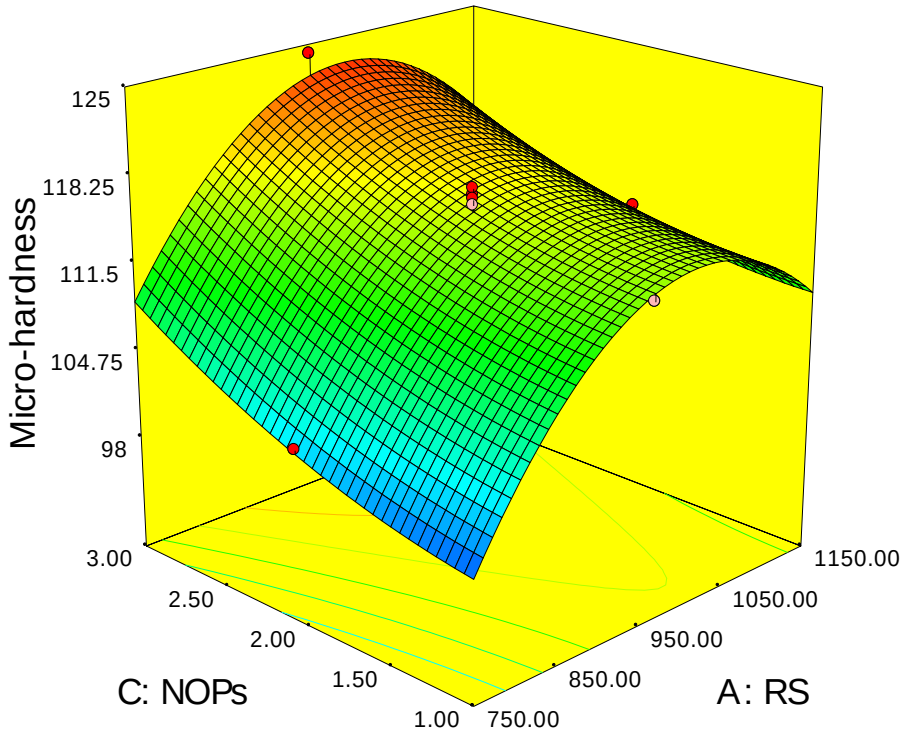
Micro-hardness
125
118.25
111.5
104.75
98
3.00
2.50
2.00
1.50
1.00
C: NOPs
750.00
850.00
950.00
1050.00
1150.00
A: RS

`

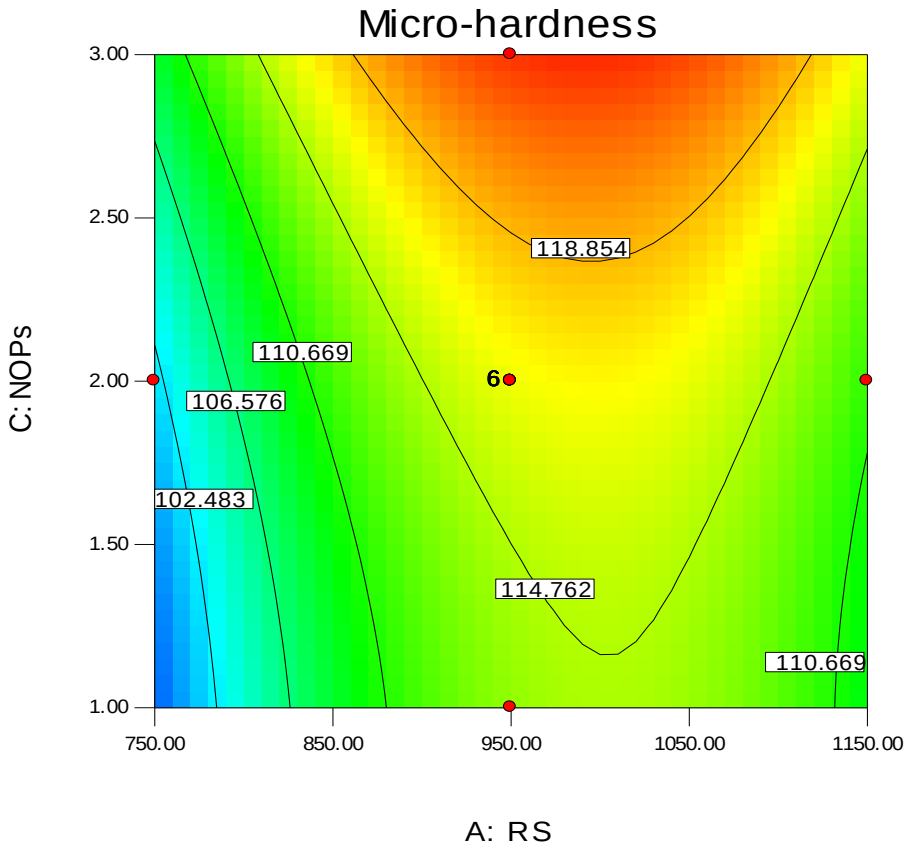
Micro-hardness
3.00
2.50
2.00
1.50
1.00
C: NOPs
118.854
110.669
106.576
102.483
114.762
110.669
6
750.00
850.00
950.00
1050.00
1150.00
A: RS

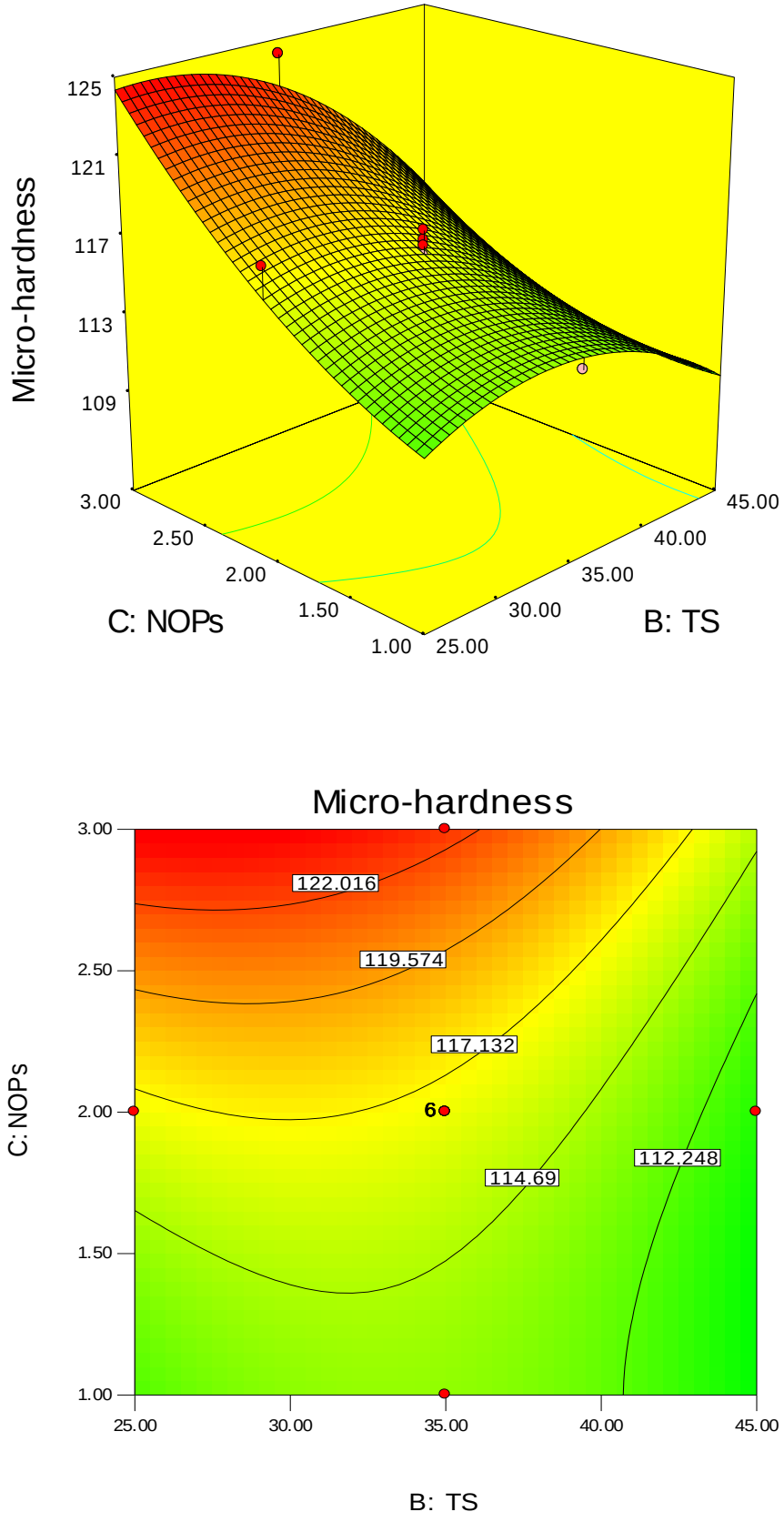

Figure 5.10: 3D response contour and surface plot of micro-hardness at SZ of reinforced FSWed joints embedded with Al_2O_3-mp

The maximum value of tensile strength (254.42 MPa), microhardness (124.5 HV) was observed at 950 rpm, 35 mm/min after three passes of FSW. On increasing the value of traverse speed, the tensile strength decreases, whereas microhardness and %elongation first increases from 25mm/min to 35mm/min and then decreases from 35 to 45 mm/min. The increased number of FSW passes enhanced the microhardness, tensile strength and %elongation of reinforced joints as shown in Fig. 5.8-5.10.

5.3 MULTI RESPONSE OPTIMIZATION: DESIRABILITY

5.3.1 DESIRABILITY FUNCTION

Desirability is a multiple response technique that was explained by Derringer and Suich [162]. This method is used to optimize a variety of quality characteristic issues that are essential to industry. The approach converts a predicted response into a scale-free value (di) called desirability, using desirability function. The geometric mean of weightage of each response's individual desirability is known as the composite desirability. The ideal parameter circumstances are regarded to be the factor settings that have the highest overall desirability. The optimization is carried through using:

(i) Determining each response's specific desirability (d);

(ii) Obtained the reinforced desirability (D) by combining each response's specific desirability;

(iii) Finding the optimal settings by maximizing the obtained reinforced desirability.

In the present investigation, desirability function is employed to obtained the optimal parameters for reinforced FSWed joints to optimize responses. In order to recognize the optimal combination of variables and their levels for friction stir welding of AA6061 and AA5083, a second order CCD with three input variables (RS, TS and NOPs) with three levels was utilized. The desirability function was used to achieve the multi-response optimization.

5.3.2 MULTI-RESPONSE OPTIMIZATION

To resolve the problems with single-response optimization of contradictory responses, multi- response optimization was performed using RSM. To effectively assess the effect of each response on overall desirability, limits and goals for each response were

specified. Weights are applied in order to highlight a goal value, the upper or lower boundaries, or both. According to the particular industry, importance is allocated. Importance varies 1 to 3, 1 is allocated for the least important and 3 to the most important.

The goals and importance of processing parameters such as RS, TS and NOPs, and the response parameters like tensile strength, microhardness and %elongation are tabulated in Table 5.6. Tensile strength, %elongation and micro-hardness all have been assigned with an importance of 3, lower and upper weight for tensile strength, %elongation, micro-hardness is to be assigned 1. Finding an optimal setting of parameters that will meet all the goals is the major objective of optimization process. The value of desirability does not mandatory to be 1 as if the any one response is increases then the other decreases. For the given design space constraints, seven optimal solutions are derived as tabulated in Table 5.7. The set of optimal parameters having higher desirability required for get the desired response parameters within the constraints is tabulated in Table 5.7.

The ramp function graph (Figures 5.11) derived from Design Expert (7) software, demonstrates the desirability for tensile strength, %elongation and microhardness. Each ramp's dot indicate the response characteristic's factor setting or response prediction. The height of the dot indicates how desired it is. Since each parameter's weight was set to 1, a linear ramp function was established. The range of desirability, ranging 0 to 1, depends on how closely the response comes to achieving the target.

Table 5.6: Range and importance of Input and Response Parameters for Desirability

Name	Goal	Lower Limit	Upper Limit	Lower Weight	Upper Weight	Importance
RS	is in range	750	1150	1	1	3
TS	is in range	25	45	1	1	3
NOPs	is in range	1	3	1	1	3
Tensile strength	maximize	178.95	254.42	1	1	3
%elongation	maximize	17.2	30.9	1	1	3
Microhardness	maximize	95.1	124.2	1	1	3

Table 5.7: Set of Optimal Solutions

Number	RS	TS	NOPs	Tensile strength	%elongation	Micro-hardness	Desirability	
1	**995.38**	**29.79**	**2.99**	**258.09**	**31.31**	**124.70**	**1**	**Selected**
2	980.95	31.35	2.98	257.71	31.16	124.23	1	
3	1007.92	25.71	2.99	256.55	30.94	124.91	1	
4	1029.71	30.25	3.00	258.29	31.58	124.37	1	
5	1010.61	31.85	3.00	258.88	31.56	124.20	1	
6	1020.50	33.75	3.00	259.08	31.58	123.40	0.991	
7	958.56	34.21	3.00	256.94	30.90	123.28	0.989	

3D-plots of desirability were first developed with input parameters and tensile strength, %elongation and micro-hardness at maximum. Employing this methodology, several objective functions may be optimized. The desirable value for the optimized input and responses parameters is 1.

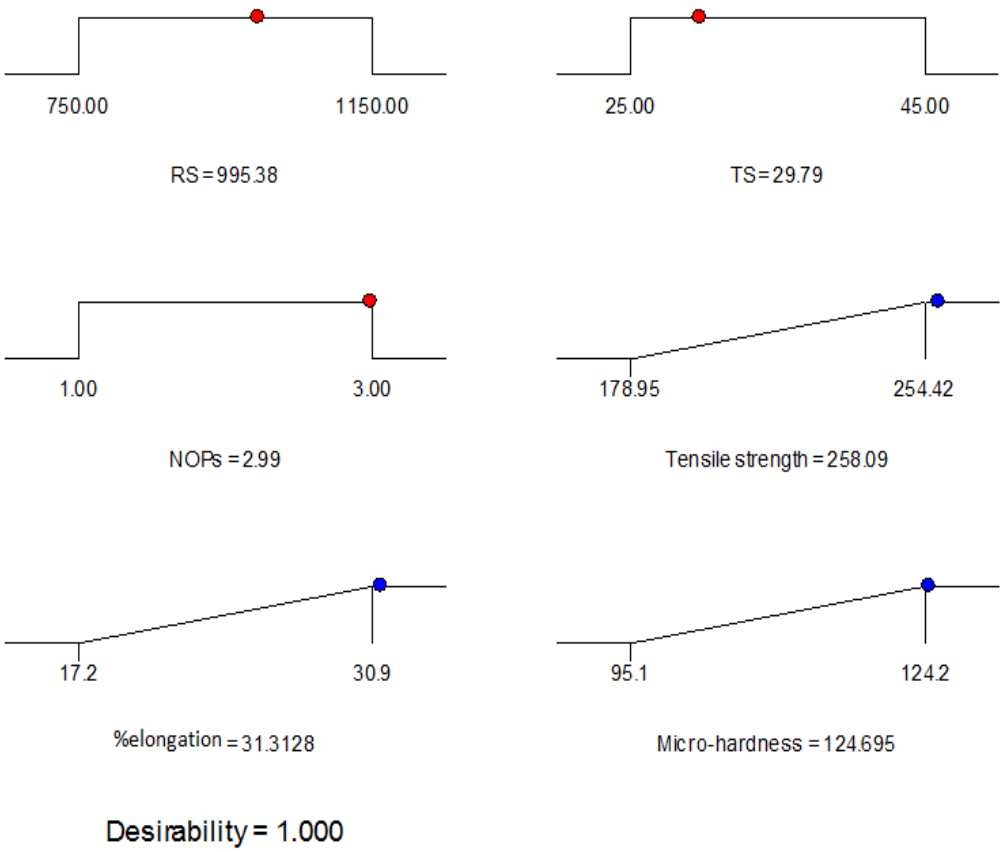

Figure 5.11: Ramp fraction plots of multi response optimization

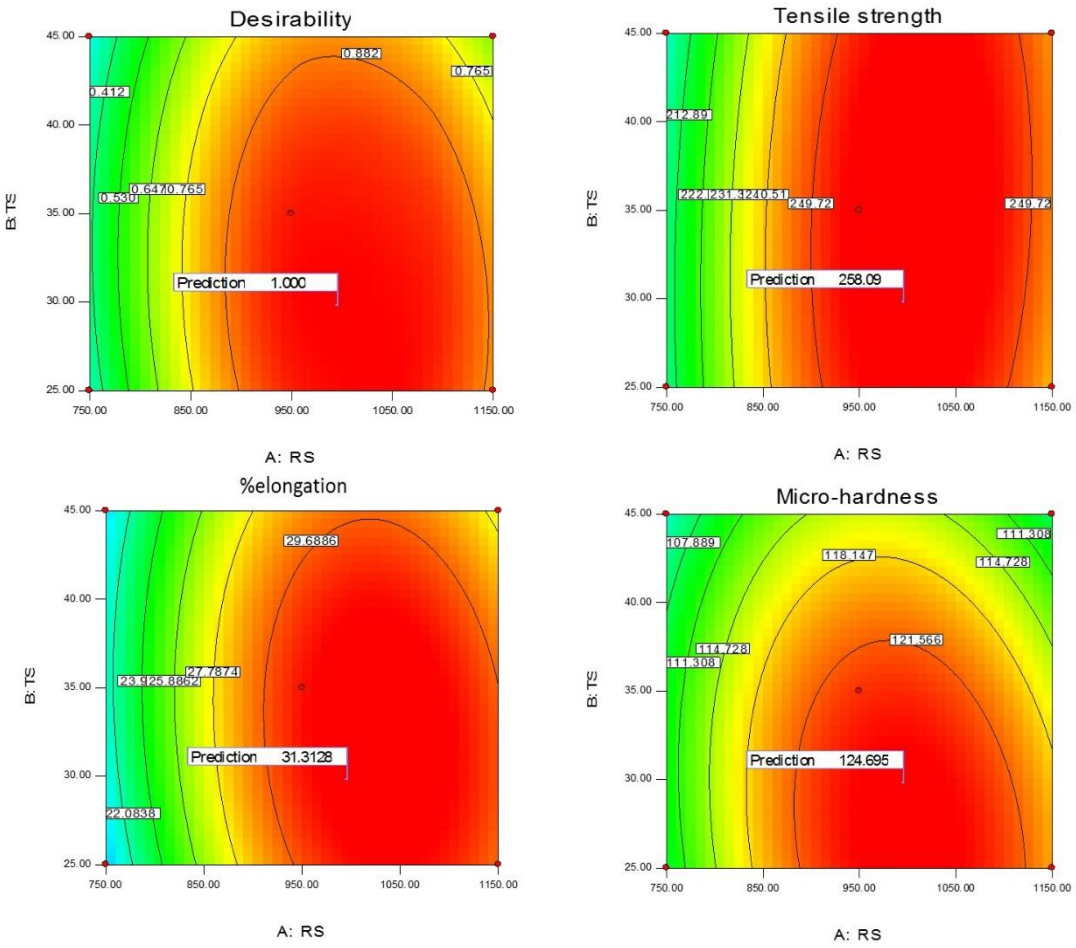

Figure 5.12: Optimized out responses of reinforced FSWed joints embedded with Al_2O_3-mp

The multi-optimized value of response parameters such as tensile strength, microhardness at the SZ and %elongation are 258.09 MPa, 124.70 HV and 31.31%, respectively, whereas the optimum value of process variables such as RS, TS and NOPs are 995.38 rpm, 29.79 mm/min and three passes of FSW, respectively as depicted in Fig. 5.11. Fig. 5.12 shows the desirability plots of desired responses for reinforced joints of AA 6061 and AA5083, according to RS, TS and NOPs. It can be shown that overall desirability is first increases with increasing the RS and then decreases. As the TS decreases, the desirability increases as shown in Fig. 5.12.

5.4 MICROSTRUCTURAL ANALYSIS OF REINFORCED FSWED JOINTS EMBEDDED WITH AL_2O_3-mp

The study related with particle distribution and grain structure in the stir zone under various process conditions was performed to investigate the influence of microparticles of Al_2O_3 along with multi-pass FSW on microstructural refinement. Fig. 4.3 a and d

show the optical micrographs of the base metals AA6061 and AA5083, which have average grain sizes of ~37 and ~41 m, respectively. ImageJ software was used to evaluate the average grain size. Due to severe plastic deformation and dynamic recrystallization (DRX), the weld zone of AA5083 and AA6061 after FSW was refined in the stir zone (SZ), heat affected zone (HAZ) and thermo mechanical affected zone (TMAZ) [163]. By adding reinforcing particles and increasing the number of passes, the grain size in the SZ may be further diminished [164]. Compared to the TMAZ and HAZ, the SZ exhibited a higher level of grain structure refinement [165].

Grain size was the most significant factor of the mechanical properties of an unreinforced FSWed joint. whereas, other parameters, such as the size of the RPs, the bonding quality between the matrix and the RPs, the RPs dispersion pattern, and the location produced by matrix's unequal thermal expansion coefficient, all contribute to the mechanical characteristics of the reinforced FSWed joint [166]. After FSW, the stretched microstructure of AA6061 and AA5083 was turned into dynamically recrystallized equiaxed grains structure in the SZ by the tool's stirring action. The annealing effect, DRX, and the influence of dispersion pattern of RPs in the metal matrix of the SZ all contribute to grain refining during FSW. All of these phenomena compete for dominance, and the grain size is determined by the dominant factors. DRX caused by plastic deformation at high temperatures, resulting in the conversion of high angle to low angle boundaries and nucleate new grains at preferential locations, reducing grain size. The impact of annealing is caused by a high heat input at higher value of RS and lower value of TS, which promotes grain growth and coarsen the grains [167]. The RPs in the SZ act as barriers to grain boundaries, through pinning effect and impede the grain growth [168]. Consequently, in the reinforced joints produced at different values of RS and TS, the DRX phenomenon and the influence of dispersion pattern of RPs (Al_2O_3-mp) and annealing effect are dominating factors for deciding the grain size [169]. The FESEM micrograph (Fig 5.13 a) of the SZ of specimen no. 19 produced at RS and TS of 750 rpm and 45 mm/min, respectively with one pass of FSW depicts the clusters of Al_2O_3-mp together with poor bonding with surrounding metal matrix caused by unusual material mixing as a result of the insufficient plastic strain at low RS value [170].

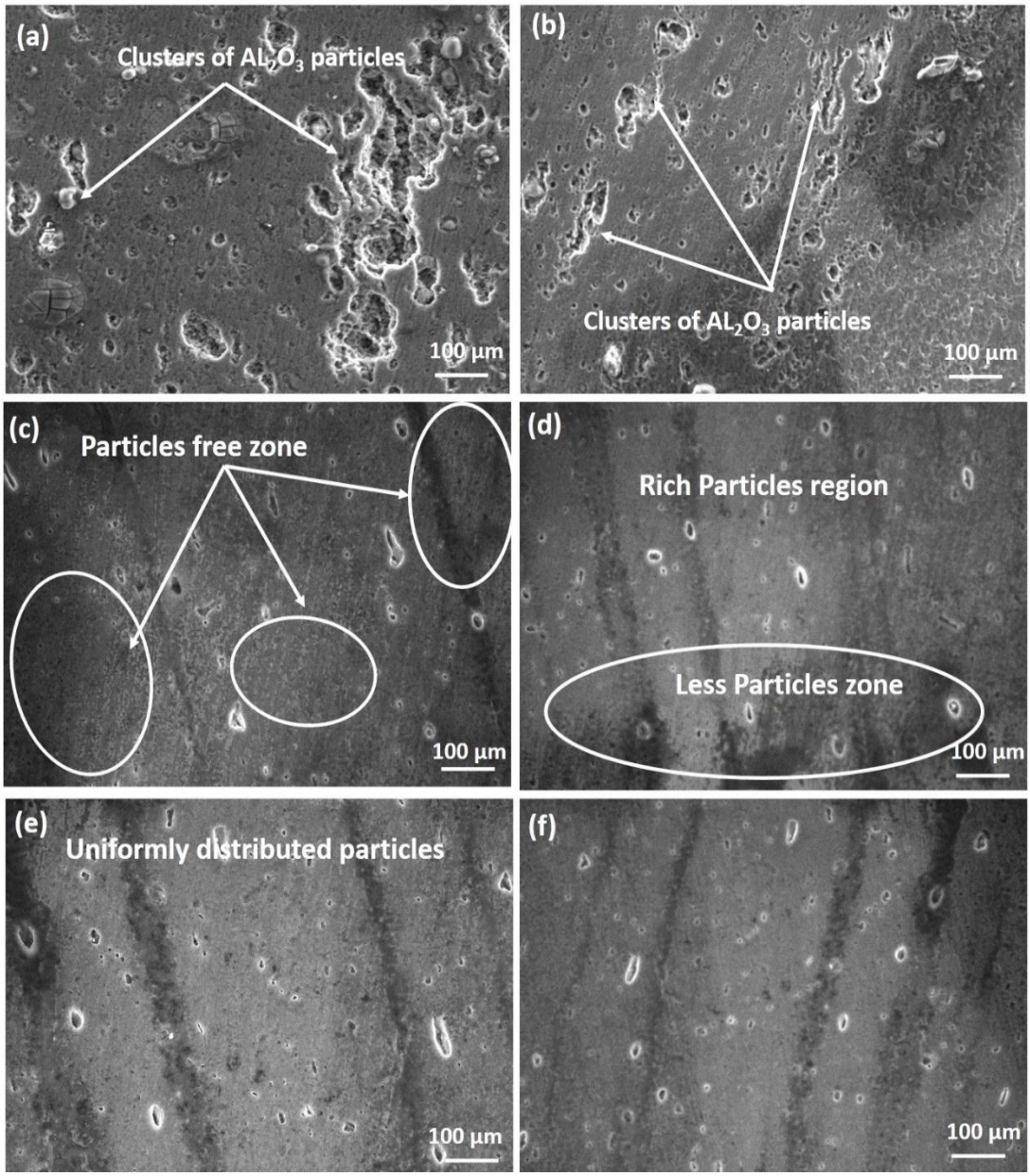

Figure 5.13: FESEM micrograph of particles distribution in the SZ, (a-b) at 750 rpm after, a) one pass, (b) Three Passes; (c-e) at 950 rpm after, (a) one pass, (b) two Passes, (c) three passes, (f) at 1150 rpm after three passes

The mean grain size was observed as 13.4 µm as depicted in Fig. 5.14 a. The clustering of Al_2O_3-mp reduces on increasing the number of passes from one to three produced at RS of 750 rpm and TS of 45 mm/min (specimen no. 1), but still small clusters Al_2O_3-mp were observed after three passes of FSW, as depicted in Fig.5.13 b. Therefore, the mean grain size in the SZ was found to be 10.5 µm, as demonstrated in Fig. 5.14 b. Fig. 5.13 (c-e), depicts the SZ of multi-pass reinforced FSWed joints at RS of 950 rpm, TS 35 mm/min and also confirms the RPs dispersion pattern.

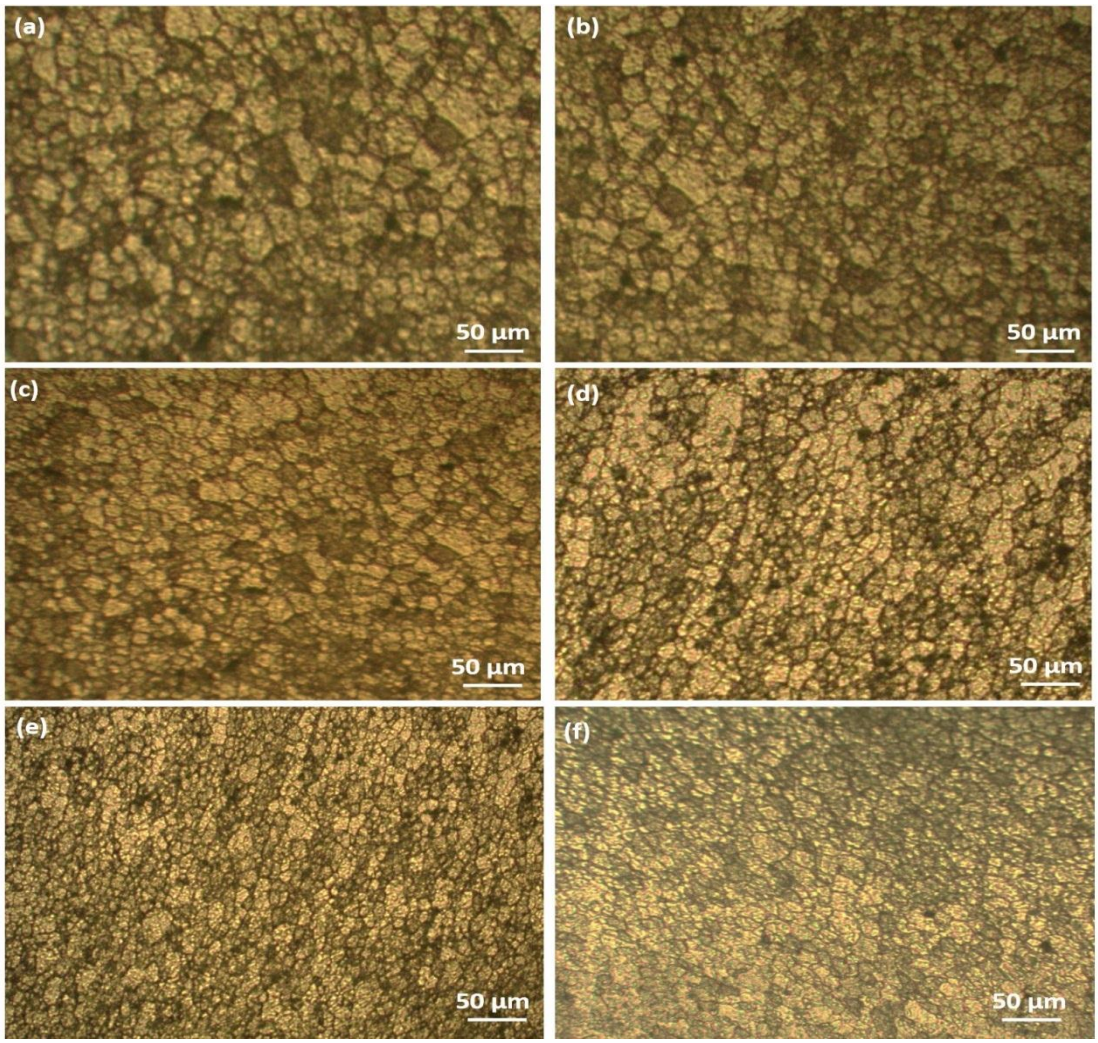

Figure 5.14: Grain structure of various reinforced FSWed joints; (a-b) at 750 rpm after, (a) one pass, (b) Three Passes; (c-e) at 950 rpm after, (c) one pass, (d) Two Passes, (e) three passes, (f) at 1150 rpm after three passes

The clusters of Al_2O_3-mp were found absent at higher RS of 950 rpm, TS of 35 mm/min after one pass of FSW (specimen no. 16) due to enhanced stirring action of tool at higher rotational speed. Rich particles zone and particles free zone in the SZ were observed after one pass of FSW as shown in Fig. 5.13 c. Therefore, it is obvious that one pass of FSW at RS of 950 rpm was also not sufficient for the homogeneous dispersion of the Al_2O_3-mp [171]. The particles free zones were found absent after two passes of FSW (specimen no. 14) due to repeated strain produced by repeated passes of FSW which promotes the dispersion of Al_2O_3 particles in the SZ. Moderate dispersion of Al_2O_3-mp, including less-particles region and rich-particles region was noticed in the reinforced FSWed joint produced after two passes of FSW as delineated in Fig. 5.13 d. The distribution of Al_2O_3-mp was more pronounced and uniform, after implementing three

passes of FSW (specimen no. 9), as observed in Fig. 5.13 e. Therefore, it is obvious in Fig 5.14 (c-e) that particle dispersion was found improved due to repeated strain on increasing number of passes from one to three passes of FSW. Thus, the increment in the number of passes from one to three reduced the size of grain due to more uniform dispersion of Al_2O_3-mp particles that resulted in higher dislocation sources and enhanced dynamic-recovery and recrystallization [172]. Therefore, according to Fig. 5.14 (c-e), the reinforced joints produced at RS and TS of 950 rpm and 35 mm/min, respectively after one, two and three passes revealed the mean grain size of 7.8, 6.2 and 4.1 µm in the SZ, respectively. The more uniform dispersion of particles of particles were also observed in the SZ of reinforced FSWed joint produced at RS of 1150 rpm, TS of 25 mm/min and after three passes of FSW (specimen no. 12), as depicted in Fig. 5.13 f. The increased mean grain size of 6.4 µm (Fig. 5.14 f) was found due to the domination of annealing effect at higher heat input at RS of 1150 rpm after three passes of FSW. Therefore, the optical microstructure illustrates that DRX and pinning effect caused by the uniform dispersion of Al_2O_3-mp led to the formation of fine and equiaxed grains.

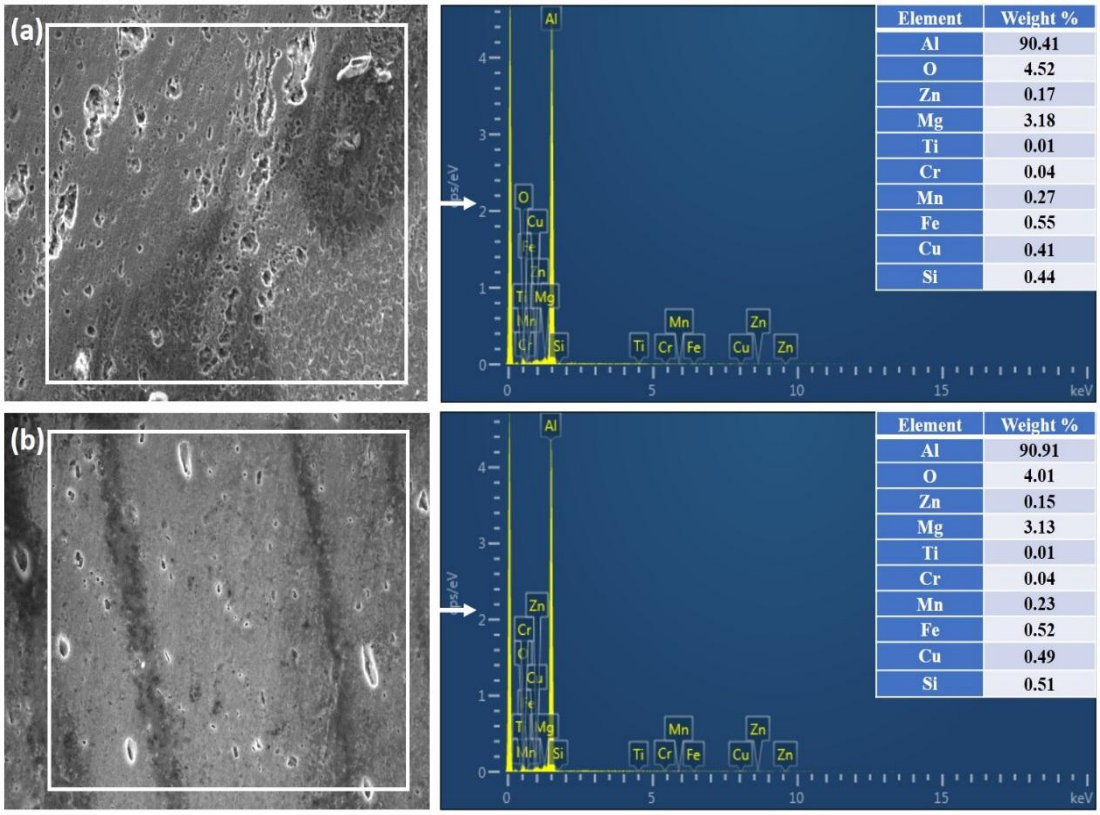

Figure 5.15: EDS analysis of reinforced FSWed joints; (a) at 750 rpm, 45mm/min with three FSW passes (b) at 950 rpm, 35 mm/min with three.

Fig. 5.15 a and b depicts the peaks of the EDS results of reinforced FSWed joints produced after three passes of FSW with RS of 750 rpm and 950 rpm respectively. The EDS findings of reinforced FSWed joint demonstrated the presence of Al_2O_3-mp in the SZ. The elemental characterization obtained by EDS analysis also revealed that the SZ of reinforced FSWed joint contained 4.52 and 4.01% of oxygen. These findings reveal the inclusion of Al_2O_3-mp to the SZ by FSW.

5.4.1 Fracture Surface analysis

Fig. 5.16 shows the morphology of the fractured surfaces of tensile samples obtained from different reinforced joints. In order to identify the failure mechanism, the microstructure of fractured surfaces was analyzed using FESEM.

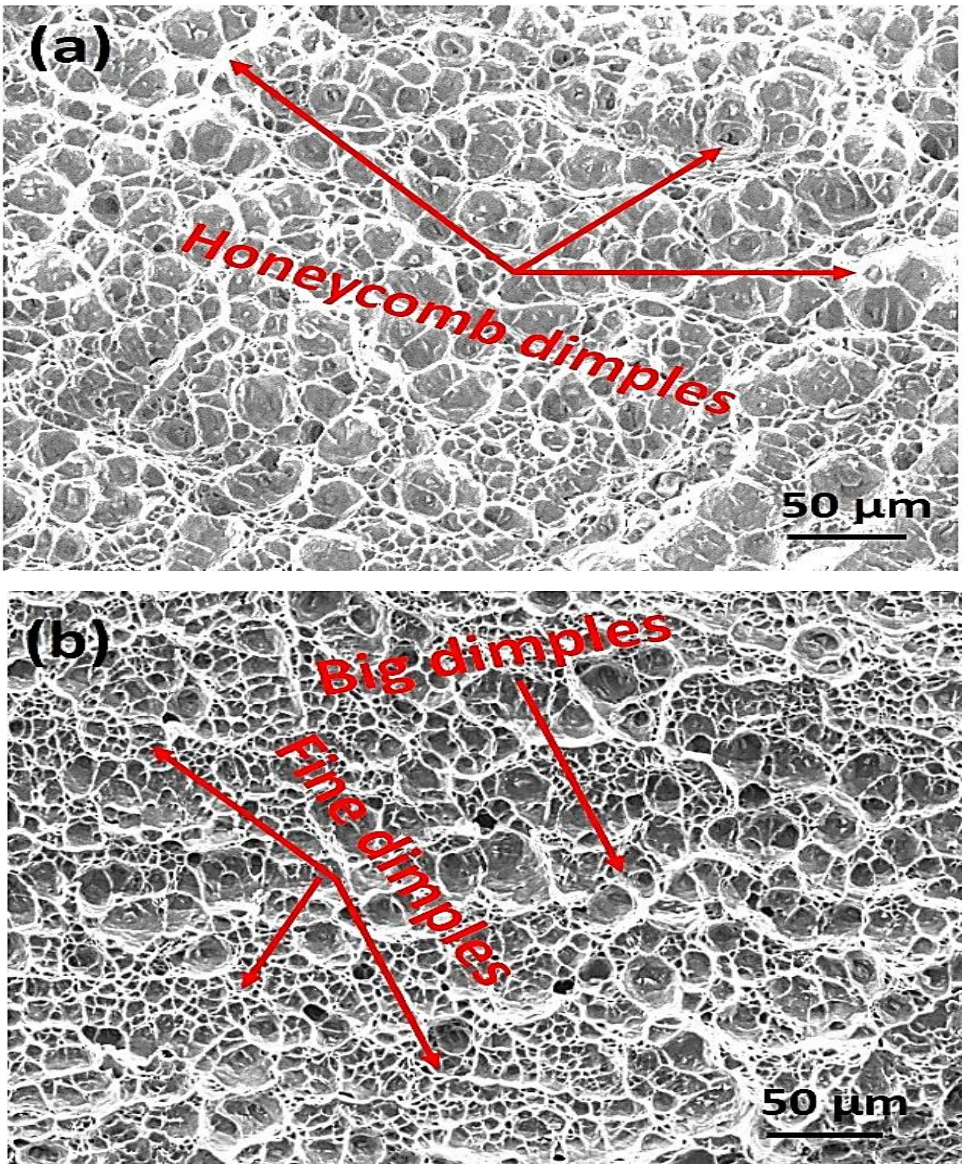

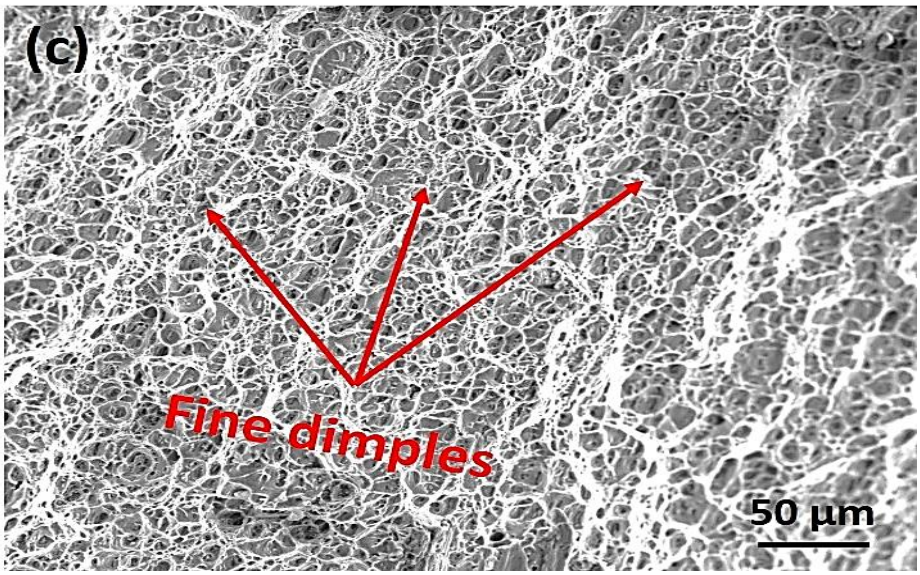

Figure 5.16 FESEM images of fractured surfaces of various Al_2O_3-mp, reinforced FSWed joints, (a) at 750 rpm, 45 mm/min after three FSW passes, (b, c) at 950 rpm, 35 mm/min after, (c) one FSW pass, (d), three FSW passes.

Interestingly, during tensile loading, some samples were fractured from the welded region whereas some samples were fractured in heat affacted zone (HAZ) region towards softer base material i.e. AA 5083, where the strength and hardness were minimal. Previous studies were also revealed that the FSWed joints generally fractured at the HAZ towards weaker base material in case of FSWed dissimilar aluminum alloys [173]. Honeycomb dimples like structure was observed, in the fractured surface micrograph of all the reinforced joints. which represent the ductile mode of failure during tensile loading. The presence of dimples indicates significant plastic deformation before failure. Any reinforced matrix's probability of strengthening depends on how well stress is transferred from the base material to the reinforcing particles. Poor interfacial contact increases the chance of the interface failing before stress is transferred to the particles, which prevents strengthening [174]. The test samples' edges were formed with a shear plane of cup-cone configuration. During the tensile loading, the cup-cone shaped shear plane was produced along the periphery of the test samples. Honeycomb dimples are a common feature of FSWed joints and refer to the visible depressions that are left on the surface of the weld after the process. These dimples are the result of the material being displaced and rearranged during the welding process, and can have a significant impact on the strength and integrity of the weld. The

size and shape of the honeycomb dimples can vary depending on several factors, including the welding parameters, the material being welded, and the tool design. Generally, larger dimples indicate a more severe deformation of the material, while finer dimples indicate a smoother and more controlled deformation. The effect of honeycomb dimples on the fracture of FSWed joints depends on several factors, including the size, shape, and distribution of the dimples. In general, FSW joints with larger and more irregular dimples tend to have lower fracture toughness and strength, as the deformation of the material is more severe and less controlled. In contrast, FSWed joints with smaller and more uniform dimples tend to have higher fracture toughness and strength, as the deformation of the material is more controlled and consistent. Overall, the presence of honeycomb dimples in FSW joints is an important consideration when assessing the strength and integrity of the weld. Welding parameters and tool design can be adjusted to control the size and distribution of the dimples and optimize the mechanical properties of the joint. In addition, the fractured surface micrograph of the reinforced FSWed joint produced at RS of 750 rpm, revealed large and deep dimples (Fig. 5.16 a). Whereas smaller dimples were noticed in the fractured surface micrograph of reinforced joint produced at RS of 950 rpm, TS of 35 mm/min after three FSW passes (Fig. 5.16 b). The dimple size found further decreases after three FSW passes, as depicted in Fig. 5.16 c. The existence of finer dimples indicates the improvement of material ductility before failure [176]. This can be ascribed to the reduced grain size, homogenous dispersion of Al_2O_3-mp and strong connection between the Al_2O_3-mp and the aluminum metal matrix, which led to higher resistance to fracture [172]. The ductile fracture of reinforced joints is caused by the development of cavities or voids, which then increase and consolidate. If the cavity nucleation could be inhibited, the ductility may be improved [174]. Fine and equiaxed dimples were produced by the coalescence of micro voids at the fractured surface [175]. The fractured metal matrix identified at HAZ was confirmed by variance in microhardness, which led to increased ductility. According to the study of the tensile samples' fractured surface, the addition of Al_2O_3-mp enhanced the tensile strength of reinforced joints.

5.5 OPTIMIZATION OF PROCESS PARAMETERS OF SiC MICROPARTICLES REINFORCED FSWed JOINTS

The friction stir welding was performed to successfully fabricate the dissimilar reinforced joints of AA5083 and AA6061 embedded with of 6% volume fraction of SiC microparticles (SiC-mp) is depicted in Fig. 5.17, in order to investigate the effects of FSW parameters, SiC-mp and multi-pass FSW on the mechanical and micro-structural characteristics, the reinforced FSWed joints was compared with unreinforced joint.

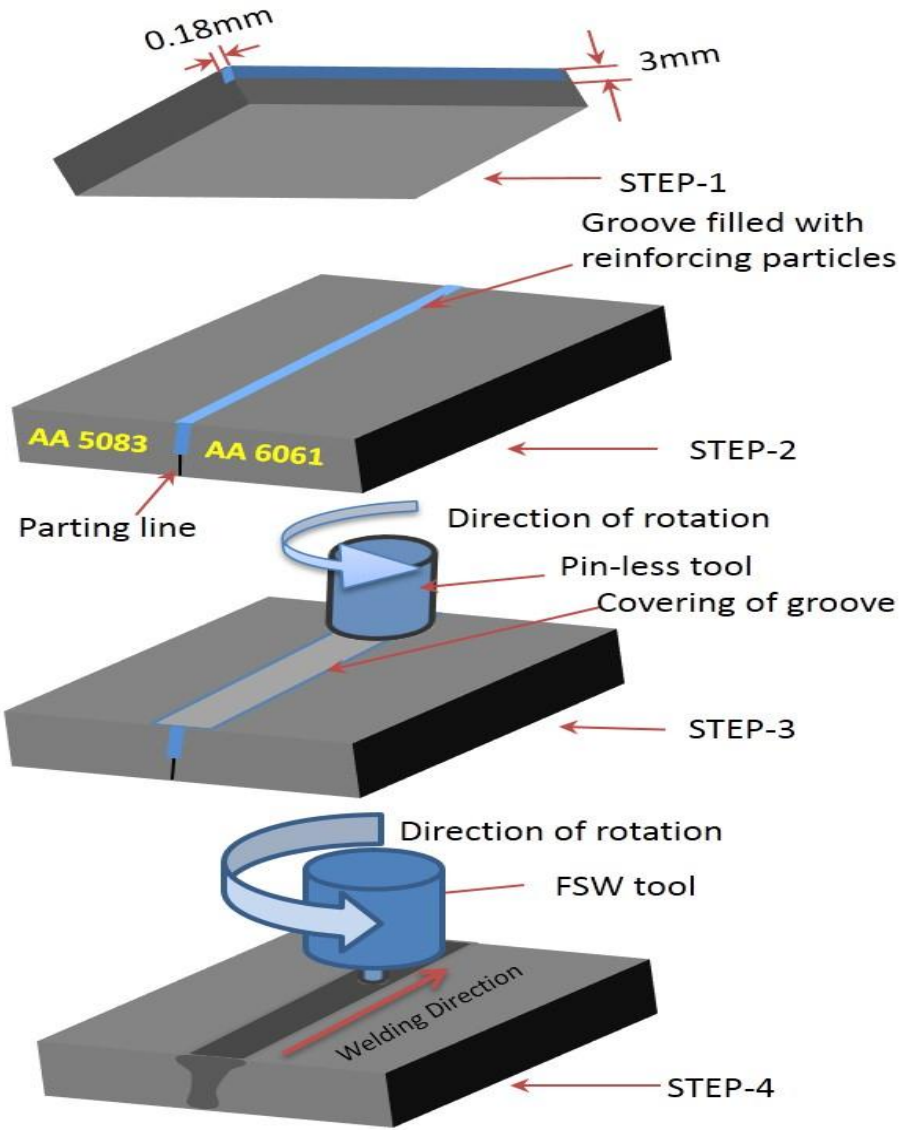

Figure 5.17: Reinforced FSWed joint incorporated with SiC microparticles

A non-consumable with threaded profiled pin manufactured of tool steel (H13) was utilized for experimentation. The input processing parameters for FSW approach have been taken as tool rotational speed (750–1150 rpm), traverse speed (25-45 mm/min)

and number of passes (1-3). The dimensional features of tensile test sample were taken according to ASTME8-standard as mentioned in the Fig. 5.18. The tensile samples were extruded from the welded plates using wire-cut CNC EDM. Multi-FSW passes were employed to fabricate FSWed joints embedded with 6% SiC microparticles as shown in Fig. 5.18. The computer controlled UTM machine was employed to analyzed the tensile test.

Three tensile samples were tested from each reinforced joint and average result was reported. As per design expert software recommendation, there are twenty FSWed reinforced joints embedded with SiC microparticles were fabricated as per design of experiment.

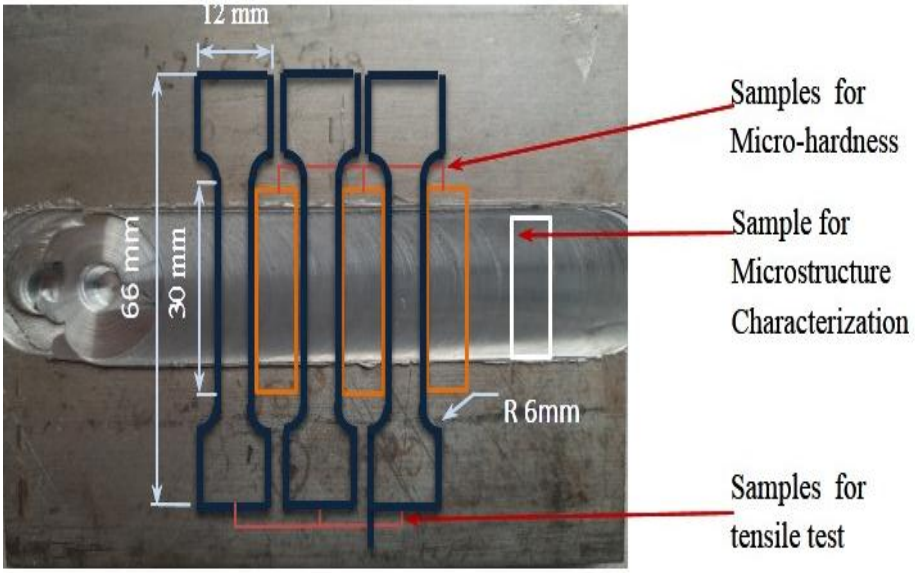

Figure 5.18:Dimension of reinforced FSWed test samples

Various researchers have utilized a variety of experimental design strategies for the development of regression equations but central-reinforced design is one of the best and most accurate design approaches [147, 148]. To obtained the design of experiments using full factorial central-reinforced design the process parameters and their levels were assigned, where the upper and lower values were coded as +1 and -1, respectively. The face-centered central reinforced design contains twenty experimental combinations with three independent input parameters namely tool rotational speed (RS), traverse speed (TS) and number of FSW passes (NOPs) with their three levels. The Processing parameter of FSWed and their levels are tabulated in Table 5.8.

Table 5.8: Processing parameter of SiC reinforced FSWed joints with their levels

Parameters	Symbols	Units	Range	Levels		
				-1	0	1
Rotational Speed (RS)	A	rpm	750-1100	700	900	1100
Traverse speed (TS)	B	mm/min	25-45	25	35	45
Number of FSW passes (NOPs)	C	----	1-2	1	2	3

5.5.1 TENSILE STRENGTH

In order to investigate the influence of rotational speed, traverse speed and number of FSW passes on the tensile properties of dissimilar reinforced FSWed joint of AA5083 and AA6061, embedded with 6% volume fraction of SiC micro-particles, the tensile samples were extruded transversely to weld joint using Wire-cut CNC EDM for better dimensional accuracy. Thereafter, the tensile samples were tested at room temperature, and the strength of various reinforced FSWed joints was measured. The average tensile strength and %elongation of reinforced FSWed joints under various processing conditions and unreinforced FSWed joint were tabulated in Table 5.9.

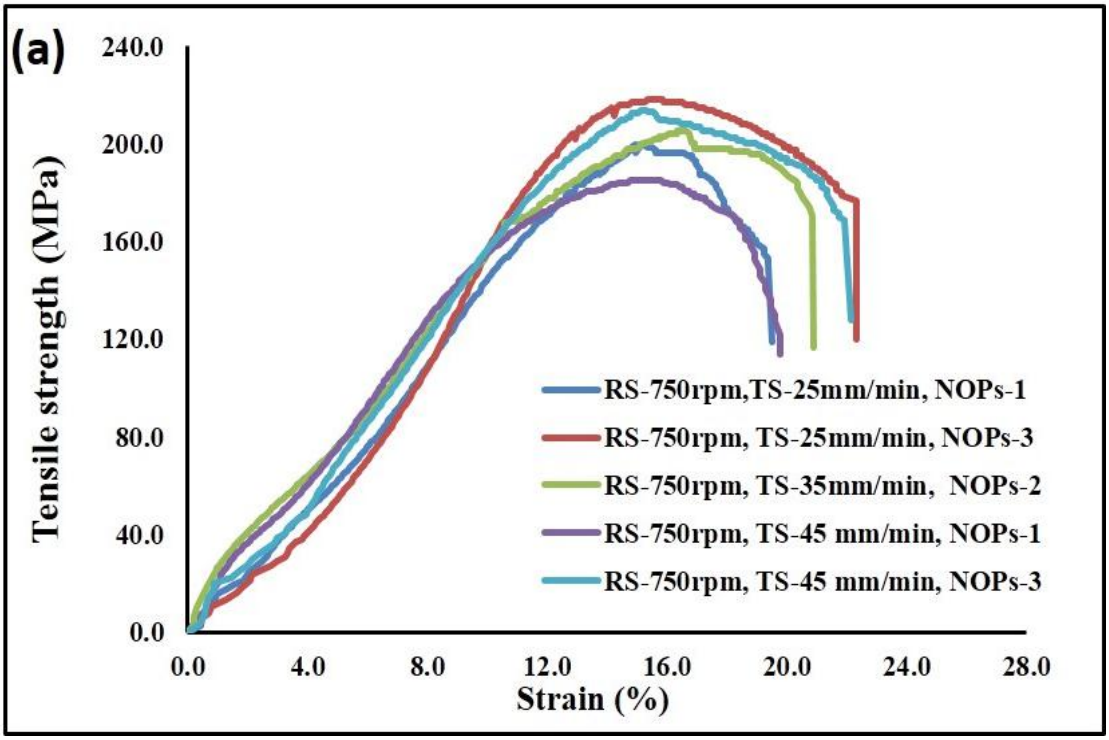

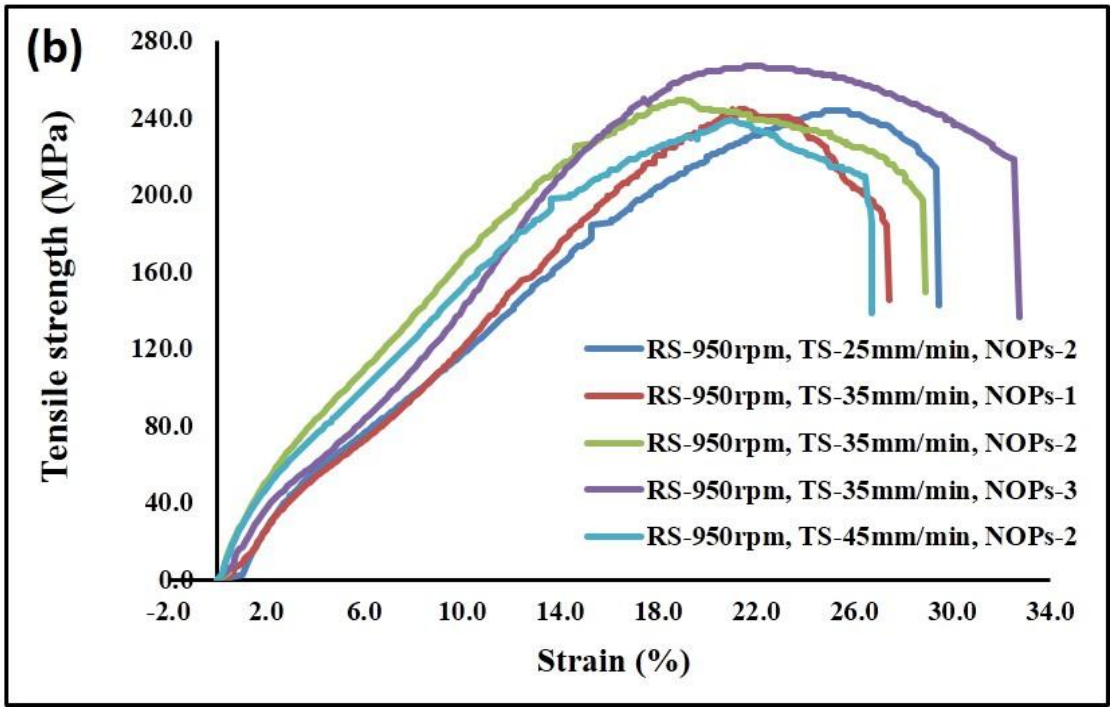

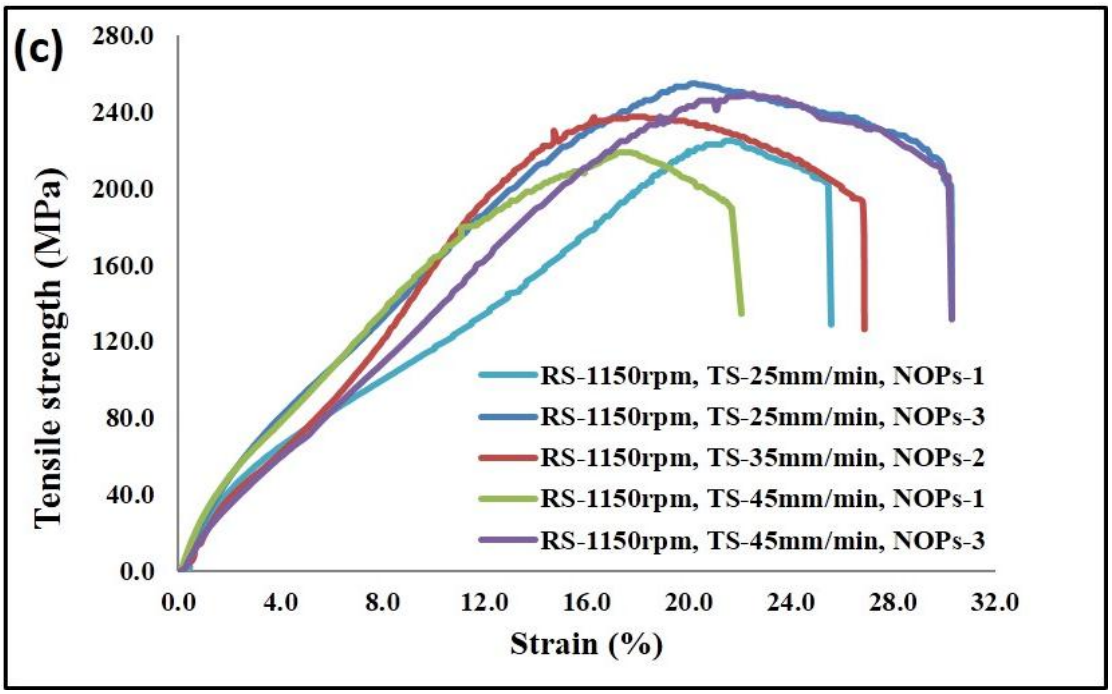

Figure 5. 19: Stress strain plots of reinforced FSWed joints produced at, (a) 750 rpm, (b) 950 rpm, (c) 1150 rpm

Under various parametric settings, the reinforced joints' tensile strength ranges from 185.93 MPa to 266.97 MPa. Fig. 5.19 shows the stress-strain diagram of FSWed joints embedded with SiC-mp under tensile loading. All FSWed joints' tensile strength is found to be lower than that of the base materials AA 6061 and AA 5083. Grain size was the main factor in determining the mechanical properties of the FSWed joint when

no reinforcing particles were used. But with the addition of SiC-mp particles, additional factors like RPs size, the strength of the bonding between the matrix and the precipitates, RPs dispersion pattern, and the location created by the matrix's uneven thermal expansion coefficient all contribute to the mechanical properties of the reinforced FSWed joint [150].

Table 5.9: Mechanical properties of various reinforced FSWed joints

Specimen no.	Process parameters			Response parameters			
	RS (rpm)	TS (mm/min)	NOPs	UTS (MPa)	Joint efficiency (%)	%elongation (%)	Micro-hardness (HV)
1	750	45	3	213.34	73.51	22.1	109.2
2	750	25	3	218.45	75.28	22.3	108.3
3	950	35	2	247.32	85.22	28.5	119.3
4	950	45	2	238.56	82.21	26.7	113.5
5	1150	25	1	224.43	77.34	25.6	112.4
6	950	35	2	249.66	86.03	28.9	120.1
7	1150	35	2	237.54	81.85	26.9	115.3
8	950	35	2	248.98	85.80	29.1	119.8
9	950	35	3	266.97	92.00	32.7	128.4
10	1150	45	3	249.64	86.02	30.3	110.4
11	750	35	2	205.43	70.79	20.9	102.4
12	1150	25	3	254.54	87.71	30.3	122.3
13	950	25	2	243.56	83.93	29.4	121.4
14	950	35	2	251.64	86.71	29.6	120.8
15	950	35	2	249.67	86.03	29.5	118.1
16	950	35	1	244.28	84.18	27.4	116.4
17	750	25	1	199.56	68.77	19.5	94.3
18	1150	45	1	219.32	75.58	22	107.5
19	750	45	1	185.95	64.08	19.7	96.3
20	950	35	2	248.78	85.73	29.1	118.4

The bonding between the RPs and the parent metal, dislocation density, and grain size all affect the reinforced FSWed joint's tensile strength [151]. The increasing rotational speed and the number of FSW passes enhanced the dispersion of RPs in the SZ. More homogenous dispersion of particles provides higher obstacles to prevent grain growth, which further reduces grain size [152].

Figure 5.20: Tensile strength of various reinforced joints

The tensile strength for as received AA5083 and AA6061 were observed to be 290.20 and 310.04 MPa, respectively, whereas %elongation was observed to be 20 and 21.9 %, respectively. After the execution of multi-pass SiC reinforced FSW, the tensile properties were enhanced simultaneously. Therefore, the SiC reinforced FSW joint produced at RS of 950 rpm, TS of 35 mm/min after three passes of FSW reveals the maximum tensile strength of 266.87 MPa which is nearly 92% of the tensile strength of the AA5083 (base material) and %elongation of 32.7%, among all the weld joints. These results were consistent with the findings of Jamalian et al. [175]. It is obvious from the 95 % confidence interval reveals that on increasing the value of RS, the microhardness, tensile strength and %elongation increases.

5.5.2 MICROHARDNESS

Vickers hardness testing was employed to analyses the distribution of micro-hardness in the processed zone of reinforced FSWed joints of AA6061 and AA5083 processed under various processing conditions as shown in Fig. 5.21. Using a Vickers micro-hardness tester with a gap of 1 mm between the indentations, the hardness profile was assessed at a load of 100 gm for dwell time of 15s. As we know that the reinforced joint is a heterogeneous reinforced with varying mechanical characteristics at its interface [177]. Fig. 5.22, showed the fluctuation of the microhardness from the weld center of the reinforced joints embedded with SiC-mp.

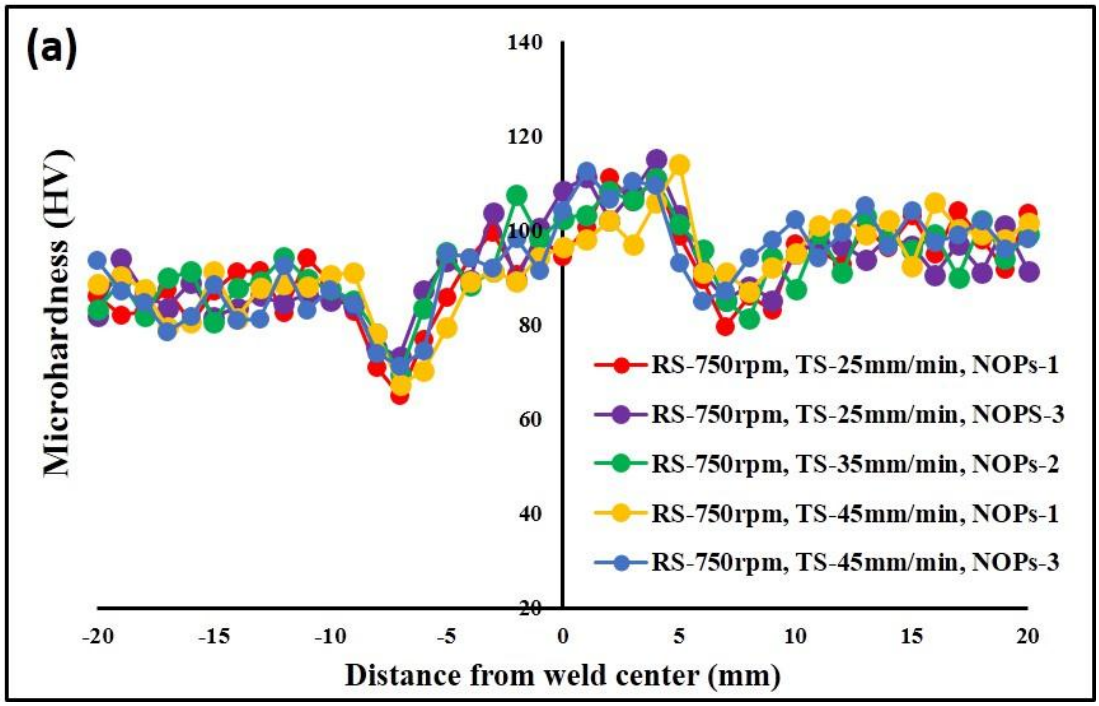

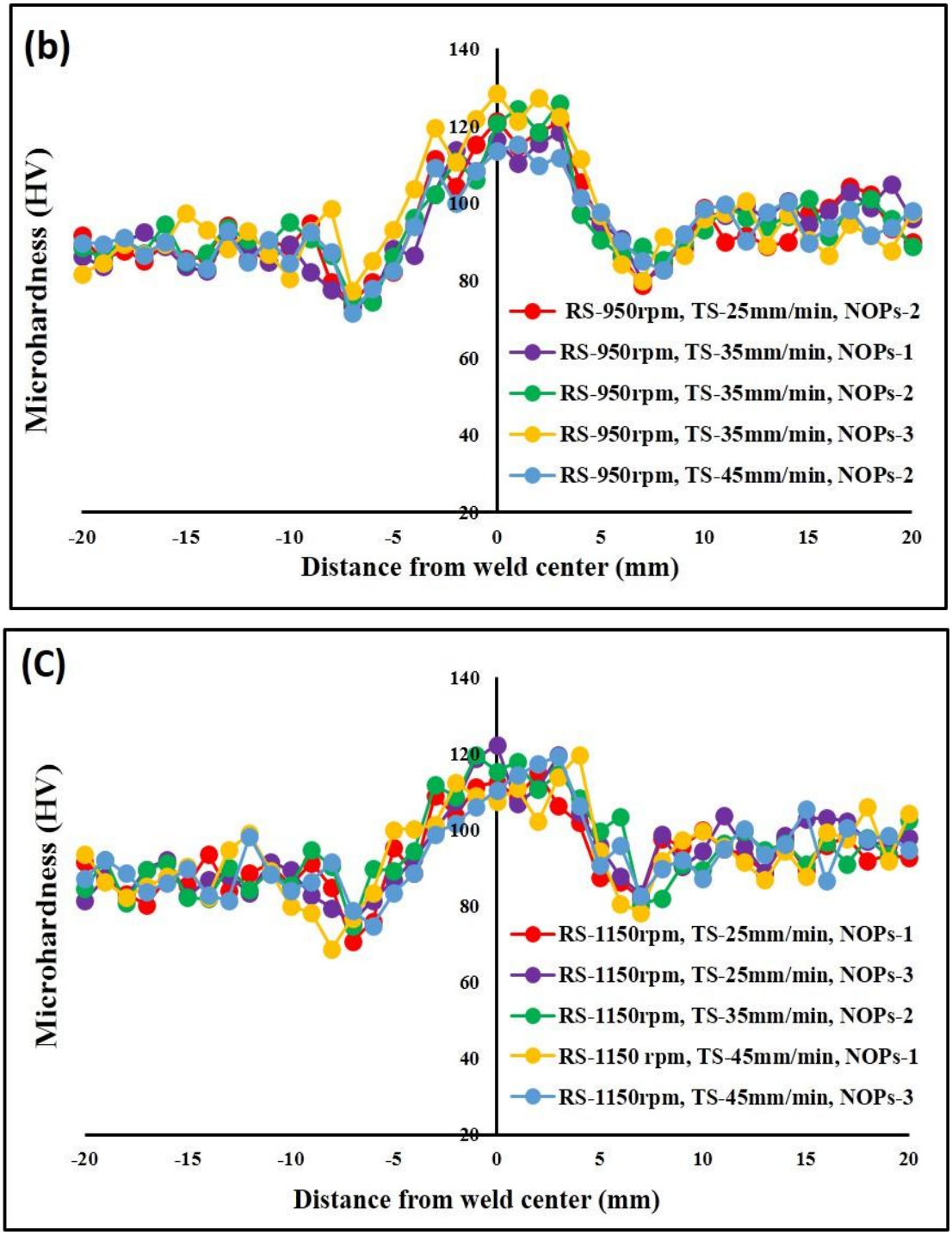

Figure 5.21: (a-c) Micro-hardness distribution of reinforced FSWed joints (a) at 750 rpm, (b) at 950 rpm, (c) at 1150 rpm

The average microhardness results along the center of the weld line are tabulated in Table 5.9. The microhardness of AA5083 and AA6061 (base materials) was found to be 85.4 and 98.1 HV, respectively. The micro-hardness profile of all the FSWed joints is delineated in Fig 5.21. The hardness of the SZ may be ascribed to the dispersion pattern of SiC-mp and grain refinement and in the SZ [160]. The micro-hardness of

SiC reinforced FSWed joints can be attributed to grain size, volume fractions of SiC particles, dislocation density, and heat input [160]. The minimum hardness of 94.3 HV was found at lower RS of 750 rpm and TS of 25 mm/min after one pass of FSW (specimen no. 17) due to low heat input and clustering of SiC-mp in the SZ. Among all the reinforced joint, the reinforced joint (specimen no. 9) produced at TS of 35 mm/min and RS of 950 rpm after three-passes of FSW reveals the maximum microhardness of 128.4 HV due to the dynamic recrystallization, higher grain refinement via pinning effect and enhanced material mixing rule homogenous dispersion of SiC-mp in the SZ as compared to other FSWed joints.

Figure 5.22: Micro-hardness of various reinforced joints

The micro-hardness of the reinforced FSWed joints was also enhanced due to the addition of hard SiC-mp. The highest micro-hardness was observed in the SZ in comparison with the other adjacent zones due to fine and equiaxed grain structure due to pinning effect of SiC-mp and dynamic recrystallization, whereas TMAZ and HAZ exhibit low micro-hardness due to coarsening of grain, elevated temperatures, over aging during the FSW [159]. According to the Hall-Patch relation, smaller grains reveal higher hardness [160]. Therefore, the three-pass SiC reinforced FSWed joint produced at RS of 950 rpm and TS of 35 mm/min showed the maximum hardness of 128.4 HV due to the more homogenous dispersion of SiC particles in the SZ as compared to other FSWed joints.

When no reinforcing particles were utilized, grain refinement by DRX was the key determinant of the joint's mechanical characteristics. However, the mechanical properties of FSPed composite joints is mainly influenced by grain refinement, pinning effect produced by reinforcing particles and bonding between reinforcing particles and metal-matrix. As a result of the higher grain refinement due to pinning effect of the uniformly distributed reinforcing particles, composite joints exhibit the finer grains resulting in improved mechanical properties [133,156].

5.5.3 DEVELOPING THE MATHEMATICAL MODEL

Twenty experiments are utilized as input data to generate mathematical equation using RSM. The response functions are tensile strength, %elongation and microhardness at stir zone whereas input parameters are rotational speed-A, traverse speed-B and Number of FSW passes-C. At a confidence level of 95%, the significance of each coefficient was assessed and tested. By employing the ANOVA technique and second order regression equations, the final mathematical model for the reinforced FSWed joint incorporating SiC-mp is presented below. The standard F value must be higher than the predicted value of F for a model to be accepted with a 95% confidence level. Tables 5.10 to 5.12 provide the results of the ANOVAs for the responses variables for reinforced joints. The final mathematical empirical equation that was developed has been provided below in coded form.

$$\textbf{Tensile strength} = +249.17 + 16.27 \times A - 3.37 \times B + 12.94 \times C + 1.09 \times A \times B + 1.77 \times A \times C + 1.09 \times B \times C - 27.43 \times A^2 - 7.86 \times B^2 + 6.71 \times C^2 \quad (5.7)$$

$$\textbf{\%elongation} = +29.09 + 3.06 \times A - 0.63 \times B + 2.35 \times C - 0.45 \times A \times B + 0.98 \times A \times C + 0.40 \times B \times C - 5.14 \times A^2 - 0.99 \times B^2 + 1.01 \times C^2 \quad (5.8)$$

$$\textbf{Microhardness} = +119.75 + 5.74 \times A - 2.18 \times B + 5.17 \times C - 2.46 \times A \times B - 1.76 \times A \times C - 1.01 \times B \times C - 11.40 \times A^2 - 2.80 \times B^2 + 2.15 \times C^2 \quad (5.9)$$

The final mathematical model equations in terms of actual variables are represented in equations 5.10-5.12.

$$\textbf{Tensile strength} = +249.17 + 16.27 \times \text{Rotational speed} - 3.37 \times \text{Traverse speed} + 12.94 \times \text{Number of FSW Passes} + 1.09 \times \text{Rotational speed} \times \text{Traverse speed} + 1.77 \times \text{Rotational speed} \times \text{Number of FSW Passes} + 1.09 \times \text{Traverse speed} \times \text{Number of FSW Passes} - 27.43 \times \text{Rotational speed}^2 - 7.86 \times \text{Traverse speed}^2 + 6.71 \times \text{Number of FSW Passes}^2 \quad 5.10$$

$$\textbf{\%elongation} = +29.09 + 3.06 \times \text{Rotational speed} - 0.63 \times \text{Traverse speed} + 2.35 \times \text{Number of FSW Passes} - 0.45 \times \text{Rotational speed} \times \text{Traverse speed} + 0.98 \times \text{Rotational speed} \times \text{Number of FSW Passes} + 0.40 \times \text{Traverse speed} \times \text{Number of FSW Passes} - 5.14 \times \text{Rotational speed}^2 - 0.99 \times \text{Traverse speed}^2 + 1.01 \times \text{Number of FSW Passes}^2 \quad 5.11$$

$$\textbf{Micro-hardness} = +119.75 + 5.74 \times \text{Rotational speed} - 2.18 \times \text{Traverse speed} + 5.17 \times \text{Number of FSW Passes} - 2.46 \times \text{Rotational speed} \times \text{Traverse speed} - 1.76 \times \text{Rotational speed} \times \text{Number of FSW Passes} - 1.01 \times \text{Traverse speed} \times \text{Number of FSW Passes} - 11.40 \times \text{Rotational speed}^2 - 2.80 \times \text{Traverse speed}^2 + 2.15 \times \text{Number of FSW Passes}^2 \quad 5.12$$

The tool rotational speed coefficient (A) is positive, it implies that the tensile strength increases when the RS increases, because at lower RS produced insufficient heat input causes unusual material mixing resulting in clustering of SiC particles. The number of FSW passes is also significantly affecting the tensile strength. Higher number of FSW passes shows the higher tensile strength, microhardness and %elongation.

5.5.4 ADEQUACY OF DEVELOPED MODEL

Table 5.10 to 5.12 presents the statistical findings of the empirical correlation that was developed. when R^2 is 1, the value of predicted empirical relationship perfectly matched the experimental value. The empirical relationships are sufficient and may be used to predict the responses without a substantial amount of error when the value of R^2 approaches 1 and the standard error is smaller.

Table 5.10: ANOVA table surface quadratic model for tensile strength

Tensile Strength						
Sources	SS	DOF	MS	F-value	P-value	
Model	8649.91	9	961.10	348.29	< 0.0001	significant
A-RS	2648.43	1	2648.43	959.75	< 0.0001	
B-TS	113.77	1	113.77	41.23	< 0.0001	
C-NOPs	1674.44	1	1674.44	606.79	< 0.0001	
AB	9.48	1	9.48	3.44	0.0935	
AC	25.03	1	25.03	9.07	0.0131	
BC	9.48	1	9.48	3.44	0.0935	
A^2	2069.46	1	2069.46	749.94	< 0.0001	
B^2	169.78	1	169.78	61.52	< 0.0001	
C^2	123.73	1	123.73	44.84	< 0.0001	
Residual	27.60	10	2.76			
Lack of Fit	17.57	5	3.51	1.75	0.2765	not significant
Pure Error	10.02	5	2.00			
Cor Total	8677.51	19				
Std. Dev.	1.66	R^2		0.9968		
Mean	234.88	Adjusted R^2		0.9939		
C.V. %	0.71	Predicted R^2		0.9676		

		Adeq Precision	69.15

Table 5.11: ANOVA table surface quadratic model for %elongation

%elongation						
Sources	SS	DOF	MS	F-value	P-value	
Model	298.92	9	33.21	76.23	< 0.0001	significant
A-RS	93.64	1	93.64	214.90	< 0.0001	
B-TS	3.97	1	3.97	9.11	0.0129	
C-NOPs	55.23	1	55.23	126.74	< 0.0001	
AB	1.62	1	1.62	3.72	0.0827	
AC	7.61	1	7.61	17.45	0.0019	
BC	1.28	1	1.28	2.94	0.1173	
A^2	72.68	1	72.68	166.80	< 0.0001	
B^2	2.70	1	2.70	6.20	0.0320	
C^2	2.80	1	2.80	6.43	0.0296	
Residual	4.36	10	0.44			
Lack of Fit	3.55	5	0.71	4.39	0.0651	not significant
Pure Error	0.81	5	0.16			
Cor Total	303.28	19				
Std. Dev.	0.66	R^2		0.9856		
Mean	26.53	Adjusted R^2		0.9727		
C.V. %	2.49	Predicted R^2		0.8030		
		Adeq Precision		28.91		

Table 5.12: ANOVA surface quadratic model for micro-hardness

Micro-hardness						
Sources	SS	DOF	MS	F-value	P-value	
Model	1445.10	9	160.57	70.61	< 0.0001	significant
A-RS	329.48	1	329.48	144.88	< 0.0001	
B-TS	47.52	1	47.52	20.90	0.0010	
C-NOPs	267.29	1	267.29	117.54	< 0.0001	
AB	48.51	1	48.51	21.33	0.0010	
AC	24.85	1	24.85	10.93	0.0079	

BC	8.20	1	8.20	3.61	0.0868	
A^2	357.11	1	357.11	157.03	< 0.0001	
B^2	21.49	1	21.49	9.45	0.0118	
C^2	12.77	1	12.77	5.61	0.0393	
Residual	22.74	10	2.27			
Lack of Fit	17.43	5	3.49	3.28	0.1089	not significant
Pure Error	5.31	5	1.06			
Cor Total	1467.84	19				

Std. Dev.	1.51	R^2	0.9845
Mean	113.73	Adjusted R^2	0.9706
C.V. %	1.33	Predicted R^2	0.8624
		Adeq Precision	31.26

The increased variance and more significant variables in the present model are suggested by the higher adjusted R^2 value. In this developed model, results give a higher R^2 value of 0.9968, 0.9856, and 0.9845and adjusted R^2 value of 0.9939, 0.9727 and 0.9706 for tensile strength, %elongation and microhardness at SZ, respectively. When the RS of tool is 750 rpm then the clustering of SiC-mp at RS was observed caused by insufficient of material maxing due to low heat generation, whereas at higher RS of 950 rpm after three FSW passes uniform dispersion of SiC-mp was observed due to sufficient material mixing caused by repeated plastic strain caused by multi-pass of FSW. ANOVA (Table 5.10) for tensile strength of reinforced joints of AA5083 and AA6061 embedded with SiC-mp shows the Fisher's F value of 348.29 for the tensile strength indicating that the model is significant. The ANOAVA Table 5.11 shows the %elongation of reinforced FSWed joint, value of the fisher's F is 76.23, indicates that the model is significant. The R^2 value demonstrates how well the models are fit. Value of R^2 which is 0.9968 for tensile strength indicating 99.68% of the complete variability which is evaluated by the model after taking into account the essential factors. The difference between the value of R^2 (99.68%) and adjusted R^2 (99.39%) is 0.29%, indicating that the model does not explain 0.29 % of the total variation and the model is not over fitted. According to ANOVA surface quadratic model (Table 5.12) the F-value for microhardness at SZ (70.61) demonstrated that the model is significant.

5.5.1 EFFECTS ON RESPONSE PARAMETERS

The predicted values vs actual values plots for tensile strength, microhardness and %elongation of reinforced FSWed joints embedded with SiC-mp as shown in Fig. 5.23.

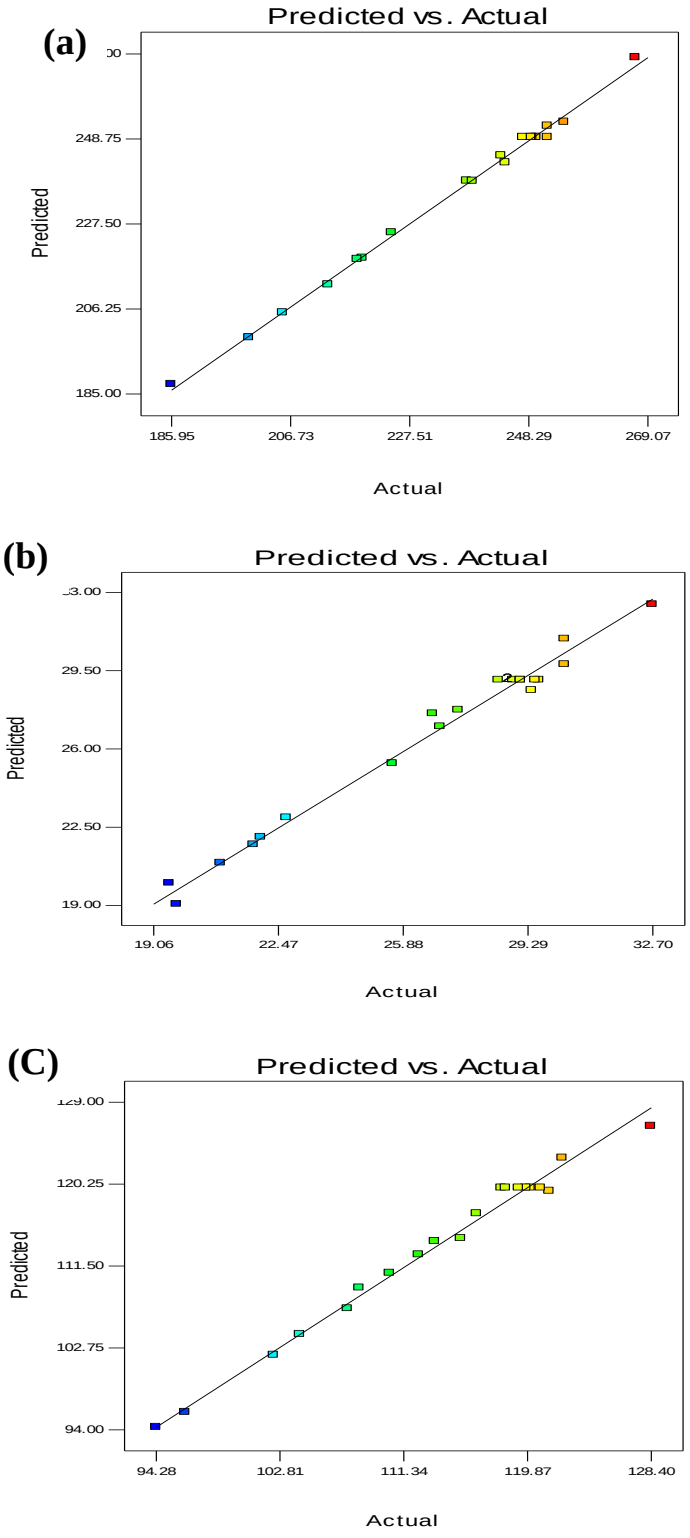

Figure 5.23: Predicted vs actual plots for, (a) Tensile strength, (b) %elongation, (c) Micro-hardness

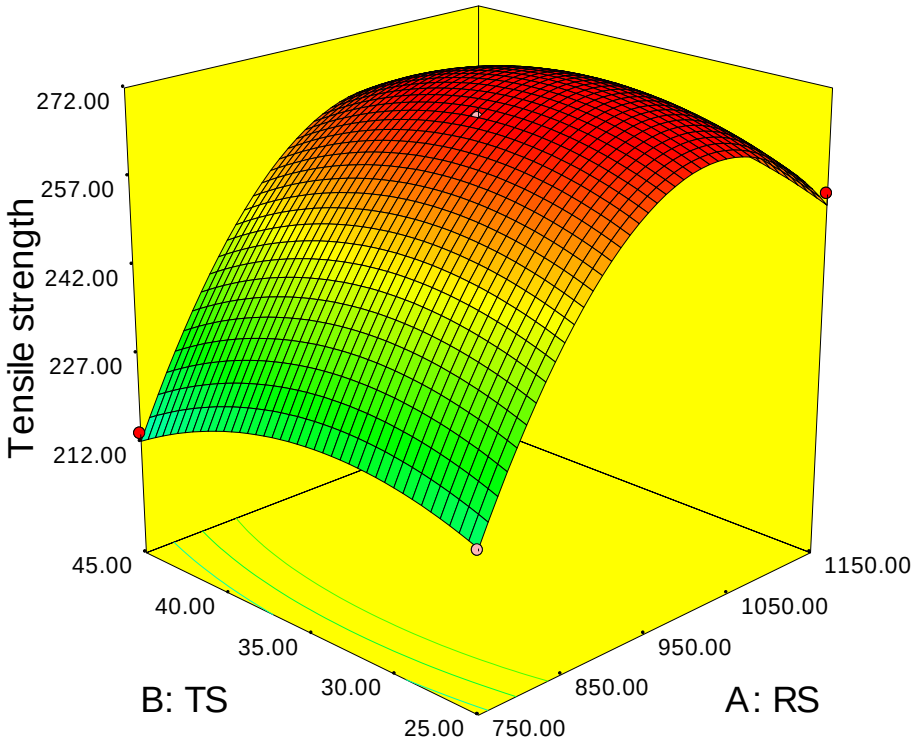
Tensile strength
272.00
257.00
242.00
227.00
212.00
45.00
40.00
35.00
30.00
25.00
B: TS
750.00
850.00
950.00
1050.00
1150.00
A: RS

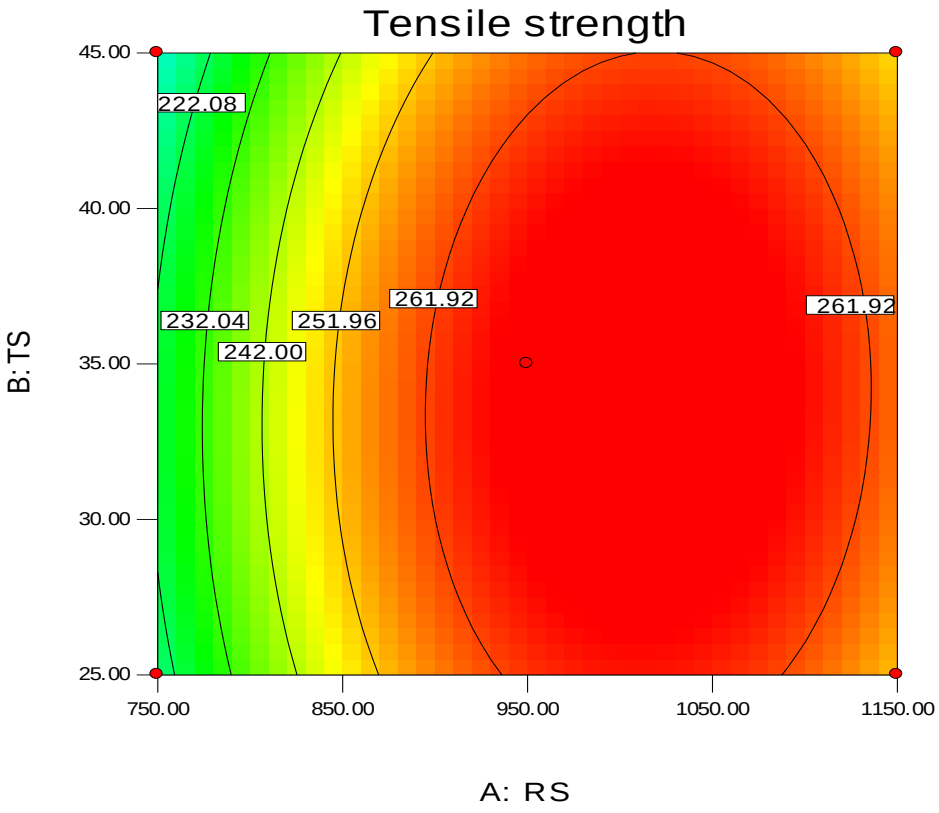
Tensile strength
45.00
40.00
35.00
30.00
25.00
B: TS
222.08
232.04
242.00
251.96
261.92
261.92
750.00
850.00
950.00
1050.00
1150.00
A: RS

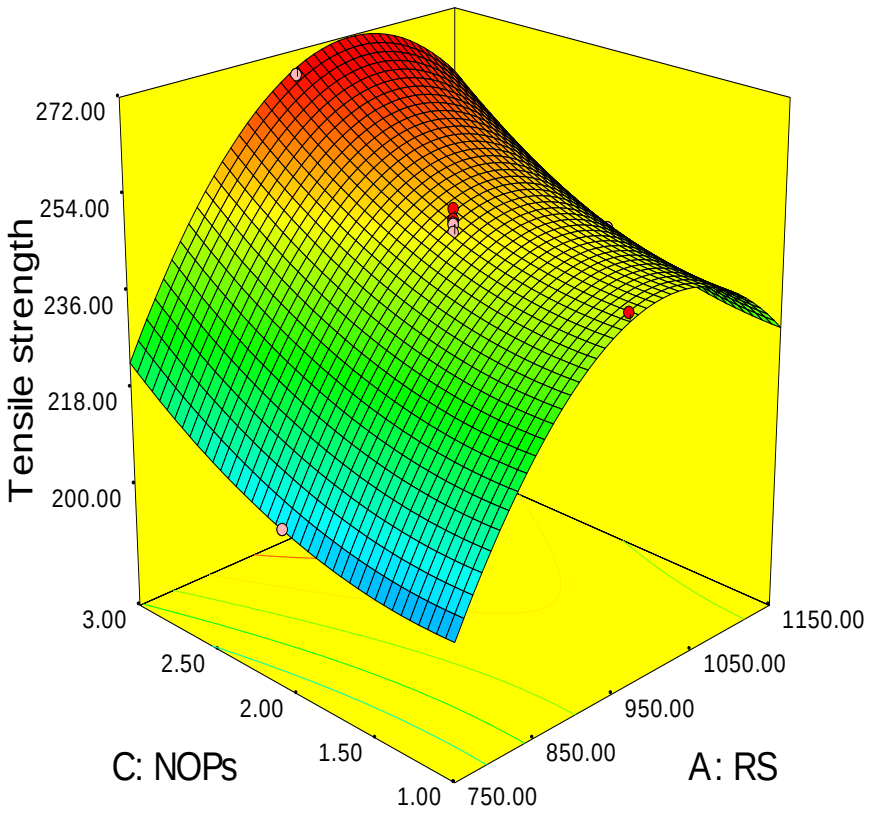
Tensile strength
272.00
254.00
236.00
218.00
200.00
3.00
2.50
2.00
1.50
1.00
C: NOPs
750.00
850.00
950.00
1050.00
1150.00
A: RS

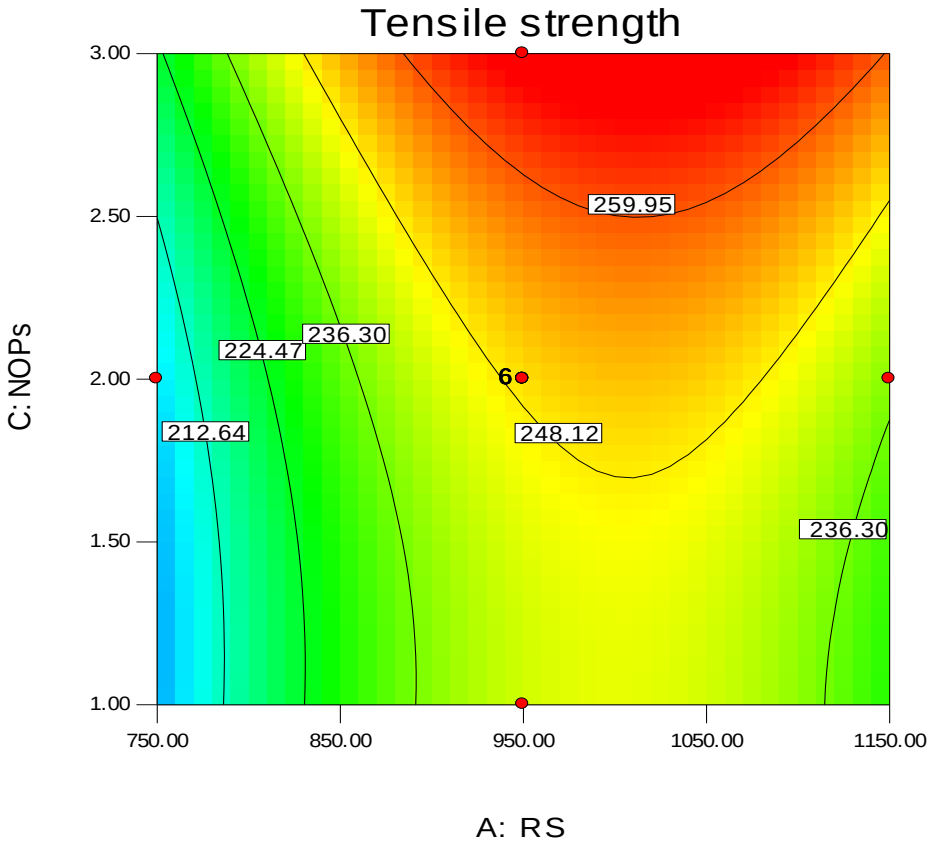
Tensile strength
3.00
2.50
2.00
1.50
1.00
C: NOPs
259.95
236.30
224.47
212.64
248.12
236.30
6
750.00
850.00
950.00
1050.00
1150.00
A: RS

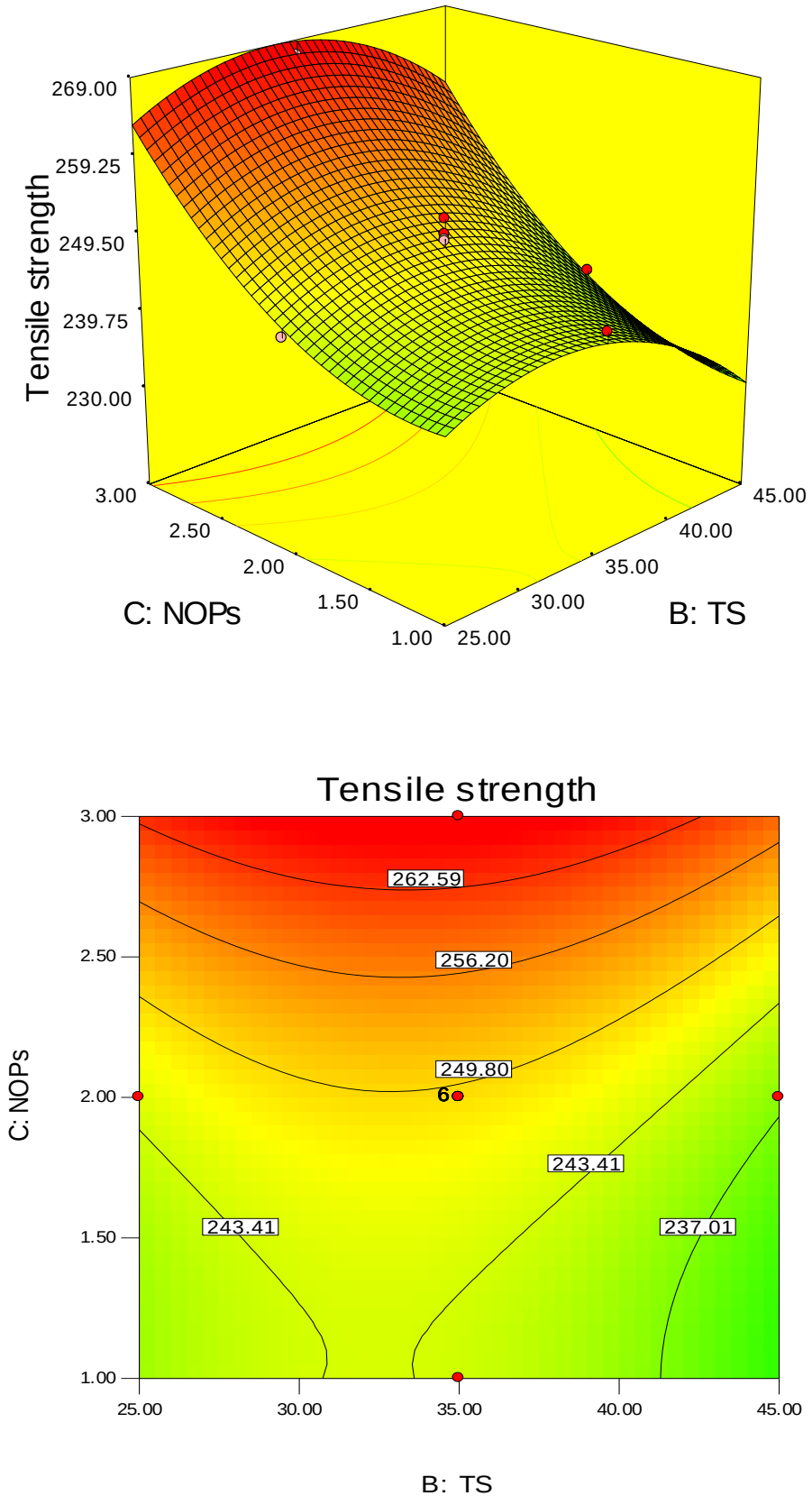

Figure 5.24: 3D response contour and surface plot of Tensile strength of reinforced FSWed joint embedded with SiC-mp

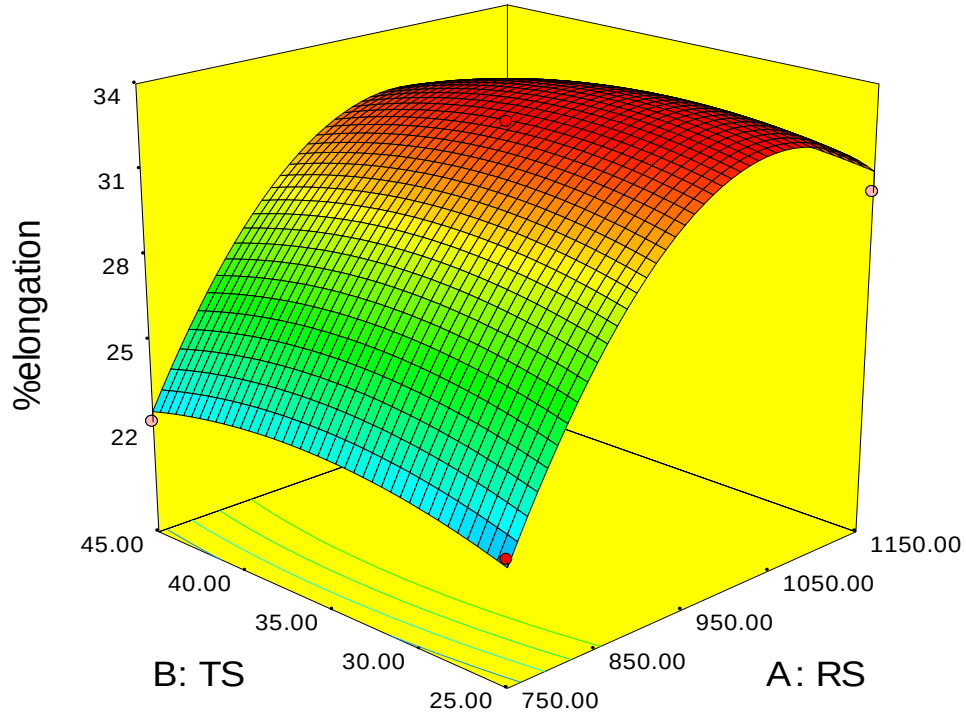
%elongation
34
31
28
25
22
45.00
40.00
35.00
30.00
25.00
B: TS
750.00
850.00
950.00
1050.00
1150.00
A: RS

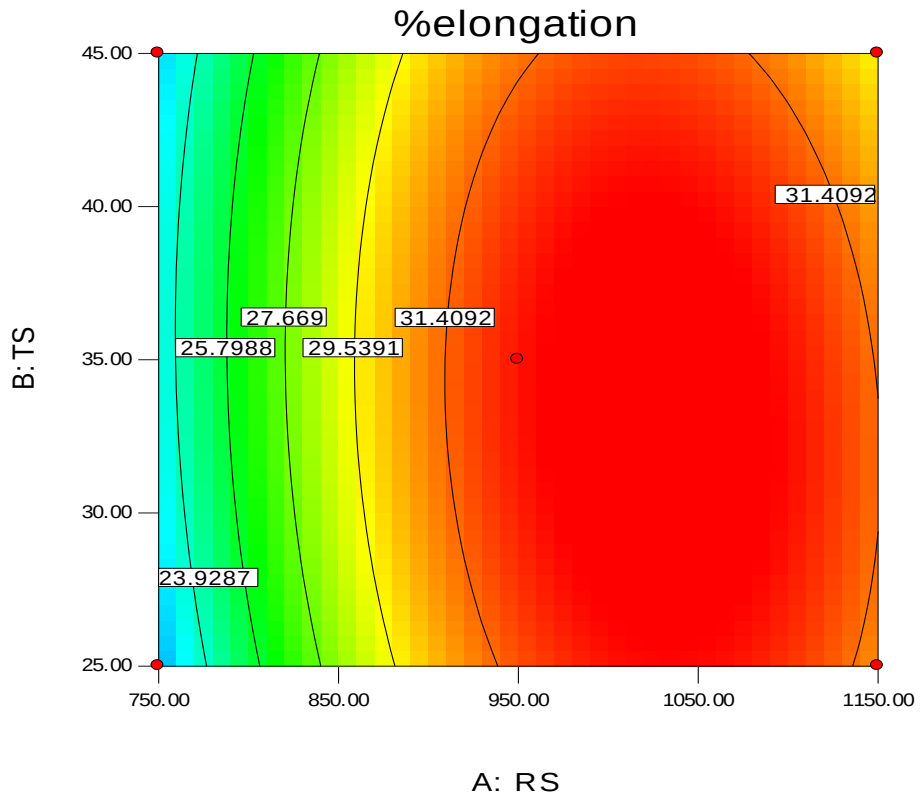
%elongation
45.00
40.00
35.00
30.00
25.00
B: TS
31.4092
27.669
31.4092
25.7988
29.5391
23.9287
750.00
850.00
950.00
1050.00
1150.00
A: RS

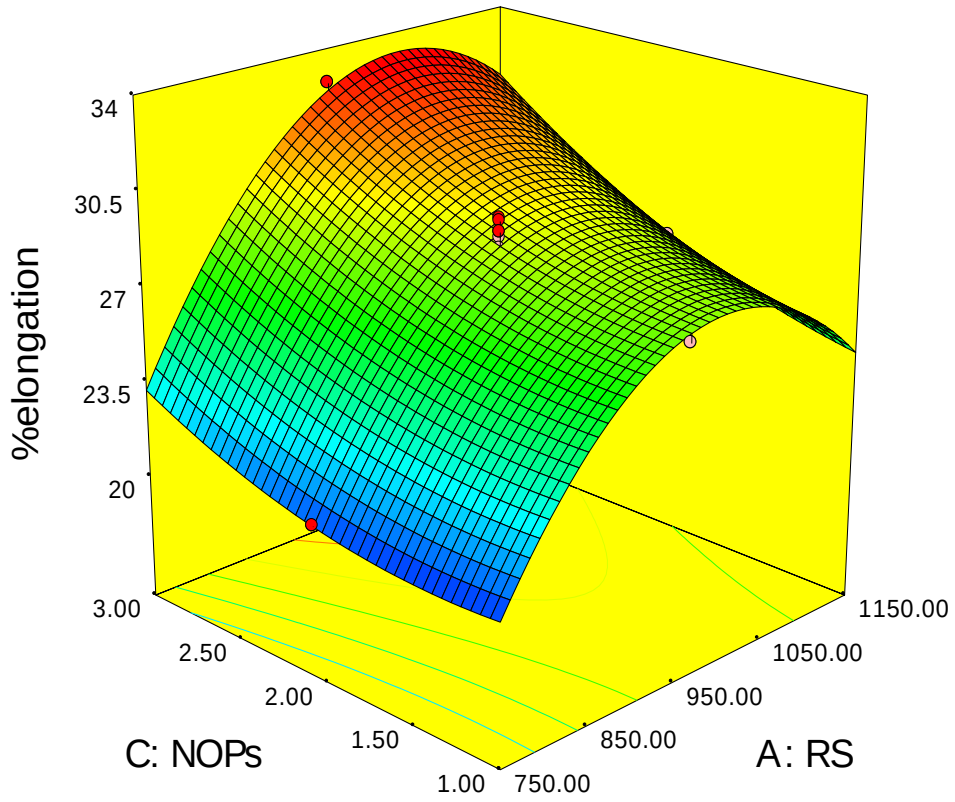
%elongation
34
30.5
27
23.5
20
3.00
2.50
2.00
1.50
1.00
C: NOPs
750.00
850.00
950.00
1050.00
1150.00
A: RS

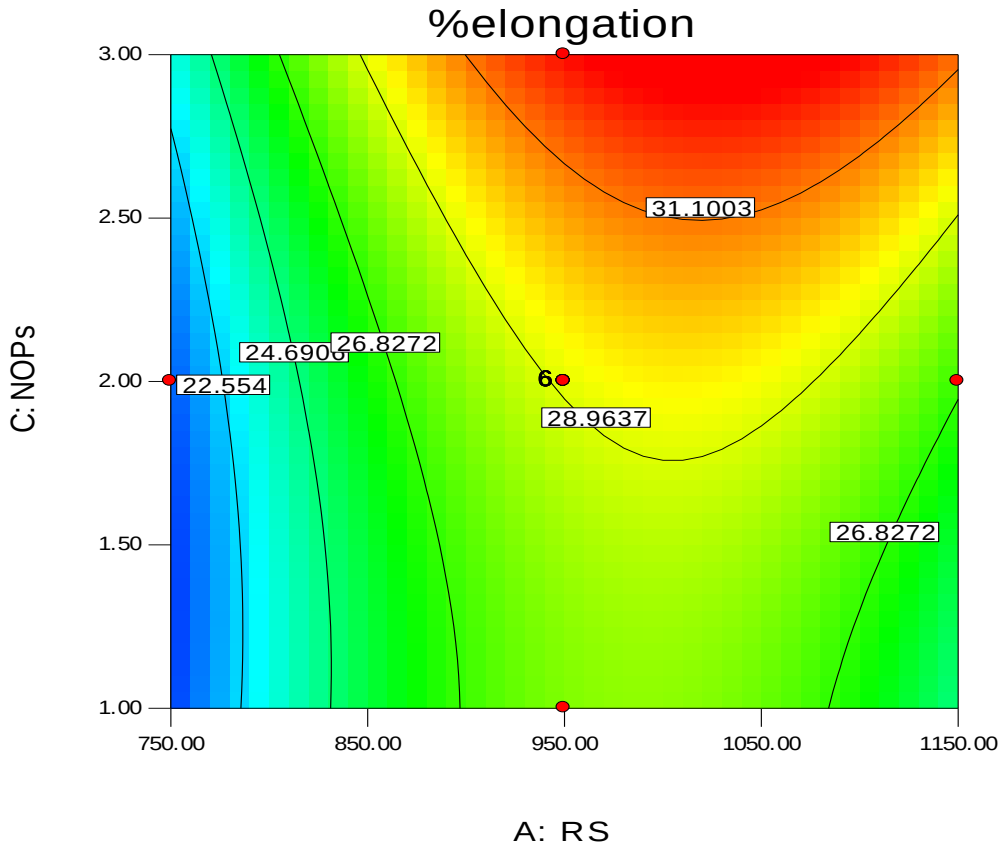
%elongation
3.00
2.50
2.00
1.50
1.00
C: NOPs
31.1003
24.6903
26.8272
22.554
6
28.9637
26.8272
750.00
850.00
950.00
1050.00
1150.00
A: RS

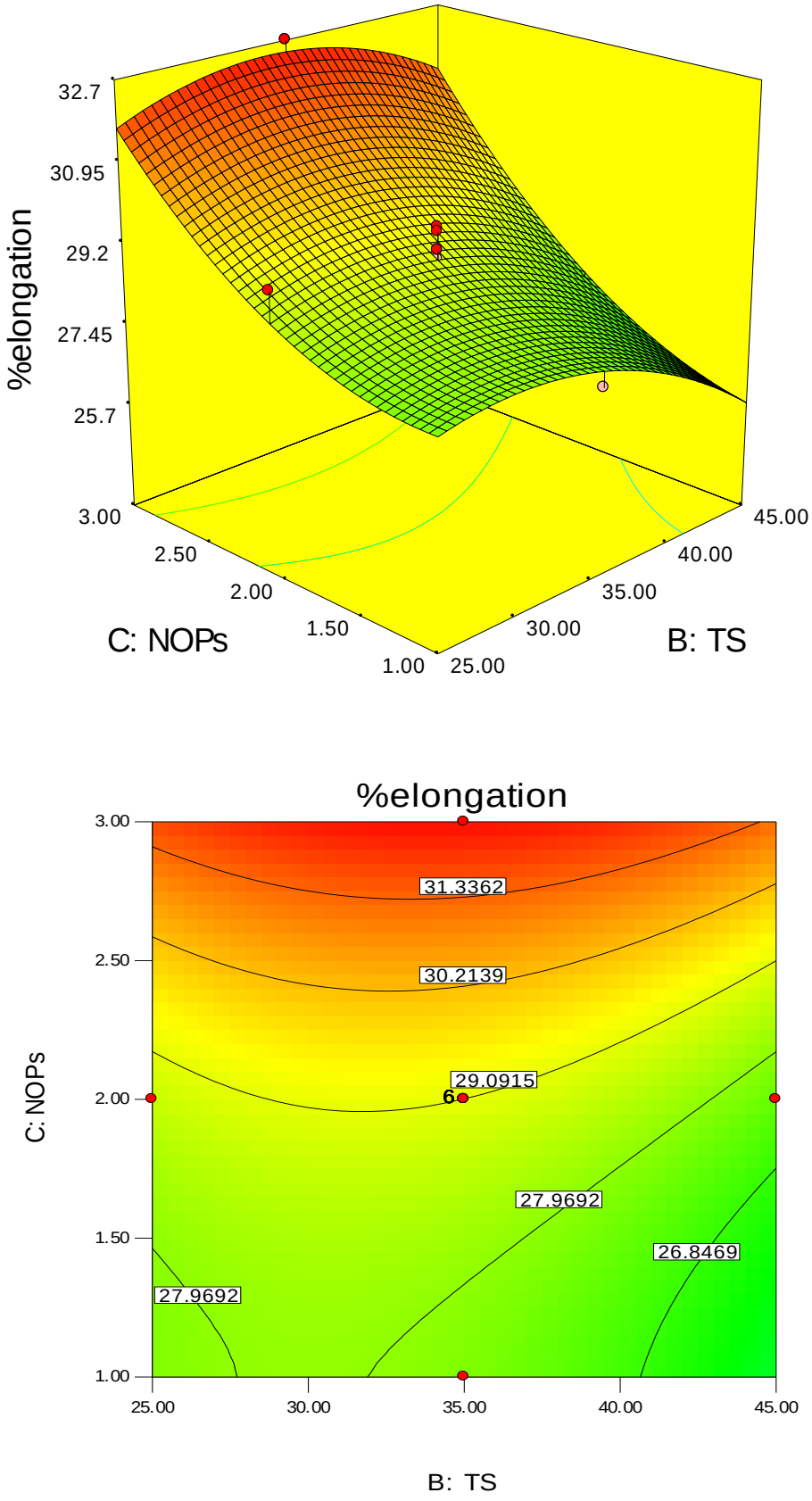

Figure 5.25: 3D response surface and contour plots of %elongation of reinforced joints embedded with SiC-mp

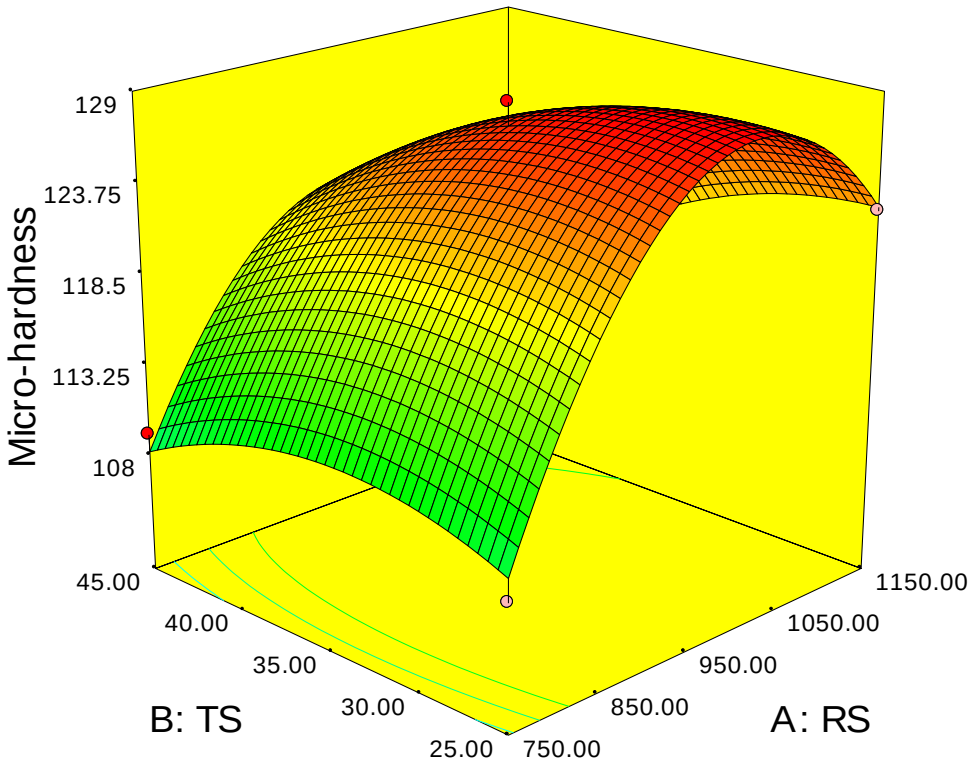
Micro-hardness
129
123.75
118.5
113.25
108
45.00
40.00
35.00
30.00
25.00
B: TS
750.00
850.00
950.00
1050.00
1150.00
A: RS

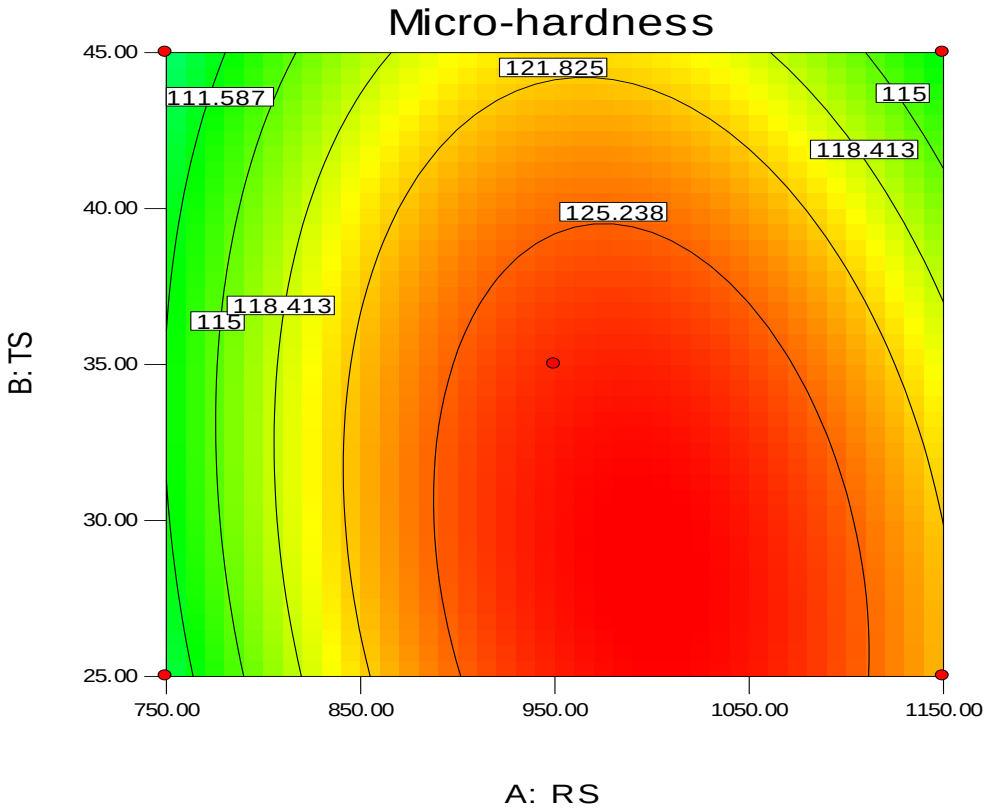
Micro-hardness
121.825
111.587
115
118.413
125.238
118.413
115
45.00
40.00
35.00
30.00
25.00
B: TS
750.00
850.00
950.00
1050.00
1150.00
A: RS

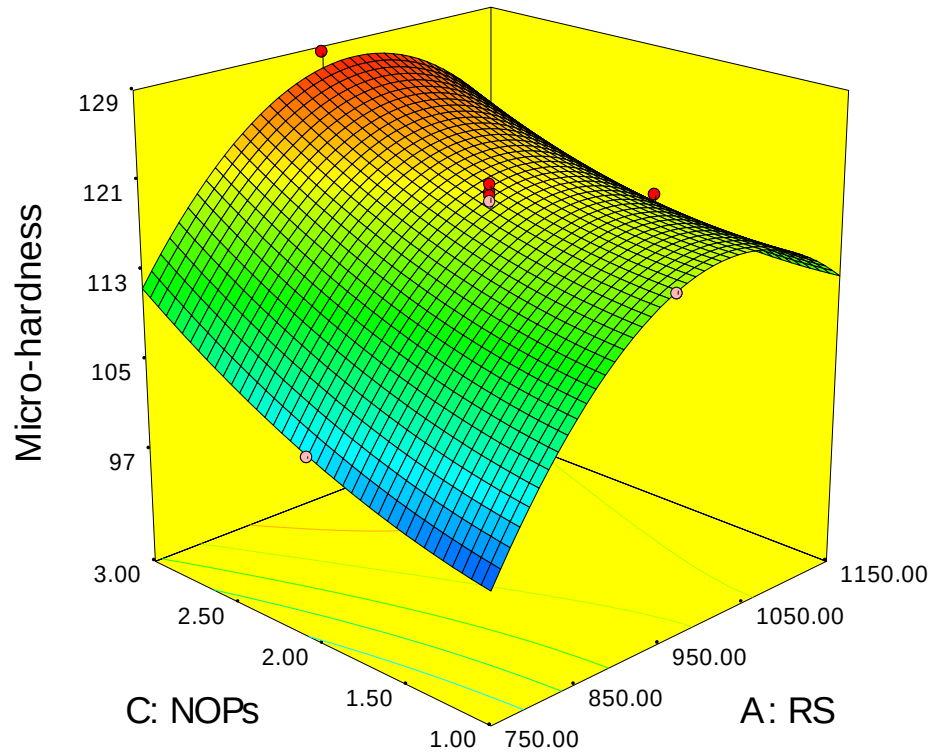
Micro-hardness
129
121
113
105
97
3.00
2.50
2.00
1.50
1.00
C: NOPs
750.00
850.00
950.00
1050.00
1150.00
A: RS

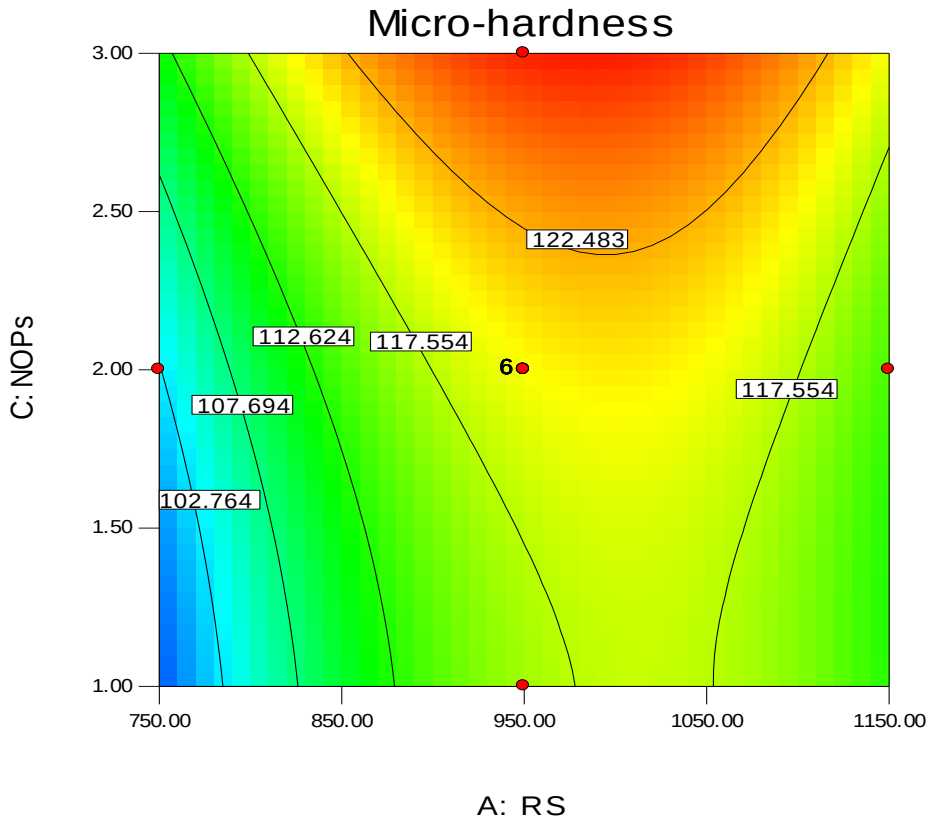
Micro-hardness
3.00
2.50
2.00
1.50
1.00
C: NOPs
122.483
112.624
117.554
6
107.694
117.554
102.764
750.00
850.00
950.00
1050.00
1150.00
A: RS

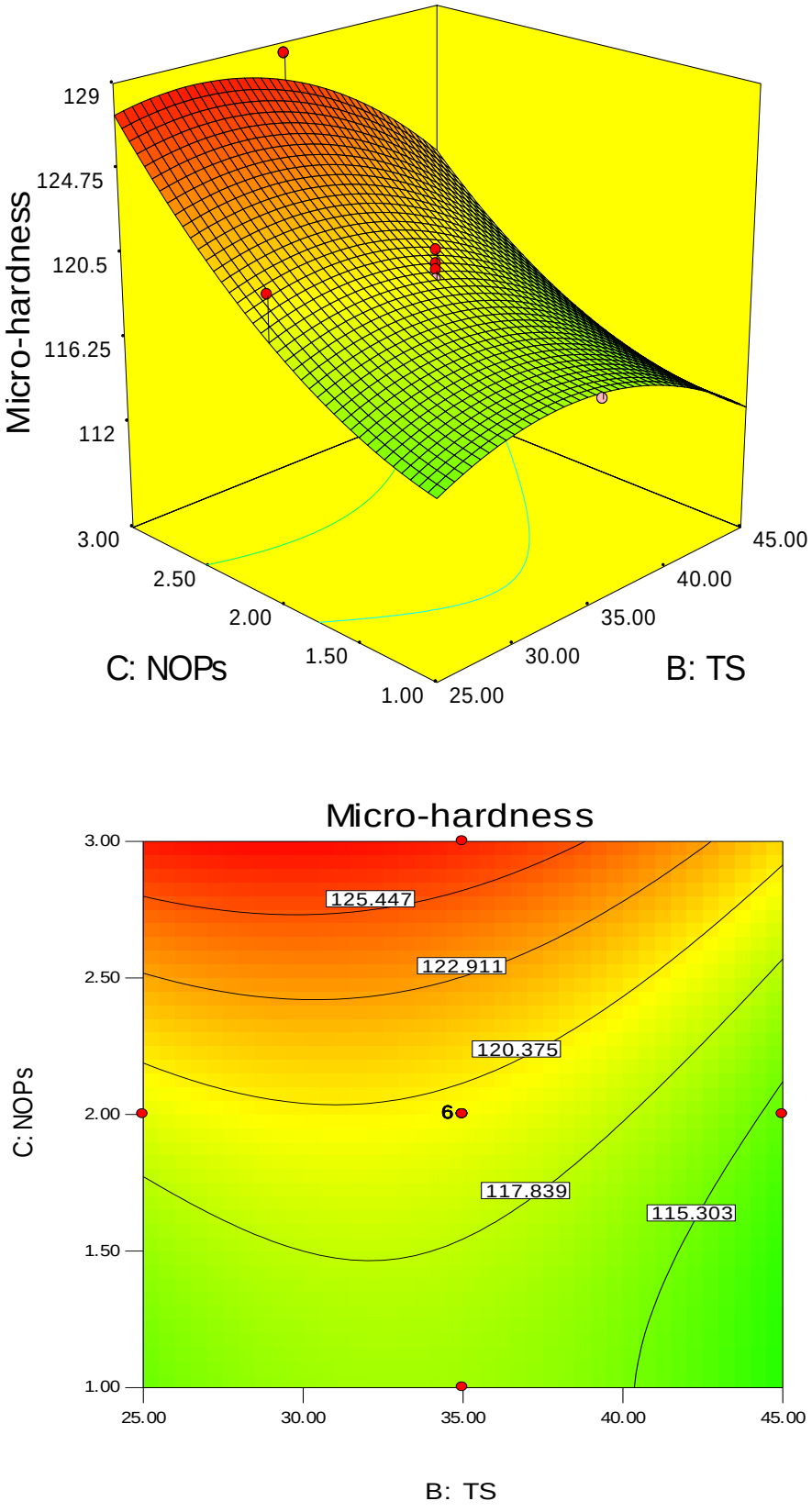

Figure 5.26: 3D response surface and contour plots of micro-hardness at stir zone of reinforced joints embedded with SiC-mp

The significance of grain refinement can be revealed by dynamic recrystallisation and pinning effect caused by SiC-mp. It can be observed that increasing RS value from 750 rpm to 950 rpm and number of passes from one to three enhances the tensile strength due to more uniform dispersion of SiC-mp resulting in enhanced pinning effect and reduced the grain size. The highest value of tensile strength (266.9 MPa) was found at RS of 950 rpm, TS of 35 mm/min after three passes of FSW. The minimum tensile strength of.171.70 MPa was found at RS of 750 rpm, TS of 45 mm/min after one pass of FSW due to clustering of SiC particles caused by inadequate tool stirring action. When the TS decreases from 45 to 35 mm/min, the tensile strength increases and on further decreasing TS, tensile strength decreases. Microhardness increases as traverse speed decreases. Increasing number of FSW passes increases the tensile strength, %elongation and microhardness due to improved material mixing in stir region leading to improvement in the tensile strength, %elongation and microhardness of the reinforced joints as depicted in Fig. (5.24-5.26).

5.6 MULTI RESPONSE OPTIMIZATION: DESIRABILITY

5.6.1 DESIRABILITY FUNCTION

Desirability is a multiple response technique that was explained by Derringer and Suich [162]. This technique is utilized for the optimization of various quality characteristic problems which is relevant to industry. The approach converts a predicted response into a scale-free value (di), which is designated as desirability, using desirability function, D(X). The geometric mean of weightage of each response's individual desirability is known as the composite desirability. The ideal parameter circumstances are regarded to be the factor settings that have the highest overall desirability. The optimization is carried through using:

(i) Determining each response's specific desirability (d);

(ii) Obtained the reinforced desirability (D) by combining the specific desirability;

(iii) Identifying the optimal settings by maximizing the obtained reinforced desirability.

In the present investigation, desirability function is employed to obtained the optimal parameters for reinforced FSWed joints to optimize tensile strength, microhardness and %elongation. In order to determine the best combination of variables and levels for the FSW of AA5083 and AA6061, a second order CCD with three variables (RS, TS, and

NOPs) each at three levels was utilized. The desirability function was used to achieve the multi-response optimization.

5.6.2 MULTIRESPONSE OPTIMIZATION

To effectively assess the effect of each response on overall desirability, limits and goals for each response were specified. Weights are applied in order to highlight a goal value, the upper or lower boundaries, or both. According to the particular industry, importance is allocated. Importance varies 1 to 3, 1 is allocated for the least important and 3 to the most important.

The goals and importance of input parameters like RS, TS and NOPs, and the response parameters like tensile strength, microhardness and %elongation are tabulated in Table 5.13. all response variables have been assigned with an importance of 3, lower and upper weight for tensile strength, microhardness is and %elongation to be assigned 1. The main purpose of the optimization process is to identify an optimal set of conditions that will satisfy all the criteria. The value of desirability does not mandatory to be 1 as if the any one response is increases then the other decreases. For the given design space constraints, seven optimal solutions are derived as tabulated in Table 5.14. The set of optimal parameters having higher desirability needed to provide the desired response parameters within the constraints is tabulated in Table 5.14.

Table 5.13: Range and importance of Input and Response parameters

Name	Goal	Lower Limit	Upper Limit	Lower Weight	Upper Weight	Importance
RS	is in range	750	1150	1	1	3
TS	is in range	25	45	1	1	3
NOPs	is in range	1	3	1	1	3
Tensile strength	maximize	185.95	266.97	1	1	3
%Elongation	maximize	19.5	32.7	1	1	3
Microhardness	maximize	94.3	128.4	1	1	3

The ramp function graph (Fig. 5.27) derived from Design Expert (7) software, demonstrates the desirability for tensile strength, %elongation and microhardness. Each ramp's dot indicates the response characteristic's factor setting or response prediction. The height of the dot indicates how desired it is. The range of desirability, ranging 0 to

1, depends on how closely the response comes to achieving the target. Employing this technology, several objective functions may be optimized. The desirable value for the optimized input and responses parameters is 1. The optimal value of tensile strength, microhardness and %elongation are 269.62 MPa, 128.47 HV and 32.75% respectively, whereas the optimized value of RS, TS and NOPs are 994.57 rpm, 29.40 mm/min, and after 3 passes, respectively as shown Fig. 5.27.

Table 5.14: Set of Optimal Solutions

Number	TRS	TS	NOPs	Tensile strength	%elongation	Micro-hardness	Desirability	
1	994.57	29.4	2.98	269.62	32.75	128.47	1	Selected
2	1003.62	28.39	3	269.64	32.82	128.82	1	
3	1025.31	28.13	2.98	268.91	32.83	128.55	1	
4	1026.04	29.28	2.99	270.15	33.00	128.50	1	
5	1008.28	30.55	2.99	270.99	33.02	128.41	1	
6	974.3	32.8	3	270.91	32.83	127.74	0.99	
7	1016.38	37.23	3	271.50	33.14	125.60	0.97	

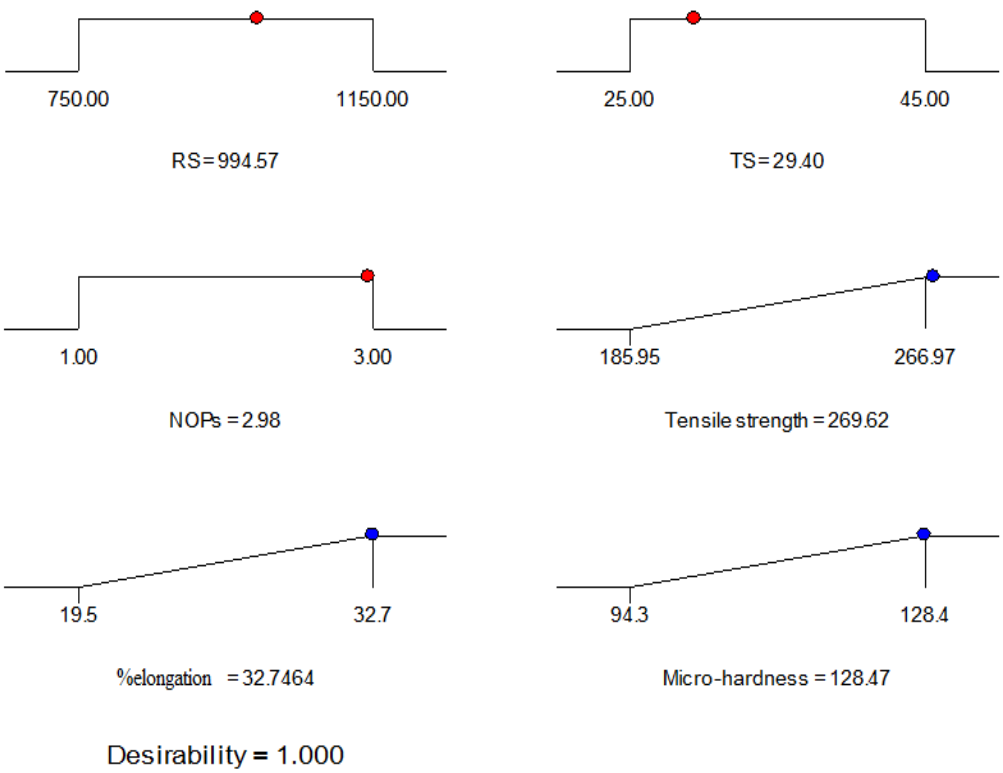

Figure 5.27: Ramp function graph for optimization of input and multi response parameters for reinforced FSWed joints embedded with SiC-mp

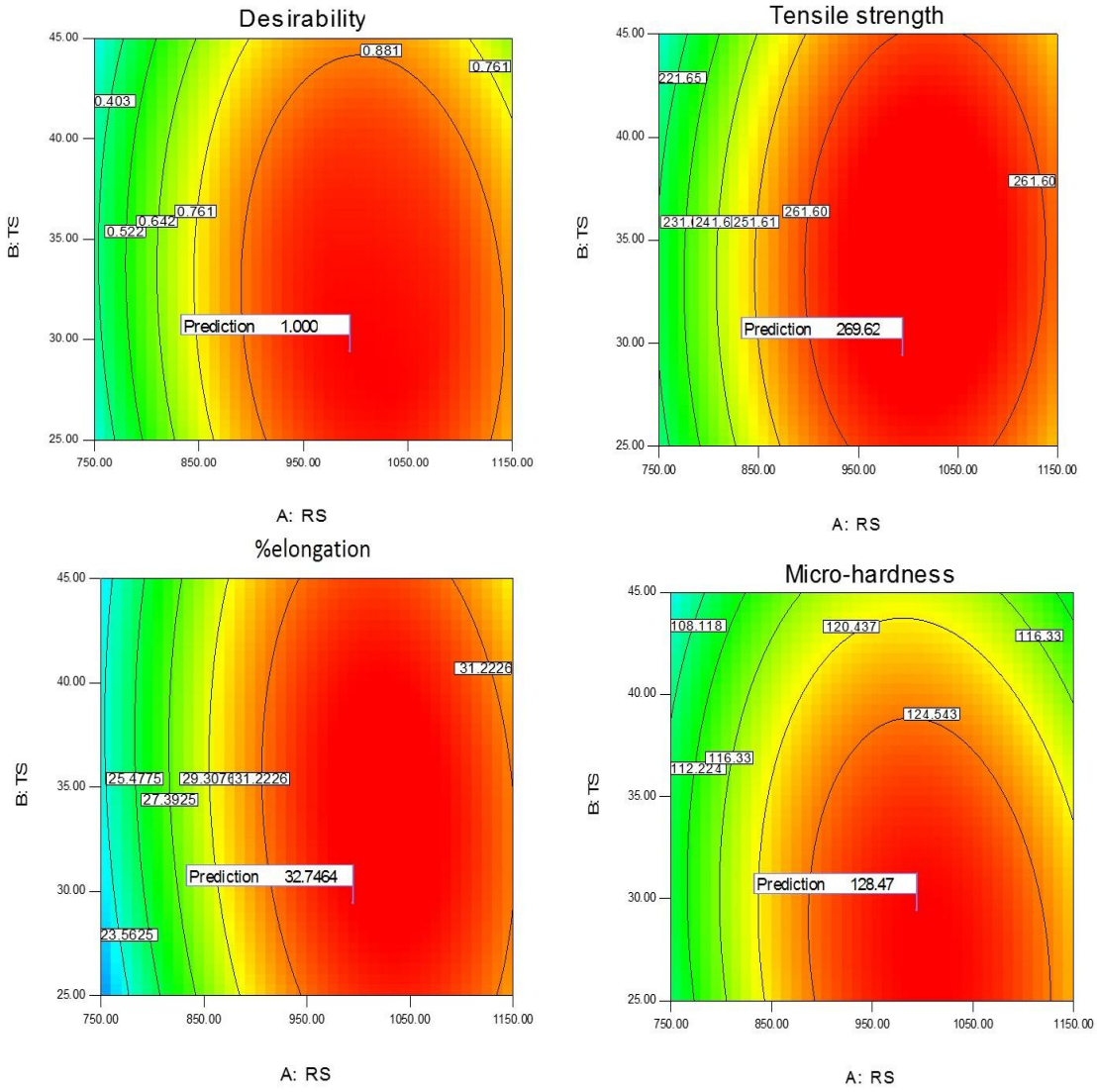

Figure 5.28: Optimized out responses of reinforced FSWed joints embedded with SiC-mp

5.7 MICROSTRUCTURE ANALYSIS OF REINFORCED JOINTS INCORPORATED WITH SiC MICROPARTICLES

The microstructure images of reinforced FSWed joints of AA6061 and AA5083 embedded with 6 % volume fraction of SiC-mp were taken from stir zone with different processing conditions. These were compared to each other on the basic dispersion pattern of SiC-mp and grain size. The weld zone of the reinforced FSWed joints includes stir zone (SZ), Heat affected zone (HAZ) and thermo-mechanical affected zone (TMAZ). From Fig. 5.29, it can be noticed that the grain size continues to reduce from HAZ to TMAZ and subsequently to SZ [163-165].

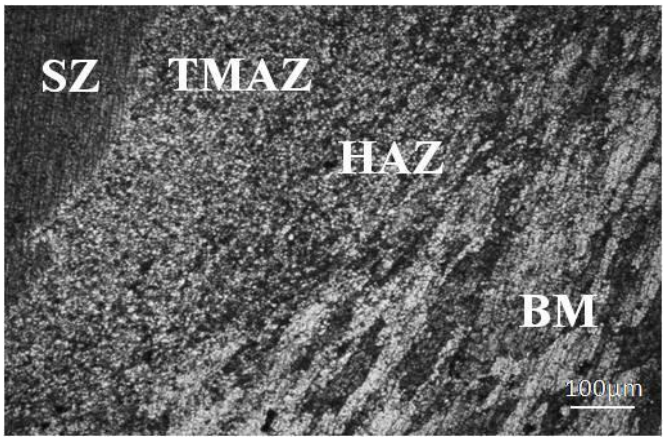

Figure 5.29: Various zones in the weld zone of reinforced FSWed joint

Grain size was the most significant factor of the mechanical properties of an unreinforced FSWed joint. whereas, other parameters, such as the size of the RPs, the bonding quality between the matrix and the RPs, the RPs dispersion pattern, and the location produced by matrix's unequal thermal expansion coefficient, all contribute to the mechanical characteristics of the reinforced FSWed joint [166]. After FSW, the stretched microstructure of AA6061 and AA5083 was turned into dynamically recrystallized equiaxed grains structure in the SZ by the tool's stirring action. The annealing effect, DRX, and the influence of dispersion pattern of RPs in the metal matrix of the SZ all contribute to grain refining during FSW [167]. All of these phenomena compete for dominance, and the grain size is determined by the dominant factors. DRX caused by plastic deformation at high temperatures, resulting in the conversion of high angle to low angle boundaries and nucleate new grains at preferential locations, reducing grain size [168].

The impact of annealing is caused by a high heat input at higher value of RS and lower value of TS, which promotes grain growth and coarsens the grains [136]. The RPs in the SZ behaves as barriers to grain boundaries and prevent the grain expansion via pinning effect [137]. Consequently, in the reinforced FSWed joints produced at different values of RS and TS, the DRX phenomenon and the influence of dispersion pattern of RPs (SiC-mp)and annealing effect are dominating factors for deciding the grain size [138]. The FESEM micrograph (Fig 5.30 a) of the SZ of specimen no. 19 processed at RS of 750 rpm and TS of 45 mm/min with one pass of FSW depicts the clusters of SiC-mp caused by inadequate material mixing as a result of insufficient plastic strain at low RS value [139].

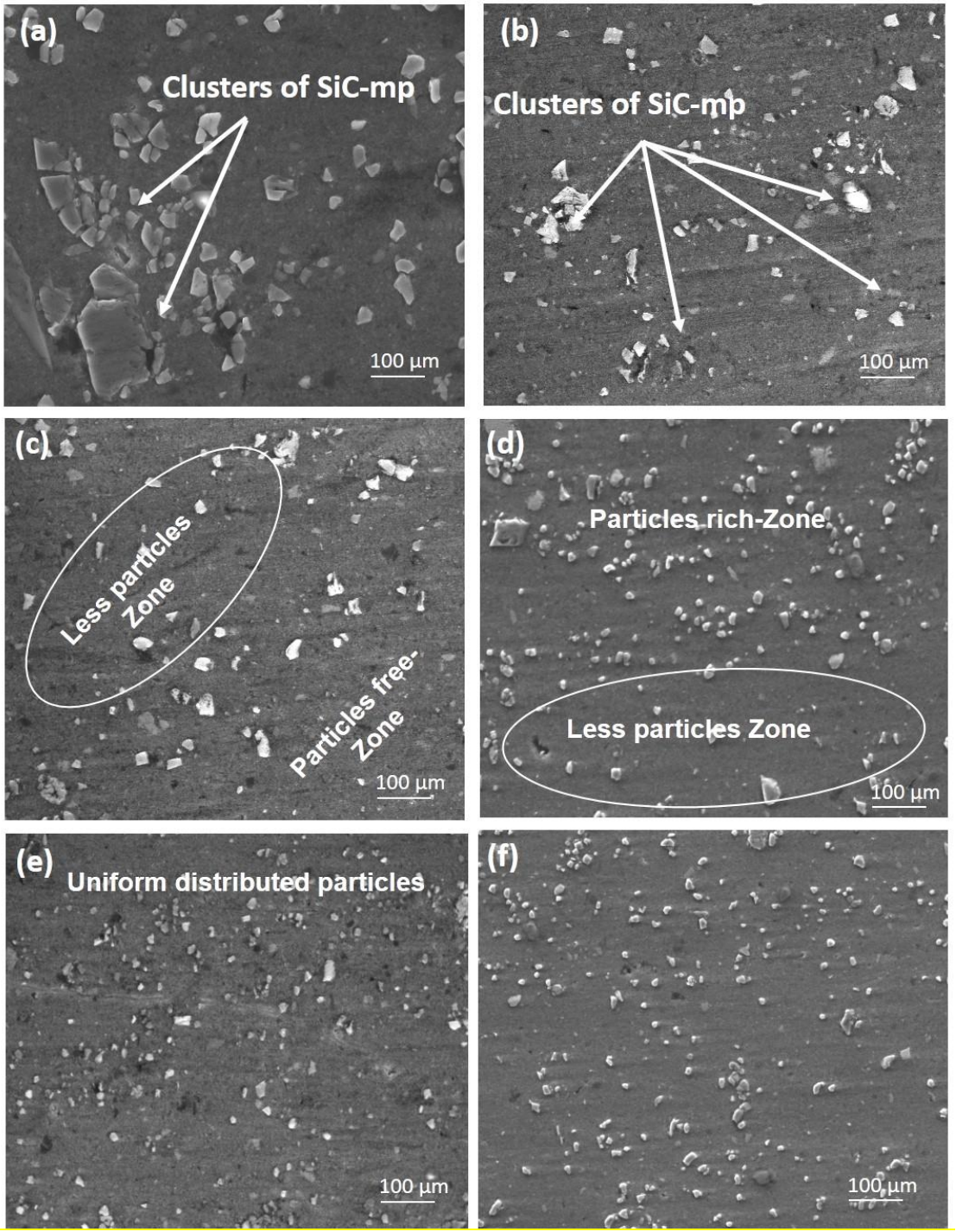

Figure 5.30: FESEM micrograph of particles distribution in the SZ, (a-b) at 750 rpm after, a) one pass, (b) Three Passes; (c-e) at 950 rpm after, (a) one pass, (b) Two Passes, (c) three passes, (f) at 1150 rpm after three passes

The clustering of SiC-mp reduces on increasing the number of passes from one to three processed at RS of 750 rpm and TS of 45 mm/min (specimen no. 1), but still small clusters SiC-mp were observed after three passes of FSW, as depicted in Fig.5.30 b. Therefore, the mean grain size in the SZ was observed as 10.1 µm as depicted in Fig.

5.31 a. Fig. 5.30 (c-e), depicts the SZ of multi-pass reinforced FSWed joints at RS of 950 rpm and TS 35 mm/min and also confirms the RPs dispersion pattern.

The clusters of SiC-mp were found absent at higher RS of 950 rpm, TS of 35 mm/min and one-pass of FSW (specimen no. 16) due to enhanced stirring action of tool at higher rotational speed. Rich particles zone, less particles zone and particles free zone were observed after one pass of FSW as depicted in Fig. 5.30 c. Therefore, it is obvious that one pass of FSW at 950 rpm was also not sufficient for the homogeneous dispersion of the SiC-mp [140]. The particles free zones were found absent after two passes of FSW (specimen no. 14) due to repeated strain produced by repeated passes of FSW which promotes the dispersion of SiC particles in the SZ.

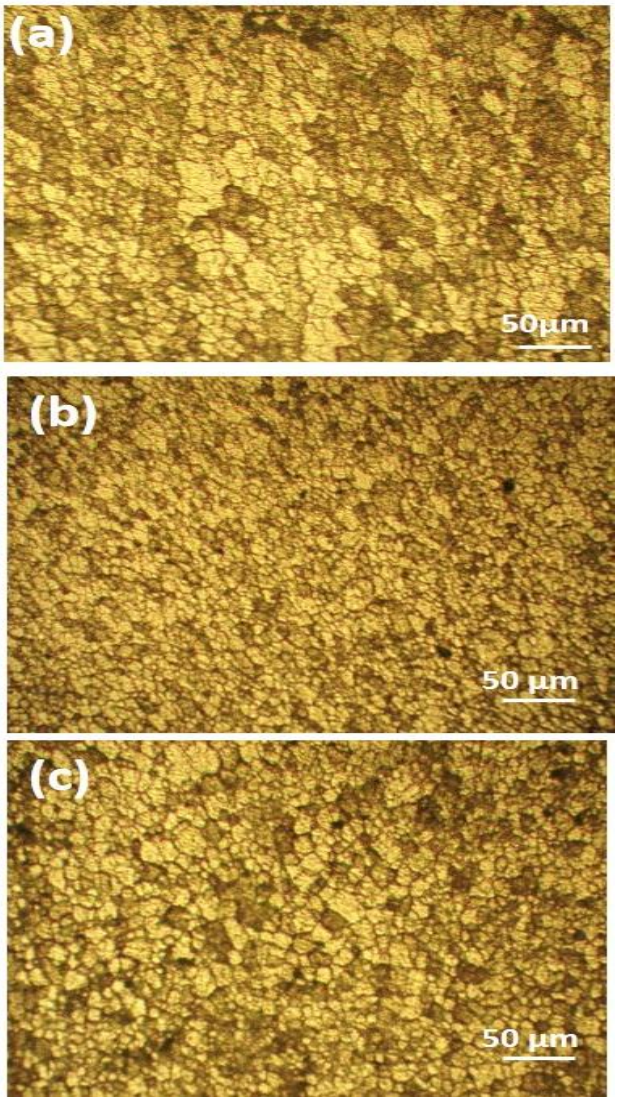

Figure 5.31: Grain structure of the SZ of various reinforced FSWed joints, (a) at 750 rpm after three Passes; (b) at 950 rpm after three passes, (f) at 1150 rpm after three passes

Moderate dispersion of SiC-mp, including less-particles region and rich-particles region was observed in the reinforced FSWed joint produced after two passes of FSW as delineated in Fig. 5.30 d. The dispersion of SiC-mp was more pronounced and uniform, after implementing three passes of FSW (specimen no. 9), as observed in Fig. 5.30 e. The particle dispersion was found improved due to repeated strain on increasing number of passes from one to three passes of FSW as obvious in Fig 5.30 (c-e). Thus, the increment in the number of passes from one to three reduced the size of grain due to more uniform dispersion of SiC-mp particles that resulted in higher dislocation sources and enhanced dynamic-recovery and recrystallization [172]. The SZ of the reinforced joints produced at RS of 950 rpm, TS of 35 mm/min after three passes of FSW, exhibited the mean grain size of 3.7 µm, as depicted in Fig. 5.31 (b).

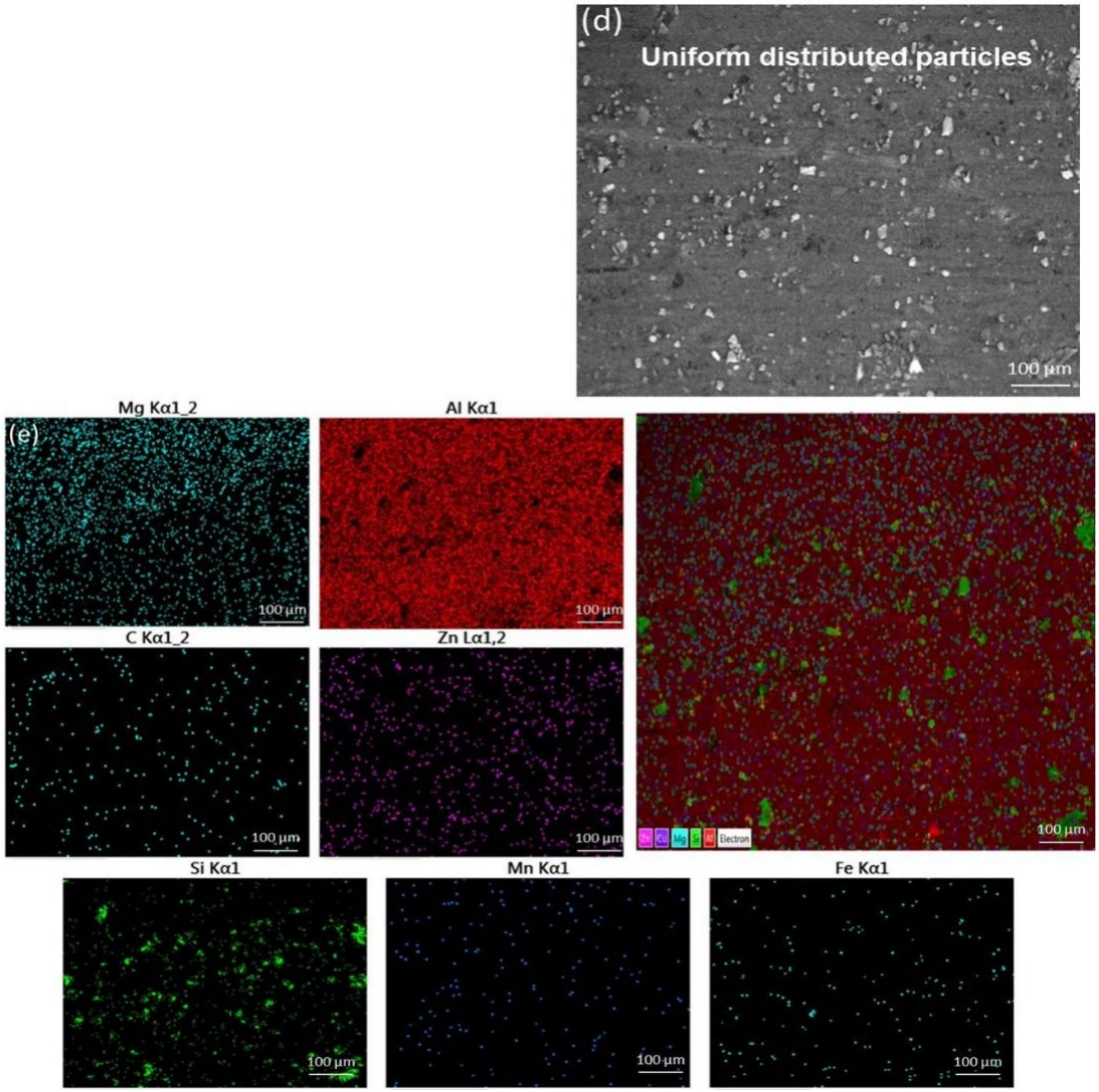

Figure 5. 32: Elemental mapping of the SZ at 950 rpm, 35 mm/min after three passes (specimen no. 9)

The more uniform dispersion of particles of particles were also noticed in reinforced FSWed joint produced at RS of 1150 rpm, TS of 25 mm/min and after three passes of FSW (specimen no. 12), as demonstrated in Fig. 5.30 f. The increased mean grain size of 5.8 µm (Fig. 5.31 c) was observed in the SZ due to domination of annealing effect at higher heat input at RS of 1150 rpm after three passes of FSW. Therefore, the optical microstructure reveals that DRX and pinning effect caused by the uniform dispersion of SiC-mp resulting in the formation of fine and equiaxed grains. Fig. 5.32 delineates the elemental mapping of the SZ after three-pass FSWed joint embedded with the SiC particles. The silicon mapping also confirms the uniform dispersion of SiC-mp after three-pass FSW. Fig. 5.33 a and b depicts the peaks of the EDS results of reinforced FSWed joints produced after three passes of FSW with RS of 750 rpm (specimen no. 1) and 950 rpm(specimen no. 9), respectively. The EDS findings of reinforced FSWed joint demonstrated the presence of SiC-mp in the SZ. The elemental characterization obtained by EDS analysis also revealed that the SZ of specimen no. 1 and specimen no. contained 5.65% and 5.57% of Si, and 4.72% and 4.02% of C, respectively. These findings reveal the inclusion of SiC-mp to the SZ of reinforced FSWed joints.

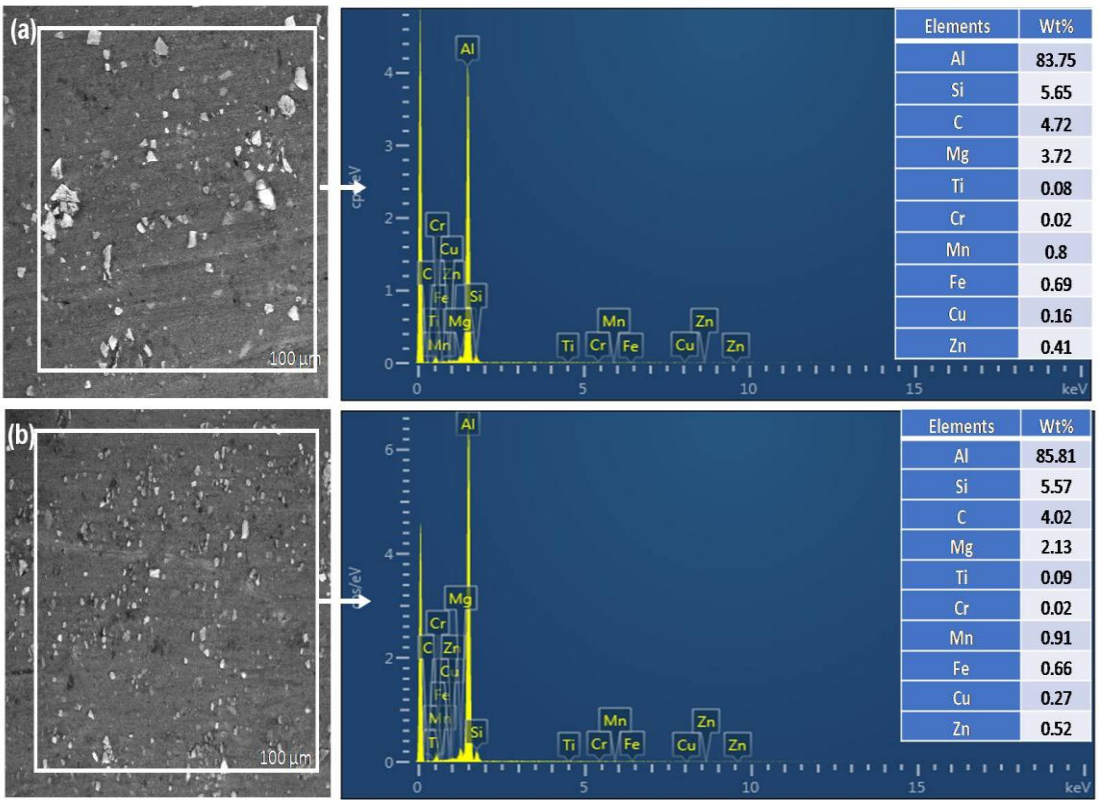

Figure 5. 33: EDS peak of reinforced FSWed joints at stir zone, (a) Specimen no.-1, (b) Specimen no.-9

5.7.1 FRACTURE SURFACE ANALYSIS

Fig. 5.34 shows the microstructure of the fractured surfaces of different reinforced FSWed joints. In order to recognize the microstructure of the failure pattern of the reinforced joint, FESEM was utilized. Interestingly, during tensile loading, some samples were fractured from the welded region whereas some samples were fractured in heat affacted zone (HAZ) region towards softer base material i.e. AA 5083, where the strength and hardness were minimal. Previous studies were also revealed that the FSWed joints generally fractured at the HAZ towards weaker base material in case of FSWed dissimilar aluminum alloys [173]. This may lead to an enhanced degree of dispersion of SiC particles, which resist the migration of dislocations under axial stress.

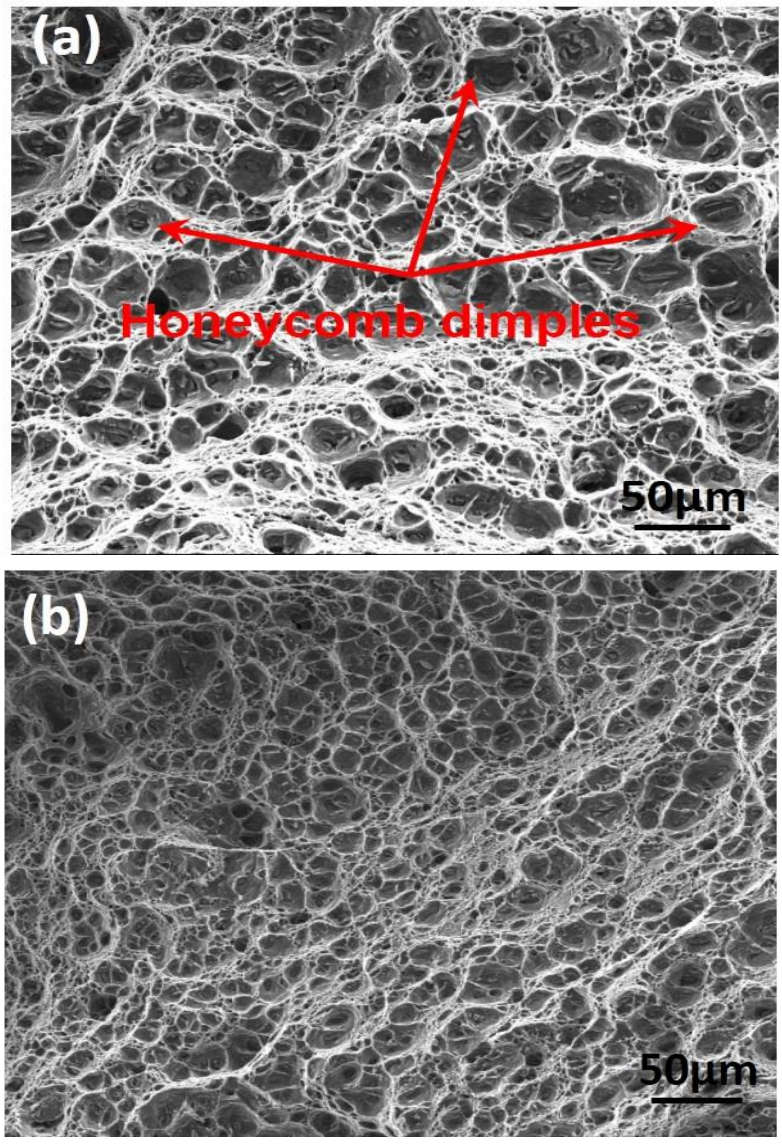

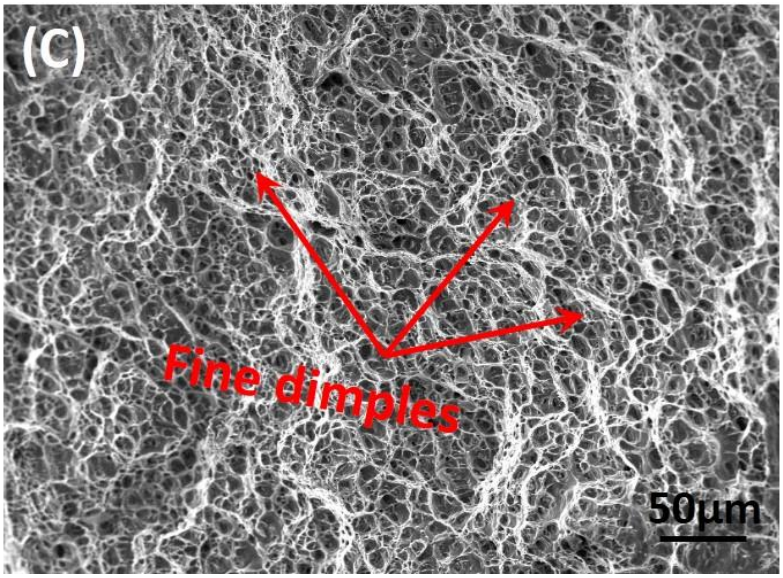

Figure 5.34: Fractured surface morphology of SiC reinforced FSWed joints, (a) at 750 rpm, 45 mm/min after three FSW passes, (b, c) at 950 rpm and 35 mm/min after, (b) one FSW pass, (c) three FSW passes

The fractured surface for SiC-mp reinforced FSWed joint showing tiny and equiaxed dimples, signifying fracture of ductile mode (Fig. 5.34 c) compared with that of other reinforced FSWed joints (Fig. 5.34 a, b). As depicted in Fig. 5.34 a, honeycomb dimples with a ductile fracture were observed in reinforced joint produced at RS of 750 rpm, TS of 45 mm/min after three FSW passes depicted the regularly separated features of cleavage and plastic deformation [174]. All of the reinforced FSWed joints were developed under various parametric settings, which led to a reduction in grain size, effective material mixing, and the development of fine, equiaxed dimples. The fractured metal matrix identified at HAZ was confirmed by variance in microhardness, which led to increased ductility. According to the study of the tensile samples' fractured surface, the addition of SiC-mp enhanced the tensile strength of reinforced joints.

5.8 COMPARATIVE ANALYSIS of Al_2O_3 and SiC REINFORCED FSWED JOINTS

To evaluate the comparative analysis of reinforced FSWed joints embedded with micro-sized Al_2O_3 and SiC particles, their maximum tensile strength, %elongation, and microhardness were compared as tabulated in Table 5.15. The comparative analysis reveals that reinforced FSWed joints embedded with SiC microparticles shows higher

maximum tensile strength, % elongation and microhardness as compared to those of the reinforced FSWed joints embedded with Al_2O_3 micro particles.

Table 5.15: Comparative analysis between reinforced FSWed joints embedded with Al_2O_3 and SiC microparticles

Response parameters	Al_2O_3-mp reinforced FSWed joints	SiC-mp reinforced FSWed joints	% improvement
Tensile strength (MPa)	254.42	266.97	4.93
%elongation (%)	30.9	32.7	5.82
Microhardness (HV)	124.2	128.4	3.38

5.9 RESEARCH CONTRIBUTION

To investigate the effects of micro-sized Al_2O_3 and SiC particles on the weld quality of dissimilar aluminum alloys AA5083 and AA6061, the joint efficiency, %elongation and microhardness of reinforced FSWed joints were compared with those of previous studies and tabulated in Table 5.16. It was observed that the incorporation of micro-sized Al_2O_3 and SiC particles significantly improved the joint efficiency, %elongation and micro-hardness of dissimilar weld joint of AA5083 and AA6061.

Table 5.16: Comparison between present research work with previous research work

Parametric Condition	Weld joint	Joint efficiency	Micro-hardness-	% Elongation	Author
RS-630 and 1600 rpm TS-16, 25 and 40 mm/min	AA6061/AA5083	71.2%	Less than both AA6061 and AA5083	------	Chiteka et al. [178]
RS-700 - 2500 rpm TS-25-400 mm/min Shoulder dia. - 10-14 mm Pin dia. - 2-4 mm	AA6061/AA5083	72.3%	Less than both AA6061 and AA5083	------	Ghaffarpour et al. [179]

TRS-900,1000, 1100 rpm TS- 100, 150, 190 mm/min Plunge depth- 0.1, 0.2, 0.3 mm	AA6061/AA5083	76.80 %	higher than both AA5083 and AA 6061	------	Krishnan and Subramaniama [180]
RS-950 rpm TS- 35 mm/min Number of pass- 1,2,3. VF of Al_2O_3-mp- 6%	AA6061/AA5083	87.6 %	45.4 % higher than AA5083	higher than both AA5083 and AA6061	Preety and Mishra
RS-950 rpm TS- 35 mm/min Number of pass- 1,2,3. VF of Al_2O_3-mp- 6%	AA6061/AA5083	91.98 %	50.3 % higher than AA5083	higher than both AA5083 and AA6061	Preety and Mishra [181]

5.10 EFFECT OF Al_2O_3 NANOPARTICLES INCORPORATION THE DISSIMILAR REINFORCED JOINTS

The friction stir welding was also performed to successfully fabricate the dissimilar reinforced joints of AA5083 and AA6061 embedded with of 6 % volume fraction of Al_2O_3 nano-particles (Al_2O_3-np), in order to investigate the effects of FSW parameters, Al_2O_3 particles and multi-pass FSW on the microstructural and mechanical characteristics of the reinforced FSWed joints. The FSW was performed at constant rotational speed, traverse speed, and tool tilt angle of 950 rpm, 30 mm/min, and 1˚, respectively. The reinforcement conditions of Al_2O_3-np with the different number of passes are tabulated in Table 5.17. The FSWed specimens after implementation of different number of FSW passes and reinforcement condition.

Table 5. 17: FSWed Specimens welding conditions

S/No.	Rotational speed (RPM)	Traverse speed (mm/min)	No. of FSW passes	Reinforcement condition
1	950	30	One-pass (1P)	Without Al_2O_3-np
2	950	30	One-pass (1P)	With Al_2O_3-np
3	950	30	Two-pass (2P)	With Al_2O_3-np
4	950	30	Three-pass (3P)	With Al_2O_3-np

5.10.1 MICROSTRUCTURAL ANALYSIS

Grain size was the most significant factor of the mechanical properties of an unreinforced FSWed joint. whereas, other parameters, such as the size of the RPs, the bonding quality between the matrix and the RPs, the RPs dispersion pattern, and the location produced by matrix's unequal thermal expansion coefficient, all contribute to the mechanical characteristics of the reinforced FSWed joint [150]. After FSW, the stretched microstructure of AA6061 and AA5083 was turned into dynamically recrystallized equiaxed grains structure in the SZ by the tool's stirring action. The annealing effect, DRX, and the influence of dispersion pattern of RPs in the metal matrix of the SZ all contribute to grain refining during FSW. All of these phenomena compete for dominance, and the grain size is determined by the dominant factors. DRX caused by plastic deformation at high temperatures, resulting in the conversion of high angle to low angle boundaries and nucleate new grains at preferential locations, reducing grain size. The impact of annealing is caused by a high heat input at higher value of rotational speed and lower value of traverse speeds, which promotes grain growth and coarsen the grains [167].

The RPs in the SZ behave as barriers to grain boundaries and prevent the grain expansion [168]. Consequently, at rotating speed of 950 rpm and traverse speed 30 mm/min, the DRX phenomenon and the influence of dispersion pattern of RPs (Al_2O_3-np) are dominating factors in the grain size reduction. Due to the absence of Al_2O_3-np in unreinforced FSWed joints, only the DRX effect is prominent, and decreased the grain size. However, in Al_2O_3-np reinforced FSW joints, both DRX and the impact of Al_2O_3-np are dominating for the grain size reduction [169].

Fig. 5.35 depicts the FESEM micrographs of all the FSWed joints. Fig. 5.35 (a) depicts the micrograph of 1P-unreinforced FSWed joint. whereas Fig. 5.35 (b-d) depicts micrographs of reinforced joints subjected to multi-pass FSW. The SZ of 1P-unreinforced FSWed joint (Fig. 5.35 a) demonstrated appropriate intermixing of both the alloys without any defect. Fig. 5.35 (b-d), depicts the SZ of multi-pass reinforced FSWed joints and also confirms the RPs dispersion pattern. The clustering of Al_2O_3-np were observed in the SZ of 1P-reinforced FSWed joint as depicted in Fig. 5.35 b. Therefore, it is obvious that 1P-FSW was not sufficient for the homogeneous dispersion of the particles due to asymmetrical material flow [170].

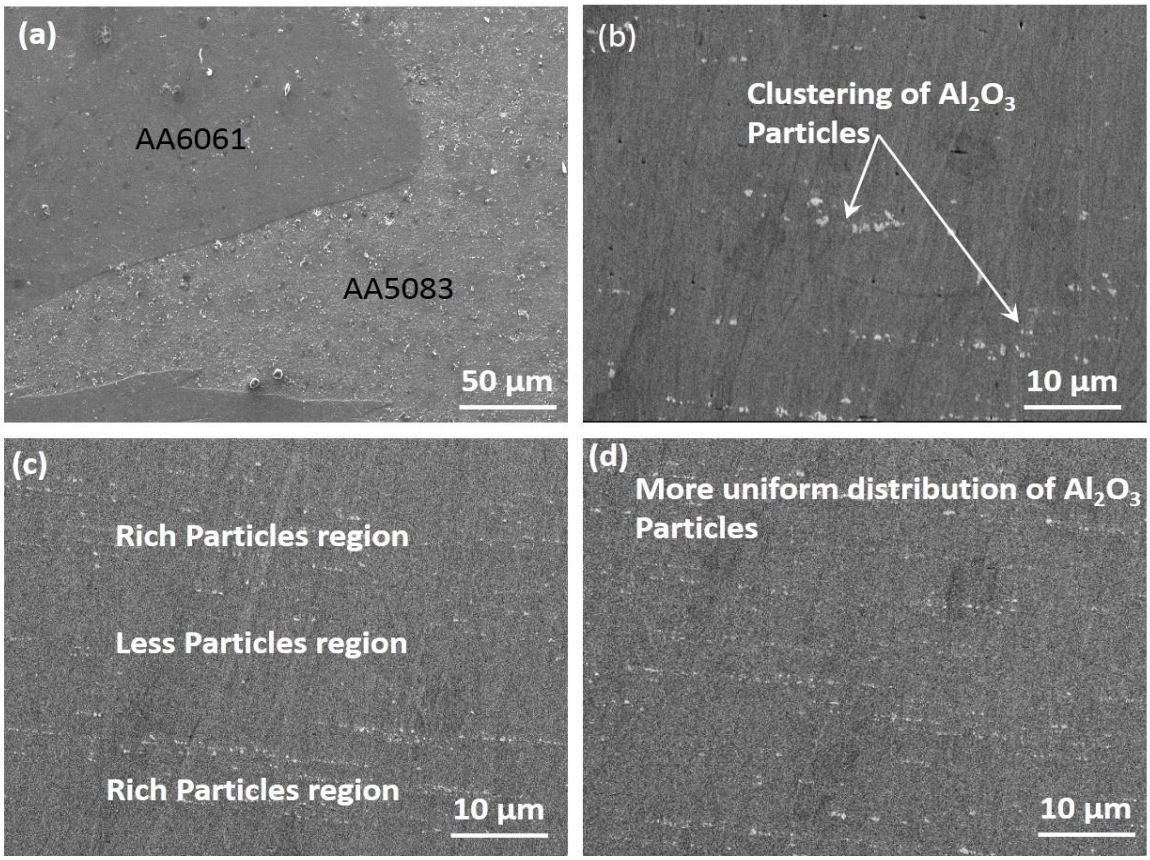

Figure 5. 35: FESEM micrograph (a) 1P- unreinforced FSWed joint, (b-d) Al_2O_3-np reinforced FSWed joint, (b) 1P, (c) 2P, (d) 3P.

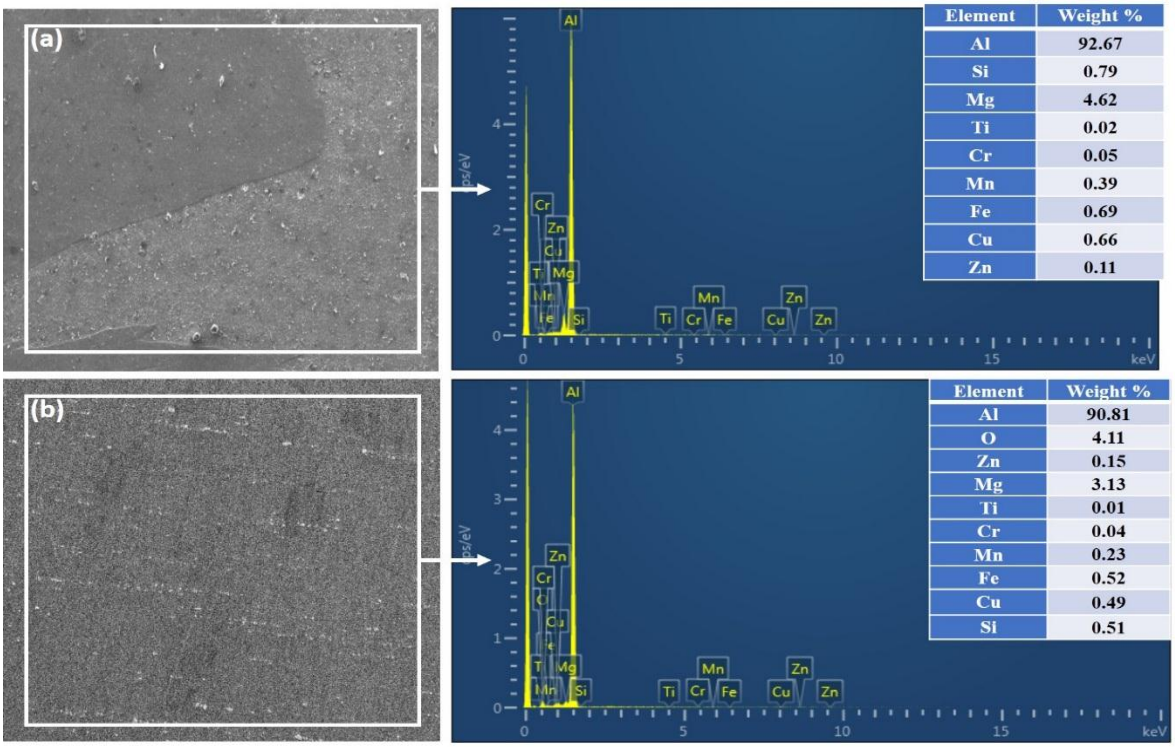

Figure 5. 36: EDS peaks of FSWed joints, (a) 1P-unreinforced FSWed joint, (b) 3P-reinforced FSWed joint

The clustering of Al_2O_3-np was found absent after 2P-FSW and the moderate dispersion of particles including rich-particle zone and less-particle zone were observed, as depicted in Fig. 5.35 c. The dispersion of Al_2O_3-np was more pronounced and uniform, after implementing 3P-FSW, as observed in Fig. 5.35 d. Therefore, it is obvious in Fig 5.35 (b-d) that particle dispersion was found to improve by breaking clusters of Al_2O_3-np on increasing number of passes from 1P to 3P. Thus, the increment in the number of passes from 1P to 3P reduced the size of grain due to more uniform dispersion of Al_2O_3-np particles that resulted in higher dislocation sources and enhanced dynamic-recovery and recrystallization [171].

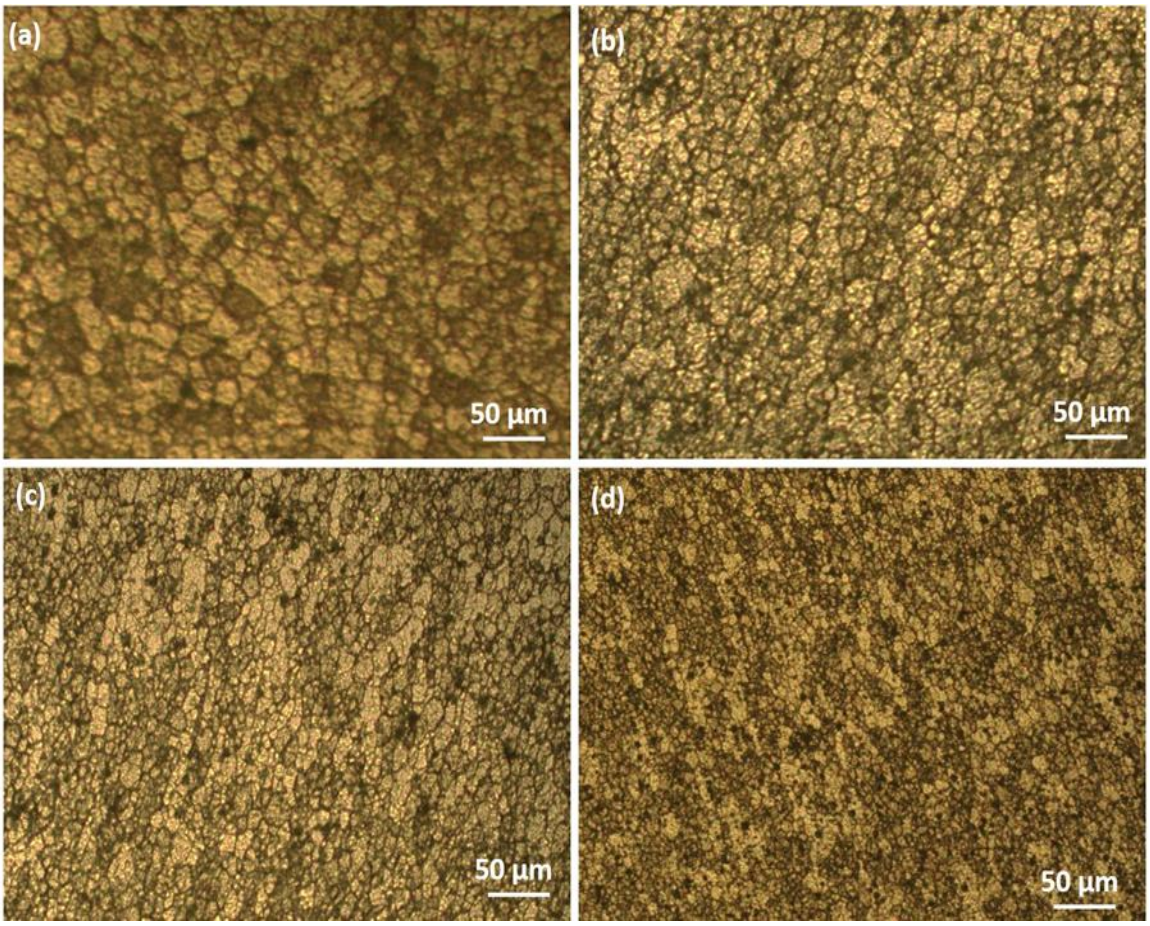

Figure 5. 37: Grain structure macrographs, (a) 1P-unreinforced FSWed joint, (b-d) Al_2O_3-np reinforced FSWed joint, (b) 1P, (c) 2P, (d) 3P.

Thus, the optical microstructure indicates that fine and equiaxed grain structures were formed due to DRX and pinning effect caused by the uniform dispersion of Al_2O_3-np. Fig. 5.36 depicts the peaks of the EDS results of 1P-unreinforced FSWed joint and 3P-reinforced FSWed joint. The EDS findings of 3P-reinforced FSWed joint demonstrated the presence of Al_2O_3-np in the SZ. The elemental characterization obtained by EDS

analysis also revealed that the SZ of 3P-reinforced FSWed joint contained 4.11 % of oxygen. These findings reveal the inclusion of Al_2O_3-np to the SZ by FSW.

5.10.2 GRAIN SIZE CHARACTERIZATION

The grain structure of 1P-unreinforced FSWed joint and multi-pass Al_2O_3-np reinforced FSWed joints was studied. Fig. 5.37 depicts the grain structure of unreinforced FSWed joints and multi-pass Al_2O_3-np reinforced FSWed joints. AA6061 and AA5083 were observed as coarse grain structures with a grain size of 37 and 41 μm, respectively. Whereas, in the SZ of 1P-unreinforced FSW contains fine recrystallized grains of size 17 μm (Fig. 5.37 a), compared with base materials due to severe plastic deformation and DRX [172]. The grain structure of 1P-reinforced FSWed joint was observed to be finer with a granular size of 10.4 μm (Fig. 5.37 b). The grain structure was further diminished as the number of passes were increased from 1P to 3P. This can be attributed to the presence of Al_2O_3-np in the SZ as the other FSW conditions were same for all FSWed joints. More uniformly dispersed Al_2O_3-np offer more hindrances against grain boundaries and prevent grain growth. The particle induced nucleation-based DRX is possible when dislocations start accumulating due to RPs during plastic deformation [173]. Consequently, the grain size of the Al_2O_3-np reinforced FSWed joint after 2P and 3P was observed as 3.9 μm and 2.8 μm, respectively (Fig. 5.37 c, d). Consequently, it can be concluded that the incorporation of Al_2O_3-np with multi-pass FSW reduced the grain size.

Table 5. 18: Ultimate tensile strength (UTS), %elonation and micro-hardness of various FSWed Joints

FSW conditions	UTS (MPa)	Joint's efficiency (%)	%elongation	Micro-hardness (HV)
1P-unreinforced FSW	205.8	71.32	20.7	108.5
1P-reinforced FSW	227.3	78.38	24.4	127.1
2P-reinforced FSW	257.4	88.76	26.8	136.4
3P-reinforced FSW	272.7	94.03	30.7	145.7

5.10.3 INFLUENCE ON TENSILE STRENGTH

From Table 5.18, it can be observed that the tensile strength of the 1P-unreinforced FSWed joint is less than the base materials due to softening of the aluminum metal matrix [174]. Prior to the investigation of the number of FSW passes, a comparison was made between the tensile strength of 1P-unreinforced and reinforced FSWed joint. The tensile strength of 1P- reinforced FSWed joint was observed higher than the 1P-unreinforced FSWed joint. This can be attributed to the presence Al_2O_3-np of that prevent the movement of dislocation boundaries and reduce the grain growth, which cause the smaller gain size [175].

The tensile strength of the reinforced FSWed joint influenced by the grain size, dislocation density, and bonding strength between the metal matrix and the RPs . On increasing in the FSW passes from 1P to 3P enhanced the dispersion of RPs in the SZ. More homogenous dispersion of particles provides higher obstacles to prevent grain growth, which further reduces grain size [176].

The mean tensile strengths of AA6061and AA5083 was determined to be 310 and 290 MPa, respectively. Furthermore, the %elongation was found to be 21.9 and 20, respectively. The tensile properties of the reinforced FSWed joint was observed improved in comparison with unreinforced FSWed joint after implementing multi-pass FSW. Consequently, 3P-reinforced FSWed joint exhibits the highest tensile strength of 272.7 MPa which is nearly 94% of as-received AA5083. These results are in agreement with the findings of Jamalian et al. [177]. The %elongation of reinforced FSWed joints was found higher than the unreinforced FSWed joint and base materials. The enhanced %elongation of reinforced FSWed after one, two and three passes was observed as 24.4, 26.8 and 30.7, respectively. Fig. 5.38 depicts the FESEM micrographs of fractured surfaces of all the weld joints. In all FSWed joints, failure happened in the HAZ on the side of AA5083 during the tensile test due to minimal hardness. Dimples like structure was observed, in the fractured surface micrograph of all the joints, which represent the ductile mode of failure during tensile loading. In addition, the fractured surface micrograph of the unreinforced FSWed joint revealed large and deep dimples (Fig. 5.38 a). Whereas smaller dimples were noticed in the fractured surface micrograph 1P Al_2O_3-np reinforced FSWed joint (Fig. 5.38 b) in comparison with 1P-unreinforced joint. Big and small sized dimples were observed (Fig. 5.38 c) in the 2p-reinforced

FSWed joint due to rich and less particles regions as revealed by FESEM micrograph (Fig. 5.38 c). The dimple size found further decreases after three FSW passes, as depicted in Fig. 5.38 (d). This can be ascribed to the reduced grain size, homogenous Al_2O_3-np dispersion and strong connection between the Al_2O_3-np and the aluminum metal matrix, which led to higher resistance to fracture [178].

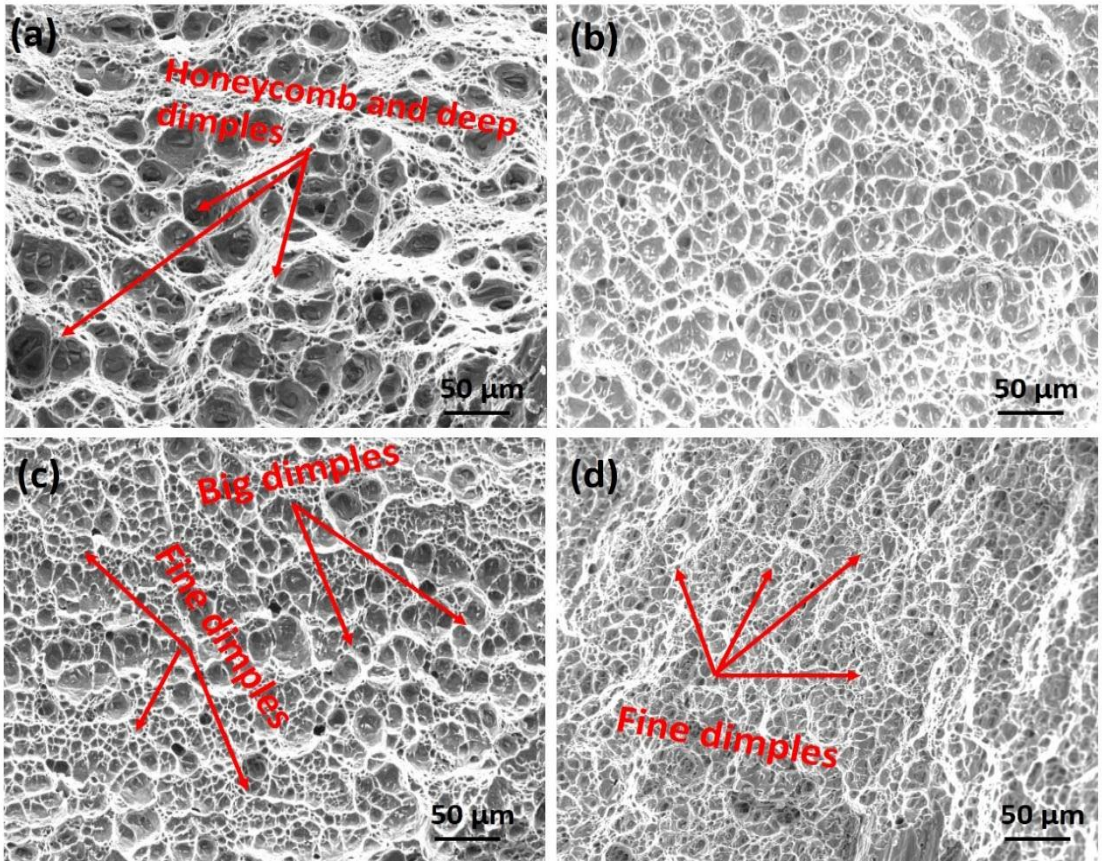

Figure 5. 38: Fractured surfaces morphology; (a) 1P-unreinforced FSWed joint; (b-d) Al_2O_3-np reinforced FSWed joint, (b) 1P, (c) 2P, (d) 3P.

5.10.4 INFLUENCE ON MICRO-HARDNESS

Table 5.18, also summarizes the average micro-hardness results at the center of weld line. The micro-hardness profile of all the FSWed joints is depicted in Fig 5.39. The micro-hardness of as received AA6061 and AA5083 was observed as 98 and 85 HV, respectively. The micro-hardness of 1P-unreinforced FSWed joint was found to be higher than the base materials. This can be ascribed to grain refinement via DRX. However, the micro-hardness of a 1P-reinforced FSWed joint was observed higher than that of 1P-unreinforced FSWed joint. The micro-hardness of reinforced FSWed joints can be ascribed to grain refinement, presence of Al_2O_3-np, dislocation density, and heat input [179]. Smaller grain size exhibits higher micro-hardness as per Hall-Patch

relationship [180]. The micro-hardness of the reinforced FSWed joints was also enhanced due to the addition of hard Al_2O_3-np. Therefore, the microhardness after 1P, 2P and 3P-reinforced FSWed joint was observed as 127.1, 136.4 and 145.7 HV, respectively. Thus, 3P-reinforced FSWed joint exhibits the maximum hardness of 145.7 HV, due to the more homogenous dispersion of Al_2O_3-np in the SZ as compared to other FSWed joints.

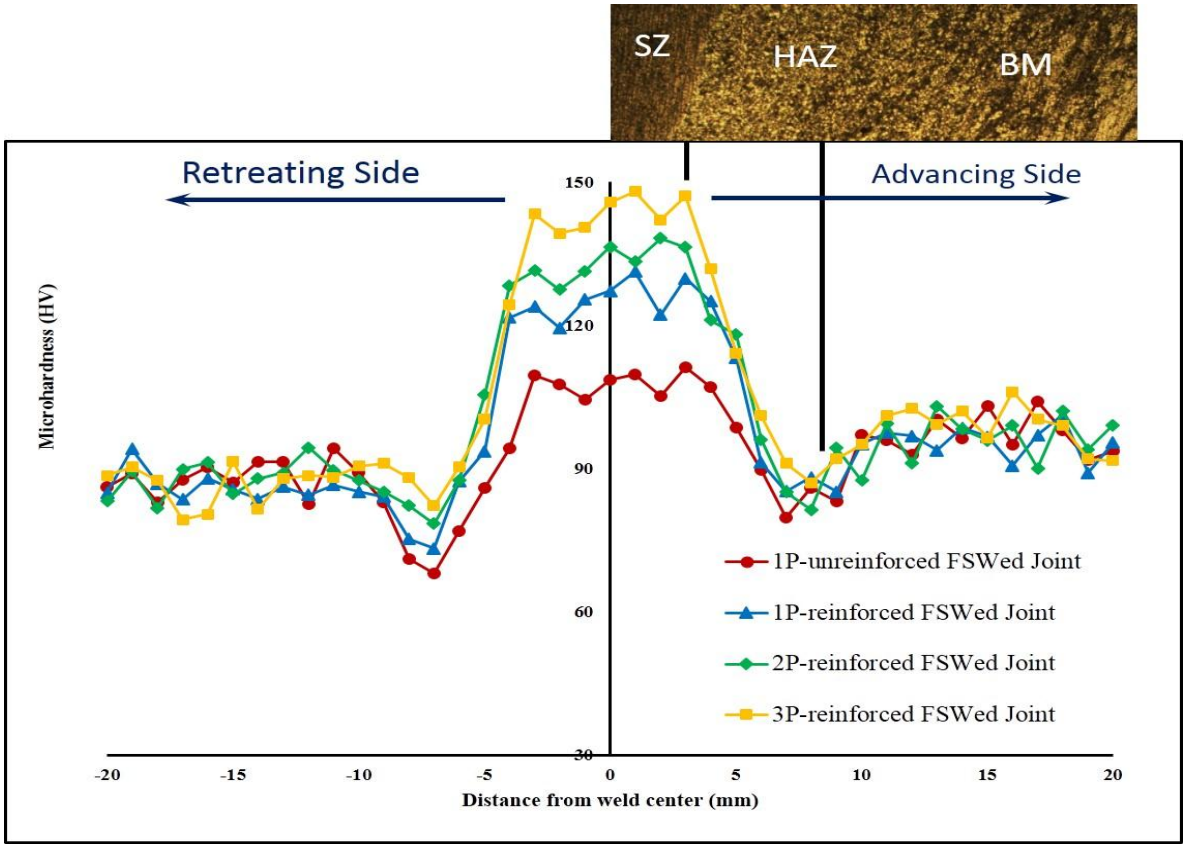

Figure 5. 39: Micro-hardness variation of Various FSWed joints

CHAPTER-6

CONCLUSIONS AND FUTURE WORK

6.1 CONCLUSIONS

The present investigation has been carried out to evaluate the influences of processing parameters of friction stir welding and incorporation of micro-sized Al_2O_3 and SiC particles on the weld quality of reinforced FSWed joints of dissimilar aluminum alloys AA5083 and AA6061. From this study following conclusions can be obtained.

- Increasing rotational speed, decreasing the traverse speed and increasing numbers of FSW passes leads to improving the dispersion pattern of reinforcing particles of (Al_2O_3 and SiC) in the SZ of reinforced FSWed joints.
- The grains structure in the stir zone of reinforced FSWed joints was observed much finer than that of the base materials.
- The highest tensile strength (254.42 MPa), %elongation (30.9%) and micro-hardness (124.2 HV) for Al_2O_3 microparticles reinforced FSWed joints were observed at rotational speed of 950 rpm, traverse speed of 35 mm/min after three passes of FSW.
- The highest tensile strength (266.97 MPa), %elongation (32.7 %) and microhardness (128.4 HV) for SiC microparticles reinforced FSWed joint were observed at rotational speed of 950 rpm, traverse speed of 35 mm/min after three passes of FSW.
- To analyze the tensile strength, %elongation and microhardness of reinforced FSWed joints of AA6061 and AA5083, empirical relationships were developed at confidence level of 95%.
- The optimum value of tensile strength, %elongation and micro-hardness at the SZ are 258.09 MPa, 31.3% and 124.69 HV respectively, whereas the optimum value of rotational speed, traverse speed and number of FSW passes are 995.38 rpm, 29.79 mm/min and 3 passes, respectively was found for Al_2O_3 microparticles reinforced FSWed joints.

- The optimum value of tensile strength, %elongation and micro-hardness at the SZ are 269.62 MPa, 32.75 % and 128.47 HV, respectively, whereas the optimum value of rotational speed, traverse speed and number of FSW passes are 994.57 rpm, 29.40 mm/min, and 3 passes, respectively was found for SiC microparticles reinforced FSWed joints.

6.2 SCOPE OF FUTURE WORK

The present experimental work has been carried out to assess the influences of friction stir welding to improve the microstructural and mechanical behaviour of dissimilar weld joints of aluminium alloys AA6061 and AA5083, and observed the optimum combination of input variables and output responses. It is recommended that the following future work should be done.

- The influence of reinforcing particles on wear resistance, corrosion resistance and residual stress etc. of reinforced FSWed joints of considered alloys may be further explored

- In this work, only threaded cylindrical pin profile is used to improve the mechanical properties of dissimilar reinforced FSWed joint of AA5083 and AA6061, different pins profile can be used to improve the reinforced joint strength.

- Influence of different reinforcements particles like TiB_2, TiC, B_4C etc. of different sizes (micro and nano) on mechanical properties can be investigated

- Influence of mixture of two or three reinforcing particles with their different proportions on mechanical properties can be investigated.

REFERENCES

[1] R. S. Mishra and Z. Y. Ma, "Friction stir welding and processing," Mater. Sci. Eng., vol. 50, pp. 1–78, 2005, doi: 10.1016/j.mser.2005.07.001.

[2] W. M. Thomas, E. D. Nicholas, J. C. Needham, M. G. Nurch, P. Temple-Smith, and C. Dawes, Friction Stir Butt Welding, G. B. (1991).

[3] Prado, R.A., Murr, L.E., Soto, K.F. & McClure, J.C. (2002). Self-optimization in tool wear for friction-stir welding of Al 6061_/20% Al2O3 MMC. Materials Science and Engineering, A, 349, (2003), 156-/165.

[4] J. Su, T. W. Nelson, and C. J. Sterling, "Microstructure evolution during FSW / FSP of high strength aluminum alloys," Mater. Sci. Eng. A, vol. 405, pp. 277–286, 2005, doi: 10.1016/j.msea.2005.06.009.

[5] J. G. (John G. Kaufman, E. L. Rooy, and American Foundry Society., Aluminum alloy castings : properties, processes, and applications. ASM International, 2004.

[6] The Aluminium Association, "International Alloy Designations and Chemical Composition Limits for Wrought Aluminum and Wrought Aluminum Alloys With Support for On-line Access From: Aluminum Extruders Council Use of the Information," Alum. Assoc. Arlington, Virginia, no. Enero 2015, p. 31, 2015, [Online] Available: https://www.aluminum.org/sites/default/files/Teal Sheets.pdf.

[7] I.Polmear, D. St. John, J. F. Nie, and M. Qian, Light Alloys: Metallurgy of the Light Metals: Fifth Ed. Elsevier Inc., 2017.

[8] C.-H. Ng, S. N. . Yahaya, and A. A. . Majid, "Reviews on aluminum alloy series andits applications," Acad. J. Sci. Res., vol. 5, no. 12, pp. 708–716, 2017, doi:10.15413/ajsr.2017.0724.

[9] E. A. Starke and S. Mridha, Encyclopedia of Materials: Science and Technology, 1st ed. Elsevier Ltd., 2001.

[10] D. Montello and A. M. Larghe, "ASM Specialty Handbook: Aluminum and Aluminum Alloys," ASM Int., no. 2, pp. 78–79, 1993.

[11] C. M. Cheng, C. P. Chou, I. K. Lee, and H. Y. Lin, "Hot cracking of welds on heat treatable aluminium alloys," Sci. Technol. Weld. Join., vol. 10, no. 3, pp. 344–352, 2005, doi: 10.1179/174329305X40688.

[12] R. S. Mishra, M. W. Mahoney, S. X. McFadden, N. A. Mara, and A. K. Mukherjee, High strain rate superplasticity in a friction stir processed 7075 Al alloy, Scripta Materialia 42(2), 163–168 (1999).

[13] R. S. Mishra, Z. Y. Ma, and I. Charit, Friction stir processing: a novel technique for fabrication of surface composite, Mater. Sci. Eng.: A 341(1–2), 307–310 (2003).

[14] Y. Gan, D. Solomon, and M. Reinbolt, Friction stir processing of particle reinforced composite materials, Materials 3(1), 329 (2010).

[15] P. B. Berbon, W. H. Bingel, R. S. Mishra, C. C. Bampton, and M. W. Mahoney, Friction stir processing: a tool to homogenize nanocomposite aluminum alloys, Scripta Materialia 44(1), 61–66 (2001).

[16] G. R. Argade, K. Kandasamy, S. K. Panigrahi, and R. S. Mishra, Corrosion behavior of a friction stir processed rare-earth added magnesium alloy, Corros. Sci. 58, 321– 326 (2012).

[17] N. Sun and D. Apelian, Friction stir processing of aluminum cast alloys for high performance applications, JOM 63(11), 44–50 (2011).

[18] Y. Hangai, T. Utsunomiya, and M. Hasegawa, Effect of tool rotating rate on foaming properties of porous aluminum fabricated by using friction stir processing, J. Mater. Process. Technol. 210(2), 288–292 (2010).

[19] S. Rathee, S. Maheshwari, and A. N. Siddiquee, Issues and strategies in composite fabrication via friction stir processing: A review, Mater. Manuf. Process. 1–23 (2017).

[20] R. M. Miranda, T. G. Santos, J. Gandra, N. Lopes, and R. J. C. Silva, Reinforcement strategies for producing functionally graded materials by friction stir processing in aluminium alloys, J. Mater. Process. Technol. 213(9), 1609–1615 (2013).

[21] M. Yang, C. Xu, C. Wu, K. C. Lin, Y. Chao, and L. An, Fabrication of AA6061/Al2O3 nano ceramic particle reinforced composite coating by using friction stir processing, J. Mater. Sci. 45(16), 4431–4438 (2010).

[22] Y. Huang, T. Wang, W. Guo, L. Wan, and S. Lv, Microstructure and surface mechanical property of AZ31 Mg/SiCp surface composite fabricated by direct friction stir processing, Mater. Des. 59(0), 274–278 (2014).

[23] S. Rathee, S. Maheshwari, A. N. Siddiquee, and M. Srivastava, Effect of tool plunge depth on reinforcement particles distribution in surface composite fabrication via friction stir processing, Defen. Technol. 13(2), 86–91 (2017).

[24] H. R. Akramifard, M. Shamanian, M. Sabbaghian, and M. Esmailzadeh, Microstructure and mechanical properties of Cu/SiC metal matrix composite fabricated via friction stir processing, Mater. Des. 54(0), 838–844 (2014).

[25] S. Rathee, S. Maheshwari, and A. N. Siddiquee, Distribution of reinforcement particles in surface composite fabrication via friction stir processing: suitable strategy, Mater. Manuf. Process. 1–23 (2017). DOI:10.1080/ 10426914.2017.1303162.

[26] L. Karthikeyan, V. S. Senthilkumar, and K. A. Padmanabhan, On the role of process variables in the friction stir processing of cast aluminum A319 alloy, Mater. Des. 31 (2), 761–771 (2010).

[27] O. El-Kady and A. Fathy, Effect of SiC particle size on the physical and mechanical properties of extruded Al matrix nanocomposites, Mater. Des. 54, 348–353 (2014).

[28] S. A. Hosseini, K. Ranjbar, R. Dehmolaei, and A. R. Amirani, Fabrication of Al5083 surface composites reinforced by CNTs and cerium oxide nano particles via friction stir processing, J. Alloy Comp. 622, 725–733 (2015).

[29] A.P. Sannino and H. J. Rack, Dry sliding wear of discontinuously reinforced aluminum composites: review and discussion, Wear 189(1), 1–19 (1995).

[30] S. R. Bakshi, D. Lahiri, and A. Agarwal, Carbon nanotube reinforced metal matrix composites — a review, Int. Mater. Rev. 55(1), 41–64 (2010).

[31] Y. B. Li, B. Q. Wei, J. Liang, Q. Yu, and D. H. Wu, Transformation of carbon nanotubes to nanoparticles by ball milling process, Carbon 37(3), 493–497 (1999).

[32] K. Kalaiselvan, N. Murugan, and S. Parameswaran, Production and characterization of AA6061–B4C stir cast composite, Mater. Des. 32(7), 4004–4009 (2011).

[33] C. S. Ramesh, S. Pramod, and R. Keshavamurthy, A study on microstructure and mechanical properties of Al 6061– TiB2 in-situ composites, Mater. Sci. Eng.: A 528(12), 4125–4132 (2011).

[34] P. M. Ashraf and S. M. A. Shibli, Development of cerium oxide and nickel oxide-incorporated aluminium matrix for marine applications, J. Alloy Compnd. 484(1–2), 477– 482 (2009).

[35] Shafiei-Zarghani, S. F. Kashani-Bozorg, and A. Zarei-Hanzaki, Microstructures and mechanical properties of Al/Al2O3 surface nano-composite layer produced by friction stir processing, Mater. Sci. Eng.: A 500(1–2), 84– 91 (2009).

[36] M. Raaft, T. S. Mahmoud, H. M. Zakaria, and T. A. Khalifa, Microstructural, mechanical and wear behavior of A390/graphite and A390/Al2O3 surface composites fabricated using FSP, Mater. Sci. Eng.: A 528(18), 5741– 5746 (2011).

[37] Sumit Jain, R.S. Mishra (2022) "Microstructural and mechanical behavior of micro-sized SiC particles reinforced friction stir processed/welded AA7075 and AA6061,",Silicon, ISSN, 1876-9918, DOI 10.1007/s12633-022-01716-5.

[38] W. M. U. Thomas, E. D. Nicholas, and A. Hall, "Friction stir welding for the transportation industries," Mater. Des., vol. 18, no. 4, pp. 269–273, 1998, doi:10.1016/S0261-3069(97)00062-9.

[39] A. Amini, C. Material, D. Engines, W. Turbines, and C. Materials, "industry Friction stir welding applications in- Marine Industry."

[40] P. J. Haagensen, O. T. Midlin, and M.Rane, "Fatigue performance of friction stir butt welds in a 6000 series aluminum allo," Comput. methods Exp. Meas. Surf. Treat. Eff. II, vol. 8, pp. 589–598, 1995, doi: 10.2495/SURF950271.

[41] M. Ericsson and R. Sandstro, "Influence of welding speed on the fatigue of friction stir welds, and comparison with MIG and TIG," vol. 25, pp. 1379–1387, 2003, doi: 10.1016/S0142-1123(03)00059-8.

[42] Bagheri, Behrouz & Abbasi, Mahmoud & Abdollahzadeh, Amin. (2021). Microstructure and mechanical characteristics of AA6061-T6 joints produced by friction stir welding, friction stir vibration welding and tungsten inert gas welding: A comparative study. International Journal of Minerals, Metallurgy and Materials. 28. 450-461. 10.1007/s12613-020-2085-1.

[43] A. Squillace, A. De Fenzo, G. Giorleo, and F. Bellucci, "A comparison between FSW and TIG welding techniques : modifications of microstructure and pitting corrosion resistance in AA 2024-T3 butt joints," J. Mater. Process. Technol., vol. 152, pp. 97–105, 2004, doi: 10.1016/j.jmatprotec.2004.03.022.

[44] C. Yeni, S. Sayer, and M. Pakdil, “Comparison of mechanical and microstructural behaviour of TIG, MIG and Friction Stir welded 7075 Aluminium Alloy,” Kov. Mater., vol. 47, no. 5, pp. 341–347, 2009.

[45] M. O. A. Sık, “Comparison between mechanical properties and joint performance of AA 2024-O aluminium alloy welded by friction stir welding,” Kov. Mater., vol. 50, no. January, pp. 131–137, 2012, doi: 10.4149/km 2012 2 131.

[46] A. Kumar, S. S. Gautam, and A. Kumar, “Heat Input & Joint Efficiency of Three Welding Processes Tig , Mig and Fsw Using Aa6061,” Int. J. Mech. Eng. Rob. Res., vol. 1, no. 1, pp. 89–94, 2014.

[47] C. Elanchezhian, B. V. Ramnath, P. Venkatesan, S. Sathish, and T. Vignesh, “Parameter Optimization of Friction Stir Welding Of AA8011-6062 Using Mathematical Method,” Procedia Eng., vol. 97, pp. 775–782, 2014, doi:10.1016/j.proeng.2014.12.308.

[48] A. K. Bodukuri, K. Eswaraiah, K. Rajendar, and A. Siddartha, “Comparison of Aluminum Alloy 5083 properties on TIGW and FSW Processes,” Mater. Today Proc., vol. 4, no. 9, pp. 10197–10201, 2017, doi: 10.1016/j.matpr.2017.06.347.

[49] L. Kumar, K. U. Yazar, and S. Pramanik, “Effect of fusion and friction stir welding techniques on the microstructure, crystallographic texture and mechanical properties of mild steel,” Mater. Sci. Eng. A, vol. 754, no. December 2018, pp. 400–410, 2019, doi: 10.1016/j.msea.2019.03.100.

[50] Khanna N Chaudhary B Airao J Dak G Badheka V, “Experimental Comparison of TIG and Friction Stir Welding Process for AA6063-T6 Aluminum Alloy,” Innov. Infrastruct., vol. 757, no. January, pp. 619–628, 2019, doi: 10.1007/978-981-13-1966-2.

[51] Moataz M. Attallah, Hanadi G. Salem, Friction stir welding parameters: a tool for controlling abnormal grain growth during subsequent heat treatment, Materials Science and Engineering A 391 (2005) 51–59.

[52] G. Buffa, J.Hua, R. Shivpuri, L. Fratini, A continuum based fem model for friction stir welding—model development, Materials Science and Engineering A 419 (2006) 389–396.

[53] S.R. Ren, Z.Y. Ma and L.Q. Chen , Effect of welding parameters on tensile properties and fracture behavior of friction stir welded Al–Mg–Si alloy, Scripta Materialia 56 (2007) 69–72.

[54] Zhang & H. W. Zhang, Material behaviors and mechanical features in friction stir welding process International Journal of Advanced Manufacturing and Technology (2007) 35:86–100.

[55] Omar S. Salih, Hangan Ou, W.Sun, D.G McCartney, "A review of friction stir welding of aluminum matrix composite", Material and Design 86 (2015) 61-71.

[56] L. Commin, M. Dumont, J.-E. Masse, L. Barrallier, Friction stir welding of AZ31 magnesium alloy rolled sheets: Influence of processing parameters, Acta Materialia 57 (2009) 326–334.

[57] Ravi kumar, Seshagiri Rao. V and Pranesh. R.V, Effect of welding parameters on macro and microstructure of friction stir welded dissimilar butt joints welded joints between AA7075 and AA6061 alloys, procedia materials science 5 (2014), 1726-1735.

[58] Jerry Wong, Patricia Zambrano, Indira Escamilla, Bernardo Gonzalez, Victor Mucino, Rafael Colás, Friction stir linear welding of an aluminum alloy, Advanced Materials Research Vol. 68 (2009) pp 116-121.

[59] Jianqing Su, Jiye Wang, R.S Mishra, Ray Xu, " Microstructure and Mechanical Properties of Friction Stir Processing Ti-6Al-4V Alloy", Material Science and Engineering A 573 (2013) 67-74

[60] J.F. Guo, H.C. Chen, C.N. Sun, G. Bi, Z. Sun, J. Wei, Friction stir welding of dissimilar materials between AA6061 and AA7075 Al alloys effects of process parameters, Materials and Design 56 (2014) 185–192.

[61] Nilesh Kumar, R.S Mishra, " Ultrafined Grained Al-Mg-Sc Alloy via friction Stir Processing", Metallurgical and Materials Transaction, 44A (2013) 934-945.

[62] W. B. Lee, Y. M. Yeon, and S. B. Jung, "Mechanical properties related to microstructural variation of 6061 Al alloy joints by friction stir welding," Mater. Trans., vol. 45, no. 5, pp. 1700–1705, 2004, doi: 10.2320/matertrans.45.1700.

[63] K. Elangovan and V. Balasubramanian, "Influences of tool pin profile and welding speed on the formation of friction stir processing zone in AA2219 aluminium alloy," Mater. Sci. Eng. A, vol. 459, no. 1–2, pp. 163–175, 2007, doi:10.1016/j.jmatprotec.2007.09.019.

[64] J. C. Hou, H. J. Liu, and Y. Q. Zhao, "Influences of rotation speed on microstructures and mechanical properties of 6061-T6 aluminum alloy joints fabricated by self- reacting friction stir welding tool," Int. J. Adv. Manuf.

Technol., vol. 73, no. 5–8, pp. 1073–1079, 2014, doi: 10.1007/s00170-014-5857-9.

[65] Q. Wang, Z. Zhao, Y. Zhao, K. Yan, and H. Zhang, "The adjustment strategy of welding parameters for spray formed 7055 aluminum alloy underwater friction stir welding joint," JMADE, 2015, doi: 10.1016/j.matdes.2015.09.038.

[66] J. Kundu and H. Singh, "Friction stir welding of dissimilar Al alloys: Effect of process parameters on mechanical properties," Eng. Solid Mech., vol. 4, no. 3, pp. 125–132, 2016, doi: 10.5267/j.esm.2016.2.001.

[67] Y. Yue, Z. Zhou, S. Ji, J. Zhang, and Z. Li, "Effect of welding speed on joint feature and mechanical properties of friction stir lap welding assisted by external stationary shoulders," Int. J. Adv. Manuf. Technol., vol. 89, no. 5–8, pp. 1691–1698, Mar. 2017, doi: 10.1007/s00170-016-9240-x.

[68] S. Shashi Kumar, N. Murugan, and K. K. Ramachandran, "Identifying the optimal FSW process parameters for maximizing the tensile strength of friction stir welded AISI 316L butt joints," Meas. J. Int. Meas. Confed., vol. 137, pp. 257–271, 2019, doi:10.1016/j.measurement.2019.01.023.

[69] C. Zhang, Y. Cao, G. Huang, Q. Zeng, and Y. Zhu, "In fl uence of tool rotational speed on local microstructure , mechanical and corrosion behavior of dissimilar AA2024 / 7075 joints fabricated by friction stir welding," vol. 49, no. November 2019, pp. 214–226, 2020, doi: 10.1016/j.jmapro.2019.11.031.

[70] Deepak Kumar and Jatinder kumar, "Optimization of Parameters in Friction Stir Welding of AA6101-T6 by Taguchi Approach," Adv. Eng. Optim. Through Intell. Tech. Adv. Intell. Syst. Comput., pp. 361–371, 2020, doi: 10.1007/978-981-13-8196-6.

[71] R. S. S. Prasanth and K. Hans Raj, "Determination of optimal process parameters of friction stir welding to join dissimilar aluminum alloys using artificial bee colony algorithm," Trans. Indian Inst. Met., vol. 71, no. 2, pp. 453–462, 2017, doi:10.1007/s12666-017-1176-9.

[72] K. T. Thilagham and S. Muthukumaran, "Process parameter optimization and characterization of friction stir welded advancing side AA6082-T6 with retreating side AA7075-T651," Mater. Today Proc., no. xxxx, 2019, doi:10.1016/j.matpr.2019.09.108.

[73] O. S. Salih, N. Neate, H. Ou, and W. Sun, "Influence of process parameters on the microstructural evolution and mechanical characterisations of friction stir

welded Al- Mg-Si alloy," J. Mater. Process. Technol., vol. 275, no. February 2019, p. 116366, 2020, doi: 10.1016/j.jmatprotec.2019.116366.

[74] H. Bin Chen, K. Yan, T. Lin, S. Ben Chen, C. Y. Jiang, and Y. Zhao, "The investigation of typical welding defects for 5456 aluminum alloy friction stir welds," Mater. Sci. Eng. A, vol. 433, no. 1–2, pp. 64–69, 2006, doi: 10.1016/j.msea.2006.06.056.

[75] Z. Barlas and U. Ozsarac, "Effects of FSW parameters on joint properties of AlMg3 Alloy," Weld. J., vol. 91, no. 1, 2012.

[76] R. Kadaganchi, M. Reddy, and H. Gokhale, "Optimization of process parameters of aluminum alloy AA 2014-T6 friction stir welds by response surface methodology," Def. Technol., vol. 11, no. 3, pp. 209–219, 2015, doi: 10.1016/j.dt.2015.03.003.

[77] L. Long, G. Chen, S. Zhang, T. Liu, and Q. Shi, "Finite-element analysis of the tool tilt angle effect on the formation of friction stir welds," J. Manuf. Process., vol. 30, pp. 562–569, 2017, doi: 10.1016/j.jmapro.2017.10.023.

[78] A. Banik, B. Saha Roy, J. Deb Barma, and S. C. Saha, "An experimental investigation of torque and force generation for varying tool tilt angles and their effects on microstructure and mechanical properties: Friction stir welding of AA 6061-T6," J. Manuf. Process., vol. 31, pp. 395–404, 2018, doi: 10.1016/j.jmapro.2017.11.030.

[79] S. Verma, M. Gupta, and J. P. Misra, "Optimization of process parameters in friction stir welding of armor-marine grade aluminium alloy using desirability approach," Mater. Res. Express, vol. 6, no. 2, 2019, doi: 10.1088/2053-1591/01.

[80] A. Goyal and R. K. Garg, "Selection of FSW tool parameters for joining Al-Mg4.2 alloy: An experimental approach," Metallogr. Microstruct. Anal., vol. 7, no. 5, pp. 524–532, Oct. 2018, doi: 10.1007/s13632-018-0468-8.

[81] M. Boz and A. Kurt, "The influence of stirrer geometry on bonding and mechanical properties in friction stir welding process," Mater. Des., vol. 25, pp. 343–347, 2004, doi: 10.1016/j.matdes.2003.11.005.

[82] K. Elangovan and V. Balasubramanian, "Influences of tool pin profile and tool shoulder diameter on the formation of friction stir processing zone in AA6061 aluminium alloy," Mater. Des., vol. 29, no. 2, pp. 362–373, 2008, doi:10.1016/j.matdes.2007.01.030.

[83] H. K. Mohanty, M. M. Mahapatra, P. Kumar, P. Biswas, and N. R. Mandal, "Effect of tool shoulder and pin probe profiles on friction stirred aluminum welds - a comparative study," J. Mar. Sci. Appl., vol. 11, no. 2, pp. 200–207, 2012, doi:10.1007/s11804-012-1123-4.

[84] R. Palanivel, P. Koshy Mathews, N. Murugan, and I. Dinaharan, "Effect of tool rotational speed and pin profile on microstructure and tensile strength of dissimilar friction stir welded AA5083-H111 and AA6351-T6 aluminum alloys," Mater. Des., vol. 40, pp. 7–16, Sep. 2012, doi: 10.1016/J.MATDES.2012.03.027.

[85] M. Yuqing, K. Liming, L. Fencheng, C. Yuhua, and X. Li, "Effect of tool pin-tip profiles on material flow and mechanical properties of friction stir welding thick AA7075-T6 alloy joints," Int. J. Adv. Manuf. Technol., vol. 88, no. 1–4, pp. 949–960, 2017, doi: 10.1007/s00170-016-8882-z.

[86] D. K. C. Udaiyakumar, M. Krishna, K. C. Udaiyakumar, D. K. Mohan Kumar, and H. Mohammed Ali, "Analysis on effect of using different tool pin profile and mechanical properties by friction stir welding on dissimilar aluminium alloys Al6061 and Al7075," IOP Conf. Ser. Mater. Sci. Eng., vol. 402, no. 1, 2018, doi: 10.1088/1757-899X/402/1/012099.

[87] X. M. Liu, Y. H. Li, Y. Zhao, and P. Chai, "Influence of pin geometry on mechanical properties of 5A05-H112 aluminum alloy during bobbin-tool friction stir welding," Mater. Res. Express, vol. 6, no. 7, 2019, doi: 10.1088/2053-1591/ab1330.

[88] M. Raturi, A. Garg, and A. Bhattacharya, "Joint strength and failure studies of dissimilar AA6061-AA7075 friction stir welds: Effects of tool pin, process parameters and preheating," Eng. Fail. Anal., vol. 96, no. December 2018, pp. 570–588, 2019, doi: 10.1016/j.engfailanal.2018.12.003.

[89] Olivier Lorrain, Véronique Favier, Hamid Zahrouni, Didier Lawrjaniec, Understanding the material flow path of friction stir welding process using unthreaded tools, Journal of Materials Processing Technology 210 (2010) 603–609.

[90] Dawood HI, Kahtan S. Mohammed, Azmi Rahmat, M. B. Uday, Effect of small tool pin profiles on microstructures and mechanical properties of 6061 aluminum alloy by friction stir welding, Trans. Nonferrous Met. Soc. China 25(2015) 2856−2865.

[91] L. Commin, M. Dumont, J. E. Masse, and L. Barrallier, “Friction stir welding of AZ31 magnesium alloy rolled sheets: Influence of processing parameters,” Acta Mater., vol. 57, no. 2, pp. 326–334, 2009, doi: 10.1016/j.actamat.2008.09.011.

[92] A. Arora, T. Debroy, and H. K. D. H. Bhadeshia, “Back-of-the-envelope calculations in friction stir welding - Velocities, peak temperature, torque, and hardness,” Acta Mater., vol. 59, no. 5, pp. 2020–2028, 2011, doi: 10.1016/j.actamat.2010.12.001.

[93] V. Saravanan, S. Rajakumar, N. Banerjee, and R. Amuthakkannan, “Effect of shoulder diameter to pin diameter ratio on microstructure and mechanical properties of dissimilar friction stir welded AA2024-T6 and AA7075-T6 aluminum alloy joints,” Int. J. Adv. Manuf. Technol., vol. 87, no. 9–12, pp. 3637–3645, 2016, doi:10.1007/s00170-016-8695-0.

[94] A. Gill, “Invastigation the effect of process parameters on impact toughness of friction stir welded aluminium,” Int. J. Mech. Prod. Eng., vol. 5, no. 10, pp. 111–119, 2017.

[95] G. R. Joshi and V. J. Badheka, “Studies on Tool Shoulder Diameter of Dissimilar Friction Stir Welding Copper to Stainless Steel,” Metallogr. Microstruct. Anal., vol. 8, no. 2, pp. 263–274, 2019, doi: 10.1007/s13632-019-00532-5.

[96] M. de Giorgi, A. Scialpi, F. W. Panella, and L. A. C. de Filippis, “Effect of shoulder geometry on residual stress and fatigue properties of AA6082 FSW joints,” J. Mech. Sci. Technol., vol. 23, no. 1, pp. 26–35, 2009, doi: 10.1007/s12206-008-1006-4.

[97] L. Trueba, G. Heredia, D. Rybicki, and L. B. Johannes, “Effect of tool shoulder features on defects and tensile properties of friction stir welded aluminum 6061-T6,” J. Mater. Process. Technol., vol. 219, pp. 271–277, 2015, doi:10.1016/j.jmatprotec.2014.12.027.

[98] G. Casalino, S. Campanelli, and M. Mortello, “Influence of shoulder geometry and coating of the tool on the friction stir welding of aluminium alloy plates,” Procedia Eng., vol. 69, pp. 1541–1548, 2014, doi: 10.1016/j.proeng.2014.03.153.

[99] Y. Kunnathur Periyasamy, A. V. Perumal, and B. Kunnathur Periyasamy, “Influence of Tool Shoulder Concave Angle and Pin Profile on Mechanical

Properties and Microstructural Behaviour of Friction Stir Welded AA7075-T651 and AA6061 Dissimilar Joint," Trans. Indian Inst. Met., vol. 72, no. 4, pp. 1087–1109, 2019, doi:10.1007/s12666-019-01584-5.

[100] Y. Javadi, S. Sadeghi, and M. A. Najafabadi, "Taguchi optimization and ultrasonic measurement of residual stresses in the friction stir welding," Mater. Des., vol. 55, pp. 27–34, Mar. 2014, doi: 10.1016/J.MATDES.2013.10.021.

[101] B. Ravi Sankar and P. Umamaheswarrao, "Modelling and Optimisation of Friction Stir Welding on AA6061 Alloy," Mater. Today Proc., vol. 4, no. 8, pp. 7448– 7456, 2017, doi: 10.1016/j.matpr.2017.07.076.

[102] M. Akbari, M. R. M. Aliha, S. M. E. Keshavarz, and A. Bonyadi, "Effect of tool parameters on mechanical properties, temperature, and force generation during FSW," Proc. Inst. Mech. Eng. Part L J. Mater. Des. Appl., vol. 233, no. 6, pp. 1033–1043, 2019, doi: 10.1177/1464420716681591.

[103] H.W. Zhang, Z. Zhang, J.T. Chen, 3D modeling of material flow in friction stir welding under different process parameters, Journal of Materials Processing Technology 183 (2007) 62–70.

[104] Indrajeet Charit, Rajiv S. Mishra, Murray W. Mahoney, "Multi sheet structure in 7475 aluminum by FSW in concert with post weld superplastic forming", Scripta Materialia 47 (2002) 631-636.

[105] Z.Y Ma, S.R Sharma, R.S Mishra, " Effect of Multipass Friction Stir Processing on Microstructure and tensile propeties of a Cast Al-Si Alloy", Scripta Materialia, 54 (2006) 1623-1626.

[106] Su, T. Nelson and C. Sterling. "Friction stir processing of large-area bulk UFG aluminum alloys". Scripta Materialia 52 (2005) pp.135-140.

[107] Z.Y.Ma, R.S Mishra, M.W. Mahoney," Super plastic deformation behavior of friction stir processed 7075Al alloy", Acta Materialia 50 (2002), 4419-4430.

[108] Khanna, N., Sharma, P., Bharati, M. et al. Friction stir welding of dissimilar aluminium alloys AA 6061-T6 and AA 8011-h14: a novel study. J Braz. Soc. Mech. Sci. Eng. 42, 7 (2020). https://doi.org/10.1007/s40430-019-2090-3.

[109] A. Barcellona, G. Buffa, L. Fratini, D. Palmeri, On microstructural phenomena occurring in friction stir welding of aluminum alloys, Journal of Materials Processing Technology 177 (2006) 340–343

[110] M. Ilangovan, S. Rajendra Boopathy, V. Balasubramanian, Microstructure and tensile properties of friction stir welded dissimilar AA6061AA5086 aluminium alloy joints, Trans. Nonferrous Met. Soc. China 25 (2015) 1080-1090

[111] Harish Suthar, Anirban Bhattacharya, Surajit Kumar Paul, Local deformation response and failure behavior of AA6061-AA6061 and AA6061-AA7075 friction stir welds, (2020), https://doi.org/10.1016/j.cirpj.2020.03.006

[112] P. Avinash, M. Manikandan, N. Arivazhagan, D. R. K, and S. Narayanan, "Friction stir welded butt joints of AA2024 T3 and AA7075 T6 aluminum alloys," Procedia Eng., vol. 75, pp. 98–102, 2014, doi: 10.1016/j.proeng.2013.11.020.

[113] P. Jayaseelan, T. V. Christy, S. J. Vijay, and R. Nelson, "Effect of tool material, profile and D/d ratio in friction stir welding of aluminium metal matrix composites," Mater. Res. Express, vol. 6, no. 9, 2019, doi: 10.1088/2053-1591/ab30b1.

[114] C. Zhang, G. Huang, Y. Cao, Y. Zhu, and Q. Liu, "On the microstructure and mechanical properties of similar and dissimilar AA7075 and AA2024 friction stir welding joints: Effect of rotational speed," J. Manuf. Process., vol. 37, no. December 2018, pp. 470–487, 2019, doi: 10.1016/j.jmapro.2018.12.014.

[115] Sameer Mohammed & Anil Kumar Birru (2019) Friction Stir Welding of AA6082 Thin Aluminium Alloy Reinforced with Al2O3 Nanoparticles, Transactions of the Indian Ceramic Society, 78:3, 137-145, DOI: 10.1080/0371750X.2019.1635046.

[116] Parumandla, N., Adepu, K. (2018). Effect of Al2O3 and SiC Nano Reinforcements on Microstructure, Mechanical and Wear Properties of Surface Nanocomposites Fabricated by Friction Stir Processing. Materials Science, 24(3), –. doi:10.5755/j01.ms.24.3.18220.

[117] Ahmadifard, S. Shahin, N., azghandi, M., Kazemi, S. (2021). Surface Hybrid Nanocomposite Produced by Friction Stir Processing : Microstructural Evolution , Mechanical Properties and Tribological Behavior, 1–16.

[118] Abdollahzadeh A, Shokuhfar A, Omidvar H, et al. (2019). Structural evaluation and mechanical properties of AZ31/SiC nano-composite produced by friction stir welding process at various welding speeds. Proceedings of the Institution of Mechanical Engineers, Part L: Journal of Materials: Design and Applications.;233(5):831-841.

[119] Bahrami, M., Farahmand Nikoo, M., & Besharati Givi, M. K. (2015). Microstructural and mechanical behaviors of nano-SiC-reinforced AA7075-O FSW joints prepared through two passes. Materials Science and Engineering A, 626, 220–228. https://doi.org/10.1016/j.msea.2014.12.009.

[120] Bozkurt Y, Uzun H, Salman S. (2011) Microstructure and mechanical properties of friction stir welded particulate reinforced AA2124/SiC/25p–T4 composite. Journal of Composite Materials.;45(21):2237-2245. doi:10.1177/0021998311401067.

[121] Cioffi, F.; Fernández, R.; Gesto, D.; Rey, P.; Verdera, D.; González-Doncel, G. (2013). Friction stir welding of thick plates of aluminum alloy matrix composite with a high volume fraction of ceramic reinforcement. Composites Part A: Applied Science and Manufacturing, 54(), 117–123. doi:10.1016/j.compositesa.2013.07.011

[122] Dragatogiannis, D. A.; Koumoulos, E. P.; Kartsonakis, I.; Pantelis, D. I.; Karakizis, P. N.; Charitidis, C. A. (2015). Dissimilar Friction Stir Welding Between 5083 and 6082 Al Alloys Reinforced with Tic Nanoparticles. Materials and Manufacturing Processes, (), 10426914.2015.1103856–. doi:10.1080/10426914.2015.1103856.

[123] Gopalakrishnan, S., Murugan, N. (2011). Prediction of tensile strength of friction stir welded aluminium matrix TiCp particulate reinforced composite. , 32(1), 462–467. doi:10.1016/j.matdes.2010.05.055.

[124] Kalaiselvan, K., Murugan. N., Parameswaran, S. (2011). Production and characterization of AA6061–B4C stir cast composite. , 32(7), 4004–4009. doi:10.1016/j.matdes.2011.03.018.

[125] Atul, K., Kaushik, P., Suhrit, M. (2017). Simultaneous improvement of mechanical strength, ductility and corrosion resistance of stir cast Al7075-2% SiC micro- and nanocomposites by friction stir processing. Journal of Manufacturing Processes, 30(), 1–13. doi:10.1016/j.jmapro.2017.09.005.

[126] Lee, S. J., Shin, S. E., Yufeng, S., Hidetoshi, F., Yongbum, P. (2018). Friction stir welding of multi-walled carbon nanotubes reinforced Al matrix composites. Materials Characterization, 145(), 653–663. doi:10.1016/j.matchar.2018.09.033.

[127] Kumar, R. A., Thansekhar, M.R. (2018). Reinforcement with alumina particles at the interface region of AA6101-T6 and AA1350 alloys during friction stir welding. Materials Research Express. doi:10.1088/2053-1591/aab8b5.

[128] Box, G.E.P., & Hunter, J.S. (1957). Multifactor experimental design, J. Ann. Math. Statistics. 28.

[129] Puri, A.B., Bhattacharyya, B. (2005). Modeling and analysis of white layer depth in a wire-cut EDM process through response surface methodology. Int J Adv Manuf Technol, 25, 301–307.

[130] Cochran, G., & Cox, G.M. (1962). Experimental design.Asia Publishing House, New Delhi.

[131] Hines, W.W., & Montgomery, D.C. (1990). Probability and statistics in engg. And management science. 3rd Edition, Wiley Publications.

[132] Deringer, G. & Suich, R. (1980). Simultaneous optimization of several response Variables.Journal of Quality Technology, 12, 214-219.

[133] Cetinel H, and Manisa MA Microstructure and Mechanical Properties of AA 5083 and AA 6061 Welds Joined with AlSi5 and AlSi12 Wires*, 3rd International Conference on Welding Technologies and Exhibition (ICWET'14) in Manisa, Turkey.

[134] W. Mirihanage, N. Munasinghe: Modification of AA 5083 weld joint characteristics, International Symposium of Research Students on Materials Science and Engineering, Chennai, India, ISRS (2004), pp. 1-6.

[135] P. Peasura, A. Watanapa: Influence of shielding gas on aluminum alloy 5083 in gas tungsten arc welding, Procedia Engineering 29 (2012), pp. 2465-2469.

[136] V.P. Singh, S.K. Patel, A. Raryan, B.K. Chen (2020) Recent research progress in solid state friction stir welding of aluminium-magnesium alloys: a critical review, Journal of Materials Research and Technology pp. 1-40.

[137] R. Chandran, S. Ramaiyan, A.G. Shanbhag, S.K.V. Santhanam Optimization of welding parameters for friction stir lap welding of AA6061-T6 Alloy Journal of Modern Mechanical Engineering, 8 (2018), pp. 31-41.

[138] O. Klog, J. Grobner, G. Wagner, R. Schmid-Fetzer, D. Eifler, Microstructural and thermodynamic investigations on friction stir welded Mg/Al-joints Int J Mater Res, 105 (2) (2014), pp. 145-155.

[139] Jain, Sumit & Mishra, R.. (2023). A Review of the Effect of Process Parameters and Temperature Variation on FSWed Dissimilar Aluminium Alloys AA7075 and AA6061. 10.1007/978-981-19-6945-4_64.

[140] B.T. Ogunsemi, T.E. Abioye, T.I. Ogedengbe, H. Zuhailawati, A review of various improvement strategies for joint quality of AA 6061-T6 friction stir weldments, Journal of Materials Research and Technology, Volume 11, 2021, 1061-1089.

[141] Sandeep Rathee, Sachin Maheshwari, Arshad Noor Siddiquee & Manu Srivastava (2017): A Review of Recent Progress in Solid State Fabrication of Composites and Functionally Graded Systems Via Friction Stir Processing, Critical Reviews in Solid State and Materials Sciences.

[142] Kumar, KS, Murigendrappa, SM, kumar, H. Experimental investigation on effects of varying volumefractions of SiC nanoparticle reinforcement on microstructure andmechanical properties in friction stir welded dissimilar joints of AA2024-T351 and AA7075-T651. Journal of Materials Research 2019; 455.

[143] Ashok Kumar, R, Ragav, GR, Nagarajan, KJ, et al. Effect of hybrid reinforcement at stirred zone of dissimilar aluminum alloys during friction stir welding. Metall. Res. Technol 2019; 116: 631.

[144] A. Shafiei-Zarghani, S. F. Kashani-Bozorg, and A. Zarei-Hanzaki, Microstructures and mechanical properties of Al/Al2O3 surface nano-composite layer produced by friction stir processing, Mater. Sci. Eng.: A 500(1–2), 84– 91 (2009).

[145] M. Raaft, T. S. Mahmoud, H. M. Zakaria, and T. A. Khalifa, Microstructural, mechanical and wear behavior of A390/graphite and A390/Al2O3 surface composites fabricated using FSP, Mater. Sci. Eng.: A 528(18), 5741– 5746 (2011).

[146] M. Ilangovan, S. Rajendra Boopathy, V. Balasubramanian, Effect of tool pin profile on microstructure and tensile properties of friction stir welded dissimilar AA 6061eAA 5086 aluminium alloy joints, Defence Technology 11 (2015) 174-184.

[147] Shanavas, S., & DHAS, J. E. R. (2017). Parametric optimization of friction stir welding parameters of marine grade aluminium alloy using response surface methodology. Transactions of Nonferrous Metals Society of China, 27(11), 2334-2344. 13.

[148] Rajakumar, S., & Balasubramanian, V. (2012). Establishing relationships between mechanical properties of aluminium alloys and optimised friction stir welding process parameters. Materials & Design, 40, 17-35.

[149] Lloyd, DJ. Particle reinforced aluminum and magnesium matrix composites. International Materials Reviews 1994; 39: 1.

[150] Yadav D, Bauri R. Processing, microstructure and mechanical properties of nickel particles embedded aluminium matrix composite. Mater Sci Eng A. 2011; 528:1326–33.

[151] Abdellah Nait Salah, Sipokazi Mabuwa, Husain Mehdi, Velaphi Msomi, Mohammed Kaddami, Prabhujit Mohapatra, Effect of Multipass FSP on Si-rich TIG Welded Joint of Dissimilar Aluminum Alloys AA8011-H14 and AA5083-H321: EBSD and Microstructural Evolutions. Silicon (2022). https://doi.org/10.1007/s12633-022-01717-4.

[152] Kumar, KS, Murigendrappa, SM, kumar, H. Experimental investigation on effects of varying volume fractions of SiC nanoparticle reinforcement on microstructure and mechanical properties in friction stir welded dissimilar joints of AA2024-T351 and AA7075-T651. Journal of Materials Research 2019; 455.

[153] Paidar M, Bokov M, Mehrez S et al Improvement of mechanical and wear behavior by the development of a new tool for the friction stir processing of Mg/B4C composite, Surface and Coatings Technology, 426, 2021, 127797.

[154] Husain Mehdi, R.S. Mishra, Investigation of mechanical properties and heat transfer of welded joint of AA6061 and AA7075 using TIG+FSP welding approach, Journal of Advanced Joining Processes, 1, 100003, (2020).

[155] Nouri, Z.; Taghiabadi, R.; Moazami-Goudarzi, M. (2020). Mechanical properties enhancement of cast Al-8.5Fe-1.3V-1.7Si (FVS0812) alloy by friction stir processing. Archives of Civil and Mechanical Engineering, 20(4), 102–. doi:10.1007/s43452-020-00106-1.

[156] Jain, Sumit & Mishra, R.. (2023). Joining of Aluminium Alloy AA6061 and Magnesium Alloy AZ-31 by Using Friction Stir Welding. 10.1007/978-981-19-6945-4_65.

[157] Yang, Kang; Li, Wenya; Niu, Pengliang; Yang, Xiawei; Xu, Yaxin (2017). Cold sprayed AA2024/Al 2 O 3 metal matrix composites improved by friction stir processing: Microstructure characterization, mechanical performance and

strengthening mechanisms. Journal of Alloys and Compounds, (), S0925838817338902–. doi:10.1016/j.jallcom.2017.11.132

[158] Husain Mehdi, Mishra, R.S. (2020). Investigation of mechanical properties and heat transfer of welded joint of AA6061 and AA7075 using TIG+FSP welding approach. Journal of Advanced Joining Processes, 1, 100003, https://doi.org/10.1016/j.jajp.2020.100003.

[159] Jain, Sumit & Sharma, Neeraj & Gupta, Rajat. (2018). Dissimilar alloys (AA6082/AA5083) joining by FSW and parametric optimization using Taguchi, grey relational and weight method. Engineering Solid Mechanics. 6. 51-66. 10.5267/j.esm.2017.10.003.

[160] V. Ebrahimzadeh, M. Paidar, M.A. Safarkhanian, O.O. Ojo, Orbital friction stir lap welding of AA5456-H321/AA5456-O aluminum alloys under varied parameters, Int. J. Adv. Manuf. Technol. 96 (2018) 1237–1254.

[161] Jain, S., & Mishra, R. S. (2021). Effect of Al2O3 nanoparticles on microstructure and mechanical properties of friction stir-welded dissimilar aluminum alloys AA7075-T6 and AA6061-T6. Proceedings of the Institution of Mechanical Engineers, Part E: Journal of Process Mechanical Engineering.

[162] Hines, W.W., & Montgomery, D.C. (1990). Probability and statistics in engg. And management science. 3rd Edition, Wiley Publications.

[163] Mishra, Radhey & Jain, Sumit. (2019). Friction stir welding (FSW) process on aluminum alloy 6082-T6 using taguchi technique. International Journal of Research in Engineering and Innovation. 3. 301-305. 10.36037/IJREI.2019.3503.

[164] El-Rayes, MM, El-Danaf, EA. The influence of multi-pass friction stir processing on the microstructural and mechanical properties of Aluminum Alloy 6082. Journal of Materials Processing Technology, Volume 212, Issue 5, 2012, Pages 1157-1168.

[165] E. G. Cole, A. Fehrenbacher, N. A. Duffie, and M. R. Zinn, “Weld temperature effects during friction stir welding of dissimilar aluminum alloys 6061-t6 and 7075-t6,” pp. 643–652, 2014.

[166] Yadav D, Bauri R. Processing, microstructure and mechanical properties of nickel particles embedded aluminium matrix composite. Mater Sci Eng A. 2011; 528:1326–33.

[167] Humphreys, FJ, Hatherly, M. Chapter 11 - grain growth following recrystallization, in: Recrystallization and Related Annealing Phenomena. Elsevier Ltd. 2004; 333–378

[168] Jain S, Mishra R. Influence of micro-sized Al2O3 particles on microstructure, mechanical, and wear behavior of dissimilar composite joint of AA6061/AA7075 by friction stir processing/welding. Proceedings of the Institution of Mechanical Engineers, Part C: Journal of Mechanical Engineering Science. 2022;236(16):9047-9060. doi:10.1177/09544062221092334.

[169] Asadi P, Faraji G, Besharati Givi MK. Producing of AZ91/SiC composite by Friction stir processing (FSP).IntJAdvManufTechnol2010;51:247–60.

[170] Husain Mehdi, Mishra R. Microstructure and mechanical characterization of tungsten inert gas-welded joint of AA6061 and AA7075 by friction stir processing. Proceedings of the Institution of Mechanical Engineers, Part L: Journal of Materials: Design and Applications. 2021;235(11):2531-2546. doi:10.1177/14644207211007882.

[171] Sarkari Khorrami, M.; Kazeminezhad, M.; Kokabi, A.H. The effect of SiC nanoparticles on the friction stir processing of severely deformed aluminum. Materials Science and Engineering: A, 602 (2014), 110–118.

[172] Jain, Sumit. (2016). UTS Maximization in Solid State Joining Process for AA6082. IOSR Journal of Mechanical and Civil Engineering. 02. 38-42. 10.9790/1684-15010020238-42.

[173] A. Nait Salah, Husain Mehdi, Arshad Mehmood, Abdul Wahab Hashmi, Chandrabhanu Malla, Ravi Kumar, Optimization of process parameters of friction stir welded joints of dissimilar aluminum alloys AA3003 and AA6061 by RSM, Materials Today: Proceedings,2021, https://doi.org/10.1016/j.matpr.2021.10.288

[174] Ebrahimzadeh, V, Paidar, M, Safarkhanian, MA, et al. Orbital friction stir lap welding of AA5456-H321/AA5456-O aluminum alloys under varied parameters. Int. J. Adv. Manuf. Technol 2018. 96: 1237–1254.

[175] Magdy M. El-Rayes; Ehab A. El-Danaf (2012). The influence of multi-pass friction stir processing on the microstructural and mechanical properties of Aluminum Alloy 6082., 212 (5), 1157–1168.

[176] Sipokazi Mabuwa and Velaphi Msomi (2020). The impact of submerged friction stir processing on the friction stir welded dissimilar joints. Mater. Res. Express 7 096513.

[177] Jamalian, HM, Ramezani, H, Ghobadi, H, Ansari, M, Yari, S, Givi, MKB, Processing–structure–property correlation in nano-SiC-reinforced friction stir welded aluminum joints, Journal of Manufacturing Processes, Volume 21,2016,Pages 180-189.

[178] Chiteka, K., & Yuvaraj, N. (2014). Mechanical and Metallurgical Characterisation of Friction Stir Welded Aluminium Alloys Aa5083-O And Aa6061-T4. i-manager's Journal on Material Science, 2(1), 7-14. https://doi.org/10.26634/jms.2.1.2758.

[179] Ghaffarpour, Morteza & Kazemi, Mohammad & Mohammadisefat, Mohammadjavad & Aziz, Ahmad & Dehghani, Kamran. (2015). Evaluation of dissimilar joints properties of 5083-H12 and 6061-T6 aluminum alloys produced by tungsten inert gas and friction stir welding. Proceedings of the Institution of Mechanical Engineers, Part L: Journal of Materials: Design and Applications. 231. 10.1177/1464420715595652.

[180] Krishnana, M., Subramaniama. S.K., Investigation of Mechanical and Metallurgical Properties of Friction Stir Corner Welded Dissimilar Thickness AA5086-AA6061 Aluminium Alloys. Materials Research. 2018; 21(4): e20171045.

[181] Preety Rani, R.S. Mishra [2022] “Influence of Reinforcement with Multi-Pass FSW on the Mechanical and Microstructural Behavior of Dissimilar Weld Joint of AA5083 and AA6061,” Silicon, ISSN 1876-9918, https://doi.org/10.1007/s12633-022-01863-9.